

University of Southampton Research Repository ePrints Soton

Copyright © and Moral Rights for this thesis are retained by the author and/or other copyright owners. A copy can be downloaded for personal non-commercial research or study, without prior permission or charge. This thesis cannot be reproduced or quoted extensively from without first obtaining permission in writing from the copyright holder/s. The content must not be changed in any way or sold commercially in any format or medium without the formal permission of the copyright holders.

When referring to this work, full bibliographic details including the author, title, awarding institution and date of the thesis must be given e.g.

AUTHOR (year of submission) "Full thesis title", University of Southampton, name of the University School or Department, PhD Thesis, pagination

UNIVERSITY OF SOUTHAMPTON
FACULTY OF ENGINEERING, SCIENCE AND MATHEMATICS
SCHOOL OF ELECTRONICS AND COMPUTER SCIENCE

Network Coding for Cooperative Multi-user Wireless Communication Systems

by

Hung Viet Nguyen

B.Eng, M.Eng

*A doctoral thesis submitted in fulfilment of
the requirement for the award of Doctor of Philosophy
at the University of Southampton*

Jan 2013

SUPERVISORS:

Dr. Soon Xin Ng

BEng, PhD , MIET, CEng, SMIEEE, FHEA

Prof. Lajos Hanzo

Dip Ing, MSc, PhD, DSc, FIEEE, FEng, FIET, EIC of IEEE Press

School of Electronics and Computer Science
University of Southampton
Southampton SO17 1BJ
United Kingdom

Dedicated to my family
with all my heartfelt gratitude, appreciation and love...

UNIVERSITY OF SOUTHAMPTON

ABSTRACT

FACULTY OF ENGINEERING AND APPLIED SCIENCE
DEPARTMENT OF ELECTRONICS AND COMPUTER SCIENCE

Doctor of Philosophy

Network Coding for Cooperative Multi-user Wireless Communication Systems

by Hung Viet Nguyen

In the first chapter, Space Time Trellis Codes (STTCs), Space Time Block Codes (STBCs) and Sphere-Packing-Space-Time Block Codes (SP-STBC) are reviewed. These schemes belong to the specific family of Multi-Input Multi-Output (MIMO) systems designed for achieving a diversity gain. The performance of the SP-STBC scheme is compared to other coded conventional modulation systems, namely to that of STBC-Phase Shift Keying or Quadrature Amplitude Modulation (STBC-PSK/QAM) and to that of STTC-Phase Shift Keying or Quadrature Amplitude Modulation (STTC-PSK/QAM). The rest of this chapter reviews other preliminaries pertaining to the context of cooperative communications and network coding.

In Chapter 2, an in-depth study of the capacity and outage probability of the Continuous-input Continuous-output Memoryless Channel (CCMC), Discrete-input Continuous-output Memoryless Channel (DCMC) and of Differential Discrete-input Continuous-output Memoryless Channel (D-DCMC) is presented. The study also considers various propagation phenomena, namely the small-scale fading and the large-scale fading. The frame-length is also taken into consideration when calculating the achievable throughput and outage probability, which serve as useful benchmarks for our near-capacity coding schemes. Extrinsic Information Transfer (EXIT) charts are used for designing Irregular Convolutional Coded Unity Rate Coded M-ary Phase Shift Keying (IrCC-URC-MPSK), Irregular Convolutional Coded Unity Rate Coded Differential M-ary Shift Keying (IrCC-URC-DMPSK) and Irregular Convolutional Coded Unity Rate Coded Space Time Trellis Coded M-ary Phase Shift Keying (IrCC-URC-STTC-MPSK) schemes.

In Chapter 3, a novel Distributed Concatenated IrCC-URC-STTC (DC-IrCC-URC-STTC) scheme is proposed for cooperative single-user systems relying on single-antenna aided relays, based on the studies conducted in Chapter 1 and Chapter 2. In this contribution, each coding arrangement of the entire DC-IrCC-URC-STTC scheme is designed for achieving decoding convergence to a vanishingly low Bit Error Ratio (BER) by employing non-binary EXIT-charts. Additionally, the EXIT charts are employed for calculating the most appropriate positions of the relays by ensuring that decoding convergence to a vanishingly low BER occurs at a similar Signal-to-Noise Ratio (SNR) both at the relays and at the destination.

In Chapter 4, Multi-User Cooperative Communications is designed for supporting M users

with the aid of near-capacity network coding. We first derive the upper and lower Frame Error Ratio (FER) performance bounds of cooperative multi-user communications systems using network coding. Then, we investigate Near-Capacity Multi-user Network-coding (NCMN) based systems using the IrCC-URC-MPSK scheme of Chapter 2. In parallel to the investigation of coherent NCMN systems, we also explored Near-capacity Non-coherent Cooperative Network-coding aided Multi-user (NNCNM) based systems using the IrCC-URC-DMPSK, which do not require channel estimation at the receiver's side. This reduces the complexity imposed, albeit this is achieved at a 3 dB SNR-loss. Moreover, a new technique referred to as the Pragmatic Algebraic Linear Equation Method (PALEM) was proposed for exactly determining the number of information sources that may be recovered from the composite NCMN stream, which results in a more accurate evaluation of the attainable FER performance of the NCMN and NNCNM based systems. The design principles presented in this contribution can be extended to a vast range of NCMN and NNCNM based systems using arbitrary channel coding schemes.

In Chapter 5, the NCMN and NNCNM based systems of Chapter 4 are generalised for introducing the Generalised NCMN (GNCMN) system, which has a multi-layer architecture and it is capable of operating in multiple modes. More specifically, the GNCMN system may operate upon employing either individually or in a combined fashion using a single Channel Coding (CC) layer plus two network coding layers, namely Network Coding 1 (NC1) and Network Coding 2 (NC2). Additionally, the GNCMN system is capable of simultaneously exploiting the advantages of all the modes available in each layer of the system as well as appropriately combining the advantageous modes across all the three layers.

Finally, in Chapter 6, the summary of our findings are presented in order to facilitate our discussions on future research.

Declaration of Authorship

I, **Hung Viet Nguyen**, declare that the thesis entitled

Network Coding for Cooperative Multi-user Wireless Communication Systems

and the work presented in it are my own and has been generated by me as the result of my own original research. I confirm that:

- this work was done wholly or mainly while in candidature for a research degree at this University;
- where any part of this thesis has previously been submitted for a degree or any other qualification at this University or any other institution, this has been clearly stated;
- where I have consulted the published work of others, this is always clearly attributed;
- where I have quoted from the work of others, the source is always given. With the exception of such quotations, this thesis is entirely my own work;
- I have acknowledged all main sources of help;
- where the thesis is based on work done by myself jointly with others, I have made clear exactly what was done by others and what I have contributed myself;
- parts of this work have been published.

Signed:

Date:

Acknowledgement

First and foremost, I would like to express my heartfelt gratitude to my supervisors Dr. Soon Xin Ng (Michael) and Professor Lajos Hanzo firstly for providing me the opportunity to join the Communications Group and subsequently for their exceptional supervision, insightful guidance and ultimately their friendship, without their fruitful support this work could not have been accomplished. Their patient step-by-step guidance along with their overall kindness and encouragement have tremendously benefited me and made known to me how an exemplary researcher should be.

The essential support in finance of Vietnam Ministry of Education and Training (MOET) represented by Vietnam International Education Department (VIED) is gratefully acknowledged. I am also thankful for the financial support provisioned by EU Optimix Project under the approval of Professor Lajos Hanzo.

I am also grateful to my collaborators, Assistant Prof. Joao Luiz Rebelatto, Assistant Prof. Yonghui Li, Miss Jing Juo and Mr. Chao Xu, for the knowledge-upbuilding discussions, suggestions and comments. To my colleagues, my thanks goes to them for enriching my experience during the past four years.

My friends in Southampton, I thank each and every one for trust and friendship. They have made my days more meaningful and enjoyable, to Mr. Terry Craft and Mrs. Bernice Craft for discussions on truthful aspects of life, to Mr. Jabez Mark for sharing joyful moments, to Vietnamese friends in Southampton for jointly enjoying unforgettable gatherings, etc.

Last but not least, I would like to dedicate this thesis to my family for their endless and unconditional supports and especially to my beloved wife Thong Bui and my dear daughter Linh Nguyen for their love and exceptional efforts during the time I was away.

To all these wonderful people, many thanks again.

List of Publications

Journals:

1. **Hung Viet Nguyen**, Soon Xin Ng, Lajos Hanzo, “Performance Bounds of Network Coding Aided Cooperative Multiuser Systems,” *IEEE Signal Processing Letters*, Vol.18, No.7, pp.435-438, July 2011.
2. **Hung Viet Nguyen**, Xu Chao, Soon Xin Ng, Lajos Hanzo , “Non-coherent Near-capacity Network Coding for Cooperative Multi-User Communications,” *IEEE Transaction on Communications*, vol.60, issue 10, pp.3059-3070, Oct. 2012.
3. **Hung Viet Nguyen**, Soon Xin Ng, Lajos Hanzo , “Irregular Convolution and Unity-Rate Coded Network-Coding for Cooperative Multi-User Communications,” *IEEE Transaction on Wireless Communications*, vol.12, issue 03, pp.1231-1243, Mar. 2013.
4. Jing Zuo, Chen Dong, **Hung Viet Nguyen**, Soon Xin Ng, Lie-Liang Yang and Lajos Hanzo, “Cross-Layer Aided Energy-Efficient Opportunistic Routing in Ad Hoc Networks,” *submitted to IEEE Transaction on Communications*, Oct. 2012.

Conferences:

1. **Hung Viet Nguyen**, Soon Xin Ng, Lajos Hanzo , “Distributed Three-Stage Concatenated Irregular Convolutional, Unity-Rate and Space-Time Trellis Coding for Single-Antenna Aided Cooperative Communications,” *IEEE 72nd Vehicular Technology Conference Fall (VTC 2010-Fall)*, Ottawa, Canada, pp.1-5, 6-9 September 2010.
2. Jing Zuo, **Hung Viet Nguyen**, Soon Xin Ng, Lajos Hanzo , “Energy-efficient relay aided ad hoc networks using iteratively detected irregular convolutional coded, unity-rate coded and Space-Time Trellis Coded transceivers,” *IEEE Wireless Communications and Networking Conference (WCNC)*, Cancun, Mexico, pp.1179-1184, 28-31 March 2011.
3. **Hung Viet Nguyen**, Soon Xin Ng, Luiz Rebelatto, Yonghui Li and Lajos Hanzo, “Near-Capacity Network Coding for Cooperative Multi-User Communications,” *IEEE 74th Vehicular Technology Conference Fall (VTC 2011-Fall)*, San Francisco, USA, pp.1-5, 5-8 September 2011.
4. **Hung Viet Nguyen**, Xu Chao, Soon Xin Ng, Luiz Rebelatto, Yonghui Li and Lajos Hanzo, “Near-Capacity Non-Coherent Network-Coding Aided Scheme for Cooperative Multi-user Communications,” *IEEE 74th Vehicular Technology Conference Fall (VTC 2011-Fall)*, San Francisco, USA, pp.1-5, 5-8 September 2011.

Contents

Abstract	ii
Declaration of Authorship	iv
Acknowledgement	v
List of Publications	vi
Glossary	xiii
List of Symbols	xviii
1 Introduction and Overview	1
1.1 Multiple Dimension Modulation	4
1.1.1 Space Time Trellis Code	8
1.1.2 Space Time Block Code	11
1.1.3 STBC-Sphere Packing	15
1.1.4 Comparison of STTC, STBC and SP-STBC	18
1.2 Cooperative Communications and Network Coding	22
1.2.1 Cooperative Communications	22
1.2.2 Network Coding	23
1.2.2.1 Linear Network Codes	24
1.3 Organisation of the Thesis	27
2 Near-capacity Coded Modulation Schemes	29

2.1	Outage probability of a single link	29
2.1.1	Continuous-Input Continuous-Output Memoryless Channel	30
2.1.2	Non-coherent detection	31
2.1.2.1	Multiple-Symbol Differential M-ary Phase-Shift Keying	31
2.1.3	Discrete-Input Continuous-Output Memoryless Channel	33
2.1.4	Differential Discrete-Input Continuous-Output Memoryless Channel	35
2.2	Outage capacity of a single link	39
2.2.1	Coherent schemes	40
2.2.2	Non-coherent schemes	43
2.3	Near-capacity channel code design	46
2.3.1	EXIT-chart based code design principle	47
2.3.2	IrCC-URC-STTC-MPSK coding scheme	48
2.3.2.1	EXIT-chart matching and optimisation of the IrCC-URC-STTC-MPSK scheme	48
2.3.2.2	Performance of IrCC-URC-STTC-MPSK coding scheme	52
2.3.3	IrCC-URC-MPSK coding scheme	54
2.3.3.1	EXIT-charts matching and optimisation	55
2.3.3.2	Performance of IrCC-URC-MPSK coding scheme	60
2.3.4	IrCC-URC-DMPSK coding scheme	64
2.3.4.1	EXIT-chart design for IrCC-URC-MSDD-aided-DMPSK	65
2.3.4.2	Performance of IrCC-URC-DMPSK coding scheme	66
2.4	The employment of sub-frames	69
2.5	Non-Coherent versus Coherent Near-Capacity Schemes	70
2.6	Chapter Summary	74
3	Distributed Three-Stage Concatenated Single-Antenna Aided Cooperation	76
3.1	Relay aided MIMO	76
3.2	Link Configuration in the Absence of the SD Link	77
3.2.1	System Model in the Absence of the SD Link	77
3.2.2	Distributed Concatenated IrCC, URC and STTC	80

3.2.3	System Capacity and Relay Selection	84
3.2.3.1	Relay Channel Capacity	84
3.2.3.2	Relay Selection	85
3.2.4	Relay Positioning and its Power Gain	87
3.3	Distributed Coding Scheme with the Presence of SD Link	92
3.3.1	System Model in the Presence of the SD Link	92
3.3.2	Encoder and Decoder in the Presence of the SD Link	92
3.3.3	Achievable Rate and Relaying Strategy	95
3.3.3.1	Dynamically Selected Relays	95
3.3.3.2	Relay Channel Capacity	97
3.3.3.3	EXIT-chart for Determining the Number of Outer Iterations	99
3.3.4	Optimal Relays versus Dynamic Relays	99
3.4	Chapter Summary	100
4	Near-Capacity Network Coding for Multi-User Cooperative Communications	102
4.1	From Network Coding to Generalised Dynamic Network Codes	102
4.2	Generalised Dynamic-Network Codes	103
4.2.1	System Model	103
4.2.2	Transfer Matrix	106
4.3	Recovering of the Information Frames at the Base Station	112
4.4	Pragmatic Method versus Rank-based Method	115
4.4.1	Purely Rank-Based Method	115
4.4.2	Pragmatic Algebraic Linear Equation Method	116
4.5	The System's Outage Probability	118
4.5.1	The Upper Bound of the Outage Probability	119
4.5.2	The Lower Bound of the Outage Probability	121
4.6	System Parameters	122
4.6.1	System Diversity Order	122
4.6.2	System Parameter Sets	122
4.7	Network Coding Design	123

4.7.1	Cooperative System Approach	123
4.7.2	Network Coding Approach	126
4.7.3	Near Capacity Multi User Network Coding Aided Systems	128
4.8	Pure Rank, Pragmatic Algebraic and SIMULation Methods	134
4.9	Performance Bounds of the Systems	134
4.10	Near-capacity Coherent/Non-coherent based System	137
4.10.1	Benefits of Network Coding	140
4.10.2	Sub-frame Transmission for Approaching the Capacity	143
4.10.3	Non-coherent versus Coherent Systems	144
4.11	Augmenting Multiplexing and Diversity Capability of Network Coding	145
4.12	Chapter summary	147
5	Generalised Near-Capacity Multi-user Network-coding: Multilayer-and-Multimode Architecture	149
5.1	Architecture of Generalised Near-Capacity Multi-user Network-coding System	150
5.1.1	Near-capacity Channel Coding	150
5.1.2	Network Coding 1	152
5.1.2.1	The Conventional mode	152
5.1.2.2	The Full Diversity mode	154
5.1.2.3	The Adaptive modes, A_1 mode and A_2 mode	159
5.1.3	Network Coding 2	162
5.1.4	Parameters of the General Near-Capacity Multi-user Network-coding systems	163
5.2	Performance Bounds in the Full Diversity Mode and the Adaptive Modes	163
5.2.1	Full Diversity Performance Bounds	163
5.2.2	Adaptive System's Performance Bounds	167
5.2.2.1	Adaptive Mode 1	167
5.2.2.2	Adaptive Mode 2	168
5.2.3	The Bounds and Monte-Carlo based Performance	170
5.3	Multiplexing and Diversity Enhancement in the Network Coding 1	172
5.3.1	Diversity Gain in Full Diversity Mode	172

5.3.2	Multiplexing and Diversity Gains from the Adaptive Mechanism	173
5.3.2.1	Maximum Adaptive Rate in Network Coding 1	173
5.3.2.2	Multiplexing Gain versus Diversity Gain in the Adaptive Network Coding	173
5.4	The Combined Modes in Network Coding 1	177
5.5	Gain by Network Coding 2	181
5.5.1	Design of Network Coding 2	181
5.5.2	Performance of the System assisted by Network Coding 2	181
5.6	Near Capacity System Performance	186
5.6.1	Achievable Capacity of the Ideal/Perfect Coding Scheme	187
5.6.2	Approaching the GNCMN capacity	187
5.6.3	Potential Solutions at Channel Coding Layer	193
5.6.4	Solutions at the Network Coding 1 Layer	193
5.6.5	Solutions at the Network Coding 2 Layer	197
5.7	Coherent versus Non-coherent Systems	199
5.8	Chapter Summary	202
6	Conclusions and Future Works	205
6.1	Conclusions	205
6.2	Future work	209
	Appendices	210
A	System's outage probability	210
A.1	Formulation of the System's Outage Probability	210
A.1.1	Outage probability of a given frame	213
A.1.1.1	Approximated maximum value of the probability $P_{o,m}(U_{m,t}^*)$	215
A.1.1.2	Approximated minimum value of the probability $P_{o,m}(U_{m,t}^*) _{ U_{m,t}^* =0}$	217
A.1.2	Bounding the system's outage probability	217
A.1.2.1	Upper bound of the system's outage probability	217
A.1.2.2	Lower bound of system's outage probability	220

B Modem Channel Emulator	221
C Adaptive mode 2: Performance Bound of the System Performance	224
C.1 Outage Probability of the System Employing the A_2 Mode	225
C.2 Outage Probability of an Information Frame in Adaptive 2	228
C.2.1 Approximation of the Probability $P_m^{A_2}(U_{m,t}^*)$	230
C.2.2 Approximation of the probability $P_m(U_{m,t}^*) _{\ U_{m,t}^*\ =0}$	232
C.3 Adaptive mode 2: Upper and Lower Bounds	233
C.3.1 Upper bound in Adaptive mode 2	233
C.3.2 Lower bound in Adaptive mode 2	236
D Additional Results	238
D.1 The FER-versus-SNR performance of the A_1 and A_2 modes	238
Bibliography	240
Subject Index	257
Author Index	260

Glossary

<i>C mode</i>	Conventional mode
<i>FD mode</i>	Full Diversity mode
16PSK	16 level Phase Shift Keying
17co-IrCC	17 component IrCC
36co-IrCC	36 component IrCC
4PSK	4-level Phase Shift Keying
8PSK	8 level Phase Shift Keying
AF	Amplify-and-Forward
AWGN	Additive white Gaussian Noise
BER	Bit Error Ratio
BICM	Bit-Interleaved Coded Modulation
BM	Branch Metric
BP	Broadcast Phase
BPS	Bit Per Symbol
BPs	Broadcast Phases
BPSK	Binary Phase-Shift Keying
BS	Base Station
CAF	Compress-And-Forward
CC	Channel Code
CC	Channel Coding
CCDF	Complementary Cumulative Distribution Function
CCMC	Continuous-input Continuous-output Memoryless Channel
CDD	Conventional Differential Detection
CNC	Convolutional Network Codes
CP	Cooperative Phase

CPs	Cooperative Phases
CSI	Channel State Information
D-DCMC	Differential Discrete-input Continuous-output Memoryless Channel
DBPSK	Differential Binary Phase Shift Keying
DC-IrCC-URC-STBC-SP	Distributed Concatenated IrCC-URC-STBC-SP
DC-IRCC-URC-STTC	Distributed Concatenated Irregular Convolutional Code, Unity-Rate Code and Space-Time Trellis Code
DC-IrCC-URC-STTC	Distributed Concatenated IrCC-URC-STTC
DCMC	Discrete-input Continuous-output Memoryless Channel
DF	Decode-and-Forward
DMPSK	Differential M-ary Phase Shift Keying
DMT	Diversity Multiplexing Trade-off
DNC	Dynamic Network Coding
DNCs	Dynamic Network Codes
DQPSK	Differential Quadrature Phase Shift Keying
EGC	Equal-Gain Combining
EXIT	Extrinsic Information Transfer
FEC	Forward Error Correction
FER	Frame Error Ratio
GDNC	Generalised Dynamic Network Code
GDNC	Generalized Distributed Network Coding
GDNCs	Generalised Dynamic Network Codes
GF	Galois Fields
GNC	Generic Network Codes
GNCMN	Generalised Near-Capacity Multi-user Network-coding
HNC	Hybrid Network Codes
i.i.d.	independent and identically distributed
IF	Information Frame
IFs	Information Frames
IIR	Infinite Impulse Response
IrCC	Irregular Convolutional Code
IrCC-URC	Irregular Convolutional Code and Unity-Rate Code

IrCC-URC-DBPSK	IrCC-URC-Differential Binary Phase Shift Keying
IrCC-URC-DMPSK	Irregular Convolutional Code-Unity Rate Code-Differential M-ary Phase Shift Keying
IrCC-URC-DMPSK	Irregular Convolutional Coded Unity Rate Coded Differential M-ary Phase Shift Keying
IrCC-URC-DMPSK	Irregular Convolutional Coded Unity Rate Coded Differential M-ary Shift Keying
IrCC-URC-DQPSK	Irregular Convolutional Code and Unity-Rate Code Differential Quadrature Binary Phase Shift Keying
IrCC-URC-MPSK	Irregular Convolutional Coded Unity Rate Coded M-ary Phase Shift Keying
IrCC-URC-MPSK	Irregular Convolutional Coded-Unity Rate Coded M-ary Phase Shift Keying
IrCC-URC-QPSK	Irregular Convolutional Code, a Unity-Rate Code and Quadrature Phase-Shift Keying
IrCC-URC-STTC	Irregular Convolutional Coded Unity Rate Coded Space Time Trellis Code
IrCC-URC-STTC-MPSK	Irregular Convolutional Coded Unity Rate Coded Space Time Trellis Coded M-ary Phase Shift Keying
IrCCs	Irregular Convolutional Codes
LDPC	Low-Density Parity-Check
LNC	Linear Network Codes
LTE	Long Term Evolution
LTE-Advanced	Long Term Evolution-Advanced
MAC	Medium Access Control
MAP	Maximum A-Posteriori
MCEM	Modem Channel Emulator Method
MDM	Multi-Dimensional Modulation
MDS	Maximum Distance Separable
MIMO	Multi-Input Multi-Output
ML	Maximum Likelihood
MRC	Maximal-Ratio Combining
MRRC	Maximal-Ratio Receiver Combining
MSDD	Multiple-Symbol Differential Detection
MSDD-aided-DEM	MSDD-aided DEModulation
MSDD-aided-DMPSK	Multiple-Symbol Differential Detection aided Differential M-ary Phase-Shift Keying
MSDSD	Multiple-Symbol Differential Sphere Detection
NC1	Network Coding 1

NC2	Network Coding 2
NCMN	Near-Capacity Multi-user Network-coding
NLNC	Non-linear Network Codes
NNCNM	Near-capacity Non-coherent Cooperative Network-coding aided Multi-user
PALEM	Pragmatic Algebraic Linear Equation Method
PAM	Pulse-Amplitude Modulation
PC	Product Codes
PFs	Parity Frames
PHY	Physical Layer
PRBM	Pure Rank Based Method
PSK	Phase-Shift Keying
Q²PSK	Quadrature-Quadrature Phase-Shift Keying
QAM	Quadrature Amplitude Modulation
QPSK	Quadrature Phase-Shift Keying
R-D	Relay-Destination
RNC	Random Network Codes
RNC	Random Network Coding
RS	Reed Solomon
RSC	Recursive Systematic Convolutional
S-D	Source-Destination
S-R	Source-Relay
SC	Selection Combining
SC	Subspace Codes
SISO	Single-Input Single-Output
SNC	Secure Network Codes
SNC	Static Network Codes
SNR	Signal-to-Noise Ratio
SP	Sphere Packing
SP-STBC	Sphere-Packing-Space-Time Block Codes
STBC	Space Time Block Codes
STBC	Space Time Block Coding
STBC-PSK/QAM	STBC-Phase Shift Keying or Quadrature Amplitude Modulation
STBC-SP	STBC-Sphere Packing
STBCs	Space Time Block Codes

STBCs	Space-Time Block Codes
STC	Space Time Coding
STTC	Space Time Trellis Code
STTC	Space Time Trellis Coded
STTC	Space Time Trellis Codes
STTC	Space Time Trellis Coding
STTC-PSK/QAM	STTC-Phase Shift Keying or Quadrature Amplitude Modulation
STTC-QPSK	Space Time Trellis Code Quadrature Shift Keying
STTCs	Space Time Trellis Codes
STTCs	Space-Time Trellis Codes
TS	Time Slot
URC	Unity-Rate Code
URC-DMPSK	Unity Rate Coded Differential M-ary Phase Shift Keying
URC-DQPSK	Unity-Rate Code Differential Quadrature Binary Phase Shift Keying
URC-QPSK	Unity-Rate Code and Quadrature Phase-Shift Keying
URC-STTC_{2×1}-QPSK	URC-STTC-QPSK having two transmit and one receive antennas
URC-STTC-MPSK	Unity Rate Coded M-ary Phase Shift Keying
URC-STTC-QPSK	Unity Rate Coded Space Time Trellis Code Quadrature Shift Keying
VMIMO	Virtual MIMO

List of Symbols

General notation

- The superscript $*$ is used to indicate complex conjugation. Therefore, a^* represents the complex conjugate of the variable a .
- The superscript T is used to indicate matrix transpose operation. Therefore, \mathbf{a}^T represents the transpose of the matrix \mathbf{a} .
- The superscript H is used to indicate complex conjugate transpose operation. Therefore, \mathbf{a}^H represents the complex conjugate transpose of the matrix \mathbf{a} .

Special symbols

- (S): Source node.
- (R): Relay node.
- (D): Destination node.
- $x_{k,i}$: Symbols transmitted over the transmit antenna T_{xi} , where i is the antenna index.
- d : Distance from source (s) to destination (d).
- d_{sr} : Distance from source (s) to relay (r).
- d_{rd} : Distance from relay (r) to destination (d).
- g_{sr} : Geometrical power gain expressed as a function of the source-to-relay distance.
- g_{rd} : Geometrical power gain expressed as a function of the relay-to-destination distance.
- G_{sr} : Geometrical power gain in dB for source-relay link.
- G_{rd} : Geometrical power gain in dB for relay-destination link.
- SNR_t : Ratio of the power transmitted from the transmitter to the noise power encountered at the receiver.
- $SNR_{t(source)}$: SNR_t for the source node.
- $SNR_{t(relay)}$: SNR_t for the relay node.
- SNR_r : Ratio of received power to noise power at receiver.
- $SNR_{r(relay)}$: SNR_r at relay.
- $SNR_{r(dest.)}$: SNR_r at destination.
- M_r : SNR_r The number of relay nodes.
- N_s : The number of symbols per frame transmitted from source node.
- k : The k^{th} symbol in the set of N_s symbols per frame transmitted from source node.
- $y_{r_i,k}$: The k^{th} received signal at the i^{th} relay node during the first transmission period.
- $h_{sr_i,k}$: Complex-valued Rayleigh fading coefficient between the source node and the i^{th} relay node at instant k .
- $n_{r_i,k}$: Additive White Gaussian Noise (AWGN) process having a variance of $N_0/2$ per dimension, which is associated with the complex-valued Rayleigh fading coefficient $h_{sr_i,k}$.

- $y_{d,l}$: The l^{th} received symbol at the destination node during the second transmission period.
- N_r : The number of symbols per frame transmitted from relay node.
- l : The l^{th} symbol in the set of N_r symbols per frame transmitted from relay node.
- $y_{d,l}$: The l^{th} symbol at the destination node during the second transmission period.
- $h_{r_i,d,l}$: Complex-valued Rayleigh fading coefficient between the i^{th} relay node and the destination node at instant l .
- $n_{d,l}$: Additive White Gaussian Noise (AWGN) process having a variance of $N_0/2$ per dimension, which associates with complex-valued Rayleigh fading coefficient $h_{r_i,d,l}$.
- c : Coded sequence.
- x : Transmitted symbol sequence.
- y_{ri} : Signal received at the i^{th} relay node.
- u_i : Recovered information bit sequence at the i^{th} relay node.
- y_d : Received signal sequence at destination.
- u' : Decoded information bit sequence at destination.
- R_{xyz} : Coding rate of the coding arrangement xyz .
- N_i : The number of information bits transmitted within a duration of $(N_s + N_r)$ symbol periods.
- η : Overall throughput of the two-hop cooperative system.
- C_{CCMC}^{relay} : Achievable capacity of a full duplex relay aided Continuous-input Continuous-output Memoryless Channel (CCMC).
- C_{DCMC}^{relay} : Achievable capacity of a half duplex relay aided Discrete-input Continuous-output Memoryless Channel (DCMC).
- X : Signal sequence transmitted from a source node.
- Y_{ri} : Signal sequence received at the i^{th} relay node.
- Y_d : Signal sequence received at the destination node.
- I : The number of iterations between a URC decoder and STTC decoder.
- α_i : The i^{th} weighting coefficient of the i^{th} IrCC component code.
- J : The number of iterations between an IrCC decoder and aggregate URC-STTC decoder.

- A : The difference in dB between the convergence SNRs of two concatenated coding arrangements considered in a specific relay aided system.
- a : The difference in terms of the ratio between the convergence SNR of two concatenated coding arrangements considered in a specific relay aided system
- N : Frame length, either in bits or symbols
- N_{sub} : The number of sub-frames constructed from a channel-encoded frame.
- x : The transmitted signal when considering a single transmission link.
- y : The received signal when considering a single transmission link.
- h : The complex-valued fading coefficient of the channel.
- h_s : The slow (block, large-scale or quasi-static) fading coefficient, which is one component of the channel coefficient h and remains constant for all symbols within a frame.
- h_f : The fast (small-scale) fading coefficient, which is one component of the channel coefficient h and fluctuates on a symbol-by-symbol basis.
- n : The AWGN process having a variance of $N_0/2$ per dimension.
- R : The data rate or throughput.
- P_e : The outage probability.
- $C|h$: The channel capacity, given the channel's fading coefficient h .
- η : The number of modulated bits per symbol.
- R_n : The normalised throughput, which is equal to R/η .
- $SNR_r|_R$: The value of SNR_r specified on the capacity curve corresponding to a given throughput R .
- $SNR_r^{EXIT}|_R$: The value of SNR_r specified on the capacity curve constructed with the aid of EXIT charts corresponding to a given throughput R .
- ε : The outage value used for specifying the outage capacity
- R_c : Coding rate.
- L : Modulation levels.
- α_i : IrCC coding coefficients representing the i^{th} fraction of the input stream, which is encoded by the i^{th} component code, $i = [1, 2, \dots, 17]$ or $i = [1, 2, \dots, 36]$

- β_i : IrCC component code (subcode) rates representing the coding rate of the i^{th} component code, $i = [1, 2, \dots, 17]$ or $i = [1, 2, \dots, 36]$.
- J : The number of outer coding iterations.
- I : The number of inner coding iterations.
- f_d : Doppler frequency.
- θ : The normalised channel estimation accuracy.
- \hat{h} : The estimated value of the fading channel coefficient h .
- n_{est} : The estimated value of the noise n .
- SNR_{est} : The nominal estimated value of SNR .
- N_w : The size of the window representing the number of symbols observed for demodulating in MSDD scheme.
- $C_n(\epsilon)$: The normalised outage capacity associated with the outage probability ϵ .
- R : The throughput or information rate of a link.
- R_n : The normalised throughput.
- θ : The channel estimation accuracy.
- N_s : The number of symbols transmitted by the source node.
- N_r : The number of symbols transmitted by the relay nodes.
- γ : The dynamic threshold used for selecting relays.
- I_{in} : The number of iterations within a coding scheme at the relay and destination.
- I_{out} : The number of iterations between two a coding scheme at the destination.
- M : The number of users supported by the system.
- k_1 : The number of information frames transmitted by each user during cooperative phases.
- k_2 : The number of parity frames transmitted by each user during broadcast phases.
- $I_m(t)$: An information frame (packet or message) transmitted by User m during the specific broadcast phase t .
- B_i : The i^{th} broadcast phase.
- C_i : The i^{th} cooperative phase.
- G**: Transfer matrix.

\mathbf{I} : Unity matrix.

\mathbf{P} : Parity matrix.

\mathbf{G}' : Modified transfer matrix.

\mathbf{I}' : Modified unity matrix.

\mathbf{P}' : Modified parity matrix.

$I_m^{Co}(t)$: an entry at row m and column t of the identity matrix.

$P'_{m,s}(t)$: an entry of the modified parity matrix defined by Equations 4.5, 4.6 and 4.7.

P_o : The system outage probability P_o .

P_o^{Upper} : Upper bound of the system outage probability P_o .

P_o^{Lower} : Lower bound of the system outage probability P_o .

D : Diversity order.

R_{NCMN} : Information rate of the NCMN system.

R_{info} : Information rate of the network coding used in NCMN systems.

R_e : Equivalent transmission rate.

$k_{2,j}$: The adaptive value of k_2 applied for User j .

R_{info,A_1} : The adaptive information rate in the A_1 mode.

R_{info,A_2} : The adaptive information rate in the A_2 mode.

H : The number of frames at the input of the Network Coding 2 layer.

Θ : The number of encoded frames at the output of the Network Coding 2 layer.

FD : Full diversity mode.

C : Conventional mode.

A_1 : Adaptive 1 mode.

A_2 : Adaptive 2 mode.

P_o^{FD} : Outage probability P_o of the system in the FD mode.

$P_o^{Upper,FD}$: Upper bound of the outage probability P_o^{FD} of the system operating in the FD mode.

$P_o^{Lower,FD}$: Lower bound of the outage probability P_o^{FD} of the system operating in the FD mode.

- Ω_1 : Multiplexing gain of the system operating in the A_1 mode.
- Ω_2 : Multiplexing gain of the system operating in the A_2 mode.
- Φ_1 : Diversity gain of the system operating in the A_1 mode.
- Φ_2 : Diversity gain of the system operating in the A_2 mode.
- Σ_1 : Sum of the diversity and multiplexing gains of the system operating in the A_1 mode.
- Σ_2 : Sum of the diversity and multiplexing gains of the system operating in the A_2 mode.

Introduction and Overview

The design of an attractive channel coding and modulation scheme depends on a range of conflicting factors [1], which are illustrated in Figure 1.1. Different solutions accrue when optimising different codec features. For example, in many applications the most important codec parameter is the achievable coding gain, which quantifies the amount of bit-energy reduction attained by a codec at a certain target Bit Error Ratio (BER). Naturally, attaining a transmit power reduction is extremely important in battery-powered devices. This transmitted power reduction is only achievable at the cost of an increase implementational complexity, which itself typically, increases the power consumption and hence erodes some of the power gain. Viewing this system optimisation problem from a different perspective, it is feasible to transmit at a higher bit rate in a given fixed bandwidth by increasing the number of bits per modulated symbols. However, when aiming for a given target BER, the channel coding rate has to be reduced in order to increase the transmission integrity. Naturally, this reduces the effective throughput of the system and results in an overall increased system complexity [2].

An anecdotal research road map leading towards the introduction of multi-user cooperative systems is represented in Figure 1.2. More specifically, we commence with the ultimate goal of designing a wireless communication system for creating reliable high data rate links. These links may be supported by utilising different forms of diversity, which are made available by introducing various techniques, for example multidimensional modulation and coding schemes.

Accordingly, we have conducted a study of Multi-Dimensional Modulation (MDM), which leads us to the need of investigating Multi-Input Multi-Output (MIMO) systems, where MDM and coding are combined. As a result of exploring further a range of MIMO-related areas, upon combining idea of the cooperative communications with that of virtual MIMO systems exploiting the concept of space time coding concatenated with turbo codes, our single-user cooperative relay aided systems were designed in Chapter 3. Furthermore, in the context cooperative communication, network coding was then invoked for constructing the multi-user, multi-layer, multi-mode cooperative system concept relying on realistic near-capacity coding schemes advocating the turbo

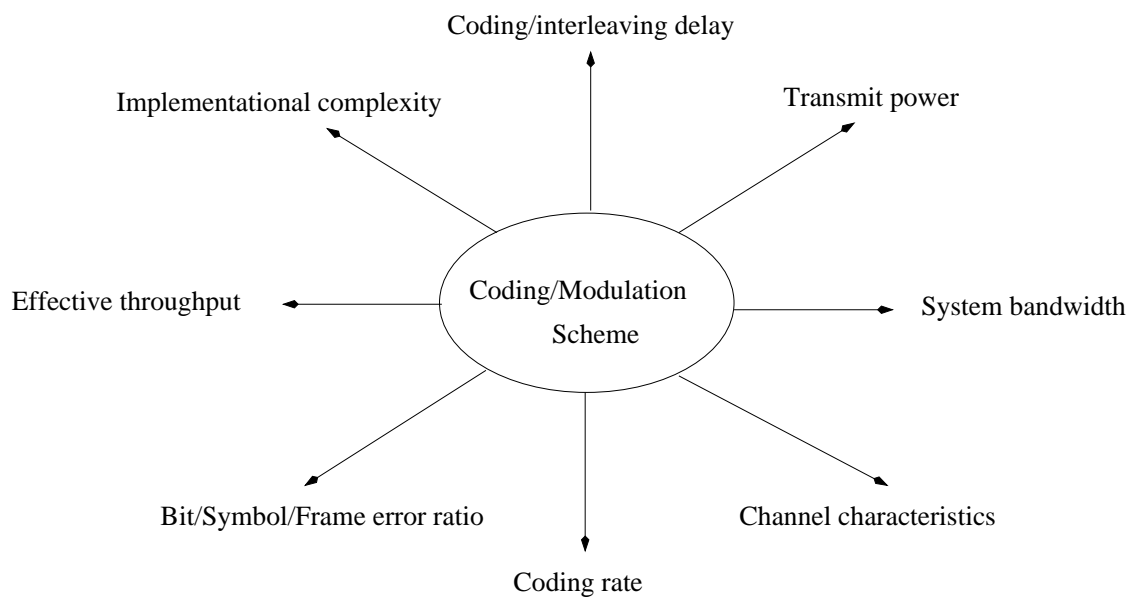


Figure 1.1: Factors affecting the design of channel coding and modulation scheme [1].

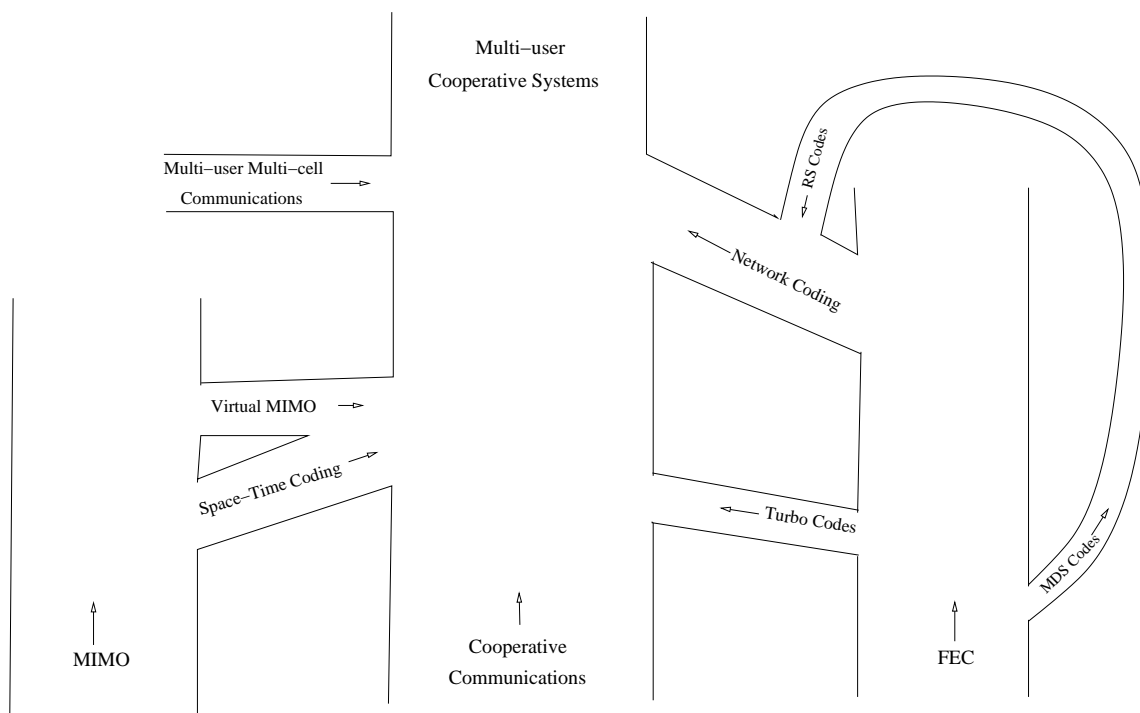


Figure 1.2: Research road map of the thesis.

principle, as detailed in Chapter 4 and Chapter 5. Accordingly, Table 1.1 and Table 1.2 summarises the important milestones related to the road map of research portrayed in Figure 1.2.

The major novel contributions presented in the thesis can be summarised as follows:

1. We formulated the complementary cumulative distribution function (CDF) $F(SNR_r|R)$ of the receiver's SNR for characterising the family of DCMC/D-DCMC channels [3,4].
2. We formulated the outage capacity of the differentially encoded modulation scheme corresponding to different outage probability values ϵ . This outage capacity is employed as our bench-marker for the realistic coding schemes both in a single-link scenario and in a network coding based scenario [3,4].
3. We conceived the EXIT-chart based design principle that is applied for near-capacity non-coherent/coherent coded modulation schemes, namely for designing Irregular Convolutional Code-Unity Rate Code-Differential M-ary Phase Shift Keying (IrCC-URC-DMPSK) [5] and an Irregular Convolutional Coded-Unity Rate Coded M-ary Phase Shift Keying (IrCC-URC-MPSK) scheme [6].
4. We amalgamated the ideas of distributed space time coding [7,8] and near-capacity channel coding with the cooperative DF approach employing several single-antenna aided relays and our IrCC-URC-STTC coding arrangement for designing a near-capacity coding scheme. In other words, we designed a near-capacity coding scheme for optimising the overall system and devised algorithms for finding relays for cooperation in the most appropriate locations in order to provide the best possible performance [9].
5. We derived the upper and lower Frame Error Ratio (FER) performance bounds of cooperative multi-user communications systems using network coding [10]. These bounds guided our network coding design as well as assist in estimating the FER performance of the systems without running extremely time-consuming Monte-Carlo simulations.
6. We proposed the detection process to be employed at the Base Station (BS) of the cooperative multi-user communications systems using network coding. Based on the algorithms employed for recovering the frames at the BS, we proposed a new method that we refer to as the Pragmatic Algebraic Linear Equation Method (PALEM), which is capable of accurately characterising the system's FER performance. The system's performance estimated by the PALEM is identical to that obtained by the Monte-Carlo simulations [3].
7. We improved the attainable diversity gain of our system by extending the idea suggested in [11] for a network coding aided system relying on an idealised channel coding scheme operating exactly at the CCMC capacity. We then formulated the performance bound of the system operating in the full-diversity mode [4].

8. We also incorporated the idea of adaptive network coding suggested in [12] into our system for the joint treatment of channel-and network-coding in order to form two adaptive modes for our system. These adaptive modes may be activated for improving the multiplexing capability of the network coding scheme used in our system. The performance bounds corresponding to the adaptive modes are also derived [4].
9. We propose an additional random network coding layer in order to allow our system to have a three-layer coding architecture, which may facilitate the further improvement of our system's performance [4].
10. We introduce a novel family of multi-user multi-layer multi-mode cooperative communication systems that is capable of simultaneously exploiting the advantages of all the modes available in our system [4].

In this chapter, we first review MDM, which is in a broad sense capable of providing more independently fading dimensions by increasing the dimensionality of the signal space. More specifically, the attainable diversity gain may be increased by making use of multiple antennas. Hence, several MDM aided schemes employing multiple antennas are compared by using the framework presented in Figure 1.1, namely Space Time Trellis Codes (STTC), Space Time Block Codes (STBC) and STBC-Sphere Packing (STBC-SP) schemes. Cooperative communications constitutes another solution conceived for enhancing the diversity gain, where single-antenna aided relays are employed for constructing virtual Multi-Input Multi-Output (MIMO) antennas. Additionally, network coding is introduced as a general method used for combining the benefits of coding and cooperative communications. After introducing the concept of MDM aided schemes, we aim for presenting multi-user cooperative systems in the subsequent chapters.

1.1 Multiple Dimension Modulation

The idea of MDM was embedded into Shannon's fundamental theorem itself, which relies on increasing the dimensionality of the signal space in order to increase the bandwidth efficiency [51]. Slepian [52] and Ottoson [53] proposed modulation schemes based on equal-energy signals that were defined as M points on a sphere in the N -dimensional Euclidean space.

The motivation for employing MDM may be readily highlighted by referring to the gain achieved with the aid of the classic two-dimensional constellation over the one-dimensional constellation. For example, a 16-Pulse-Amplitude Modulation (PAM) signal loses as much as 9.3 dB over 16-Quadrature Amplitude Modulation (QAM) at the same spectral efficiency, when comparing their capacity curves. Furthermore, each additional bit per transmitted signal costs an extra 6 dB in PAM systems, whereas the associated cost in QAM is only 3 dB. The implication of this is that upon considering infinitely large constellations, the Signal-to-Noise Ratio (SNR) loss of one-dimensional constellations with respect to two-dimensional constellations is unbounded [54].

<i>Year</i>	<i>Author</i>	<i>Milestone</i>
1948	Shannon [13]	Shannon's capacity theorem was introduced.
1950	Hamming [14]	Hamming codes were discovered.
1955	Elias [15]	Convolutional codes were introduced.
1957	Prange [16]	Cyclic codes were proclaimed.
1959	Brennan [17]	Three diversity systems, namely Selection Combining (SC), Maximal-Ratio Combining (MRC) and Equal-Gain Combining (EGC), were analysed.
1960	Reed and Solomon [18]	Reed Solomon (RS) codes were defined over certain finite Galois fields.
1966	Forney [19]	Concatenated codes were introduced.
1971	van der Meulen [20]	A simple relay channel constituted by a source, a destination and a relay was introduced.
1972	Bahl <i>et al.</i> [21]	The Maximum A-Posteriori (MAP) algorithm was invented.
1974	Bahl <i>et al.</i> [22]	The symbol based MAP algorithm was proposed.
1977	van der Meulen [23]	The model of [20] was generalised and the transmission efficiency of relays was studied.
1979	Cover and El Gamal [24]	Capacity analysis of the full duplex relay channel was presented.
1993	Berrou <i>et al.</i> [25]	Turbo codes were discovered.
1997	Tarokh <i>et al.</i> [26]	Space Time Trellis Coding (STTC) was introduced.
1996	Foschini <i>et al.</i> [27]	Diagonal BLAST was conceived for achieving a MIMO multiplexing gain.
1998	Alamoti <i>et al.</i> [28]	Space Time Block Coding (STBC) was introduced.
	Sendonaris <i>et al.</i> [29]	The relay model was generalised to the system supporting multiple nodes, which are capable of transmitting their own data as well as of serving as relays for others.
1999	Tarokh <i>et al.</i> [30–32]	Alamouti's scheme of [28] was generalised for supporting systems exploiting more than two transmit antennas.
2000	Ahlsvede <i>et al.</i> [33]	Widely acknowledged concept of network coding was formally published.
2002	Hanzo, Liew and Yeap [2]	Turbo algorithms were characterised.
2003	Laneman and Wornell [34]	Various cooperative diversity protocols were developed for exploiting spatial diversity in a cooperative scenario.

Table 1.1: Milestones related to the research road map presented in Figure 1.2 (Part 1).

<i>Year</i>	<i>Author</i>	<i>Milestone</i>
2004	Laneman <i>et al.</i> [7]	Performances of various cooperative diversity protocols, namely of Decode-and-Forward (DF), of Amplify-and-Forward (AF) and of relay selection are compared in terms of their outage behaviours.
	Janani <i>et al.</i> [35]	The diversity of coded cooperation was increased by borrowing ideas originated from STCs in conjunction with the application of turbo codes to the proposed relay aided system.
2005	Snessens <i>et al.</i> [36]	A soft DF signalling strategy capable of outperforming the conventional DF and AF was proposed.
	Hu and Li <i>et al.</i> [37]	Slepian-Wolf cooperation exploiting distributed source coding in wireless cooperative communication was advocated.
2006	Li <i>et al.</i> [38]	Soft information relaying applied in a BPSK modulated system employing turbo coding was proposed.
	Hu <i>et al.</i> [39]	Wyner-Ziv cooperation relying on the Slepian-Wolf cooperation of [37] in conjunction with a Compress-And-Forward (CAF) signalling strategy was proposed.
	Yeung and Cai [40,41]	Existence of Maximum Distance Separable (MDS) network codes was shown.
	Ho <i>et al.</i> [42]	Random Network Coding (RNC) was introduced for a non-coherent network model.
2007	Xiao <i>et al.</i> [43]	The concept of network coding was introduced in the context of cooperative communications.
2008	Wang <i>et al.</i> [44]	The complex field network coding approach capable of mitigating the throughput loss in conventional cooperative signalling schemes and of attaining full diversity gain was introduced.
2009	Hanzo <i>et al.</i> [45]	Low-complexity cooperative MIMOs and distributed turbo codes designed for two users cooperating for the sake of improving their attainable BER performance were presented.
	Ming and Skoglund [46]	A basic example of the applications of MDS network coding was introduced in multi-user relay networks.
2010	Rebelatto <i>et al.</i> [47]	Generalized Distributed Network Coding (GDNC) designed based on RS codes was introduced for cooperative communications.
2011	Rebelatto <i>et al.</i> [12,48]	Adaptive GDNC was introduced in the context of cooperative communications.
2012	Maric <i>et al.</i> [49]	Multi-hop network coding based systems relying on an AF mechanism were studied.
	Xiao <i>et al.</i> [50]	MDS network codes were investigated in scenarios in the presence or absence of the direct source-BS links and relying on orthogonal/non-orthogonal channels.

Table 1.2: Milestones related to the research road map presented in Figure 1.2 (Part 2).

Unfortunately, the same reasoning does not hold when we extend this concept from two-dimensional constellations to higher-dimensional constellations. In practice, conventional modulation schemes, like QAM and Phase-Shift Keying (PSK), use two-dimensional signals facilitated by the in-phase and quadrature components of a sinusoidal carrier. Four-dimensional signal spaces can be realised in a similar way by simultaneously exploiting two channels, which can be for example two orthogonally polarised electromagnetic waves, or time-division or frequency-division multiplexed signals transmitted over a common medium [51]. Commencing from the concept of permutation codes introduced by Slepian [52], Welton and Lees [55] designed a four-dimensional vector space, while another design implemented by Zetterberg [56] was inspired from an algebraic point of view. The problem is that for a given carrier frequency f_0 , there are only two orthogonal functions, namely $\sin(2\pi f_0 t)$ and $\cos(2\pi f_0 t)$, which can be used for modulating a base-band signal without expanding its bandwidth. Hence, only the transition from one-dimensional signalling to two-dimensional signalling allows us to double the transmitted information bit rate, provided those signalling schemes are based on the use of an in-phase quadrature-phase carrier. By contrast, a BER performance improvement was reported when evolving from two-dimensional-signalling to four-dimensional-signalling [55, 57], which was not accompanied by a throughput improvement.

Additionally, the seminal paper by Saha and Birdsall [58] suggested that the four-dimensional modulation referred to as Quadrature-Quadrature Phase-Shift Keying (Q²PSK) transmits twice as many bits per second at a given bandwidth compared to that of Quadrature Phase-Shift Keying (QPSK) without any SNR penalty. The evolution from QPSK to Q²PSK was presented in a way analogous to the transition from BPSK to QPSK. However, the appealing benefits of Q²PSK eroded after Visintin *et al.* investigated the minimum bandwidth required for each of those modulations [57]. This research clearly showed that the bandwidth efficiency of QPSK and Q²PSK are, in fact, identical, and that there is no advantage in using Q²PSK on Additive white Gaussian Noise (AWGN) channels. Visintin also suggested that in order to get a benefit from using a four-dimensional basis, a channel coded scheme should be used [57].

Following the idea of the coded multi-dimensional scheme, the joint designs between MDM and coding, namely group codes, trellis codes as well as convolutional and block codes were proposed [51, 53, 56, 59, 60]. The MDM concept was also applied to Bit-Interleaved Coded Modulation (BICM) in the context of multi-antenna channels in the form of spatial mapping (mapping across antennas) [61–65]. Later, MDM was combined with Space Time Coding (STC) and BICM in the form of coded modulation aided MIMO systems [63–66]. In such coded modulation systems, multidimensional bit-to-symbol mapping is used between the channel coded words and multidimensional constellations.

Advances in channel coding made it feasible to approach Shannon's capacity limit in systems equipped with a single antenna. However, these capacity limits can be further extended with the aid of multiple antennas. MIMO systems provide a linearly increasing capacity as a function of the transmit power, provided that the extra power is assigned to additional antennas [67]. MIMO

schemes can be briefly categorised as diversity techniques, multiplexing schemes, multiple access arrangements and beamforming techniques [45]. In what follows, we consider various MDM aided diversity techniques, namely Space Time Trellis Codes (STTC), Space Time Block Codes (STBC) and STBC-Sphere Packing (STBC-SP).

1.1.1 Space Time Trellis Code

Space Time Trellis Codes (STTCs) [31, 68–70] were proposed by Tarokh *et al.*, which incorporate jointly designed channel coding, modulation, transmit diversity and optional receiver diversity. The performance criteria for designing STTCs were listed in [68] with the assumption that the channel is fading slowly and that the fading is non-dispersive. It was illustrated in [68] that the systems performance is determined by matrices constructed from pairs of distinct code sequences. The diversity gain and coding gain of the codes are determined by the minimum rank and the minimum determinant [68], respectively. The results were then also extended to fast-fading channels [71]. The STTCs proposed in [68] strike the best trade-off among the data rate, diversity gain and trellis complexity. The effect of multiple propagation paths on the performance of STTCs were investigated in [31] for transmission over slowly varying Rayleigh fading channels. It was shown in [31] that the presence of multiple paths does not decrease the diversity order guaranteed by the design criteria used for constructing the STTCs. The results provided in [31] were then also extended to rapidly-fading dispersive and non-dispersive channels.

Having presented a rudimentary introduction to STTCs, let us now detail encoding and decoding processes with the aid of an example, namely that of the 4-state, 4-level Phase Shift Keying (4PSK) STTC using two transmit antennas, $N_t = 2$. More sophisticated STTCs were designed for 4PSK and 8PSK [68] by increasing the number S of trellis states to $S = \{8, 32\}$. In the 4-state-4PSK-STTC encoder, at any time instant k , the 4-state 4PSK-STTC encoder transmits the symbols $x_{k,1}$ and $x_{k,2}$ over the transmit antennas T_{x1} and T_{x2} , respectively. The symbols transmitted at the time instant k are given as follows [68]:

$$x_{k,1} = 0.d_{k,1} + 0.d_{k,2} + 1.d_{k-1,1} + 2.d_{k-1,2}, \quad (1.1)$$

$$x_{k,2} = 1.d_{k,1} + 2.d_{k,2} + 0.d_{k-1,1} + 0.d_{k-1,2}, \quad (1.2)$$

where $d_{k,i}$ represents the current input bits, whereas $d_{k-1,i}$ the previous input bits and $i = \{1, 2\}$ is the antenna index.

In the 4-state-4PSK-STTC decoder, at any transmission instant, having symbols x_1 and x_2 transmitted from the antennas T_{x1} and T_{x2} , we would receive:

$$y_1 = h_{1,1}x_1 + h_{1,2}x_2 + n_1, \quad (1.3)$$

$$y_2 = h_{2,1}x_1 + h_{2,2}x_2 + n_2, \quad (1.4)$$

at the receiver antennas R_{x1} and R_{x2} , where $h_{1,1}$, $h_{1,2}$, $h_{2,1}$ and $h_{2,2}$ are the corresponding complex-valued time-domain channel coefficients. With the aid of a channel estimator, the Viterbi Algorithm based maximum likelihood sequence estimator [68] first finds the branch metric associated with every transition in the decoding trellis diagram, which is identical to the state diagram. For each trellis transition, we have two estimated transmit symbols, namely \tilde{x}_1 and \tilde{x}_2 , for which the Branch Metric (BM) is given by:

$$\begin{aligned} BM &= |y_1 - h_{1,1}\tilde{x}_1 - h_{1,2}\tilde{x}_2|^2 + |y_2 - h_{2,1}\tilde{x}_1 - h_{2,2}\tilde{x}_2|^2, \\ &= \sum_{i=1}^2 |y_i - h_{i,1}\tilde{x}_1 - h_{i,2}\tilde{x}_2|^2, \\ &= \sum_{i=1}^2 \left| y_i - \sum_{j=1}^2 h_{ij}\tilde{x}_j \right|^2. \end{aligned} \quad (1.5)$$

We can generalise Equation (1.5) to N_t transmit antennas and N_r receive antennas as follows:

$$BM = \sum_{i=1}^{N_r} \left| y_i - \sum_{j=1}^{N_t} h_{ij}\tilde{x}_j \right|^2. \quad (1.6)$$

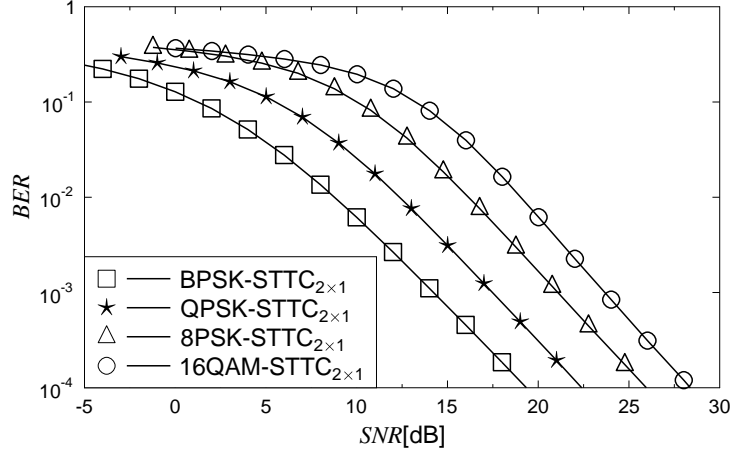
Bearing in mind the framework illustrated in Figure 1.1, let us fix the frame length (interleaving delay) to $N = 10000$ bits, in order to study BER and Frame Error Ratio (FER) performances for various system throughputs, as summarised in Table 1.3. The BER and FER performances of STTC systems having two transmit antennas and a single receive antenna are presented Figure 1.3a and Figure 1.3b. These performance curves were recorded for transmission over fast-Rayleigh fading channels with respect to various modulation schemes offering different Bit Per Symbol (BPS) throughputs, namely $BPS = \{1, 2, 3, 4\}$, as given in Table 1.3. As seen in Figure 1.3a and Figure 1.3b, an increase of 3 dB in SNR is required for attaining the same BER or FER, when the throughput increases by 1 BPS.

Modulation Scheme	Coded Modulation Schemes	Throughput (<i>BPS</i>)
BPSK	STTC2x1-BPSK	1.0
QPSK	STTC2x1-QPSK	2.0
8PSK	STTC2x1-8PSK	3.0
16QAM	STTC2x1-16QAM	4.0

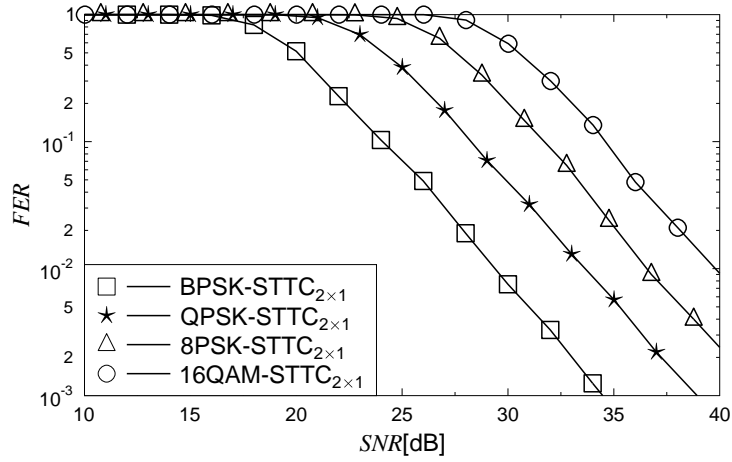
Table 1.3: Throughput of STTC2x1-MPSK systems, when different modulation schemes, namely BPSK, QPSK, 8PSK and 16QAM, are employed.

Let us take the throughput of the system into account by comparing the system performance from BER/FER-versus- E_b/N_0 perspective, where the values of E_b/N_0 and SNR have to satisfy the following relationship:

$$\frac{E_b}{N_0} \times BPS = SNR. \quad (1.7)$$



(a) BER-versus-SNR performance of the STTC2x1 scheme



(b) FER-versus-SNR performance of the STTC2x1 scheme

Figure 1.3: The BER/FER-versus-SNR performance of the STTC2x1 schemes having throughputs of $BPS = \{1, 2, 3, 4\}$, as listed in Table 1.3, provided that the frame length is fixed to $N = 10^4$ bits, when communicating over fast Rayleigh fading channels.

Equation (1.7) may be represented in the logarithmic domain as

$$\frac{E_b}{N_0}_{dB} + \log_{10}(BPS) = SNR_{dB}. \quad (1.8)$$

Accordingly, our BER/FER-versus- E_b/N_0 performance comparison is represented in Figure 1.4

Furthermore, in order to study the effect of the frame length N on the attainable performance of the system, let us investigate the STTC2x1 scheme relying on the QPSK modulation. Different values of the frame length, namely $N = [10^2, 10^3, 10^4, 10^5]$, are used for the QPSK-STTC2x1 scheme. As seen in Figure 1.5a, the BER-versus- E_b/N_0 performance curves of the QPSK-STTC2x1 scheme remain almost unchanged, when different frame lengths are applied. By contrast, the shorter the frame, the better the FER-versus- E_b/N_0 performance becomes, as seen in Figure 1.5b. It is plausible that for a fixed BER, a higher FER is associated with a longer frame. This is because although a longer frame is employed, no interleaver is invoked for exploiting the benefit of having a longer

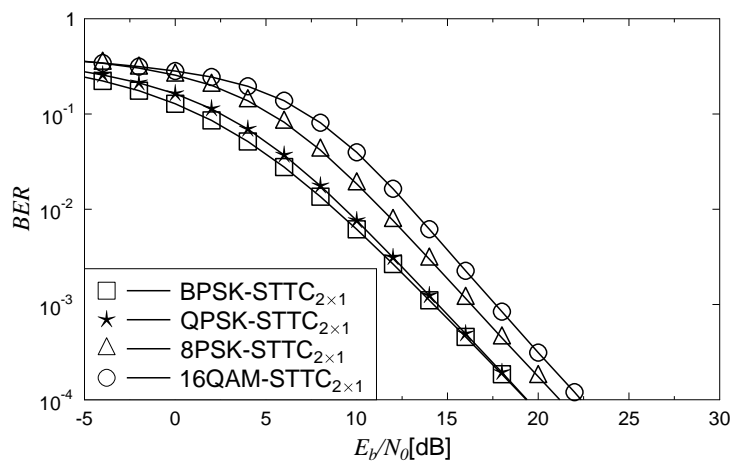
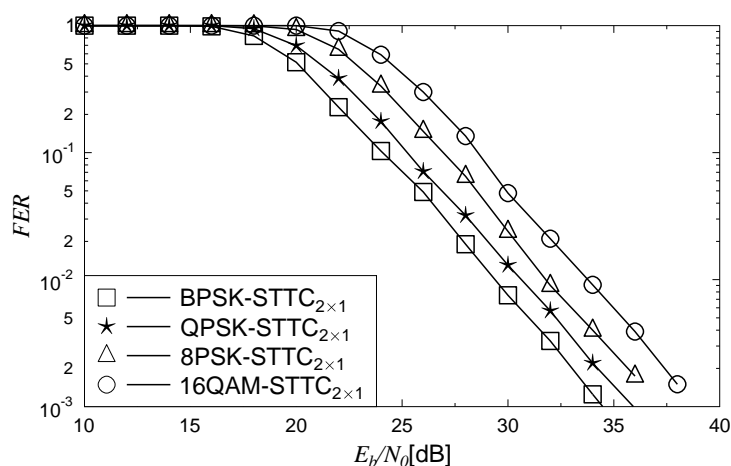
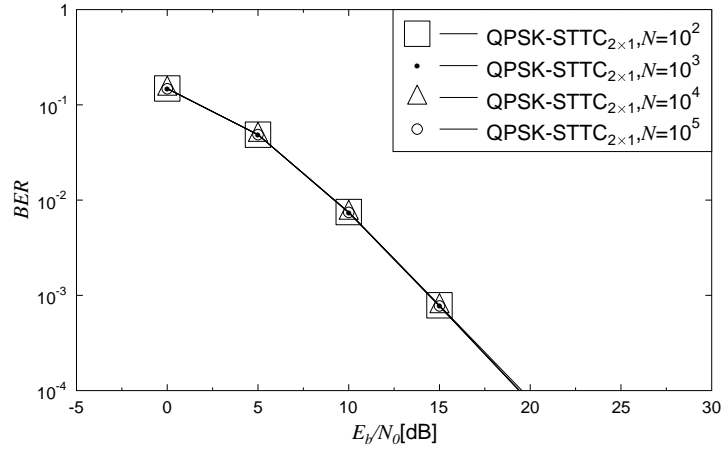
(a) BER-versus- E_b/N_0 performance of the STTC2x1 scheme(b) FER-versus- E_b/N_0 performance of the STTC2x1 scheme

Figure 1.4: The BER/FER-versus- E_b/N_0 performance of the STTC2x1 scheme across various bandwidths of $BPS = \{1, 2, 3, 4\}$ listed in Table 1.3, when communicating over fast Rayleigh fading channel, provided that the frame length is fixed to $N = 10^4$ bits.

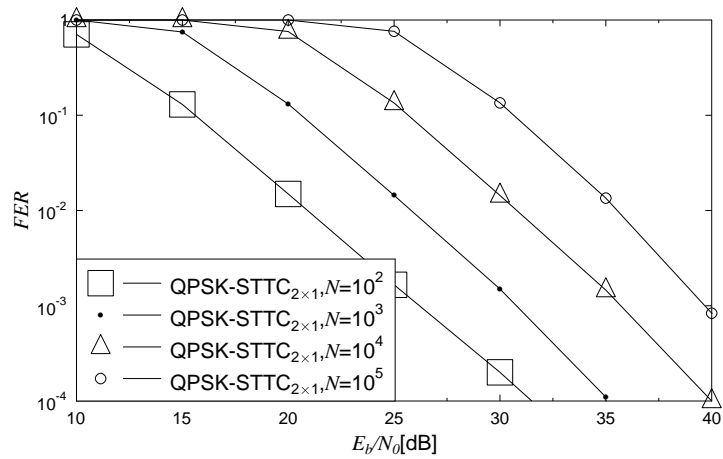
frame. This issue will be further explored in Section 2.3.2.2, where interleavers are invoked in concatenated coding schemes.

1.1.2 Space Time Block Code

The Space Time Block Coding (STBC) concept was conceived by Alamouti in [72] as a simple two-branch transmit diversity scheme. Using two transmit antennas and a single receive antenna, the scheme provides the same diversity order as Maximal-Ratio Receiver Combining (MRRC) with one transmit antenna and two receive antennas, provided that the two antennas experience independent fading. It was also shown in [72] that the scheme can be readily generalised to two transmit antennas and N_r receive antennas for providing a diversity order of $2N_r$. In order to exploit both the spatial and the temporal diversities offered by a MIMO system, an STBC transmits



(a) BER-versus- E_b/N_0 performance of the QPSK-STTC $_{2 \times 1}$ scheme



(b) FER-versus- E_b/N_0 performance of the QPSK-STTC $_{2 \times 1}$ scheme

Figure 1.5: The BER/FER-versus- E_b/N_0 performance of the QPSK-STTC $_{2 \times 1}$ scheme for the frame lengths of $N = [10^2, 10^3, 10^4, 10^5]$, when communicating over fast Rayleigh fading channels.

a signal matrix \mathbf{S} conveying the source information using both spatial and temporal dimensions. Considering a MIMO system having N_t transmit and N_r receive antennas, an STBC scheme can be designed for transmitting Q symbols using T time slots. Hence, the STBC scheme may be described by a set of parameters $(N_t N_r Q T)$ having the normalised throughput of $R = Q/T$. In other words, the concept of STBCs is based on a set of matrices \mathbf{S} satisfying both the throughput and the diversity order requirements under certain complexity constraints [73].

A STBC describes the relationship between the original transmitted signals x and the signal replicas artificially created at the transmitter for transmission over independently fading diversity channels can be defined by an $N_t \times T$ element transmission matrix [2]. The entries of the matrix are constituted by linear combinations of the input symbols and their conjugates. Hence, a general form of the transmitted matrix of an STBC scheme may be illustrated as follows:

$$\mathbf{G}_{N_t} = \begin{bmatrix} g_{11} & g_{21} & \cdots & g_{N_t 1} \\ g_{21} & g_{22} & \cdots & g_{N_t 2} \\ \vdots & \vdots & \cdots & \cdots \\ g_{T1} & g_{T1} & \cdots & g_{N_t T} \end{bmatrix}, \quad (1.9)$$

where the entries g_{ij} represent a linear combination of the symbols x_1, x_2, \dots, x_k and of their conjugates. More specifically, the entries g_{ij} represent the elements that are transmitted from antenna $i, i = 1, 2, \dots, N_t$ within time slot $j, j = 1, 2, \dots, T$.

Alamouti proposed the simplest version of STBC in [72], where the transmit matrix of the STBC was specified as follows:

$$\mathbf{G}_2 = \begin{bmatrix} x_1 & x_2 \\ x_2^* & x_1^* \end{bmatrix}. \quad (1.10)$$

As we can see from the transmit matrix \mathbf{G}_2 , at a given time instant T , two signals are simultaneously transmitted from the pair of antennas T_1 and T_2 . In the next time slot, x_2^* and x_1^* , which are the conjugates of the symbols x_1 and x_2 , are simultaneously transmitted from the antennas T_1 and T_2 . Assuming that the complex-valued fading envelope is constant across the corresponding two consecutive time slots, and independent noise samples are added at the receiver in each time slot, the received signals can be expressed with the aid of Equation (1.10) as:

$$y_1 = h_1 x_1 + h_2 x_2 + n_1, \quad (1.11)$$

$$y_2 = -h_1 x_2^* + h_2 x_1^* + n_2, \quad (1.12)$$

where y_1 and y_2 are the signals received during the two time slots. In order to extract the signals x_1 and x_2 from the received signals y_1 and y_2 , we combine the received signals as follows:

$$\begin{aligned} \tilde{x}_1 &= h_1^* y_1 + h_2 y_2^*, \\ &= h_1^* h_1 x_1 + h_1^* h_2 x_2 + h_1^* n_1 - h_2 h_1^* x_2 + h_2 h_2^* x_1^* + h_2 n_2^*, \\ &= (|h_1|^2 + |h_2|^2) x_1 + h_1^* n_1 - h_2 n_2^*. \end{aligned} \quad (1.13)$$

Similarly, for signal x_2 we have:

$$\begin{aligned}
\tilde{x}_2 &= h_2^* y_1 - h_1 y_2^* , \\
&= h_2^* h_1 x_1 + h_2^* h_2 x_2 + h_2^* n_1 + h_1 h_1^* x_2 - h_1 h_2^* x_1^* - h_1 n_2 , \\
&= (|h_1|^2 + |h_2|^2) x_2 + h_2^* n_1 - h_1 n_2^* .
\end{aligned} \tag{1.14}$$

After cancelling the unwanted signal x_2 and x_1 in Equation (1.13) and Equation (1.14), respectively, both signals \tilde{x}_1 and \tilde{x}_2 are passed to a maximum likelihood detector for determining the most likely transmitted symbols.

Modulation Scheme	Coded Modulation Schemes	Throughput (<i>BPS</i>)
BPSK	G2-STBC2x1-BPSK	1.0
QPSK	G2-STBC2x1-QPSK	2.0
8PSK	G2-STBC2x1-8PSK	3.0
16QAM	G2-STBC2x1-16QAM	4.0

Table 1.4: Throughput of G2-STBC2x1 systems, when employing different modulation schemes, namely BPSK, QPSK, 8PSK and 16QAM.

Again, upon employing the framework illustrated in Figure 1.1, let us first set the frame length (interleaving delay) to $N = 10^4$ bits, and embark on studying the BER and FER performances for various system throughput values, as listed in Table 1.4. The BER and FER performances of the G2-STBC system employing a single receive antenna are depicted in Figure 1.6a and Figure 1.6b, respectively. We employed the modulation schemes given in Table 1.4, namely BPSK, QPSK, 8PSK and 16QAM, which correspond to the system throughput values of 1BPS, 2BPS, 3BPS and 4BPS, respectively.

Similar to the manner advocated in Section 1.1.1, the throughput of the G2-STBC systems corresponding to the different modulation schemes summarised in Table 1.4 are compared by investigating both their BER-versus- E_b/N_0 and FER-versus- E_b/N_0 performances. The relationship between the values of SNR and E_b/N_0 were given by Equation (1.7) or Equation (1.8). As a result, the BER-versus- E_b/N_0 and FER-versus- E_b/N_0 performances corresponding to the different modulation schemes of Table 1.4 are plotted in Figure 1.7.

The effect of using different frame lengths is also studied for the G2-STBC2x1 scheme, where the BPSK modulation is investigated for a range of frame lengths, namely $N = [10^2, 10^3, 10^4, 10^5]$. As seen in Figure 1.8a, the BER-performance of the G2-STBC2x1-BPSK scheme remains unchanged, when different frame lengths are employed. By contrast, when a longer frame is employed, a degraded FER-performance is seen in Figure 1.8b, because no interleaver is invoked for exploiting the advantage of a long frame.

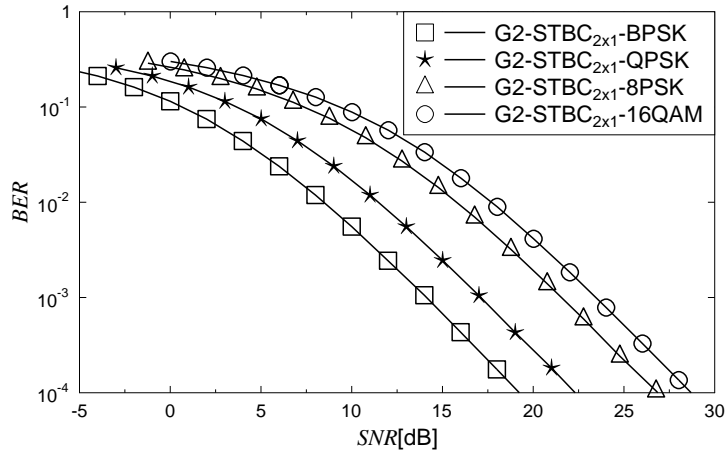
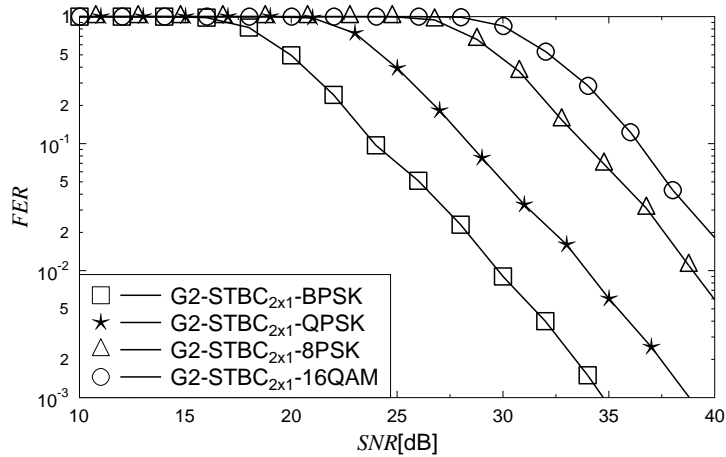
(a) BER-versus-SNR performance of the G2-STBC_{2x1} scheme(b) FER-versus-SNR performance of the G2-STBC_{2x1} scheme

Figure 1.6: The BER/FER-versus-SNR performance of the G2-STBC_{2x1} scheme for the throughput values of $BPS = \{1, 2, 3, 4\}$ given in Table 1.4, when communicating over fast Rayleigh fading channels for frame length of $N = 10^4$ bits.

1.1.3 STBC-Sphere Packing

In line with the approach suggested in [57], Sphere Packing (SP) modulation was designed jointly with STBC in [74] for two transmit antennas and for various number of receive antennas, in order to exploit the benefits of multi-dimensional modulation. In [74], the signals transmitted from two transmit antennas are chosen from L legitimate space-time signals, which are designed over the four-dimensional real-valued Euclidean space \mathbf{R}^4 . In other words, the L legitimate space-time signals transmitted are selected from the four-dimensional real-valued Euclidean space by ensuring that they have the highest possible minimum Euclidean distance from all other $(L - 1)$ legitimate signals. In Table 1.5, the value of L and its corresponding throughput and block sizes are listed. The FER and BER performances of various SP-STBC schemes having $L = \{4, 16, 64, 256\}$ and employing two transmit and one receive antennas are presented in Figure 1.9a and Figure 1.9b.

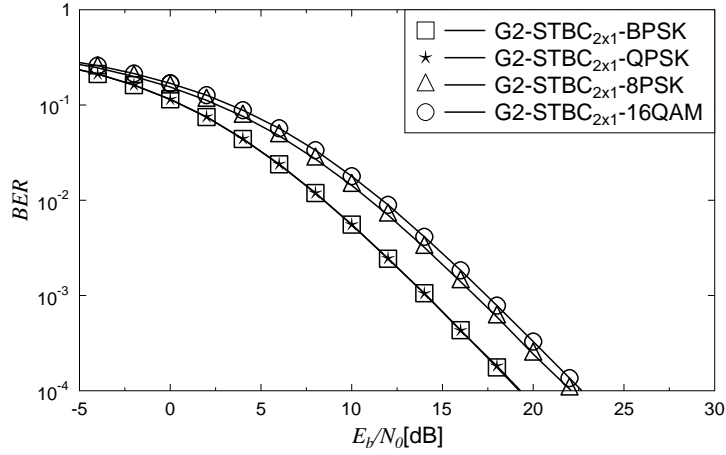
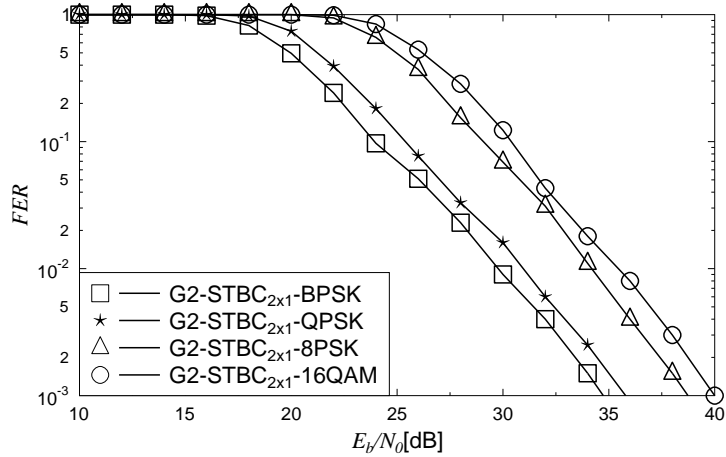
(a) BER-versus- E_b/N_0 performance of the G2-STBC2x1 scheme(b) FER-versus- E_b/N_0 performance of the G2-STBC2x1 scheme

Figure 1.7: The BER/FER-versus- E_b/N_0 performance of the G2-STBC2x1 scheme for the throughput values of $BPS = \{1, 2, 3, 4\}$ given in Table 1.4, when communicating over fast Rayleigh fading channels, while the frame length was set to $N = 10^4$ bits.

The SP-STBC-G2 scheme was also concatenated with other channel coding schemes, namely with Low-Density Parity-Check (LDPC) codes in [75] and with BICM in [76].

In harmony with our approach of conducting the comparisons in Section 1.1.1 and Section 1.1.2, the throughput of the scheme associated with different signal set sizes, as listed in Table 1.5, the relationship between the SNR and E_b/N_0 values formulated in Equation (1.7) or Equation (1.8) may be employed for taking the throughput into account in our performance comparisons. As a result, the BER/FER-versus- E_b/N_0 performance is plotted in Figure 1.10, when different signal set sizes, namely $L = 4, 16, 64, 128$ were employed for communicating over fast Rayleigh fading channels using a frame length of $N = 10^4$ bits.

Additionally, let us consider the 4-SP-STBC-G2 scheme for studying the influence of applying different frame lengths, namely $N = [10^2, 10^3, 10^4, 10^5]$ on the performance of the system.

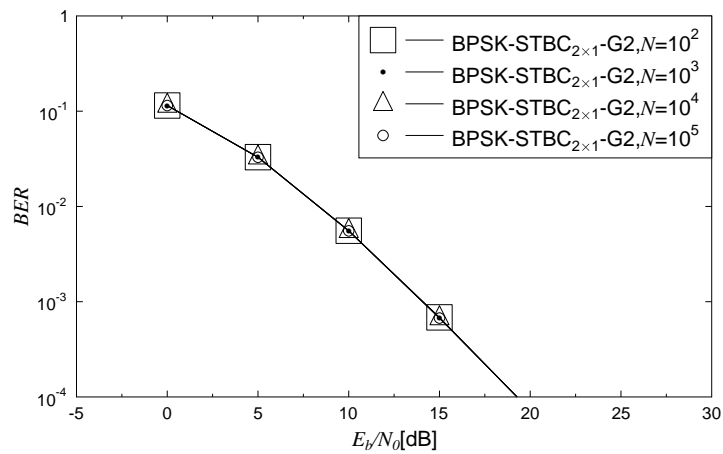
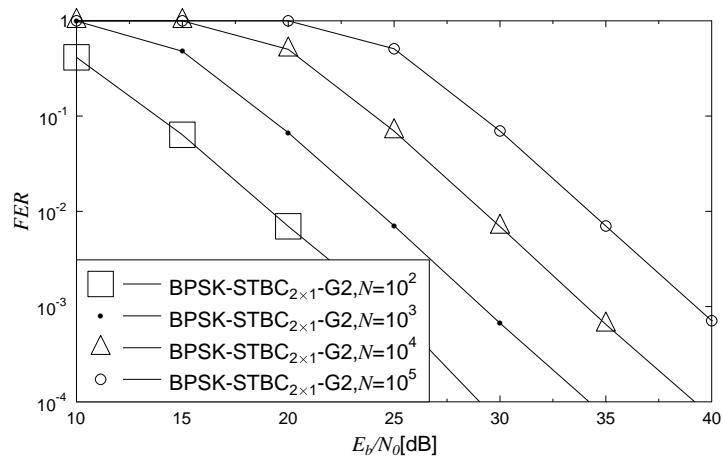
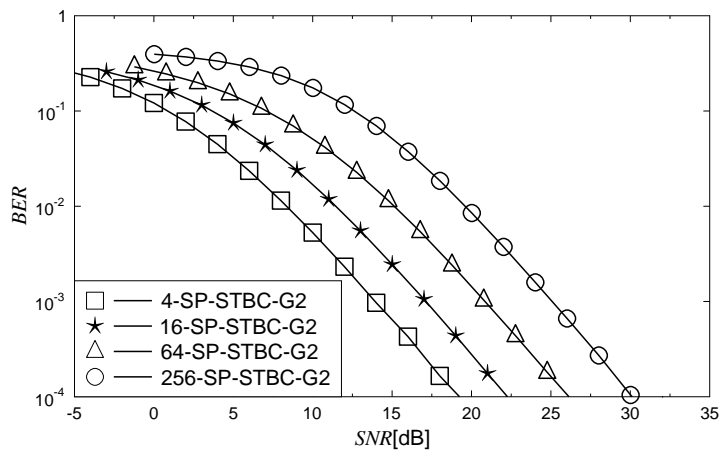
(a) BER-versus- E_b/N_0 performance comparison(b) FER-versus- E_b/N_0 performance comparison

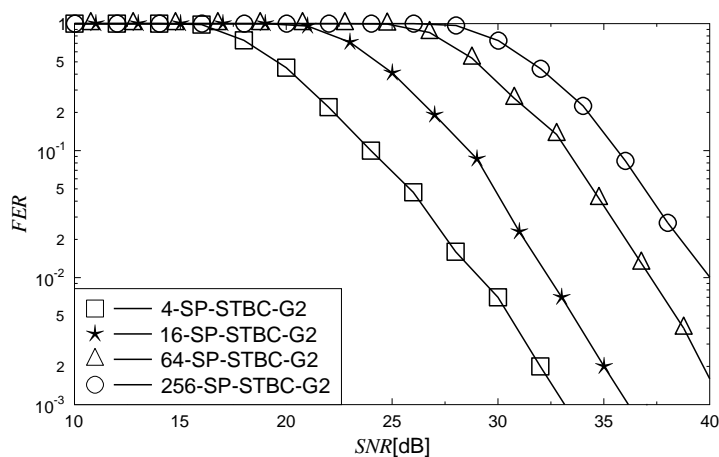
Figure 1.8: The BER/FER-versus- E_b/N_0 performance of the G2-STBC $_{2 \times 1}$ scheme compared over different frame lengths, namely $N = [10^2, 10^3, 10^4, 10^5]$, when communicating over fast Rayleigh fading channel.

L	Block size (bits)	Throughput (BPS)
4	2	1.0
8	3	1.5
16	4	2.0
32	5	2.5
64	6	3.0
128	7	3.5
256	8	4.0

Table 1.5: Throughput of SP-aided G₂ systems for different SP signal set sizes L [45].



(a) BER-versus-SNR performance comparison



(b) FER-versus-SNR performance comparison

Figure 1.9: The BER/FER-versus-SNR performance of the SP-STBC 2×1 -G2 scheme relying on different values of the SP signal set sizes mentioned in Table 1.5, when communicating over fast Rayleigh fading channels.

It can be seen in Figure 1.11a that the BER-versus- E_b/N_0 performance of the scheme remains unchanged, when the frame length is increased from $N = 10^2$ bits to $N = 10^5$ bits. However, the FER-versus- E_b/N_0 performance of the scheme seen in Figure 1.11b varies, when the frame length changes. More specifically, the longer the frame length, the worse the FER-versus- E_b/N_0 performance becomes. This again is because no interleavers are employed in the 4-SP-STBC-G2 scheme.

1.1.4 Comparison of STTC, STBC and SP-STBC

Having separately studied the transmit diversity techniques of STTC, STBC and SP-STBC, let us now compare the BER/FER performances of these techniques at each of the different throughputs of $BPS = 1, 2, 3, 4$. In order to highlight the benefits of having a coding gain, the performance

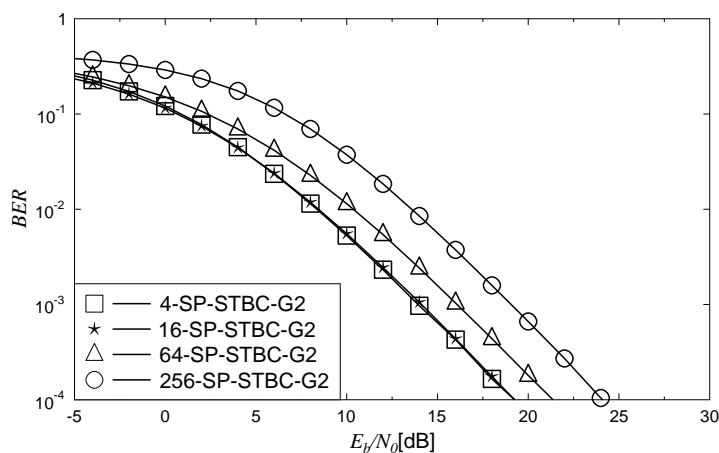
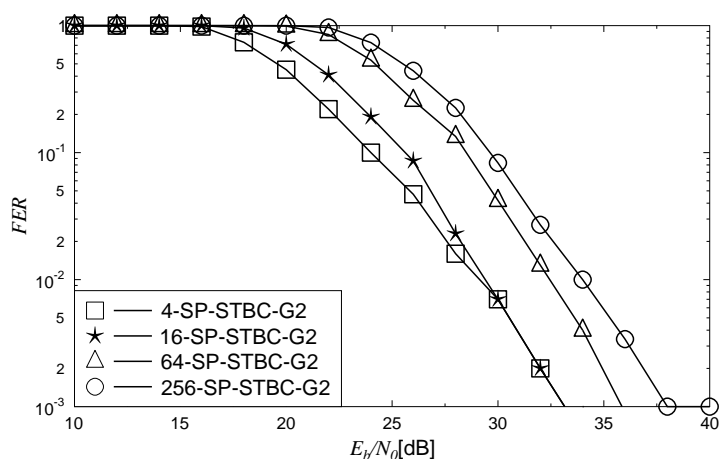
(a) BER-versus- E_b/N_0 performance comparison(b) FER-versus- E_b/N_0 performance comparison

Figure 1.10: The BER/FER-versus- E_b/N_0 performance of the SP-STBC 2×1 -G2 scheme relying on different values of the SP signal set sizes mentioned in Table 1.5, when communicating over fast Rayleigh fading channels.

of the corresponding system operating without channel coding is also considered. For example, the performance curve of the BPSK scheme is also included, when comparing the performances of the STTC 2×1 -BPSK, G2-STBC 2×1 -BPSK and 4-SP-STBC-G2 systems. As a result, Figure 1.12 presents performance curves of the above-mentioned schemes, when the frame length of $N = 10^4$ is employed, provided that the channel imposes fast Rayleigh fading. More specifically:

BPS = 1: As shown in Figure 1.12a and Figure 1.12b, in the high SNR region STBC 2×1 -BPSK provides a slightly better performance than those of STTC 2×1 -BPSK and 4-SP-STBC in terms of both BER and FER performances, while STTC 2×1 -BPSK exhibits a marginal improvement in comparison to 4-SP-STBC.

BPS = 2: The performances of SP-STBC and STBC-BPSK are virtually identical as we can see in Figure 1.12c and Figure 1.12d. The STTC-based systems are capable of providing a better

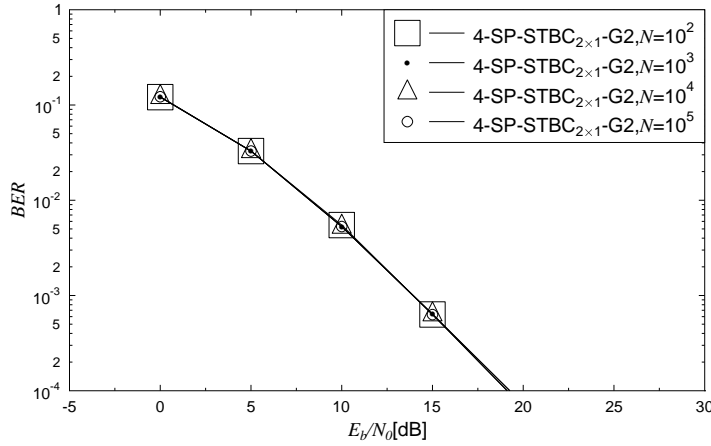
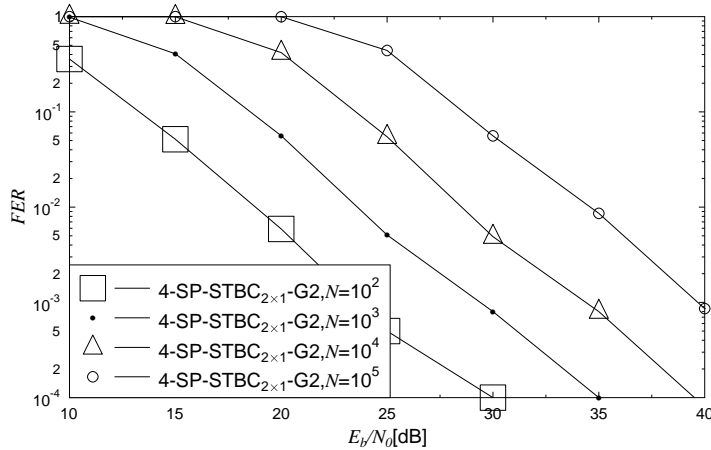
(a) BER-versus- E_b/N_0 performance comparison(b) FER-versus- E_b/N_0 performance comparison

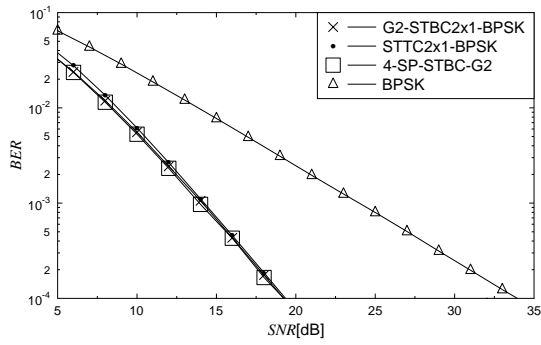
Figure 1.11: The BER/FER-versus- E_b/N_0 performance of the 4-SP-STBC $_{2 \times 1}$ -G2 scheme using different frame lengths, namely $N = [10^2, 10^3, 10^4, 10^5]$, when communicating over fast Rayleigh fading channels.

BER and FER performance than that of the other two.

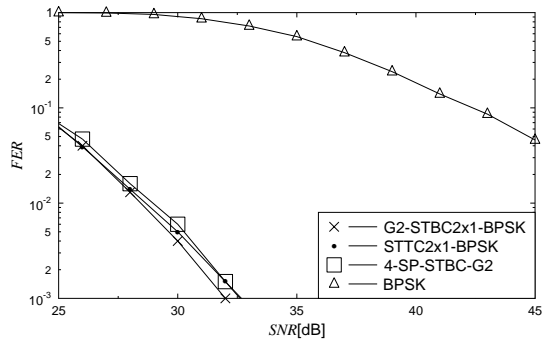
BPS = 3: It is shown in Figure 1.12e and Figure 1.12f that SP-STBC exhibits a better performance than that of STBC-8PSK. However, STTC-8PSK still has the best performance, especially in terms of its FER.

BPS = 4: As seen in Figure 1.12g and Figure 1.12h, the descending performance order of the various schemes is given by STTC, SP-STBC, STBC-QAM and 2x1-QAM, respectively.

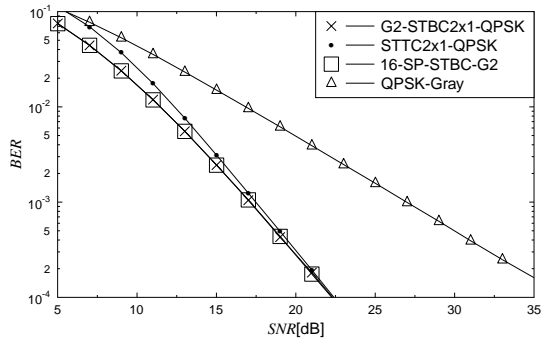
In summary, the STTC $_{2 \times 1}$ scheme exhibits a superior BER/FER performance in comparison to the other schemes, namely to G2-STBC $_{2 \times 1}$ and SP-STBC $_{2 \times 1}$ -G2, especially at sufficiently high SNRs, as seen in Figure 1.12. As a result, the STTC scheme is chosen for our cooperative system investigated in Chapter 3.



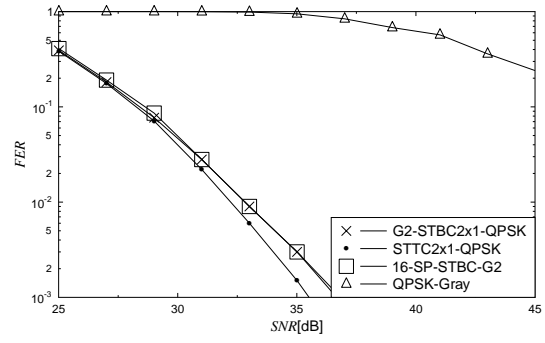
(a) BER performance, BPS = 1



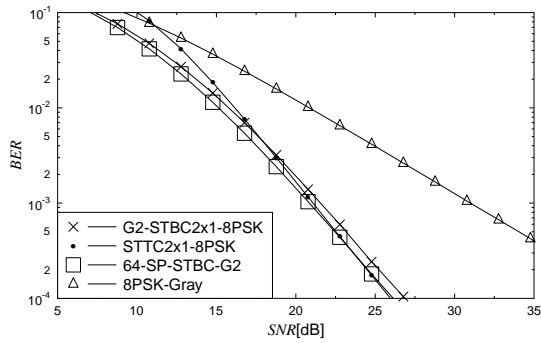
(b) FER performance, BPS = 1



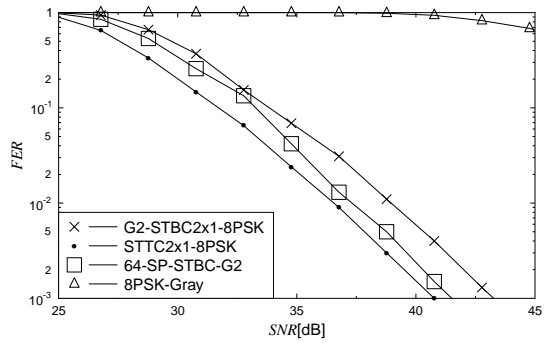
(c) BER performance, BPS = 2



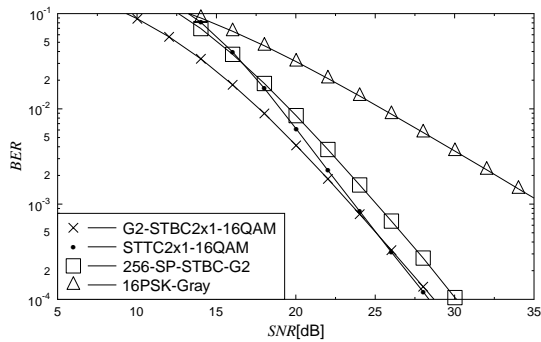
(d) FER performance, BPS = 2



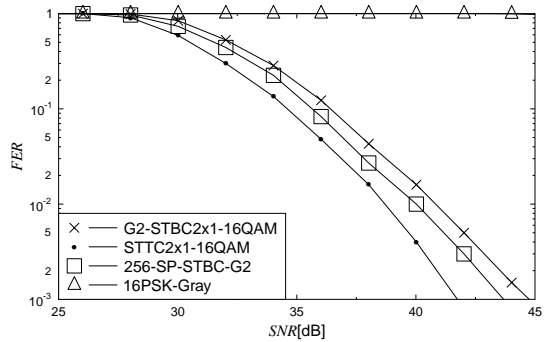
(e) BER performance, BPS = 3



(f) FER performance, BPS = 3



(g) BER performance, BPS = 4



(h) FER performance, BPS = 4

Figure 1.12: The BER/FER performance of the STTC2x1, G2-STBC2x1, SP-STBC2x1-G2 schemes, for the throughput values of BPS = 1,2,3,4, when communicating over fast Rayleigh fading channels.

1.2 Cooperative Communications and Network Coding

1.2.1 Cooperative Communications

Classically, relays have been used to extend the range of wireless communication systems [24, 77–82]. However, in recent years, numerous exciting new applications of relay aided communications have emerged [83–85]. The applications of cooperative and relay aided communications involve the Physical Layer (PHY) [86, 87], the Medium Access Control (MAC) [88], the network layer as well as their cross-layer operation [89], as seen in Figure 1.13. One of the emerging applications is based on supporting communications between the source and destination nodes with the aid of cooperative protocols. By designing sophisticated medium access between the source and relay nodes [88, 90], in conjunction with appropriate modulation and coding [91, 92], it has been found that the diversity gain of the system can be substantially improved [93]. Moreover, in multi-user systems, different users can also act as cooperating partners or relays in order to share resources and assist each other in their information transmission [94]. Another emerging application is the exchange of information between multiple users through relay(s). In some cases, the total throughput of these systems can be drastically increased by exploiting the knowledge of one's own transmitted signal [83].

Based on cross-layer operation techniques relying on the PHY, MAC and network layers, cooperative networks have recently received significant research attention [95, 96]. As seen in Figure 1.13, cooperative networking may be classified into the following categories:

- Coding [97–104] in the PHY layer
- Power allocation [105–110] in the PHY layer
- Cooperative transmission [111–113] in the PHY layer
- Relay-selection-and-routing in the network layer [114, 115]
- Service-quality improvement [116–118] in cooperative networks
- Channel access [119–121] in cooperative networks.
- Routing [122–124] in cooperative networks.
- Scheduling [125, 126] in cooperative networks.
- Topology control [127, 128] in cooperative networks.
- Resource management [129, 130] in cooperative networks
- Cross-layer design [97] in cooperative networks

Section 1.2.2 is dedicated to reviewing the literature of network coding.

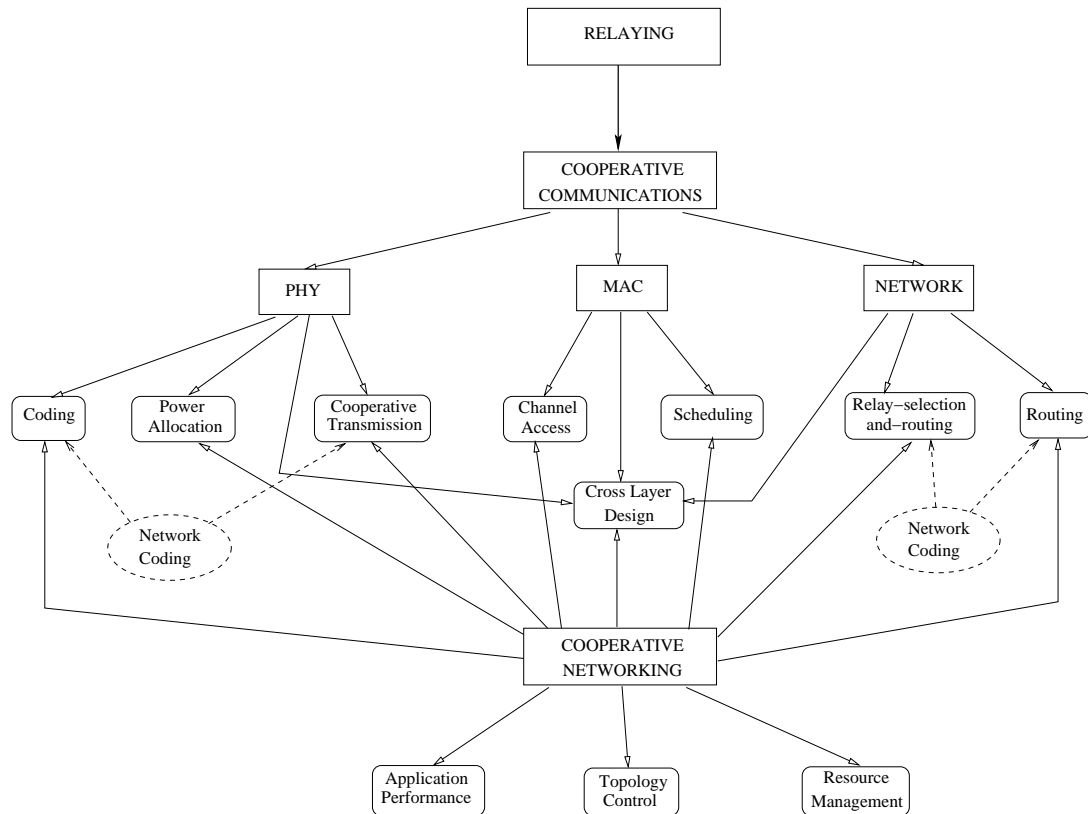


Figure 1.13: Cooperative Networking

1.2.2 Network Coding

Network coding is capable of increasing the throughput, while minimising the amount of energy required per packet as well as the delay of packets travelling through the network [131, 132]. This is achieved by allowing intermediate nodes in a communication network to combine multiple data packets received via the incoming links before transmission to the destination [133]. According to [134], the connections between the network coding and other disciplines can be illustrated in Figure 1.14.

Although, the theory of network coding has been well documented for a single communication session, the field of concurrent communication sessions still constitutes an open theoretical challenge [135]. Moreover, transmission errors may appear in a communication network that employs network coding. These may be random errors, erasures due to lost packets, or more seriously, errors caused by intentional attacks inflicted by malicious nodes in the network. As discussed briefly in [136], the employment of classic error correction coding leads to network error correction coding. Additionally, as explored in [137], it is paramount importance to determine the fundamental limit of confidential communication in networks in the presence of malicious eavesdroppers.

Network codes may be classified based on different perspectives. For example on the basis of how the information streams are processed at the relays [134], or depending on the construction

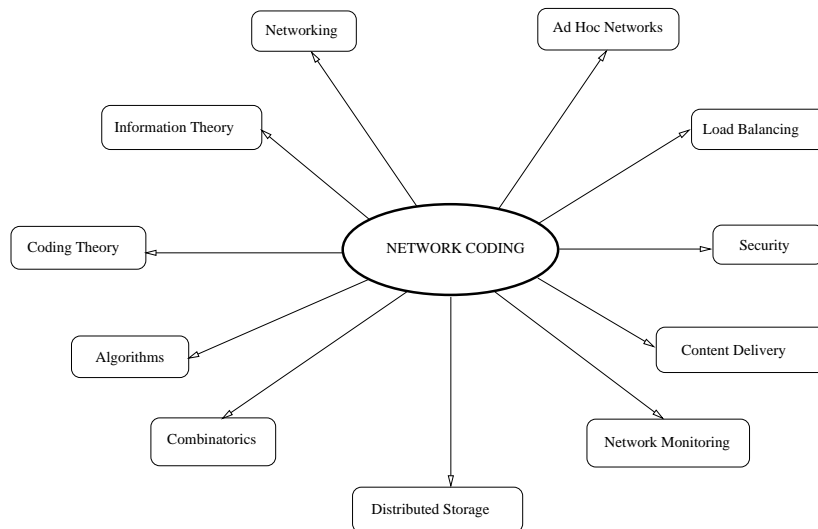


Figure 1.14: Network Coding: Connections with other disciplines [134].

of network codes [136], depending on the specific the architecture of networks employing network coding [138], the layer in networks where the network coding operates [139], just to name a few. As seen in Figure 1.15, let us classify network codes into three main categories, namely the Linear Network Codes (LNC), Non-linear Network Codes (NLNC) and the family of so-called Hybrid Network Codes (HNC)¹.

It should be noted that the capacity of single-source multicast communications in a network can be approached by solely using LNC [140], which has many attractive properties. From a theoretical standpoint, linearity is a beneficial algebraic property supported by exact mathematical foundations. From an engineering standpoint, the simplicity of linear approaches leads to relatively low complexity in the encoding and decoding processes, which makes LNC attractive [141]. Hence, our research interests are focused on LNC. It is worth noting that the specific categories of the LNC characterised in Figure 1.15 are not strictly unrelated to one another.

1.2.2.1 Linear Network Codes

Let us focus our attention on the LNC branch of the network coding taxonomy presented in Figure 1.15, where we pay particularly attention to Maximum Distance Separable (MDS) network codes and to Random Network Codes (RNC). For the details on Generic Network Codes (GNC), Static Network Codes (SNC) and Convolutional Network Codes (CNC), the interested reader might like to refer to [142]. For the details on Product Codes (PC) seen in Figure 1.15, please refer to [136], whereas the specifics of Secure Network Codes (SNC) mentioned in Figure 1.15 can be found in [143–145]. Below, we summarise the important milestones in the evolution of MDS

¹We use the term ‘hybrid network codes’ for the network codes that do not entirely belong to either the linear network coding or non-linear network coding classes

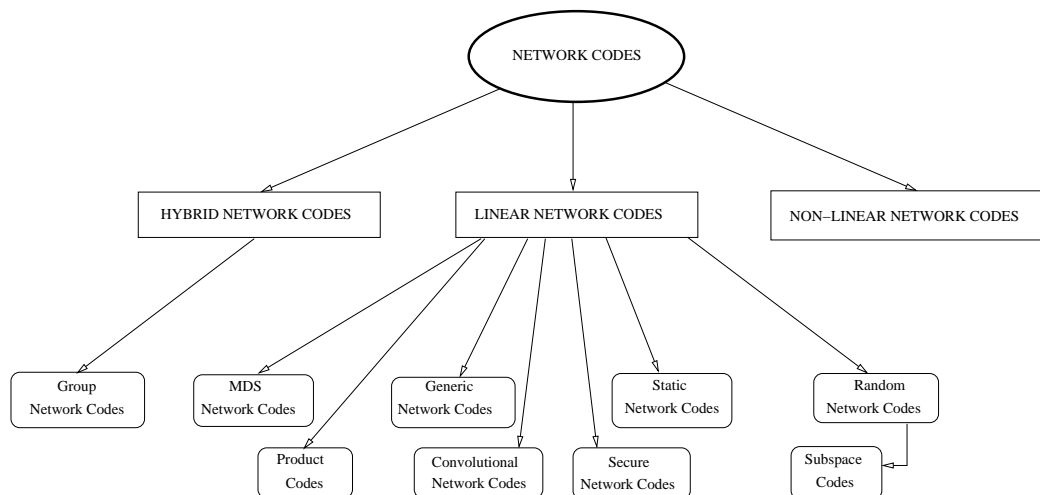


Figure 1.15: A rough classification of network codes (2000-2013)

network codes and RNCs in Table 1.6.

As seen in Table 1.6, the concept of network coding was introduced by Ahlswede *et al.* in 1998 [146], which was formally published in 2000 [33].

In 2006, the network coding concept was conceived as a generalisation of classic error correction codes in [40, 41], which also extended bounds employed in classic coding theory, namely the Singleton bound, Hamming bound and Gilbert-Vashamov bound, to the network coding field. Based on the Singleton bound, the existence of Maximum Distance Separable (MDS) network codes was proved.

In 2006, RNCs were proposed in [42]. The main benefits of RNC are their decentralised operation and robustness to network changes or link failures, which are considered in the scenario of the non-coherent network model. It was noted that research in network coding theory considered two different network models, namely coherent and non-coherent networks. In the coherent network, the transmitter and receivers are aware of the network characteristics, while in the non-coherent networks the opposite is true. Naturally, the non-coherent network model is more suitable for most practical applications [136].

In 2007, SC was introduced in [147] as a branch of RNC, which was described in more detail in 2008 [148] as a network code capable of correcting various combinations of errors and erasures.

In 2008, the author of [149] proved that the concept of minimum distance plays exactly the same role as it does in classic coding theory in terms of characterising the capability of correcting/detecting errors. This proof simplifies the design of network codes. Hence, the structure of the MDS code family established in classic coding theory may also be applied to network coding.

Relying on the initial work in [46] published in 2009, the application of the MDS network coding in multi-user relay networks was fully characterised in 2011 [150].

<i>Year</i>	<i>Author</i>	<i>Milestone</i>
1998	Ahlsvede <i>et al.</i> [146]	Seminal work on the network coding field introducing the concept of processing information frames at intermediate nodes rather than simply forwarding them.
2000	Ahlsvede <i>et al.</i> [33]	Widely acknowledged concept of the network coding was formally published.
2006	Yeung and Cai [40, 41]	Existence of Maximum Distance Separable (MDS) network codes was proved for paving the way applying classic code theory to network coding.
	Ho <i>et al.</i> [42]	Random Network Coding (RNC) was introduced for non-coherent network model, which is more suitable for most practical applications.
2007	Koetter <i>et al.</i> [147, 148]	Subspace Codes (SC) was proposed as a branch of RNC family, which is capable of correcting various combinations of errors and erasures.
	Xiao <i>et al.</i> [43]	The concept of network coding was introduced in the context of relay aided communications.
2008	Zhang [149]	Concept of minimum distance in LNC was proved to be the same as that in classic coding theory, when characterising the capability in correcting/detecting errors.
2009	Ming and Skoglund [46]	A basic example on the applications of MDS network coding in multi-user relay networks was introduced.
2010	Rebelatto <i>et al.</i> [47]	Generalized Distributed Network Coding (GDNC) was introduced, which is generalised from the basic model of [46] by allowing each user to transmit multiple frames during broadcast and cooperative phases according to a transfer matrix constructed from generating matrices of RS codes.
2011	Chao <i>et al.</i> [150]	Applications of MDS network coding in multi-user relay networks was fully introduced along with analyses on Diversity Multiplexing Trade-off (DMT).
	Rebelatto <i>et al.</i> [12, 48]	Adaptive GDNC was introduced by allowing each user in the GDNC system to transmit fewer parity frames based on the feedback from transmission during the broadcast phases
2012	Rebelatto <i>et al.</i> [99]	GDNC systems was formally introduced.
	Maric <i>et al.</i> [49]	Multi-hop network coding based systems relying on an AF mechanism were studied.
	Xiao <i>et al.</i> [50]	MDS network codes were investigated in scenarios in the presence or absence of the direct source-BS links and relying on orthogonal/non-orthogonal channels.

Table 1.6: Milestones in network coding (2000-2012) with regard to the development and applications of the Maximum Distance Separable (MDS) based network coding.

In 2011-2012, relying on the initial results of [47] disseminated in 2010, the authors of [12, 99] formally introduced Generalized Distributed Network Coding (GDNC) relying on employing the construction of Reed Solomon (RS) codes, which belong to the family of MDS codes.

This is the point where we commence our network coding related work, where our approach is in line with a recent observation² presented in [140]. More specifically, we further develop the concept of GDNC systems and incorporate near-capacity channel coding schemes into the GDNC systems, in order to conceive a family of multi-user, multi-layer, multi-mode cooperative systems.

1.3 Organisation of the Thesis

The structure of the thesis is portrayed in Figure 1.16. More specifically, various MDM schemes, namely STTCs, STBCs and Sphere Packing Modulation were introduced earlier in this chapter, which were compared. These discussion were then followed other preliminaries related to the context of cooperative multiuser systems. The capacity and outage probabilities of the Continuous-input Continuous-output Memoryless Channel (CCMC), Discrete-input Continuous-output Memoryless Channel (DCMC) and the Differential Discrete-input Continuous-output Memoryless Channel (D-DCMC) were presented in Chapter 2. Based on the findings in Chapter 1 and Chapter 2, distributed coded modulation schemes were designed for cooperative communications in Chapter 3. In Chapter 4, network coding was employed for devising cooperative multi-user communication systems. Chapter 5 was dedicated to the generalisation of the multi-user network coding aided system in Chapter 4, in order to conceive multi-user, multi-layer, multi-mode cooperative systems. Finally, in Chapter 6, our conclusions and future work ideas were presented.

²It is observed by the authors of [140] that in the area of network coding research, the gradual shift from more theoretical investigations to more practical concerns has demonstrated that network coding research has reached a level of maturity. As a result, more recent research in network coding is more focused on its practical challenges, implications and implementations [140].

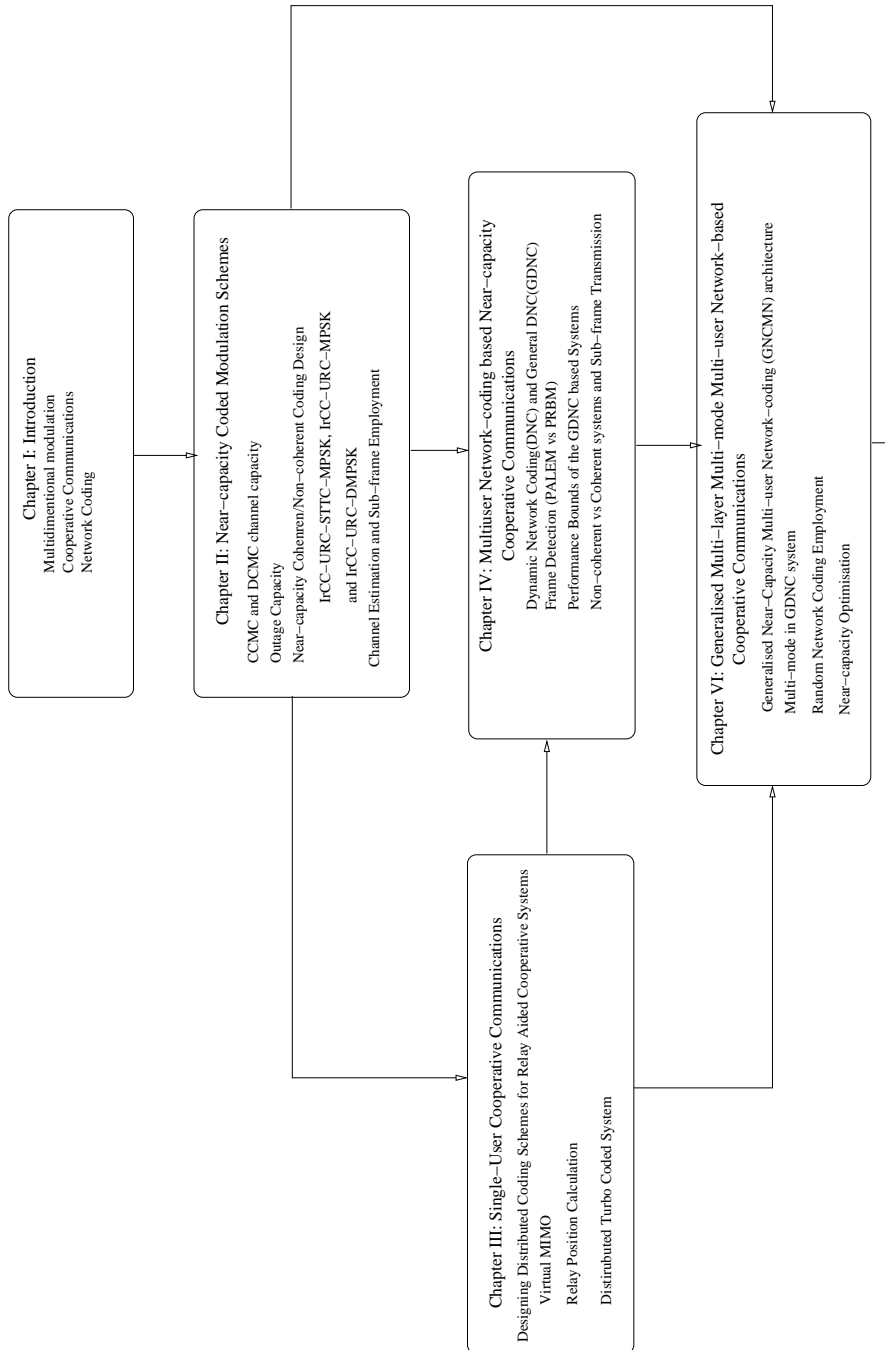


Figure 1.16: The organisation of the thesis.

Near-capacity Coded Modulation Schemes

This chapter aims for conceiving and characterising near-capacity coding schemes. The chapter commences by providing insights concerning the channel capacity of a single transmission link, including the Continuous-input Continuous-output Memoryless Channel (CCMC), Discrete-input Continuous-output Memoryless Channel (DCMC) as well as the Differential Discrete-input Continuous-output Memoryless Channel (D-DCMC). Then, in Section 2.3 we continue by detailing the design procedure of our near-capacity coding schemes with the aid of Extrinsic Information Transfer (EXIT) charts. The effects of channel estimation errors are also presented by comparing our coherent and non-coherent schemes.

2.1 Outage probability of a single link

We consider a single transmission link associated with the transmitted and received signals of x and y , respectively. The received signal can be represented as

$$y = hx + n, \quad (2.1)$$

where $h = h_s h_f$ is the complex-valued fading coefficient that comprises two components, namely a block fading coefficient (slow fading, large-scale shadow fading or quasi-static fading) h_s , which is constant for all symbols within a frame and a fast fading (small-scale fading) coefficient h_f , which fluctuates on a symbol-by-symbol basis. Finally, n is the AWGN process having a variance of $N_0/2$ per dimension.

We refer to C as the maximum achievable transmission rate of reliable communication supported by the channel characterised by (2.1). Let us assume that the transmitter encodes data at a rate of R bits/s/Hz. If the channel realisation h has a capacity of $C|_h < R$, which is lower than

required, the system is declared to be in outage, where the outage probability is given by:

$$P_e(R) = Pr \{C|h < R\} , \quad (2.2)$$

with $C|h$ being the capacity, i.e. the maximum achievable rate of the channel, when h is known.

2.1.1 Continuous-Input Continuous-Output Memoryless Channel

Assuming that x is independent and identically distributed (i.i.d.), the transmission link obeys the CCMC model. The outage probability for the interleaved channel associated with a transmission frame length of N symbols is given by [151, 152]

$$P_e^{CCMC}(R) = Pr \left\{ \frac{1}{N} \sum_{n=1}^N \log_2 (1 + |h_n|^2 SNR) < R \right\} , \quad (2.3)$$

where SNR is the signal to noise power ratio and h_n is the channel coefficient associated with the n^{th} symbol. For an infinite-length transmission frame having symbol indices spanning from $N \rightarrow \infty$, for almost all realisations of the random channel gains [151], we have

$$P_e^{CCMC}(R) = Pr \{E [\log_2 (1 + |h|^2 SNR)] < R\} , \quad (2.4)$$

where h represents a channel coefficient pertaining to a symbol in a transmitted frame. Jensen's inequality [153] suggests that if $f(u)$ is a strictly concave function of an arbitrary random variable u , then we have $E[f(u)] \leq f(E[u])$, with equality if and only if u is deterministic. Under these conditions $P_e^{CCMC}(R)$ becomes

$$\begin{aligned} P_e^{CCMC}(R) &= Pr \{ \log_2 (1 + E [|h|^2] SNR) < R \} , \\ &= Pr \left\{ E [|h|^2] < \frac{2^R - 1}{SNR} \right\} . \end{aligned} \quad (2.5)$$

Assuming that the block fading coefficient h_s is a constant for all N symbols within a transmitted frame, we have

$$P_e^{CCMC}(R) = Pr \left\{ |h_s|^2 E [|h_f|^2] < \frac{2^R - 1}{SNR} \right\} . \quad (2.6)$$

From Equation (2.6), we can directly infer that the outage probability corresponding to the case in which signals experience small-scale fading becomes

$$P_e^{CCMC,f}(R) = Pr \left\{ E [|h_f|^2] < \frac{2^R - 1}{SNR} \right\} . \quad (2.7)$$

By contrast, if the signals do suffer from block fading, but no small-scale fading, it becomes

$$P_e^{CCMC,s}(R) = Pr \left\{ |h_s|^2 < \frac{2^R - 1}{SNR} \right\} . \quad (2.8)$$

Based on Equation (2.8), in Figure 2.1 we have visualised the FER vs SNR performance corresponding to different values of the throughput R , when transmitting over block Rayleigh fading channels. To elaborate a little further, in this case, $P_e^{CCMC,large}(R)$ of Equation (2.8) is equivalent to the Frame Error Ratio (FER) of the corresponding transmission link, where we assumed that the block fading channel coefficient h_s remains constant for a transmission frame.

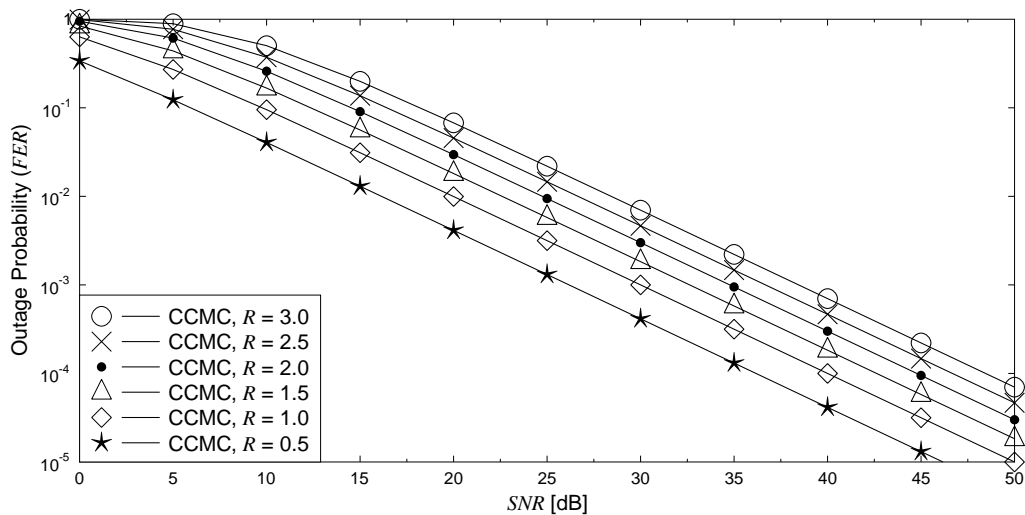


Figure 2.1: Outage probability (FER) of the CCMC channel calculated by Equation (2.8), when the transmission link corresponding to different values of throughput R experiences the block Rayleigh fading represented by h_s of Equation (2.8).

2.1.2 Non-coherent detection

Without accurate channel estimation, Conventional Differential Detection (CDD) generally exhibits a 3 dB performance degradation in comparison to the performance of the coherent detection relying on the idealised perfect channel knowledge, provided that the Doppler frequency is not excessive. Moreover, there exists an irreducible error floor due to the employment of CDD when fading channels are fluctuating rapidly. In order to alleviate this problem, Multiple-Symbol Differential Detection (MSDD) [154], which makes a joint decision on the source information by observing multiple consecutive received symbols/blocks, reduces the performance discrepancy between CDD and the coherent detection. To reduce the exponentially increasing complexity of MSDD regarding to the increased detection window length, Multiple-Symbol Differential Sphere Detection (MSDSD) is a favoured choice in order to reach the Maximum Likelihood (ML) performance with a reduced detection complexity.

2.1.2.1 Multiple-Symbol Differential M-ary Phase-Shift Keying

In cooperative communication systems, as the number of sources and relays increases, it becomes unrealistic to obtain accurate Channel State Information (CSI) for the increasing number of mobile-to-mobile channels. Inaccurate CSI may erode the performance of the near capacity coherent modulation schemes designed with the aid of EXIT charts relying on the assumption of perfect CSI estimation. Hence Differential M-ary Phase Shift Keying (DMPSK) can be chosen for the sake of eliminating the excessive complexity of channel estimation in distributed networks.

Furthermore, MSDD [154] may be employed in order to mitigate the performance loss of the non-coherent receivers. Since the differential encoder is 'recursive' – i.e. has an infinite impulse response – similar to Recursive Systematic Convolutional (RSC) codes, the (1,1) point of the EXIT chart can be approached by MSDD having a detection window length as long as the decoding frame length. However, the MSDD window length is severely limited, because its extension imposes an exponentially increasing detection complexity. As a remedy, MSDSD [155] was proposed for reducing the complexity, but the employment of a frame-sized detection window length still remains impractical. Furthermore, having a slightly degraded performance is unavoidable, since MSDSD constitutes the Max-Log-MAP – rather than MAP – algorithm of MSDD.

For DMPSK schemes, differential encoding is carried out according to:

$$s_n = \begin{cases} s_1 & n = 1 \\ x_{n-1}s_{n-1} & n > 1 \end{cases}, \quad (2.9)$$

where x_n carries the source information. For a single transmission link, the signal received over a Rayleigh fading channel may be expressed as:

$$y_n = s_n h_n + n_n, \quad (2.10)$$

where the AWGN n_n has a zero mean and a variance of N_0 , while h_n denotes the fading coefficient having a temporal correlation of $\varepsilon\{h_n h_{n+k}^*\} = J_0(2\pi k f_d)$ according to Clarke's fading model [154], where J_0 denotes the zero-order Bessel function of the first kind and f_d is the normalized Doppler frequency.

In order to observe the received signal across an MSDD decision window of N_w consecutive symbols, (2.10) may be further developed as:

$$\mathbf{y} = \mathbf{s}\mathbf{h} + \mathbf{n}, \quad (2.11)$$

where the $(N_w \times 1)$ -element matrix $\mathbf{y} = [y_{n-N_w+1}, \dots, y_n]^T$ models the received symbols within the MSDD window, while the equivalent fading channel matrix $\mathbf{h} = [h_{n-N_w+1}, \dots, h_n]^T$ and the equivalent AWGN matrix $\mathbf{n} = [n_{n-N_w+1}, \dots, n_n]^T$ are both of size $(N_w \times 1)$. The $(N_w \times N_w)$ -element equivalent transmission matrix \mathbf{s} of (2.11) is modelled as $\mathbf{s} = \text{diag}\{[s_{n-N_w+1}, \dots, s_n]\}^T$.

The MSDD aims for minimizing the a posteriori probability of [154]:

$$\Pr(\mathbf{y} | \mathbf{s}) = \frac{\exp\left[-\text{tr}\left\{\mathbf{y}^H (\mathbf{R}_{\mathbf{y}\mathbf{y}})^{-1} \mathbf{y}\right\}\right]}{\pi^{N_w} \det(\mathbf{R}_{\mathbf{y}\mathbf{y}})}, \quad (2.12)$$

where the correlation matrix $\mathbf{R}_{\mathbf{y}\mathbf{y}}$, whose determinant is a real-valued constant, is given by:

$$\mathbf{R}_{\mathbf{y}\mathbf{y}} = \mathbf{s}\mathbf{R}_{\mathbf{h}\mathbf{h}}\mathbf{s}^H + \mathbf{R}_{\mathbf{n}\mathbf{n}} = \mathbf{s}\mathbf{C}\mathbf{s}^H, \quad (2.13)$$

where the correlation of the fading channel is given by $\mathbf{R}_{\mathbf{h}\mathbf{h}} = \text{Toeplitz}\{\rho_0, \dots, \rho_{N_w-1}\}^1$. with $\rho_k = NJ_0(2\pi k f_d)$, while the correlation matrix of the AWGN is given by $\mathbf{R}_{\mathbf{n}\mathbf{n}} = N_0 \cdot \mathbf{I}_{N_w}$. The

¹This notation simply indicates that R_{hh} is a Toeplitz-structured matrix constituted by the elements $\{\rho_0, \dots, \rho_{N_w-1}\}$

channel correlation matrix in (2.13) is defined as $\mathbf{C} = \mathbf{R}_{hh} + \mathbf{R}_{nn}$. Therefore, the trace operation in (2.12) may be further formulated as:

$$\text{tr} \left\{ \mathbf{y}^H (\mathbf{R}_{yy})^{-1} \mathbf{y} \right\} = \text{tr} \left\{ \mathbf{y}^H \mathbf{s} \mathbf{C}^{-1} \mathbf{s}^H \mathbf{y} \right\} = \left\| \mathbf{L}^H \mathbf{s}^H \mathbf{y} \right\|^2, \quad (2.14)$$

where the lower triangle matrix \mathbf{L} is generated by the decomposition of $\mathbf{C}^{-1} = \mathbf{L}\mathbf{L}^H$. Based on the a posteriori probability of (2.12), the Log-MAP algorithm conceived for Multiple-Symbol Differential Detection aided Differential M-ary Phase-Shift Keying (MSDD-aided-DMPSK) may be formulated as:

$$L_e(b_k | \mathbf{y}) = \ln \left(\frac{\sum_{\mathbf{s} \in \mathbf{s}_1^k} \exp \left[\left\| \mathbf{L}^H \mathbf{s}^H \mathbf{y} \right\|^2 + \sum_{j=1, j \neq k}^{N_w(\log_2 M)} b_j L_a(b_j) \right]}{\sum_{\mathbf{s} \in \mathbf{s}_0^k} \exp \left[\left\| \mathbf{L}^H \mathbf{s}^H \mathbf{y} \right\|^2 + \sum_{i=1, i \neq k}^{N_w(\log_2 M)} b_i L_a(b_i) \right]} \right), \quad (2.15)$$

where $L_e(b_k | \mathbf{y})$ denotes the extrinsic LLR provided for the bit b_k , while \mathbf{s}_0^k and \mathbf{s}_1^k refer to the constellation set corresponding to the equivalent transmission matrix \mathbf{s} when b_k is set to 0 and 1, respectively.

2.1.3 Discrete-Input Continuous-Output Memoryless Channel

By employing the classic Monte Carlo simulation method for averaging the expectation terms, the DCMC capacity of the transmission link may be calculated by [156]:

$$C_{(\eta)}^{DCMC} = \eta - \frac{1}{L} \sum_{l=1}^L E \left[\log_2 \sum_{z=1}^L \exp(\psi_{l,z}) \Big|_{X_l} \right], \quad (2.16)$$

where $L = 2^\eta$ is the number of modulation levels, while η is the number of modulated bits and $E[A|X_l]$ is the expectation of A conditioned on the L -ary signals X_l . Note that $\psi_{l,z}$ is a function of both the transmitted signal and of the channel as defined in [156]. For the system relying on a single transmit and a single receiver antenna, we have

$$\psi_{l,z} = \frac{-|h(x_l - x_z) + n|^2 + |n|^2}{N_0}, \quad (2.17)$$

where h , x and n are the complex-valued fading coefficient, the transmitted signal and the AWGN, respectively.

We define the receiver's faded signal to noise power ratio as $SNR_r = E[|h|^2 SNR]$. At a given throughput R , we readily identify the corresponding signal to noise power ratio $SNR_r|_R$ that is defined as the SNR value associated with the capacity $C_{(\eta)}^{DCMC} = R$ on the $C_{(\eta)}^{DCMC}$ -versus- SNR capacity curve represented by Equation (2.16) and plotted in Figure 2.2, where a throughput of R may be maintained. The specific values of $SNR_r|_R$ corresponding to different throughputs R are listed in Table 2.1. Then, similar to Equation (2.5) and Equation (2.6), the outage probability of the interleaved DCMC model is equivalent to the probability of the event that we have $|h|^2 SNR <$

$SNR_r|_R$, which is expressed as

$$\begin{aligned}
 P_e^{DCMC}(R, \eta) &= Pr \{E[|h|^2 SNR] < SNR_r|_R\}, \\
 &= Pr \left\{ E[|h|^2] < \frac{SNR_r|_R}{SNR} \right\}, \\
 &= Pr \left\{ |h_s|^2 E[|h_f|^2] < \frac{SNR_r|_R}{SNR} \right\}.
 \end{aligned} \tag{2.18}$$

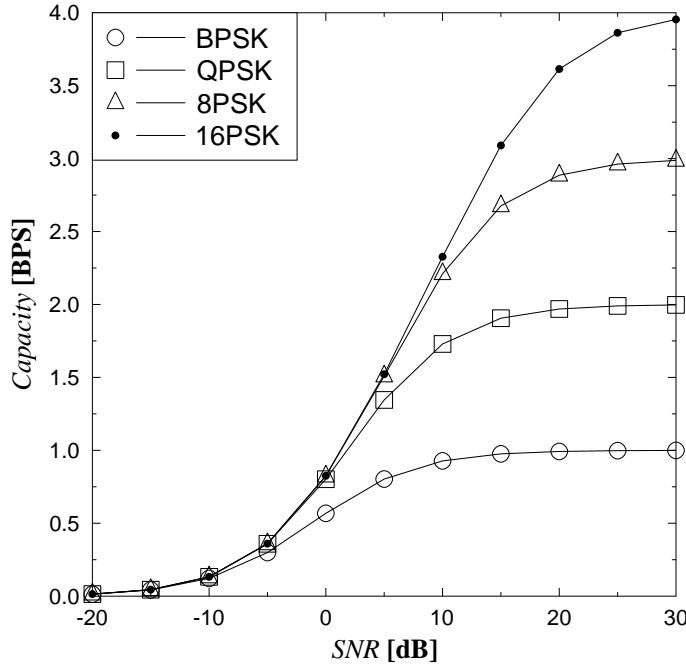


Figure 2.2: Capacity curves of the DCMC calculated by Equation (2.16) for uncorrelated Rayleigh (fast) fading channel, when employing Binary Phase-Shift Keying (BPSK), Quadrature Phase-Shift Keying (QPSK), 8 level Phase Shift Keying (8PSK) and 16 level Phase Shift Keying (16PSK) schemes.

From Equation (2.18), the outage probability corresponding to the scenario, in which the received signals experience only fast fading but no block fading can be formulated as

$$P_e^{DCMC,f}(R, \eta) = Pr \left\{ E[|h_f|^2] < \frac{SNR_r|_R}{SNR} \right\}. \tag{2.19}$$

Similarly, it can also be inferred from Equation (2.18) that the outage probability corresponding to the scenario, when the signals experience only block scale fading but no fast fading may be expressed by:

$$P_e^{DCMC,s}(R, \eta) = Pr \left\{ |h_s|^2 < \frac{SNR_r|_R}{SNR} \right\}. \tag{2.20}$$

For the sake of comparing different modulation schemes, namely BPSK and QPSK, we define the

Normalised throughput $R_n = R/\eta$	$SNR_r _{R_n}$ [dB]	
	BPSK ($\eta = 1$ Bit Per Symbol (BPS))	QPSK ($\eta = 2$ BPS)
0.01	-21.45	-18.55
0.20	-7.38	-4.40
0.40	-3.01	-0.01
0.50	-1.20	1.78
0.60	0.59	3.60
0.80	4.92	7.95
0.99	28.37	31.75

Table 2.1: $SNR_r|_R$ values calculated by the formula given in Equation (2.16) for DCMC schemes corresponding to considering different normalised throughputs, namely $R_n = \{0.01, 0.2, 0.4, 0.5, 0.6, 0.8, 0.99\}$, when communicating over uncorrelated Rayleigh fading channels.

normalized throughput R_n as

$$R_n = \frac{R}{\eta}. \quad (2.21)$$

Accordingly, the $SNR_r|_R$ values corresponding to different values of the normalised throughput R_n considered in the DCMC scheme can be calculated from Equation (2.16), as listed in Table 2.1. Then, by substituting the $SNR_r|_R$ value acquired from Equation (2.16) into Equation (2.25), the related outage probability or FER can be computed across various values of the normalised throughput R_n . As a result, we have Figure 2.3 characterising the relationship between the outage probability versus the normalised throughput R_n , when employing the BPSK and QPSK modulation schemes for transmission defined as the probability of exceeding the maximum tolerable FER over slow Rayleigh fading channel.

2.1.4 Differential Discrete-Input Continuous-Output Memoryless Channel

Let us now consider the DCMC capacity of differentially encoded schemes D-DCMC, having a throughput R given by

$$R = \eta R_c, \quad (2.22)$$

where η is the number of modulated bits and R_c is the equivalent channel coding rate.

In contrast to the DCMC capacity, where the maximum rate expression was given in Equation (2.16), we invoke EXIT charts for calculating the D-DCMC channel capacity supported by the non-coherent detection scheme detailed in Section 2.1.2.1. More specifically, we exploit a useful property [157] of EXIT charts, namely that the area under the EXIT curve of an inner receiver component of Figure 2.27 is approximately equal to the achievable capacity of the channel

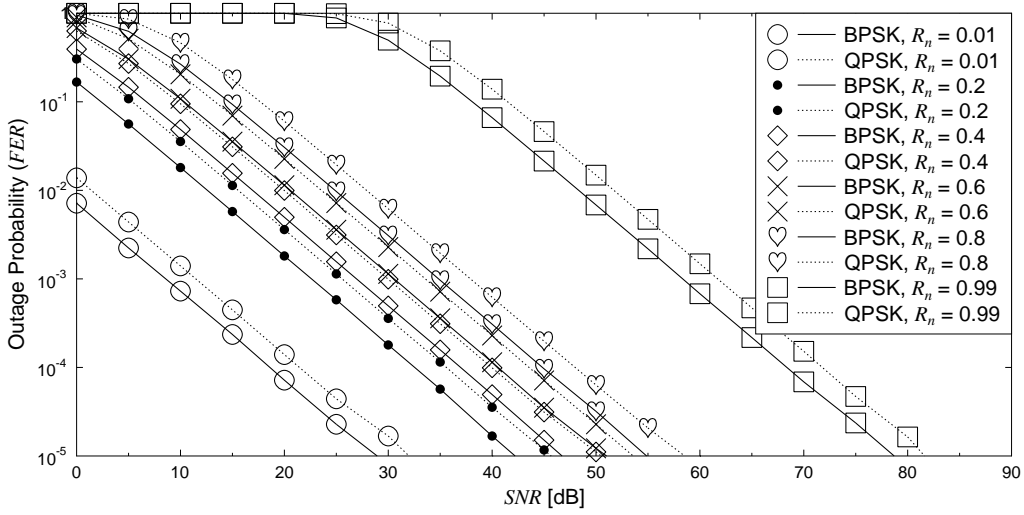


Figure 2.3: Outage probability (FER) of the DCMC calculated by Equation (2.25) for BPSK and QPSK modulation scheme for transmission over the block Rayleigh fading channel.

supported by the inner component. For example, the area under the EXIT curve of Differential Quadrature Phase Shift Keying (DQPSK) modem quantifies the attainable capacity for any system, such as for example DCMC-DQPSK Unity-Rate Code Differential Quadrature Binary Phase Shift Keying (URC-DQPSK) and Irregular Convolutional Code and Unity-Rate Code Differential Quadrature Binary Phase Shift Keying (IrCC-URC-DQPSK) systems. Accordingly, in order to obtain the capacity curves seen in Figure 2.4, we have carried out the following steps:

- We generate the EXIT curves of various differential modulation schemes, namely those of Differential Binary Phase Shift Keying (DBPSK) and Differential Quadrature Phase Shift Keying (DQPSK), for different SNR_r values, as exemplified in Figure 2.29.
- We determine a single point on the capacity curves by computing the area under an EXIT curve and its corresponding SNR_r . As a result, the capacity curves are plotted in Figure 2.4 for an uncorrelated Rayleigh fading channel, when employing DBPSK and DQPSK modulation schemes.

As an alternative method, we can obtain the D-DCMC capacity curves by shifting the corresponding DCMC capacity curves plotted in Figure 2.2 to the right by 3dB. As a result, the D-DCMC curves determined by the shifting method are also plotted in Figure 2.4.

Having plotted the D-DCMC capacity curves, at a given throughput of R , we can now specify the $SNR_r^{EXIT}|_R$ required for maintaining this specific throughput, again as seen in Figure 2.4. In our forthcoming discourse, we will opt for using the D-DCMC capacity curve determined by the

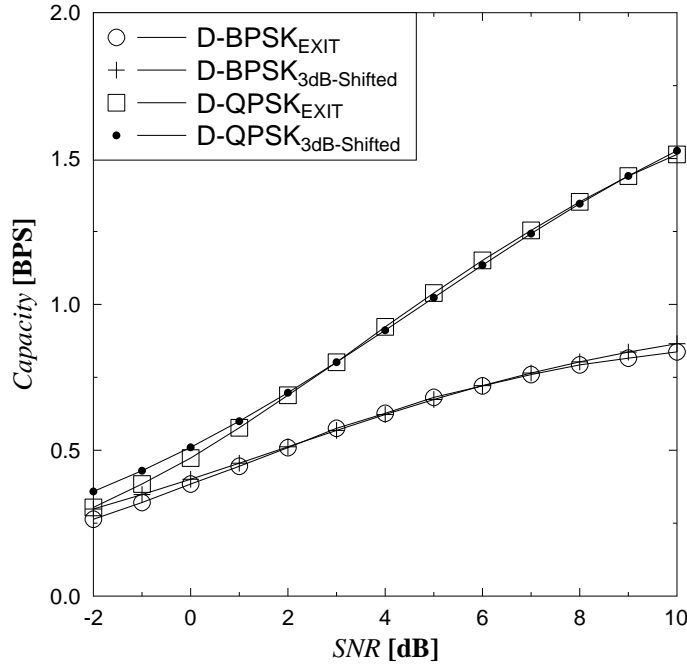


Figure 2.4: Capacity curves of the D-DCMC determined by the EXIT-chart based method or by shifting the DCMC capacity curves of Figure 2.2 to the right a distance of 3 dB, when employing BPSK and QPSK modulation schemes over uncorrelated Rayleigh (fast) fading channel.

EXIT-chart based procedure. As a result, the $SNR_r^{EXIT}|_R$ values required are listed in Table 2.2 for different values of the normalised throughput R_n .

Then, upon replacing $SNR_r|_R$ of Equation (2.18) by $SNR_r^{EXIT}|_R$, the outage probability of the D-DCMC model may be formulated as:

$$P_e^{D-DCMC}(R, \eta) = Pr \left\{ |h_s|^2 E[|h_f|^2] < \frac{SNR_r^{EXIT}|_R}{SNR} \right\}. \quad (2.23)$$

The outage probabilities for the uncorrelated Rayleigh (fast) and the block Rayleigh (slow) fading channels can also be inferred from Equation (2.23) as follows:

$$P_e^{D-DCMC,fast}(R, \eta) = Pr \left\{ E[|h_f|^2] < \frac{SNR_r^{EXIT}|_R}{SNR} \right\}, \quad (2.24)$$

and as:

$$P_e^{D-DCMC,slow}(R, \eta) = Pr \left\{ |h_s|^2 < \frac{SNR_r^{EXIT}|_R}{SNR} \right\}. \quad (2.25)$$

Accordingly, by employing Equation (2.23) and the $SNR_r^{EXIT}|_R$ values listed in Table 2.2, the resultant outage probability can be quantified for diverse values of the normalised throughput R_n for the block Rayleigh fading channel, when DBPSK and DQPSK modulation schemes are employed, as seen in Figure 2.5.

Normalised throughput $R_n = R/\eta$	$SNR_r^{EXIT} _{R_n}$ [dB]	
	DBPSK ($\eta = 1$ BPS)	DQPSK ($\eta = 2$ BPS)
0.01	-12.03	-10.31
0.20	-3.13	-0.78
0.40	0.26	2.98
0.60	3.44	6.45
0.80	7.89	11.32
0.99	28.00	32.00

Table 2.2: $SNR_r^{EXIT}|_{R_n}$ values calculated with the aid of the EXIT charts to be introduced at a later stage in Section 2.3 for a D-DCMC scheme, when various normalised throughput R_n , namely 0.01, 0.2, 0.4, 0.6, 0.8 and 0.99, are considered.

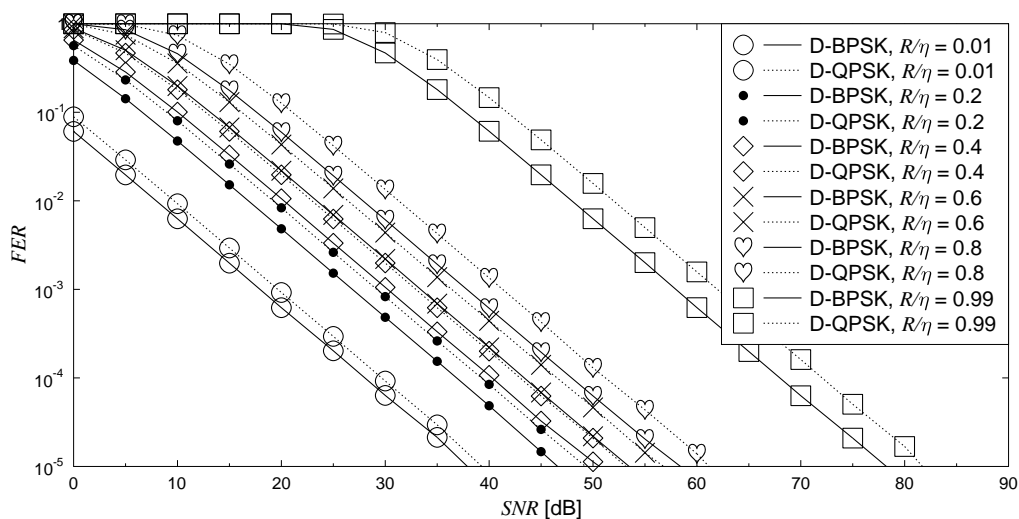


Figure 2.5: Outage probability (FER) of the D-DCMC calculated by Equation (2.23) for block Rayleigh fading channel, when DBPSK and DQPSK modulation schemes are used. The outage probability is plotted across different values of the normalised throughput R/η , namely 0.01, 0.2, 0.4, 0.6, 0.8, 0.99.

2.2 Outage capacity of a single link

As noted in [151], channel coding cannot significantly improve the achievable error probability in block fading channels, where the channel coefficients remain constant over the period of a frame. This is because in this specific scenario the channel is an AWGN channel associated with different SNRs and the system's performance is dominated by the low-SNR frames. More specifically, in the presence of the small-scale fading, where the channel coefficients change for every symbol, the transmitter can send data at the rate of $R < C|h$, while maintaining an arbitrarily low error probability. However, it may not be possible to maintain a vanishingly low Bit Error Ratio (BER) for a large-scale fading channel, where the channel coefficients remain constant over a frame duration. Hence, the capacity of large-scale fading channels may become zero in the strict sense. Alternatively, the outage capacity $C(\varepsilon)$ introduced in [151] was defined as the highest possible value of transmission rate R , which was still capable of ensuring that the outage probability (FER) becomes less than ε . It should be noted that the capacity of the quasi-static fading channels is dependent on the outage probability ε characterising the desired quality of transmission. Thus, the outage capacity is different from the capacity represented by Equation (2.16).

Similar to the formulaic relationship established for the CCMC case in [151], it can be inferred from (2.18) that the outage capacity of the DCMC channel may be formulated as:

$$SNR(\varepsilon, \eta) = F^{-1}(1 - \varepsilon), \quad (2.26)$$

where $F(SNR_r|R)$ is the Complementary Cumulative Distribution Function (CCDF) of the combined fast-and slow-fading (small-and large scale-fading) envelope of $|h|^2 = |h_s|^2|h_f|^2$, which is defined as

$$F(SNR_r|R) = Pr \left\{ |h_s|^2 > \frac{SNR_r|R}{SNR} \right\}. \quad (2.27)$$

Note that $F(SNR_r|R)$ depends on the transmission rate R , while the corresponding SNR_r may be calculated from Equation (2.16). In order to provide a fair comparison of the different-throughput modulation schemes, the CCDF $F(SNR_r|R_n)$ of the SNR_r is used at the same value of the normalised transmission rate R_n . Accordingly, Equation (2.27) becomes

$$F(SNR_r|R_n) = Pr \left\{ |h_s|^2 > \frac{SNR_r|R_n}{SNR} \right\}. \quad (2.28)$$

In this discourse, the uncorrelated Rayleigh fading is chosen for the small-scale fading scenario. Accordingly, each uncorrelated Rayleigh fading coefficient is uncorrelated and varies on symbol-by-symbol basis. By contrast, the block fading is also chosen to be Rayleigh distributed, but each block Rayleigh fading coefficient remains constant during a frame duration and varies independently on frame-by-frame basis.

2.2.1 Coherent schemes

Let us first consider the DCMC capacity. Again, at a given throughput of R and a modulation scheme characterised by η , we can have $R_n = R/\eta$, as defined by Equation (2.21). Then, we can readily identify the receive signal to noise power ratio $SNR_r|_{R_n}$ required for maintaining R_n from the DCMC capacity curve described by Equation (2.16) and portrayed in Figure 2.2. As a result, the $SNR_r|_{R_n}$ values corresponding to the normalized throughput R_n are summarised in Table 2.1. The $SNR_r|_{R_n}$ values of Table 2.1 are employed for computing the CCDF of $F(SNR_r|_{R_n})$ defined by Equation (2.28). As seen in Figure 2.6, the CCDF of $F(SNR_r|_{R_n})$ is plotted across different values of normalised throughput R_n , namely 0.01, 0.2, 0.4, 0.6, 0.8, 0.99.

Having computed the CCDF of $F(SNR_r|_{R_n})$, we can now calculate the minimum required value of the SNR at a given outage probability η by applying Equation (2.26). For the sake of comparing different modulation schemes, we define $C_n(\varepsilon)$ as the normalised outage capacity, which is given by

$$C_n(\varepsilon) = \frac{C(\varepsilon)}{\eta}, \quad (2.29)$$

where $C(\varepsilon)$ is the outage capacity determined by the relationship of Equation (2.26), while η is the number of modulated bits used for representing a symbol in the modulation scheme of consideration.

As a result, the normalised outage capacity $C_n(\varepsilon)$ of Equation (2.29) may be plotted in Figure 2.7 for a range of outage probability values ε , namely for $\varepsilon = 10^{-1}, 10^{-2}, 10^{-3}$, when the BPSK and the QPSK modulation schemes are employed in the block Rayleigh fading channel. Let us demonstrate the above-mentioned steps by a numerical example as follows.

Example 2.1. *Let us consider a specific system employing the parameters summarised in Table 2.3.*

Since QPSK modulation is employed in our system, we can substitute $\eta = 2$ and $L = 2^2 = 4$ into Equation (2.16), in order to calculate the corresponding capacity curve, which is shown in Figure 2.8. As seen in Figure 2.8, given $R = R_c\eta = 0.5 \times 2.0 = 1.0$, we have $SNR_r|_R = 1.793$ dB. Then, the value of $SNR_r|_R = 1.793$ dB is employed for calculating $F(SNR_r|_R)$ defined in Equation (2.27). Having computed the CCDF of $F(SNR_r|_R = 1.793)$ plotted in Figure 2.9, we can then compute the minimum SNR required for maintaining a given outage probability of ε by using Equation (2.26). Accordingly, given the value of $\varepsilon = 10^{-3}$, the SNR value corresponding to the outage capacity in our numerical example can be computed as:

$$SNR(\varepsilon, \eta)|_{\varepsilon=10^{-3}, \eta=2} = F^{-1}(1 - \varepsilon)|_{\varepsilon=10^{-3}}. \quad (2.30)$$

As a result, the SNR = 31.63 dB obtained from Equation (2.30) corresponds to an outage probability of $\varepsilon = 10^{-3}$, as shown in Figure 2.9. Naturally, the point having $R = 1.0$ BPS and SNR = 31.63 dB constitutes a single point on the outage capacity curve plotted in Figure 2.10.

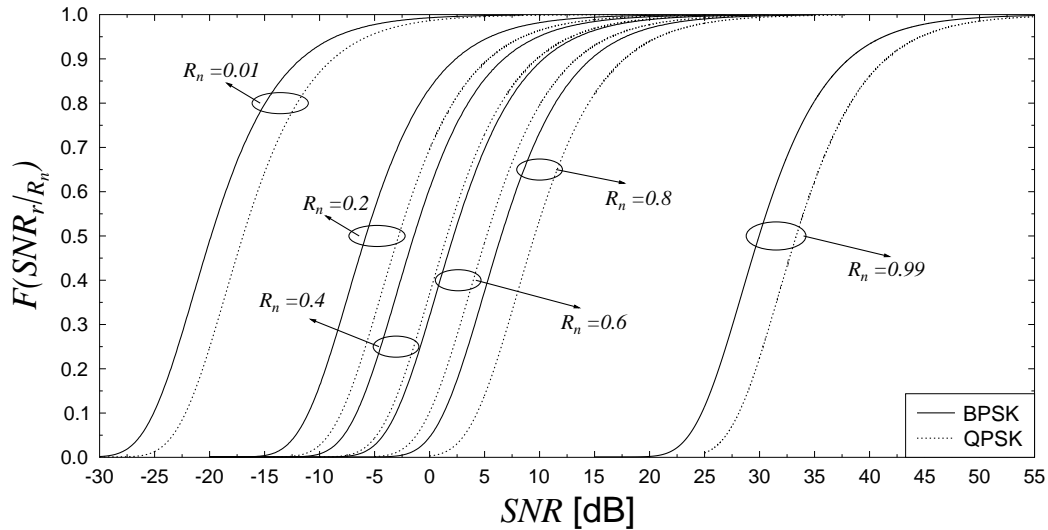


Figure 2.6: The CCDF $F(SNR_r|R_n)$ of the normalised achievable rate R_n calculated by Equation (2.28), when the BPSK and the QPSK modulation schemes are employed for communicating over the block Rayleigh fading channel. The CCDF of $F(SNR_r|R_n)$ is plotted across different values of normalised throughput R_n , namely 0.01, 0.2, 0.4, 0.6, 0.8, 0.99.

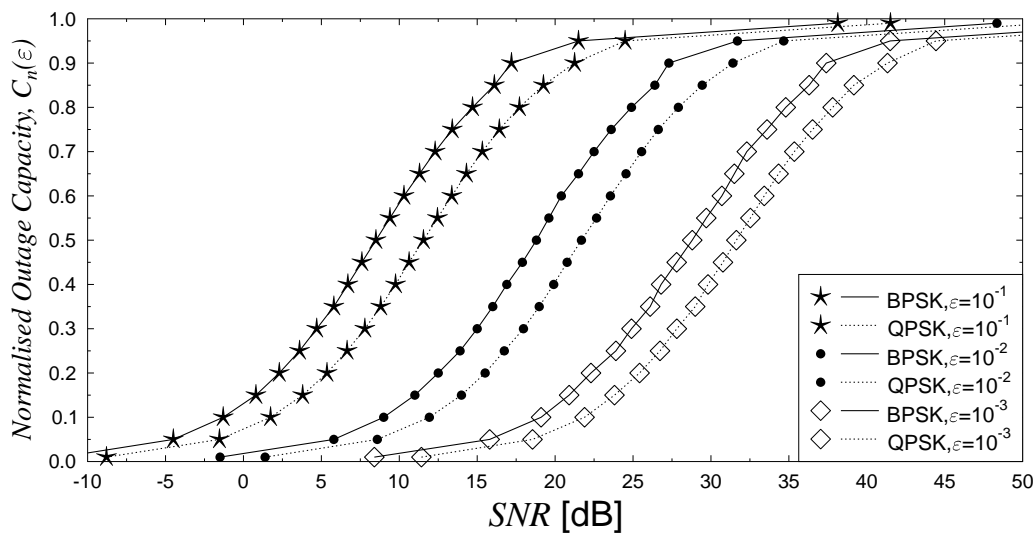


Figure 2.7: Outage capacity of the DCMC calculated by Equation (2.26) upon the CCDF of $F(SNR_r|R)$ plotted in Figure 2.6, for the range of the outage probability η , namely 10^{-1} , 10^{-2} and 10^{-3} , when the BPSK and the QPSK modulation schemes are employed for communicating over the block Rayleigh fading channel.

Parameters	$G_{4 \times 8}$ system
R [BPS]	1.0(QPSK)
Modulation	QPSK
L	4
η	2
R_c	0.5
ε	10^{-3}

Table 2.3: The relating parameters of the illustrative system employing QPSK modulation (number of modulation levels $L = 4$ and number of modulated bits per symbol $\eta = 2$) and a channel coding scheme having a coding rate $R_c = 0.5$, which results in the information rate $R = 1.0$. The outage capacity corresponding to the outage probability $\varepsilon = 10^{-3}$ is calculated upon the listed parameters.

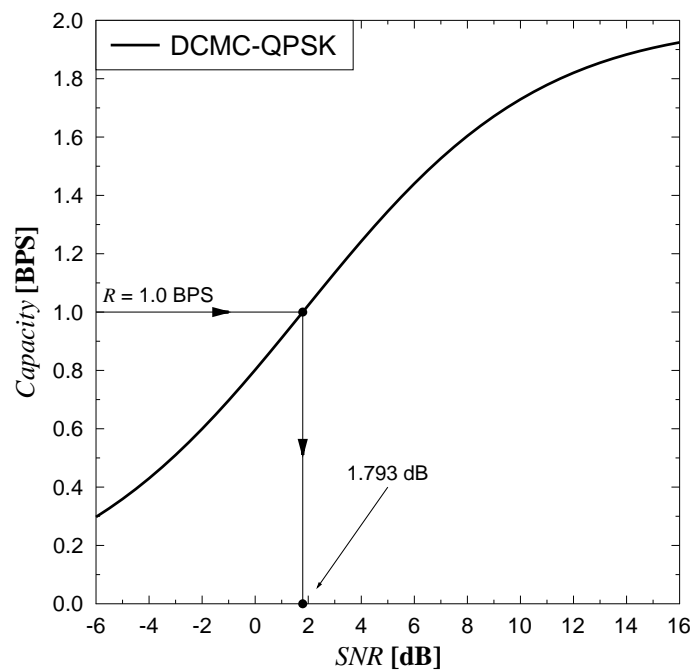


Figure 2.8: The DCMC capacity curve is plotted by using Equation (2.16) for small-scale Rayleigh fading channel, when the QPSK modulation is employed. The value of $SNR_r|_R$ corresponding to $R = R_c \eta = 0.5 \times 2.0 = 1.0$ is specified on the DCMC capacity curve.

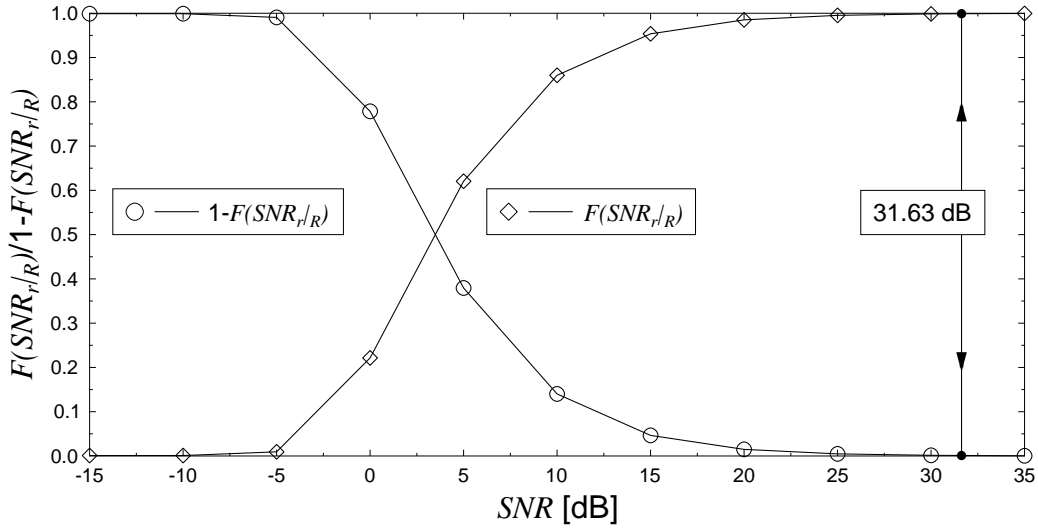


Figure 2.9: The CCDF of $F(SNR_r|R)$ given in Equation (2.27) and its offset function of $(1 - F(SNR_r|R))$ are calculated across different values of SNR for the value of $SNR_r|R = 1.793$, which is associated with the specific system having the relevant parameters listed in Table 2.1.

Similarly, other SNR values associated with different values of R may be calculated in order to form the outage capacity curve plotted in Figure 2.10, provided that the same outage probability of $\varepsilon = 10^{-3}$ is considered.

The specific point at $R = 1.0$ BPS and $SNR = 31.63$ dB for $\varepsilon = 10^{-3}$ recorded in Figure 2.10 may be interpreted as follows. If the SNR_r value is equal to or lower than 31.63 dB, the maximum outage capacity is equal to 1.0 BPS, provided that the outage probability of $\varepsilon = 10^{-3}$ is guaranteed. Viewed from a different perspective, if we have $SNR_r \leq 31.63$ dB at the receiver and the transmission rate is $R = 1$ BPS, the best possible quality of transmission is achieved at an outage probability of $\varepsilon = 10^{-3}$.

2.2.2 Non-coherent schemes

It should be noted that the general outage capacity formula of Equation (2.26) can also be used for the D-DCMC case, where the CCDF $F(SNR_r|R)$ of the achievable rate R is replaced by $F(SNR_r^{EXIT}|R)$, which can be defined as

$$F(SNR_r^{EXIT}|R) = Pr \left\{ |h_s|^2 > \frac{SNR_r^{EXIT}|R}{SNR} \right\}. \quad (2.31)$$

Note that the CCDF $F(SNR_r^{EXIT}|R)$ depends both on the transmission rate R and on the modulation scheme employed. These two parameters allow us to specify the $SNR_r^{EXIT}|R$ value on the corresponding capacity curve calculated by the EXIT-chart based method, as mentioned in Section 2.1.4, where the capacity curves of DBPSK and DQPSK are plotted in Figure 2.4. Similarly

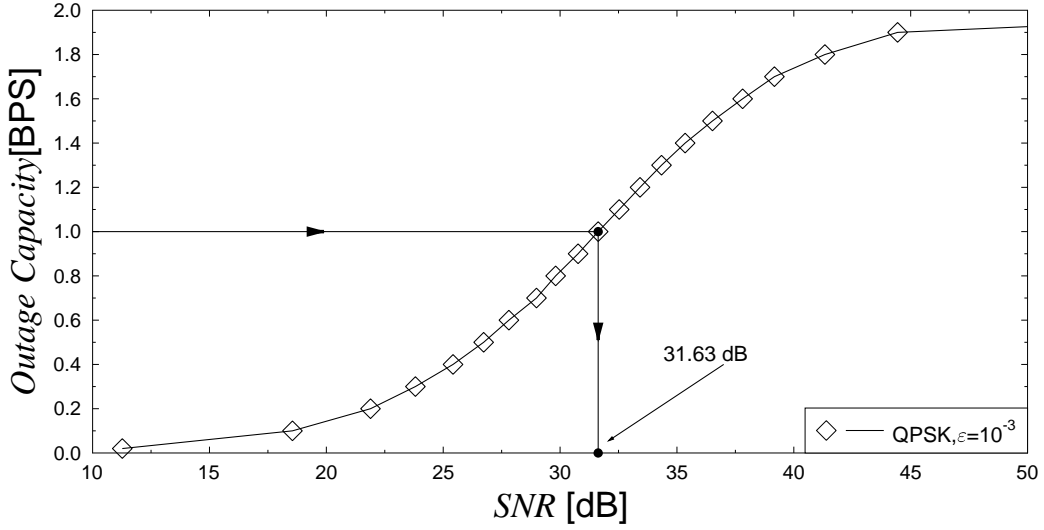


Figure 2.10: The outage capacity corresponding to $\varepsilon = 10^{-3}$ is calculated by Equation (2.30) for the system characterised by Table 2.1.

to the DCMC case, we also employ the normalised transmission rate R_n for the sake of comparing different modulation schemes, namely DBPSK and DQPSK. Hence, Equation (2.31) becomes

$$F(SNR_r^{EXIT}|_{R_n}) = Pr \left\{ |h_s|^2 > \frac{SNR_r^{EXIT}|_{R_n}}{SNR} \right\}, \quad (2.32)$$

where $SNR_r^{EXIT}|_{R_n}$ is the value corresponding to R_n on the capacity curve. Having calculated $SNR_r^{EXIT}|_{R_n}$, as listed in Table 2.2, the CCDF $F(SNR_r^{EXIT}|_{R_n})$ of Equation (2.32) is drawn in Figure 2.11 against the SNR and parameterised by different values of the normalised throughput, namely $R_n = 0.01, 0.2, 0.4, 0.6, 0.8, 0.99$, for the scenario of employing the DBPSK and DQPSK modulation schemes, when communicating over the block Rayleigh fading channel.

Then, the CCDF $F(SNR_r^{EXIT}|_R)$ of Equation (2.31) or the CCDF $F(SNR_r^{EXIT}|_{R_n})$ of Equation (2.32) can be used in conjunction with Equation (2.26) for calculating the outage capacity of a perfect D-DCMC capacity-achieving system. For the sake of comparison between different modulation schemes, namely DBPSK and DQPSK, the normalised outage capacity $C_n(\varepsilon)$ defined by Equation (2.29) is utilised for characterising the outage capacity of a perfect D-DCMC capacity-achieving system. As a result, we have Figure 2.12 showing the normalised outage capacity pertaining to a range of outage probability values ε , namely to $\varepsilon = 10^{-1}, 10^{-2}$ and 10^{-3} , when the DBPSK and DQPSK modulation schemes are used for communicating over the block Rayleigh fading channel.

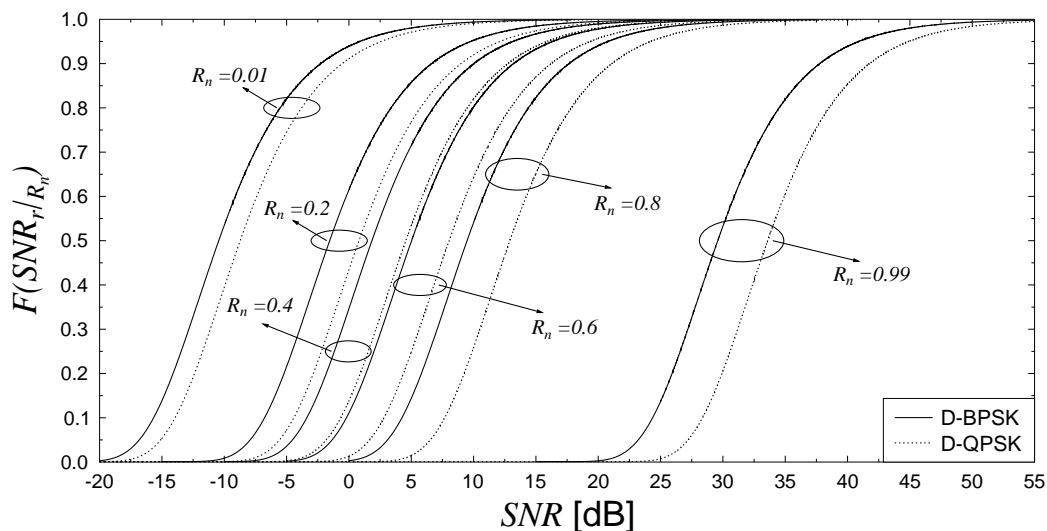


Figure 2.11: The CCDF of $F(SNR_r^{EXIT} | R_n)$ is calculated by Equation (2.32), for the cases of employing DBPSK and DQPSK modulation schemes, where corresponding values of $SNR_r^{EXIT} | R_n$ are given in Table 2.2. The CCDF of $F(SNR_r^{EXIT} | R_n)$ is calculated across different normalised throughputs R_n , namely 0.01, 0.2, 0.4, 0.6, 0.8, 0.99, when communicating over the block Rayleigh fading channel.

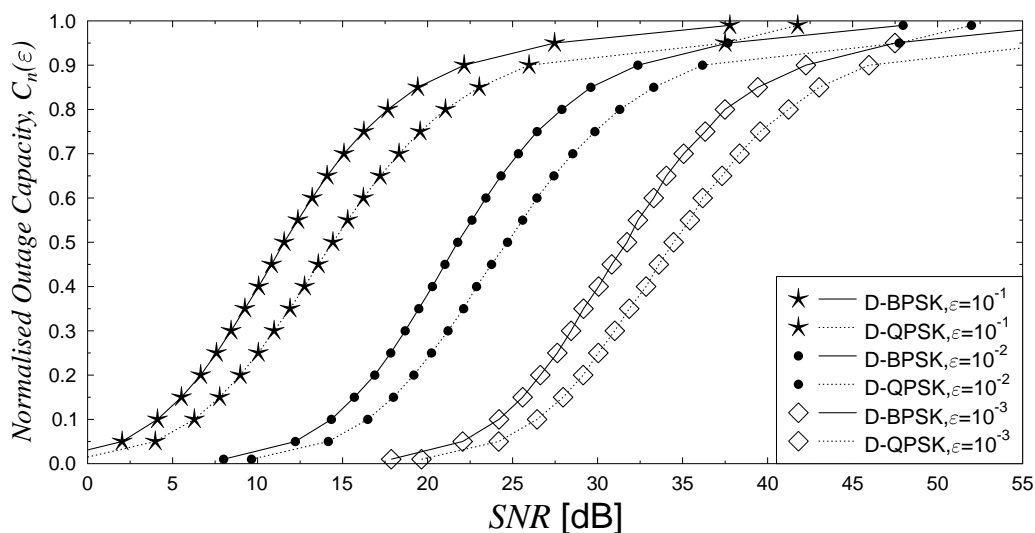


Figure 2.12: The normalised outage capacity $C_n(\epsilon)$ of the D-DCMC associated with the range of outage probability values ϵ , namely with $\epsilon = 10^{-1}, 10^{-2}$ and 10^{-3} , is calculated by Equation (2.26) and Equation (2.31) for the cases of employing the DBPSK and the DQPSK modulation schemes employed for communicating over the block Rayleigh fading channel.

2.3 Near-capacity channel code design

Tüchler and Hagenauer [158, 159] proposed the employment of Irregular Convolutional Codes (IrCCs) for serial concatenated schemes, which are constituted by a family of convolutional codes having different rates, in order to design a near-capacity system. These IrCCs were specifically designed with the aid of EXIT charts for improving the convergence behaviour of iteratively decoded systems. Briefly, these schemes were then further developed for a broad class turbo-transceiver in [45]. Each component code of the IrCCs encodes an appropriately selected fraction of the input bit stream. More explicitly, the appropriate fractions may be selected with the aid of EXIT-chart analysis in order to shape the inverted EXIT curve of the composite Irregular Convolutional Code (IrCC) for ensuring that it matches the EXIT curve of the so-called inner decoder constituted by the detector. In this manner, an open EXIT-chart tunnel can be created at low SNR values, which implies approaching the channel's capacity bound [157].

EXIT charts have been introduced as an effective tool conceived for analysing the convergence properties of iterative decoding aided concatenated coding schemes [160]. As an advantage, this can be achieved without performing time-consuming Monte-Carlo simulations. EXIT charts can be used for finding powerful codes exhibiting guaranteed convergence for a given channel [161]. Specifically, near-capacity codes have been successfully designed by applying an EXIT-chart-based technique, for example in [76, 158, 162].

As a further advance, it was shown in [163, 164] that a recursive Unity-Rate Code (URC) should be employed as an intermediate code in order to improve the attainable decoding convergence. A URC can be used as a precoder for creating an inner code component having Infinite Impulse Response (IIR) in order to reach the (1,1) point of perfect decoding convergence in the EXIT chart and hence to achieve an infinitesimally low BER [76].

According to (2.1) and (2.6), the average SNR_r per frame can be expressed as

$$SNR_r = \frac{E[|h_s|^2]E[|h_f|^2]E[|x|^2]}{N_0} = \frac{|h_s|^2}{N_0}, \quad (2.33)$$

where we have $E[|x|^2] = 1$, $E[|h_f|^2] = 1$ for an uncorrelated Rayleigh fading channel and $E[|h_s|^2] = |h_s|^2$ for a block fading Rayleigh channel. Thus, given a specific SNR_r , we can generate the EXIT chart [160] of the system. The benefits of this idea will be demonstrated throughout the rest of this section.

Furthermore, for convenience of signal processing as well as signal transmissions, each channel-encoded frame of the practical systems [165, 166] tends to be partitioned into an N_s number of sub-frames, where the average SNR_r of (2.33) may be formulated as:

$$SNR_r = \frac{E[|h_s|^2]}{N_0} = \frac{\sum_{i=1}^{N_s} |h_{s,i}|^2 / N_s}{N_0}, \quad (2.34)$$

with $h_{s,i}$ representing the block fading corresponding to the i^{th} sub-frame of the channel-encoded frame. Hence, the performance of coding schemes subsequently mentioned in this section will be

evaluated not only in the small-scale fading channel but also in the block fading channel, where the employment of sub-frame transmission is considered.

2.3.1 EXIT-chart based code design principle

A particularly useful EXIT-chart property [157] is that the area under the EXIT curve of an inner decoder component is approximately equal to the attainable channel capacity, provided that the channel's input symbols are equiprobable. This property [157] may be exploited for determining the achievable rate of Forward Error Correction (FEC) schemes relying on iterative multi-stage coding. Then, the achievable capacity may be used for selecting a specific coding scheme from the available set and may also be used for optimising coding arrangements relying on numerous parameters by using the achievable capacity as a criterion for comparing all legitimate sets of parameters used for specifying the coding arrangement.

In the context of employing IrCCs as the outer-most coding stage for a serially concatenated scheme, the design guidelines provided below illustrate, how the various advantages of IrCCs and EXIT-charts can be combined. More specifically, the designing guidelines can be formulated in the following two-step procedure:

- **Step1:** Create the EXIT curve of the amalgamated inner decoder constituted for example by the above-mentioned URC having a beneficial IIR with the inner-most detector constituted by the demodulator. The number of decoding iterations between the URC decoder and the inner-most detector is decided based on the area under the EXIT curve of this amalgamated inner decoder. Since the area under this amalgamated inner decoder represents the achievable DCMC capacity [157], while a high number of iteration would incur a high complexity, the minimum number of required iterations can be selected at the cost of a marginal capacity loss.
- **Step2:** The overall coding rate of the IrCC encoder is chosen to match the achievable capacity of the amalgamated inner decoder. We employ the EXIT curve matching algorithm of [158] for generating the optimised weighting coefficients α_i . The number of IrCC component codes can be $i = 1, \dots, 17$ or $i = 1, \dots, 36$. The matching algorithm aims for finding a set of codes facilitating decoding convergence to a vanishingly low BER at the lowest possible SNR_r , where a narrow but marginally open EXIT chart tunnel would appear in the EXIT chart.

The general principle briefly described by our two-step procedure will be demonstrated with the aid of the results in Section 2.3.2, Section 2.3.3 and Section 2.3.4 via the specific examples of designing Irregular Convolutional Coded Unity Rate Coded Space Time Trellis Coded M-ary Phase Shift Keying (IrCC-URC-STTC-MPSK), Irregular Convolutional Coded Unity Rate Coded M-ary Phase Shift Keying (IrCC-URC-MPSK) and Irregular Convolutional Coded Unity Rate Coded Differential M-ary Phase Shift Keying (IrCC-URC-DMPSK) coding arrangements, respectively.

2.3.2 IrCC-URC-STTC-MPSK coding scheme

This section is dedicated to the design of the IrCC-URC-STTC-MPSK coding arrangement portrayed in Figure 2.13. As seen in Figure 2.13, the bit stream at the transmitter side is first encoded by the IrCC encoder before it is fed into the interleaver π_1 , in order to get the interleaved input stream for feeding the URC encoder. The output of the URC encoder is again scrambled by the interleaver π_2 before being encoded by the Space Time Trellis Code (STTC) detailed in Section 1.1.1. This signal is then transmitted to the receiver side over wireless fading channels, as portrayed in Figure 2.13 .

At the receiver side, as seen in Figure 2.13, the signals provided by the receive antenna are demodulated and decoded by the STTC decoder before being processed by the I inner iterations exchanging extrinsic information between the STTC decoder and the URC decoder. The resultant soft information extracted from the received signals by the inner iterations are then used as the input data for the J outer iterations exchanging extrinsic information between the IrCC encoder and the amalgamated inner component, which is the Unity Rate Coded M-ary Phase Shift Keying (URC-STTC-MPSK) arrangement. Hence, our design goals are to determine the most appropriate number of inner and outer iterations, as well as the weighting coefficients of the IrCC subcodes used in the IrCC encoder.

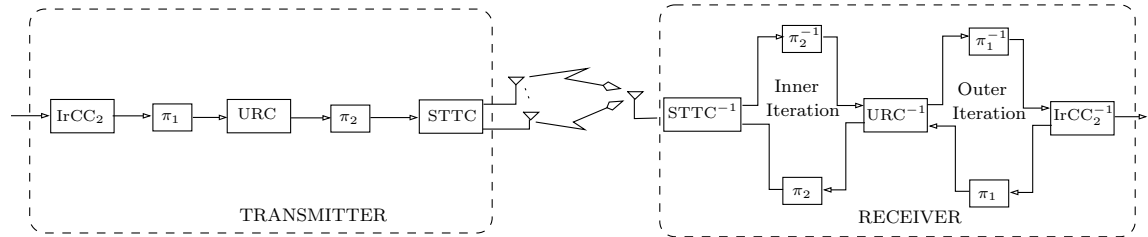


Figure 2.13: The structure of the Irregular Convolutional Coded Unity Rate Coded Space Time Trellis Code (IrCC-URC-STTC) coding scheme.

The IrCC-URC-STTC-MPSK coding arrangement featured in Figure 2.13 is later used in our relay-aided cooperative communications scheme detailed in Chapter 3. In such cooperative systems, the IrCC-URC-STTC-MPSK coding scheme is invoked for constructing a virtual Multi-Input Multi-Output (MIMO) scheme constituted by our relay-aided system. More specifically, we apply the EXIT-chart based design principles outlined in Section 2.3.1 for our IrCC-URC-STTC coding scheme relying on QPSK modulation, in order to conceive a near-capacity IrCC-URC-STTC-QPSK scheme.

2.3.2.1 EXIT-chart matching and optimisation of the IrCC-URC-STTC-MPSK scheme

In order to increase the achievable channel capacity of the amalgamated Unity Rate Coded Space Time Trellis Code Quadrature Shift Keying (URC-STTC-QPSK) inner code and to approach that

of a Space Time Trellis Coded (STTC) and STTC-QPSK aided system, an iterative decoding process exchanging extrinsic information between the URC and STTC decoders should be implemented [167]. We exploit the above-mentioned characteristics of EXIT charts [157] for calculating the DCMC capacity of the two inner-most coding arrangements, namely that of the Space Time Trellis Code Quadrature Shift Keying (STTC-QPSK) and URC-STTC-QPSK schemes. Then, based on the capacity of these two coding arrangements, we determine the most appropriate number of iterations. As a result, Figure 2.14 shows that once at least $I = 3$ iterations had been applied, the achievable channel capacities of the STTC-QPSK and URC-STTC-QPSK systems become near-identical.

The code design is continued by viewing our three-stage IrCC-URC-STTC-QPSK coding arrangement as the two-stage-concatenated IrCC outer code and the amalgamated URC-STTC-QPSK inner code. According to the design guidelines introduced in Section 2.3.1, the EXIT chart matching procedure conceived for this coding arrangement is briefly summarised as follows:

Step1: Create the EXIT chart of the URC-STTC-QPSK scheme for different receiver Signal to Noise Ratios SNR_r , as seen in Figure 2.15.

Step2: Fix the overall IrCC code rate to $R_c = 0.5$ and employ the EXIT curve matching algorithm [158] for generating the optimised weighting coefficients $\alpha_j, j = 1, \dots, 17$, of the 17-component IrCC codes corresponding to the lowest possible SNR_r that allows decoding convergence, where the decoding trajectory reaches the top-right corner of the corresponding EXIT charts. This observation suggests that a near-capacity performance can be achieved.

Once the steps mentioned above have been completed, we obtain the EXIT curves and the corresponding weighting coefficients $\alpha_j, j = 1, \dots, 17$ for the IrCC encoder, as shown in Figure 2.15. The EXIT-chart results show that if having $J = 24$ iterations were affordable, the iterative decoding trajectory would reach the $(1, 1)$ point of perfect convergence to an infinitesimally low BER.

Furthermore, the area property of EXIT-charts [157, 162] mentioned in Section 2.3.1 states that the area under the normalised EXIT curve of an inner decoder component is approximately equal to the attainable channel capacity, provided that the channels' input symbols are equiprobable. Again, by exploiting the area property of the EXIT-charts [157, 162], the achievable DCMC capacities of the MIMO $_{2 \times 1}$ -QPSK, the STTC $_2 \times 1$ -QPSK, URC-STTC $_2 \times 1$ -QPSK and IrCC-URC-STTC $_2 \times 1$ -QPSK aided systems are quantified by generating the EXIT charts of these schemes across various SNR values. Then, the areas under each of these EXIT charts corresponding to different SNR values are measured for determining the associated capacity curves, as plotted in Figure 2.14.

It should be noted that the capacity of an inner arrangement sets an upper bound for the capacity of an outer arrangement. Hence, according to the afore-listed order, the capacity associated with the inner most arrangement MIMO $_{2 \times 1}$ -QPSK sets the maximum achievable capacity for all the systems employing the other schemes, namely the STTC $_2 \times 1$ -QPSK, URC-STTC $_2 \times 1$ -QPSK

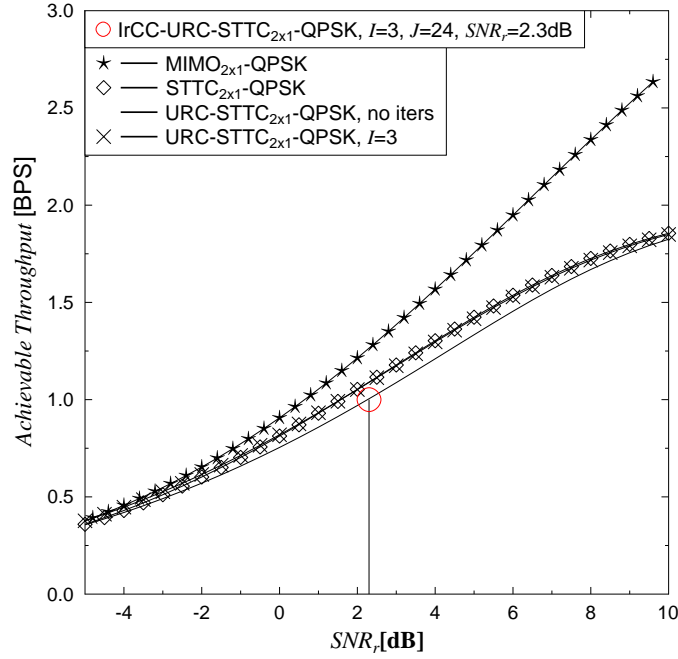


Figure 2.14: Achievable throughputs of the $\text{MIMO}_{2 \times 1}$ -QPSK, the $\text{STTC}_{2 \times 1}$ -QPSK arrangement, the $\text{URC-STTC}_{2 \times 1}$ -QPSK arrangement ($I = 0, 3$ iterations between URC and $\text{URC-STTC}_{2 \times 1}$ -QPSK) and the $\text{IrCC-URC-STTC}_{2 \times 1}$ -QPSK arrangement ($I = 3$ iterations between URC and $\text{URC-STTC}_{2 \times 1}$ -QPSK in conjunction with $J = 24$ iterations between IrCC and $\text{URC-STTC}_{2 \times 1}$ -QPSK).

and $\text{IrCC-URC-STTC}_{2 \times 1}$ -QPSK, as seen in Figure 2.14. Additionally, it can be seen from Figure 2.15 and Figure 2.14 that the IrCC-URC-STTC -QPSK scheme's capacity curve is only about $(2.3 - 1.6) = 0.7\text{dB}$ away from the STTC -based DCMC capacity curve.

Following the same procedure as illustrated by designing the IrCC-URC-STTC -QPSK, we also designed other coding arrangements relying on 8PSK and 16PSK, namely the $\text{IrCC-URC-STTC-8PSK}$ and $\text{IrCC-URC-STTC-16PSK}$ schemes. The corresponding weighting coefficients of the IrCC encoder are listed in Table 2.4. It should be noted that the 17 weighting coefficients α_i , $i = [1, 2, \dots, 17]$, as listed in Table 2.4, are the 17 coding fractions of the 17 corresponding component codes (subcodes). More specifically, the i^{th} of subcode having a code rate β_i encodes the fraction α_i of the input bit stream, where the values of β_i , $i = [1, 2, \dots, 17]$ are listed in Table 2.5. Hence, the values of the weighting coefficient α_i and β_i always have to satisfy the constraint of:

$$R_c = \sum_{i=1}^{17} \alpha_i \beta_i, \quad (2.35)$$

where R_c is the coding rate (aggregate coding rate) of the IrCC code.

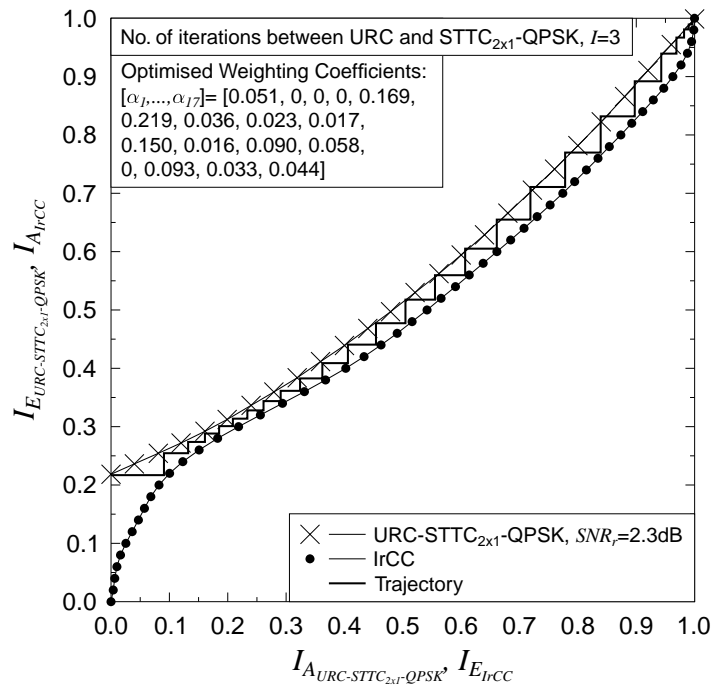


Figure 2.15: The EXIT chart curves of the URC-STTC-QPSK having two transmit and one receive antennas (URC-STTC_{2x1}-QPSK) scheme at $SNR = 2.3$ dB when $I = 3$ iterations between URC and STTC_{2x1}-QPSK are configured and of the IrCC having the overall coding rate $R_c = 0.5$.

Inner arrangement (Turbo-cliff SNR)	Coefficients: $[\alpha_1, \alpha_2, \dots, \alpha_{17}]$
URC-STTC-QPSK (2.3 dB)	[0.05, 0, 0, 0 0.169, 0.219, 0.036, 0.023, 0.0166, 0.149, 0.015, 0.089, 0.058, 0, 0.093, 0.033, 0.044]
URC-STTC-8PSK (4.4 dB)	[0 0.171, 0.093, 0, 0, 0.195, 0, 0, 0.099, 0.05, 0, 0, 0.197, 0, 0, 0.025, 0.165]
URC-STTC-16PSK (7.0 dB)	[0.203, 0, 0.093, 0 0.102, 0, 0, 0.148, 0, 0, 0 0.055, 0.149, 0, 0, 0, 0.248]

Table 2.4: Subcode weighting coefficients of the IrCC encoder associated with URC-STTC-QPSK, URC-STTC-8PSK and URC-STTC-16PSK.

Component Code (Subcode)	Code Rate $\beta_i, i = [1, 2, \dots, 17]$
1	$\beta_1=0.10$
2	$\beta_2=0.15$
3	$\beta_3=0.20$
4	$\beta_4=0.25$
5	$\beta_5=0.30$
6	$\beta_6=0.35$
7	$\beta_7=0.40$
8	$\beta_8=0.45$
9	$\beta_9=0.50$
10	$\beta_{10}=0.55$
11	$\beta_{11}=0.60$
12	$\beta_{12}=0.65$
13	$\beta_{13}=0.70$
14	$\beta_{14}=0.75$
15	$\beta_{15}=0.80$
16	$\beta_{16}=0.85$
17	$\beta_{17}=0.90$

Table 2.5: List of the component (subcode) rates for the IrCC code having 17 components (subcodes).

2.3.2.2 Performance of IrCC-URC-STTC-MPSK coding scheme

Upon employing the IrCC weighting coefficients listed in Table 2.4, we can now evaluate the BER-performance of our coding schemes, namely of IrCC-URC-STTC-QPSK, IrCC-URC-STTC-8PSK and IrCC-URC-STTC-16PSK, which rely on different modulation arrangements, such as QPSK, 8PSK and 16PSK, as shown in Figure 2.16. Observe in Figure 2.16 that our Monte-Carlo simulation results substantiate the predictions obtained by using the EXIT-charts of Figure 2.15, as we illustrated earlier in Section 2.3.2.1 by the example of the IrCC-URC-STTC-QPSK coding scheme. For the scenarios of employing 8PSK and 16PSK, the IrCC coefficients and the corresponding 'turbo-cliff' SNRs facilitating a vanishingly low BER are summarised in Table 2.4, which were obtained by our EXIT-chart based design, .

Importantly, the value of the 'turbo-cliff' SNR given in Table 2.4 indicates that as we inferred from our EXIT-chart analysis, once the SNR value exceeds this value, the BER/FER of the coding scheme is expected to become infinitesimally low. Indeed, the performance prediction provided by the EXIT-chart curves, which were created by using the procedure briefly summarised in Section 2.3.1, is satisfied by our simulation results presented in Figure 2.16. Explicitly, the BER of the system supported by our coding schemes, such as the IrCC-URC-STTC-QPSK, IrCC-URC-STTC-

8PSK and IrCC-URC-STTC-16PSK arrangements, drops to a value below 10^{-6} , when the SNR value exceeds the corresponding turbo-cliff SNR.

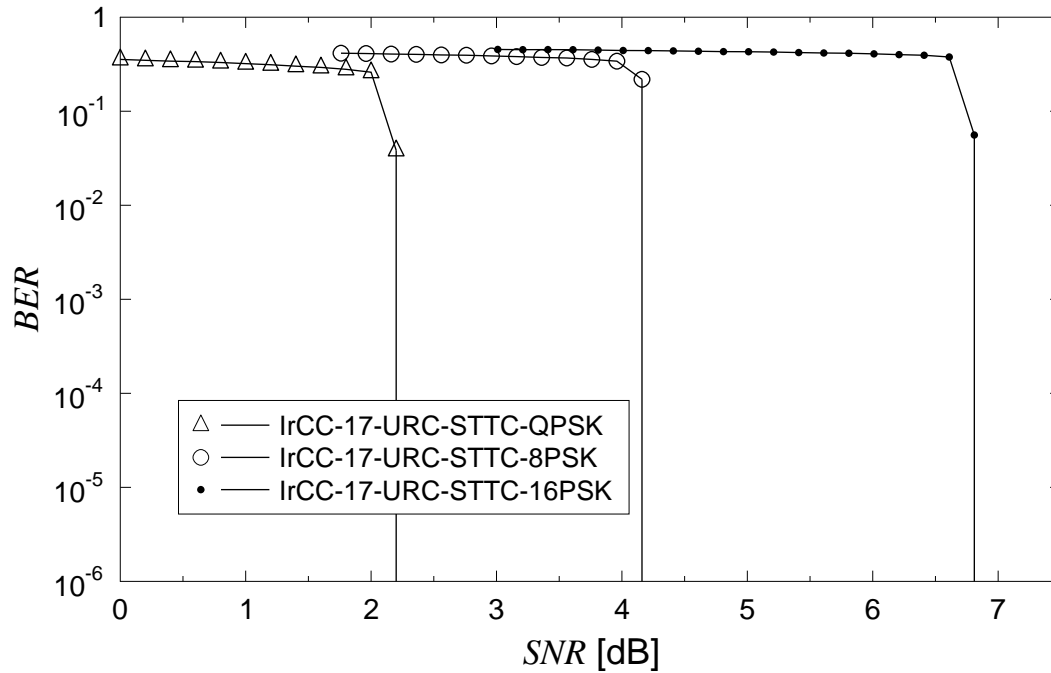


Figure 2.16: BER performance of IrCC-URC-STTC_{2×1}-MPSK corresponding to different modulation schemes, namely QPSK, 8PSK and 16PSK over Rayleigh small-scale fading channel, where the coding rate $R_c = 0.5$ and the frame length $N = 10^5$ are employed, while the weighting coefficients of the IrCC are given in Table 2.4.

Moreover, in order to apply our near-capacity coding schemes in practical systems [168], it is necessary to investigate the performance of these schemes when different transmission frame lengths are employed. Figure 2.17 characterises the performance of our IrCC-URC-STTC_{2×1}-QPSK scheme, when using different frame lengths of $N = \{112, 500, 1000, 1500, 2000, 8688, 120\,000\}$ bits. Observe from Figure 2.17 that as expected, the performance of the coding scheme degrades, when the frame length is reduced. Additionally, it was found that at a frame length of $N \leq 2000$ bits, the coding scheme employing 17 IrCC component codes would exhibit a poorer performance than the coding scheme that invokes only a single IrCC component code. This suggests that one-component IrCC encoder should be used, when the frame length is reduced to a value below a certain threshold, such as $N \leq 2000$ bits.

For the sake of characterising the relationship of the coding gain versus the interleaver length, when different numbers of iterations are employed at the receiver side, we compare the FER-performance corresponding to different configurations determined by parameters, namely the frame length, the number of the inner iterations and the number of outer iteration, at the same value of FER, say $FER = 10^{-4}$. As a result, we have the comparison of coding gain versus interleaver

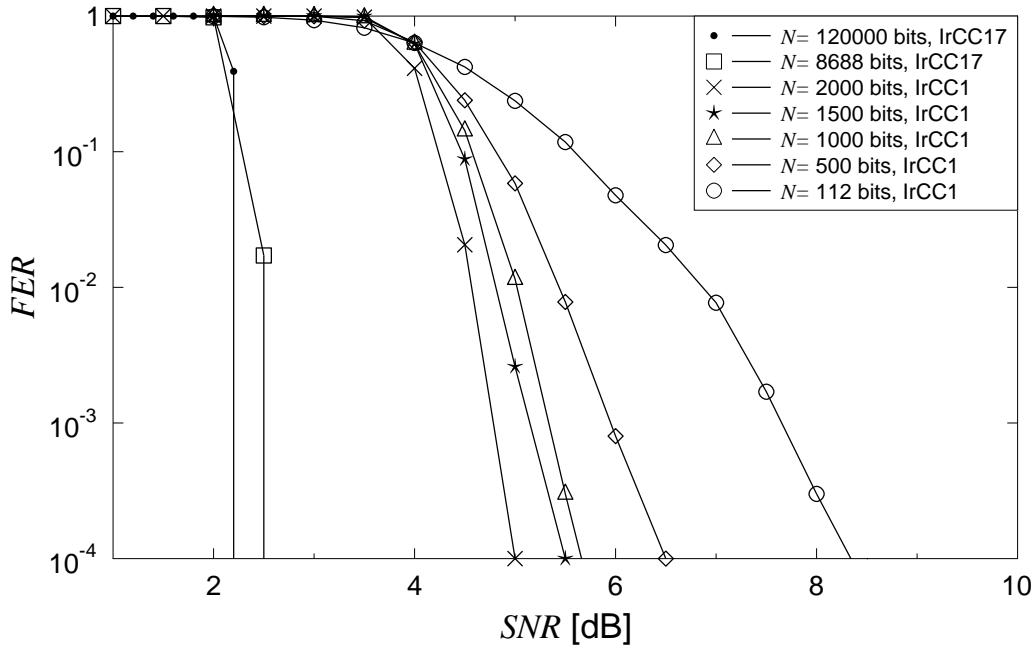


Figure 2.17: FER performance of IrCC-URC-STTC_{2×1}-QPSK corresponding to the frame length of $N = 112, 500, 1000, 1500, 2000, 8688$ and $120\,000$ bits, when communicating over Rayleigh fading channel.

length plotted in Figure 2.18. Note that we conceive a concept of referenced coding gain by referring to the zero-coding-gain corresponding frame length of $N = 112$.

2.3.3 IrCC-URC-MPSK coding scheme

In this section, we invoke our design principle summarised in Section 2.3.1 for conceiving a near-capacity IrCC-URC-MPSK scheme, which may be used in a transmission system portrayed in Figure 2.19. At the transmitter side seen in Figure 2.19, an information frame of N bits are encoded by the IrCC encoder having a coding rate of R_c , in order to produce an out-put frame having a frame length of N/R_c bits. The frame is then interleaved before being encoded again by the URC encoder for providing a URC-encoder frame of the same length, which is N/R_c bits. The frame from output of the URC encoder is modulated by a modulation scheme employing η bits for representing a symbol, before transmitting to the receiver side, as seen in Figure 2.19. It can be inferred that the SNR and the E_b/N_0 of the system are related by:

$$SNR = E_b/N_0 \frac{N\eta}{R_c} \quad (2.36)$$

At the receiver side pictured in Figure 2.19, the signals received during a single frame duration are demodulated then decoded by the URC decoder before entering the iteratively decoding process of J iterations occurring between the inner decoder and the IrCC decoder. The inner decoder com-

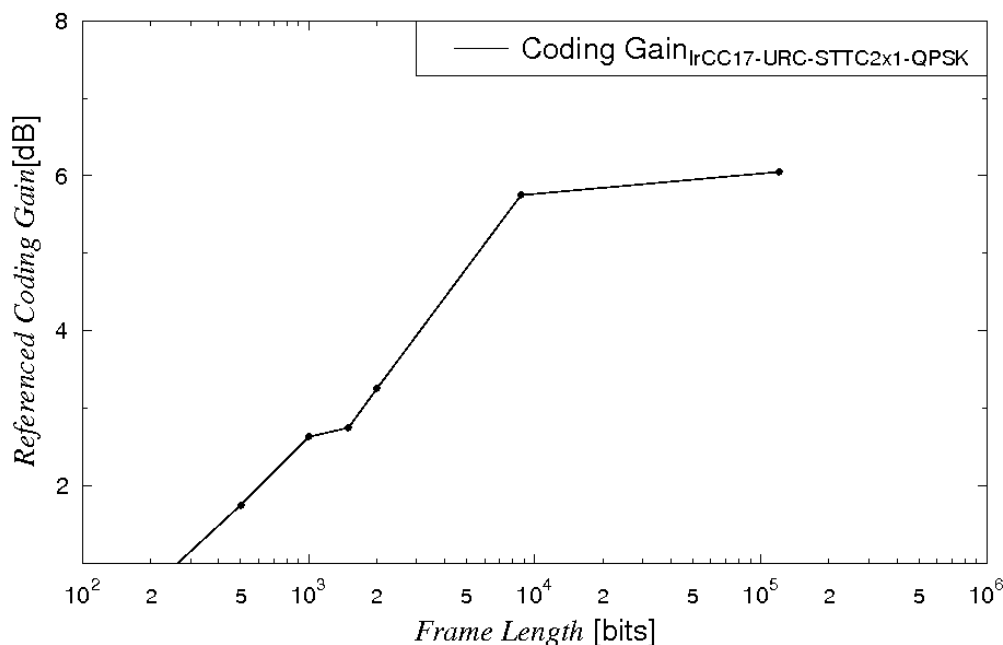


Figure 2.18: Coding gain-versus-delay comparison for IrCC-URC-STTC_{2×1}-QPSK scheme communicating over uncorrelated Rayleigh fading channel at an $FER = 10^{-4}$ and $R_c = 0.5$, when considering different frame length of $N = [112, 500, 1000, 1500, 2000, 8688, 120000]$ bits, while employing different numbers $I = 3$ and $J = 24$, which represents the number of the inner iterations and the outer iterations, respectively.

ponent is an amalgamated arrangement comprising the demodulation block and the URC decoder, as seen in Figure 2.19.

It should be noted that there is no iterations within the inner decoder component, since no improvement in the capacity is seen when performing iterative decoding at the inner decoder. Hence, our code design goal is to determine optimal IrCCs for different inner decoder components relying on different modulation schemes, namely BPSK, QPSK, 8PSK and 16PSK.

It is plausible that the more components used to form an IrCC encoder, the better its EXIT curve can match to the inner coding arrangement. This implies that the IrCC-URC-MPSK scheme can perform more closely the corresponding DCMC capacity. Thus, we also employ a more powerful IrCC code, which is constructed from 36 subcodes, in order to create an improved coding arrangement.

2.3.3.1 EXIT-charts matching and optimisation

As aforementioned at the beginning of this section, a near-capacity IrCC-URC-MPSK channel coding scheme [45] may be chosen for the sake of approaching the achievable channel capacity.

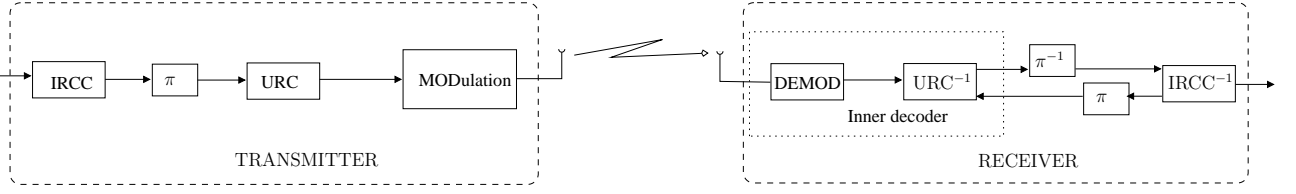


Figure 2.19: Architecture of a transmission system employing IrCC-URC-MPSK scheme.

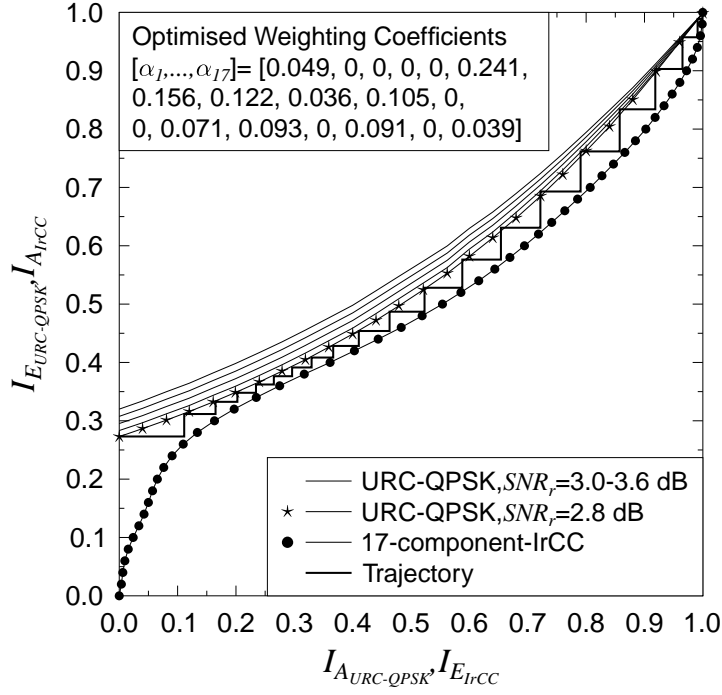


Figure 2.20: The EXIT curves of the inner decoder URC-QPSK and the outer decoder 17-component IrCC for a single transmission link along with the Monte-Carlo simulation based decoding trajectory, provided that $R_c = 0.5$.

For brevity and readability, we present the design procedure for Irregular Convolutional Code, a Unity-Rate Code and Quadrature Phase-Shift Keying (IrCC-URC-QPSK) using our generically applicable EXIT-chart aided method outlined in Section 2.3.1. The specific design procedure for IrCC-URC-QPSK are summarised as follows:

Step1: Create the EXIT curve of the inner decoder constituted by our Unity-Rate Code and Quadrature Phase-Shift Keying (URC-QPSK) scheme for different SNR_r values, namely $SNR_r = 3.6, 3.4, 3.2, 3.0$ and 2.8 dB for the 17-component IrCC, as seen in Figure 2.20, as well as namely $SNR_r = 2.7, 2.6, 2.5, 2.4$ and 2.3 dB for the 36-component IrCC, as seen in Figure 2.21;

Step2: We opt for the system throughput of $R = 1$, we fix the IrCC code rate to $R_c = 0.5$ and employ the EXIT curve matching algorithm of [158] for generating the optimised weighting coefficients $\alpha_i, i = 1, \dots, 17$ ($i = 1, \dots, 36$) of the 17 (36) different-rate component IrCC codes. The exact values of these coefficients for the 17-component IrCC code and the 36-component IrCC

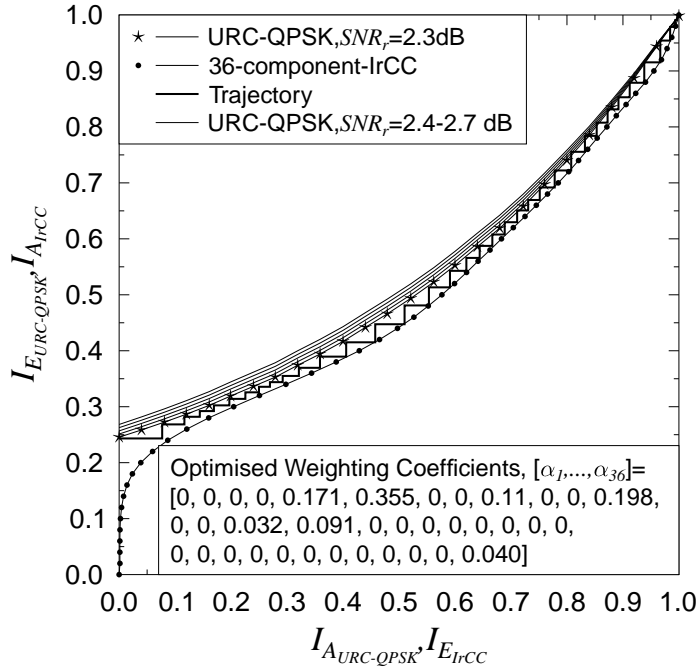


Figure 2.21: The EXIT curves of the inner decoder URC-QPSK and the outer decoder 36-component IrCC having the coding rate $R_c = 0.5$ for a single transmission link along with the Monte-Carlo simulation based decoding trajectory.

code) can be found in Figure 2.20 and Figure 2.21, respectively. More specifically, we opt for the set of codes facilitating decoding convergence to a vanishingly low BER at the lowest possible SNR_r , while ensuring that the Monte-Carlo simulation based decoding trajectory reaches the point of (1,1) at the top-right corner of the corresponding EXIT chart. This implies that a near-capacity performance can be achieved, as detailed in [45].

Having implemented the design steps mentioned above, we obtain the EXIT curves and the corresponding IrCC component-code weighting coefficients α_i , $i = 1, \dots, 17$ or $i = 1, \dots, 36$, as shown in Figure 2.20 or Figure 2.21. Again as partly detailed in [45], these weighting coefficients α_i determine the particular fraction of the input stream to be encoded by the i^{th} IrCC component code having a code rate of β_i , where the value of β_i for the 17-component IrCC and 36-component IrCC is given in Table 2.5 and Table 2.6, respectively. Similar to the condition of Equation (2.35) for the 17-component IrCC, the values of α_i and β_i for the 36-component IrCC also obey the following condition as:

$$R_c = \sum_{i=1}^{36} \alpha_i \beta_i. \quad (2.37)$$

The EXIT-chart results of Figure 2.20 (Figure 2.21) show that provided $J = 20$ ($J = 36$) iterations were affordable for the case of employing 17-component IrCC (36-component IrCC), the trajectory would reach the (1, 1) point in Figure 2.20 (Figure 2.21), which guarantees a vanishingly low BER .

Component Code (Subcode)	Code Rate $\beta_i, i = [1, 2, \dots, 36]$
1	$\beta_1=0.10$
2	$\beta_2=0.15$
3	$\beta_3=0.20$
4	$\beta_4=0.25$
5	$\beta_5=0.30$
6	$\beta_6=0.35$
7	$\beta_7=0.40$
8	$\beta_8=0.45$
9	$\beta_9=0.50$
10	$\beta_{10}=0.55$
11	$\beta_{11}=0.60$
12	$\beta_{12}=0.65$
13	$\beta_{13}=0.70$
14	$\beta_{14}=0.75$
15	$\beta_{15}=0.80$
16	$\beta_{16}=0.85$
17	$\beta_{17}=0.90$
18	$\beta_{18}=0.10$
19	$\beta_{19}=0.15$
20	$\beta_{20}=0.20$
21	$\beta_{21}=0.25$
22	$\beta_{22}=0.30$
23	$\beta_{23}=0.35$
24	$\beta_{24}=0.40$
25	$\beta_{25}=0.45$
26	$\beta_{26}=0.50$
27	$\beta_{27}=0.45$
28	$\beta_{28}=0.50$
29	$\beta_{29}=0.55$
30	$\beta_{30}=0.60$
31	$\beta_{31}=0.65$
32	$\beta_{32}=0.70$
33	$\beta_{33}=0.75$
34	$\beta_{34}=0.80$
35	$\beta_{35}=0.85$
36	$\beta_{36}=0.90$

Table 2.6: List of the component (subcode) rates for the IrCC code having 36 components (subcodes).

Again, we can utilise the area property of EXIT-charts [45, 157, 162], which states that the area under the normalised EXIT curve of an inner decoder component is approximately equal to the attainable channel capacity, provided that the channel's input symbols are equiprobable. Hence, we exploited the area property of EXIT-charts [157, 162] to determine the achievable DCMC capacities of the URC-QPSK and IrCC-URC-QPSK systems, which are quantified in Figure 2.22. It is seen in Figure 2.22 that the capacity of the URC-QPSK scheme almost coincides with the DCMC-QPSK curve. The numerical results of Figure 2.25 also show the attainable channel capacity improvements corresponding to $J = 1, 10, 20$ and 40 iterations. There is only a negligible further improvement for having $J = 40$ in comparison to $J = 20$. It is also demonstrated in Figure 2.22 that the IrCC-URC-QPSK scheme's capacity curve is only about $(2.8 - 1.8) = 1.0\text{dB}$ away from DCMC-QPSK capacity curve for $J = 20$.

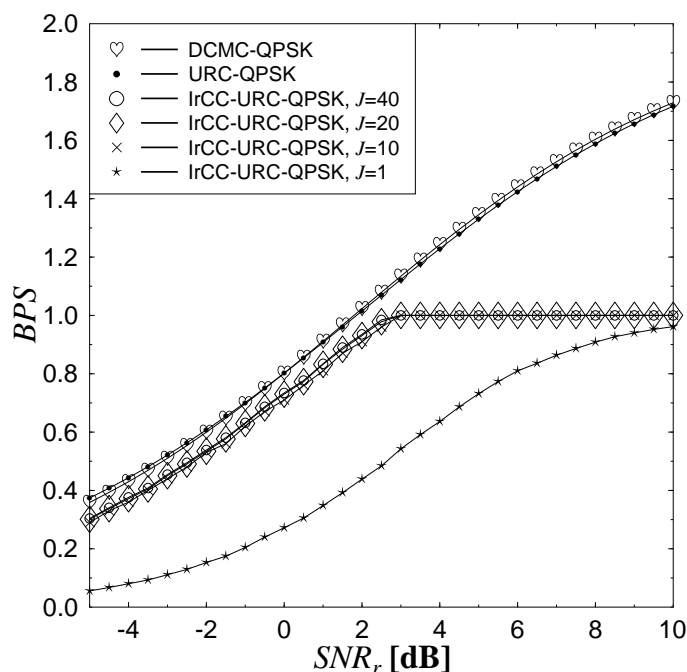


Figure 2.22: Achievable throughputs for the DCMC-QPSK, URC-QPSK and IrCC-URC-QPSK based systems, when communicating over Rayleigh small-scale fading channel.

We can further improve the performance of the IrCC-URC-MPSK by employing the IrCC codes consisting of 36 component codes. We aim to exploit the advantage of 36 component IrCC (36co-IrCC), which is capable of providing more flexible EXIT curve, so its EXIT curve match more closely to the EXIT curve of inner components than EXIT curve of 17 component IrCC (17co-IrCC). The similar manner for designing 17co-IrCC results in the EXIT chart drawn in Figure 2.21, where the 36co-IrCC-URC-QPSK scheme performs only about $(2.3 - 1.8) = 0.5\text{dB}$ away from DCMC-QPSK for $J = 40$.

We may replicate the same procedure, when considering other modulation schemes, namely

8PSK and 16PSK. As a result, the EXIT charts relating to the arrangements employing 8PSK and 16PSK modulation schemes are presented in Figure 2.23 and Figure 2.24, respectively. The weighting coefficients for the IrCC code in each modulation scheme are presented in the corresponding figures, namely in Figure 2.20, Figure 2.21, Figure 2.23 and Figure 2.24. For the sake of readability, those weighting coefficients are also listed in Table 2.7.

Inner arrangement (Turbo-cliff SNR)	Coefficients: $[\alpha_1, \alpha_2, \dots, \alpha_{17}]$
URC-QPSK (2.8 dB)	[0.049, 0, 0, 0, 0, 0.241, 0.156, 0.156, 0.122, 0.036, 0.105, 0, 0, 0.071, 0.093, 0, 0.091, 0, 0.039]
URC-STTC-8PSK (6.0 dB)	[0.062, 0, 0, 0, 0.247, 0.154, 0, 0, 0.041, 0.169, 0, 0.082, 0.049, 0, 0.090, 0.041, 0.064]
URC-STTC-16PSK (8.9 dB)	[0.022, 0, 0.202, 0, 0.116, 0.073, 0, 0.061, 0.151, 0, 0, 0, 0.202, 0, 0, 0.023, 0.145]
Inner arrangement (Turbo-cliff SNR)	Coefficients: $[\alpha_1, \alpha_2, \dots, \alpha_{36}]$
URC-QPSK (2.3 dB)	[0, 0, 0, 0, 0.071, 0.355, 0, 0, 0.11, 0, 0, 0.198, 0, 0, 0.032, 0.091, 0, 0, 0, 0, 0, 0, 0, 0, 0, 0, 0, 0, 0, 0, 0, 0, 0, 0, 0.04]
URC-8PSK (5.0 dB)	[0, 0, 0, 0.368, 0, 0, 0.072, 0.079, 0.096, 0, 0, 0.163, 0, 0, 0.09, 0, 0.08, 0, 0, 0, 0, 0, 0, 0, 0, 0, 0, 0, 0, 0, 0, 0, 0, 0, 0, 0.048]
URC-16PSK (8.5 dB)	[0, 0.1, 0.082, 0.078, 0.049, 0.053, 0.047, 0, 0.126, 0, 0, 0.099, 0, 0, 0.084, 0, 0.059, 0, 0, 0, 0, 0, 0, 0, 0, 0, 0, 0.104, 0, 0, 0, 0, 0, 0, 0, 0.052, 0.061]

Table 2.7: Subcode weighting coefficients of the IrCC17 and IrCC36 encoders corresponding to different inner components, namely URC-QPSK, URC-8PSK and URC-16PSK, when communicating over Rayleigh small-scale fading channel. Both the IrCC17 and IrCC36 have the same coding rate of $R_c = 0.5$.

2.3.3.2 Performance of IrCC-URC-MPSK coding scheme

The simulation results seen in Figure 2.25 supports the accuracy of our EXIT chart analysis presented in Figure 2.20, where $J = 20$ steps are required for the trajectory reaching the (1,1) corner at the $SNR_r = 2.8$ dB. In fact, when employing $J = 20$ iterations between the IrCC and URC components, the IrCC-URC-QPSK channel coding scheme has a vanishingly low BER for SNRs in excess of 2.8dB, provided that the transmission frame length is sufficiently high, say $N = 10^5$

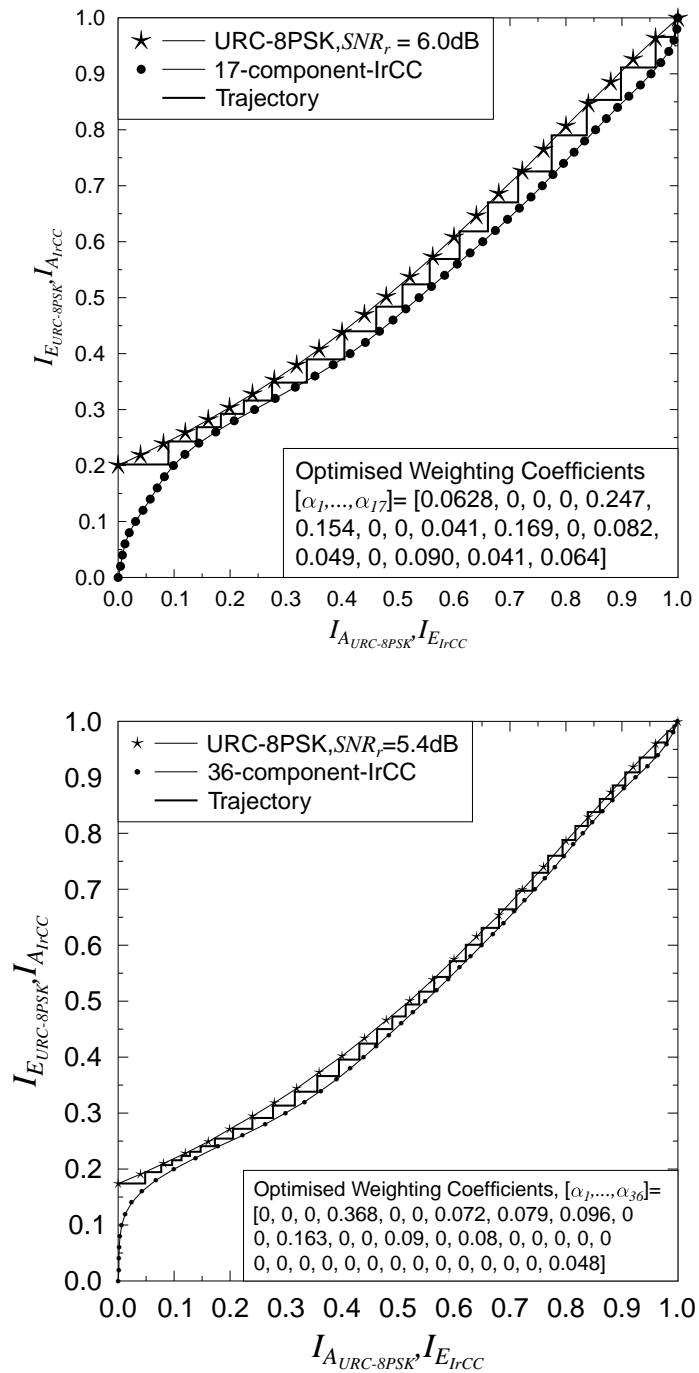


Figure 2.23: EXIT charts for the 17co-IrCC-URC-8PSK coding scheme and the 36co-IrCC-URC-8PSK coding scheme at the $SNR_r = 6.0$ dB and $SNR_r = 5.4$ dB, respectively. The same coding rate $R_c = 0.5$ is chosen, and the EXIT curves are obtained in Rayleigh small-scale fading channel.

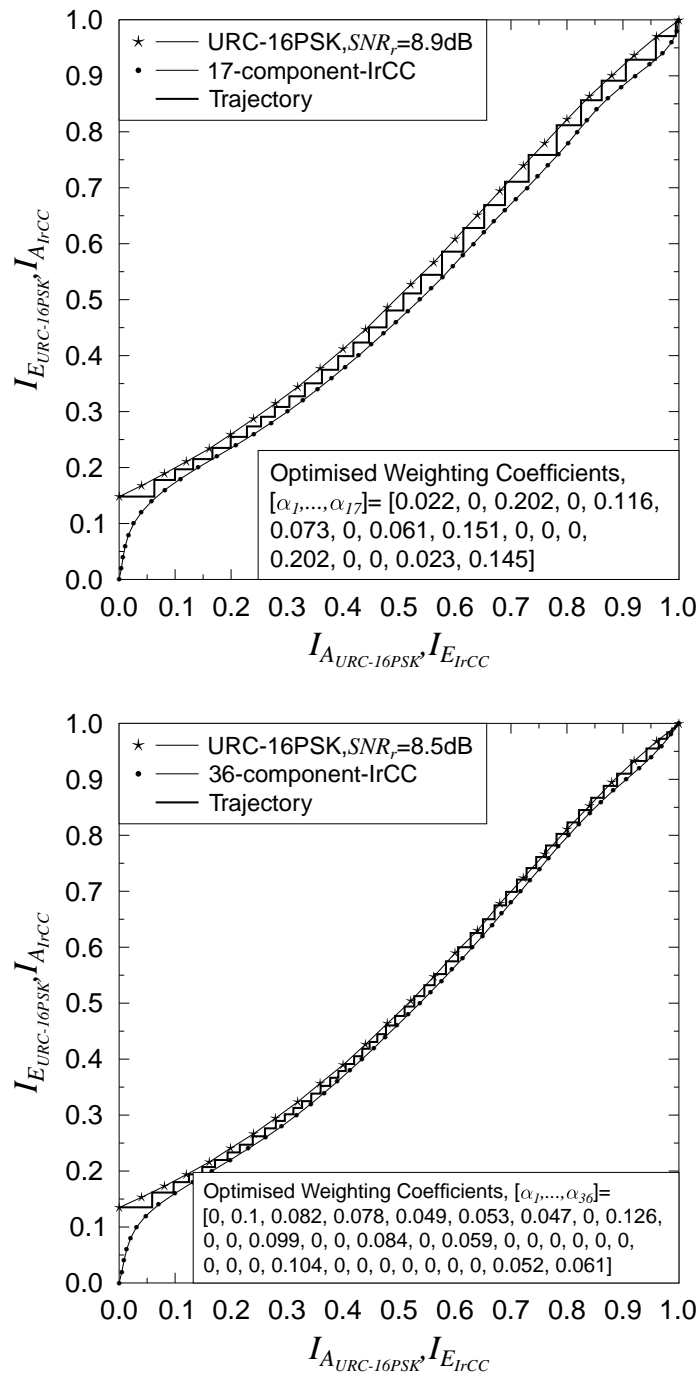


Figure 2.24: EXIT chart for the 17co-IrCC-URC-16PSK coding scheme and the 36co-IrCC-URC-16PSK coding scheme at the $SNR_r = 8.9$ dB and $SNR_r = 8.5$ dB, respectively. The same coding rate $R_c = 0.5$ is chosen, and the EXIT curves are obtained in Rayleigh small-scale fading channel.

bits, as seen in Figure 2.25.

At this stage we also define the relaying-aided pathloss-reduction instituted by the corresponding reduced-distance. Naturally, this pathloss-reduction becomes unity for each direct source-to-destination link [169]. We also observe from Figure 2.25 that as expected, a shorter frame length results in an improved FER performance, hence to strike a compromise, we may opt for a frame size of $N = 10^4$ bits for the system, where FER-performance is more important than BER-performance. In contrast, in the system, where BER-performance is paid more attention, the system duly opts for employing a frame size of $N = 10^5$ bits for the sake of maximising the system's BER-performance.

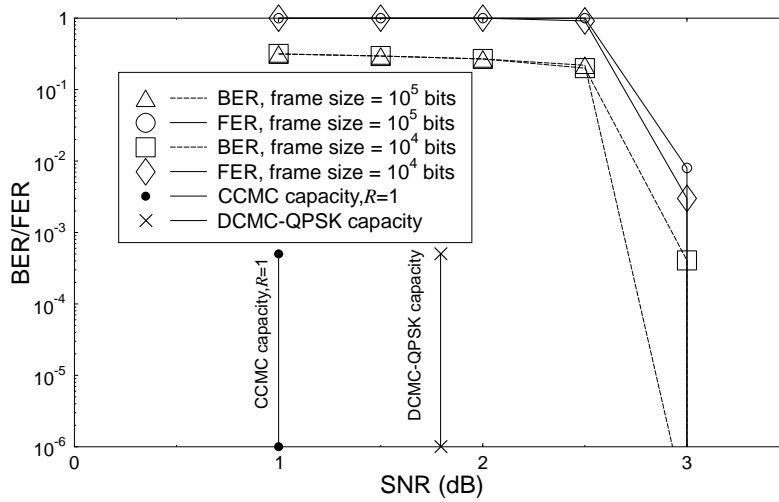


Figure 2.25: Performance of the IrCC17-URC-QPSK scheme under Rayleigh small-scale fading conditions, corresponding to different frame lengths, namely $N = 10^4, 10^5$. The scheme is relied on IrCC17 employing the coding rate $R_c = 0.5$ and having the weighting coefficients given in Figure 2.24.

For further insight, we make a comparison in the performance of IrCC-URC-MPSK in the case of employing 17co-IrCC and that of using 36co-IrCC. As a benefit of having more component codes in 36co-IrCC, the EXIT curve of 36co-IrCC is capable of matching better to the EXIT curve of the inner component, which is URC-xPSK, as seen in Figures 2.20, 2.21, 2.23 and 2.24. For example, the better matching can be seen in Figure 2.21 and Figure 2.20, where the gap between the EXIT curve of 36co-IrCC and the EXIT curve of the inner component URC-QPSK is smaller than that between the EXIT curve of 17co-IrCC. As a result, 36co-IrCC exhibits a better performance in comparison to 17co-IrCC, as presented in Figure 2.26, where an average improvement of 0.5 dB is exhibited. However, it should be noted that the better performance of coding scheme employing 36co-IrCC can be achieved with a cost of a more complexity, which is 20 extra iterations in the case of IrCC-URC-QPSK coding scheme.

Bearing in mind the improved performance of the coding scheme employing 36co-IrCC, we favour 36co-IrCC in forming the non-coherent coding scheme of IrCC-URC-DMPSK, which is

presented in the next section, Section 2.3.4.

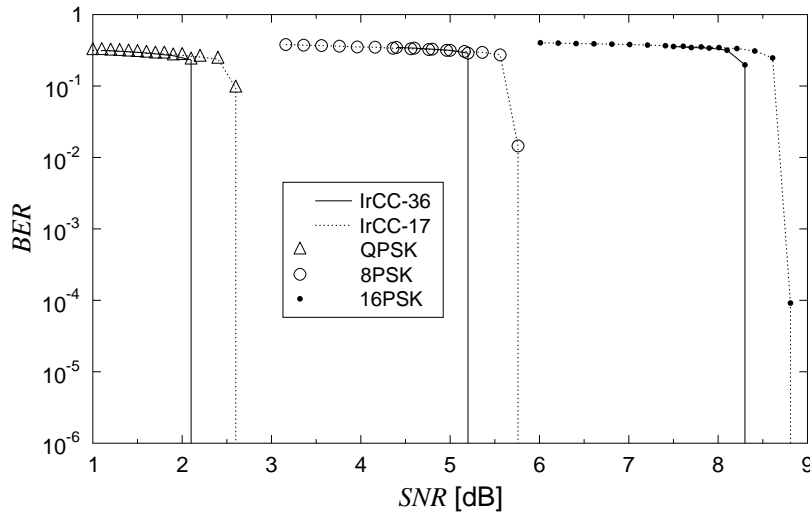


Figure 2.26: Comparison in performance corresponding to the employment of 36co-IrCC and 17co-IrCC in the IrCC-URC-MPSK arrangement, when considering different modulation schemes, namely QPSK, 8PSK and 16PSK over Rayleigh small-scale fading channel. The coding rate of $R_c = 0.5$ and the frame length of $N = 10^5$ are set for this comparison, while the weighting coefficients of 17co-IrCC and 36co-IrCC are listed in Table 2.7.

2.3.4 IrCC-URC-DMPSK coding scheme

Again, the EXIT-chart based design guidelines given in Section 2.3.1 is invoked for facilitating the near-capacity coding design of the IrCC-URC-Multiple-Symbol Differential Detection aided Differential M-ary Phase-Shift Keying (IrCC-URC-MSDD-aided-DMPSK) scheme, which may be employed in the system illustrated in Figure 2.27.

In the system described by Figure 2.27, the transmitted frame of N bits at the transmitter side is first encoded by the IrCC encoder having the coding rate R_c , in order to produce an egress frame of N/R_c bits. The egress frame is mixed by the first interleaver π_1 before being encoded by the URC in order to introduce the resultant frame of the same size. The frame at the out-put of the URC encoder is again blended by the second interleaver π_2 before being modulated by the differential modulation for transmitting over wireless channel, as seen in Figure 2.27.

At the receiver side of the system portrayed in Figure 2.1.2.1, the signals received from antenna during a single frame duration is first processed in I inner iterations by iteratively performing two steps, namely conducting demodulation using the MSDD method and decoding at the URC decoder. Once having performed the I inner iterations, the resultant frame is fed into J so-called outer iterations. It should be noted that each of J outer iterations contains I inner iterations. As

a result, the receiver illustrated by Figure 2.1.2.1 has to perform totally $I \times J$ inner iterations, in order to retrieve a frame of the received information.

Our goal for designing the IrCC-URC-MSDD-aided-DMPSK scheme is to determine the optimal values of I inner iterations, J outer iterations as well as weighting coefficients of IrCC. In particular, the EXIT-chart tool is employed for formatting the IrCC encoder as well as determining the D-DCMC capacity of the non-coherent inner most component of the coding scheme, namely the Differential M-ary Phase Shift Keying (DMPSK) and the Unity Rate Coded Differential M-ary Phase Shift Keying (URC-DMPSK).

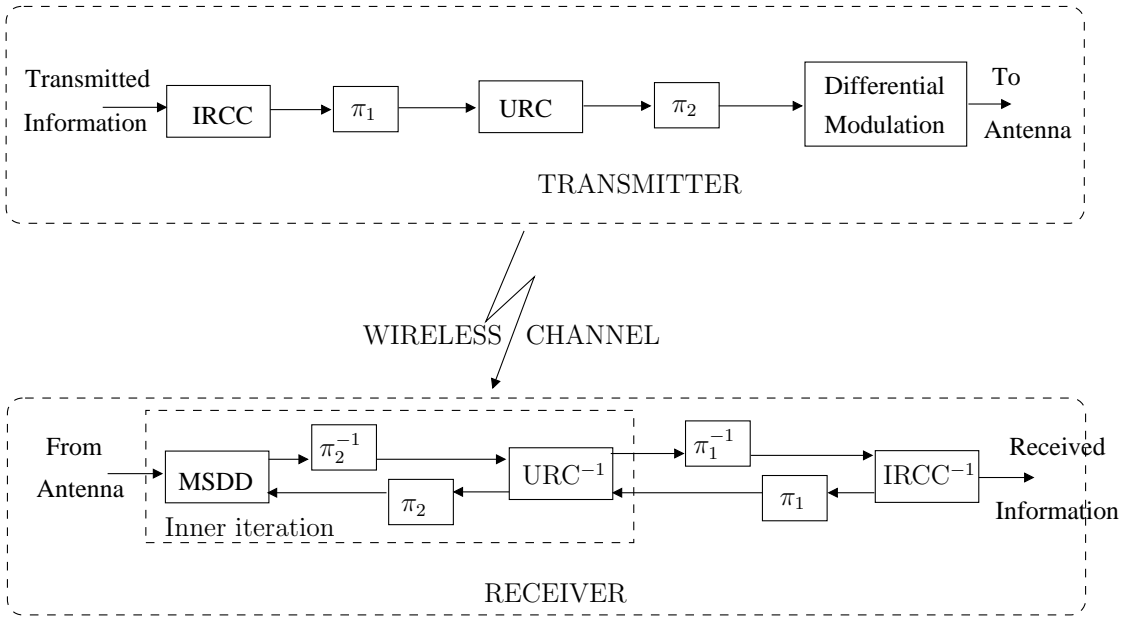


Figure 2.27: System architecture of the IrCC-URC-MSDD-aided-DMPSK scheme.

2.3.4.1 EXIT-chart design for IrCC-URC-MSDD-aided-DMPSK

Similar to the manner used to designing the coherent scheme in Section 2.3.3, for the sake of simplicity, we present our generic design procedure for the specific example of IrCC-URC-Differential Binary Phase Shift Keying (IrCC-URC-DBPSK) associated with MSDD $N_w = 4$ using our generically applicable EXIT-chart aided method, which is summarised as follows:

Step1: We optimise the number I of inner iterations between URC and MSDD-aided DEModulation (MSDD-aided-DEM), which is also similar to the inner iteration between URC and STTC detailed in Section 2.3.2. We first utilise the useful property of EXIT charts [157], which may be stated that the area under the EXIT curve of an inner decoder component is approximately equal to the attainable channel capacity, provided that the channel's input symbols are equiprobable. Hence we exploited the area property of EXIT-charts [157] to determine the achievable capacities of the URC-MSDD-aided-DBPSK(DQPSK) and IrCC-URC-MSDD-aided-DBPSK(DQPSK) systems, which

are quantified in Figure 2.28. It is seen in Figure 2.28 that the capacity curve of the URC-MSDD-aided-DBPSK(DQPSK) scheme approaches that of the MSDD-aided-DBPSK(DQPSK) arrangement, when $I > 1$ inner iterations are employed for the composite URC-MSDD-aided-DBPSK(DQPSK) decoder. It is also demonstrated in Figure 2.28 that the attainable capacity improvement becomes negligible for $I > 2$. Therefore, we fix the number of inner iterations to $I = 2$ thereafter.;

Step2: Having fixed the optimal number $I = 2$ of inner iteration, we can create the EXIT curve of the inner decoder component constituted by our URC-MSDD-aided-DBPSK scheme for different SNR_r values, namely from 2.3 dB to 3.0 dB for DBPSK scheme and from 5.2 dB to 6.0 dB for DQPSK scheme with an increasing step of 0.1 dB, as seen in Figure 2.29;

Step3: We then fix the IrCC code rate $R_c = 0.5$ and employ the EXIT curve matching algorithm of [170] for generating the optimised weighting coefficients $\alpha_i, i = 1, \dots, 36$, of the 36 different-rate component IrCC codes. More specifically, we opt for the set of codes facilitating decoding convergence to a vanishingly low BER at the lowest possible SNR_r , while ensuring that the Monte-Carlo simulation based decoding trajectory reaches the point of (1,1) at the top-right corner of the corresponding EXIT chart. This implies that a near-capacity performance can be achieved, as detailed in [45]. As a result, we obtained the weighting coefficients of the IrCC associated with SNR_r value, as noted in Figure 2.29. Then, these parameters allowed us to generate the respective trajectories, which exhibits the number J of the outer iterations between IrCC and the amalgamated arrangement URC-MSDD-aided-Q(B)PSK, as seen in Figure 2.29.

As a result of having implemented the design steps mentioned above, we obtain the EXIT curves and the corresponding IrCC component-code weighting coefficients $\alpha_i, i = 1, \dots, 36$, as shown in Figure 2.29. Again as detailed in [45], these weighting coefficients α_i determine the particular fraction of the input stream to be encoded by the i^{th} IrCC component code having a code rate of α_i . The EXIT-chart results show that provided a sufficiently high number of iterations, say J is carried out between the IrCC decoder and the composite URC-MSDD-aided-DBPSK decoder, the Monte-Carlo simulation based decoding trajectory would reach the (1,1) point in Figure 2.29, which guarantees a vanishingly low BER .

The numerical results of Figure 2.28 also show that for a sufficiently high number of say $J \geq 30$ outer iterations, the distance between the capacity curve of the IrCC-URC-MSDD-aided-DBPSK(DQPSK) scheme and that of the DCMC-MSDD-aided-DBPSK(DQPSK) arrangement is less than 0.5 dB.

2.3.4.2 Performance of IrCC-URC-DMPSK coding scheme

Setting the parameters determined in the design procedure, namely IrCC coding coefficients as given in Figure 2.29, the number of inner iterations $I = 2$, the number of outer iterations $J = 30$, we can get the performance of the coding scheme by running corresponding simulations. More

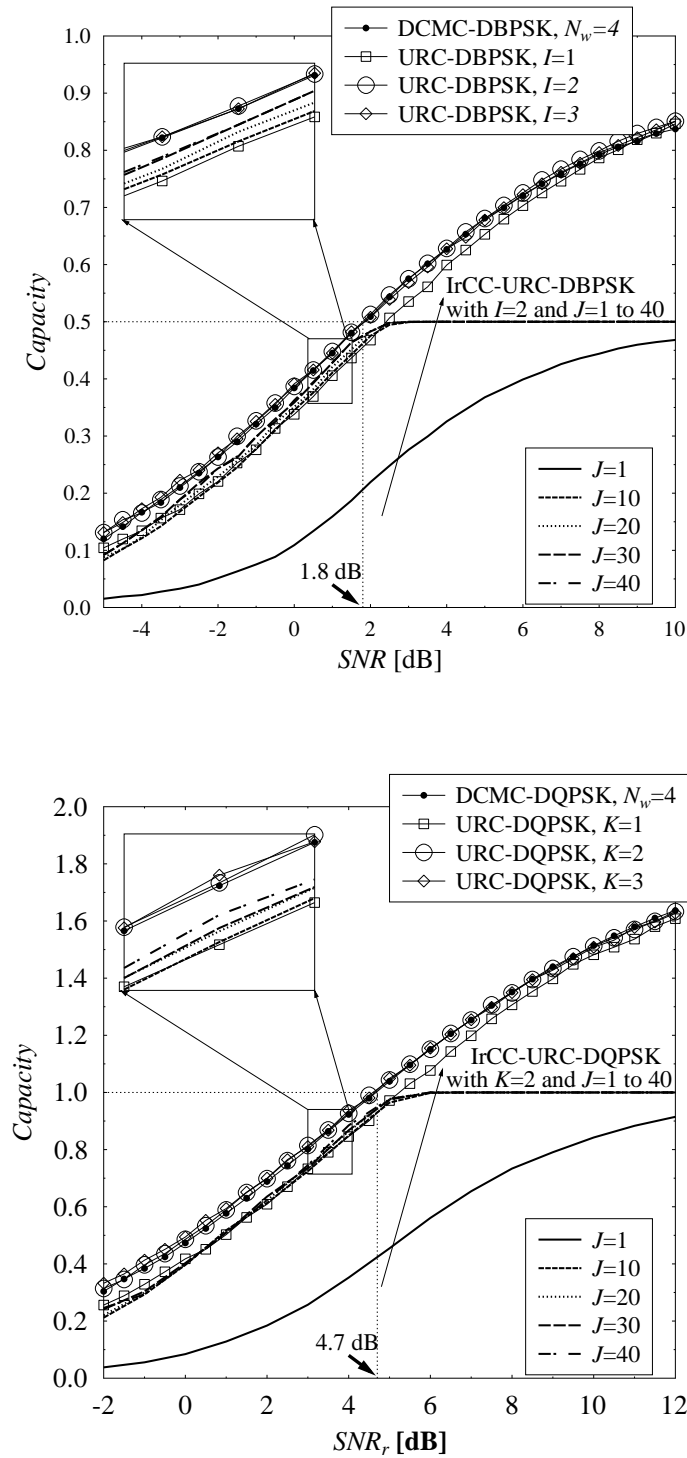


Figure 2.28: Channel capacity comparison for the MSDD-aided-DBPSK(DQPSK), URC-MSDD-aided-DBPSK(DQPSK) and IrCC-URC-MSDD-aided-DBPSK(DQPSK) based systems when $f_d = 0.03$.

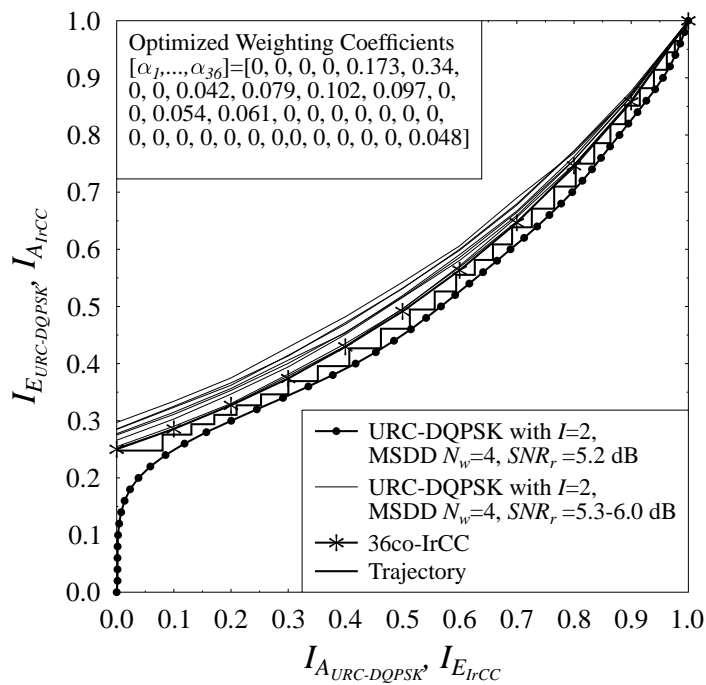
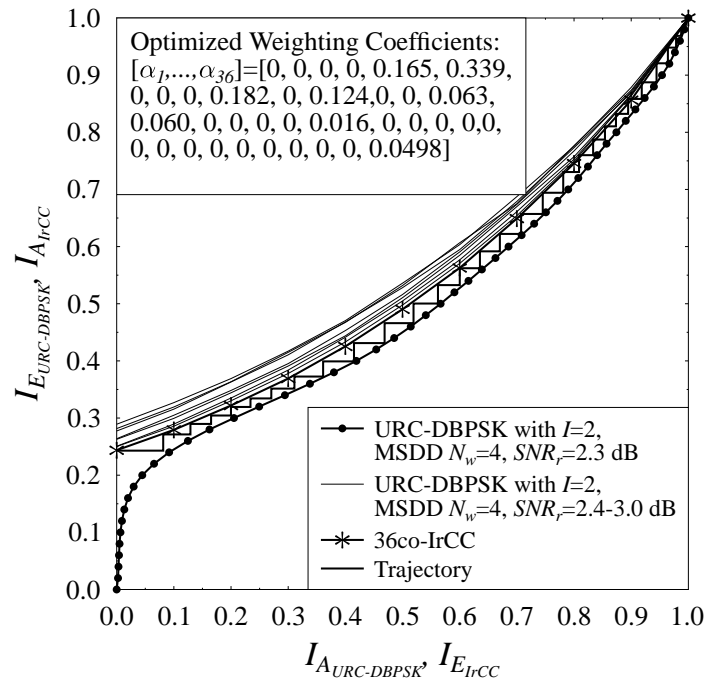


Figure 2.29: The EXIT curves of the inner decoder URC-MSDD-aided-DBPSK(DQPSK) and the outer decoder IrCC along with the Monte-Carlo simulation based decoding trajectory when $f_d = 0.03$.

specifically, the FER/BER-performance of the IrCC-URC-DBPSK(DQPSK) seen in Figure 2.33 is in line with our EXIT chart analysis detailed in Section 2.3.4.1. For example, once the outer iterations between the IrCC and URC components is set to $J = 30$, the IrCC-URC-MSDD-aided-DBPSK channel coding scheme has a vanishingly low BER for SNRs in excess of 5.1 dB, provided that the transmission frame length is greater or equal to $N = 10^6$. However, a negligible performance's degradation of 0.1 dB is recorded, when frame length of 10^5 symbols is applied in the system.

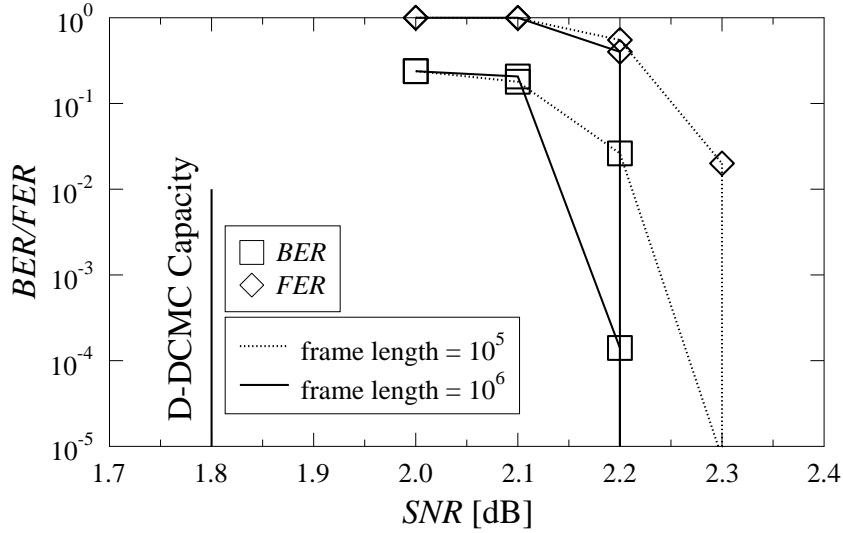


Figure 2.30: The performance of the proposed IrCC-URC-MSDD-aided-DBPSK scheme in the small-scale Rayleigh fading channel with $f_d = 0.03$.

2.4 The employment of sub-frames

In the small-scale fading channel, the transmitter can send data at the rate of $R < C|_h$, while maintaining an arbitrarily small error probability, but this idealised performance cannot be maintained for block fading channel [151]. Let us take one of the near-capacity coding scheme designed in previous sections to illustrate the scenario. Accordingly, the performance of the proposed IrCC-URC-MSDD-aided-DBPSK(DQPSK) scheme recorded for transmission over the block Rayleigh fading channel is presented in Figure 2.32. However, in the practical system [165, 166], each channel-encoded frame tends to be transmitted in an N_{sub} number of sub-frames, where the average SNR_r of (2.33) may be formulated as:

$$SNR_r = \frac{E[|h_s|^2]}{N_0} = \frac{\sum_{i=1}^{N_{sub}} |h_{s,i}|^2 / N_{sub}}{N_0}, \quad (2.38)$$

with $h_{s,i}$ representing the block shadow fading corresponding to the i^{th} sub-frame of the channel-encoded frame.

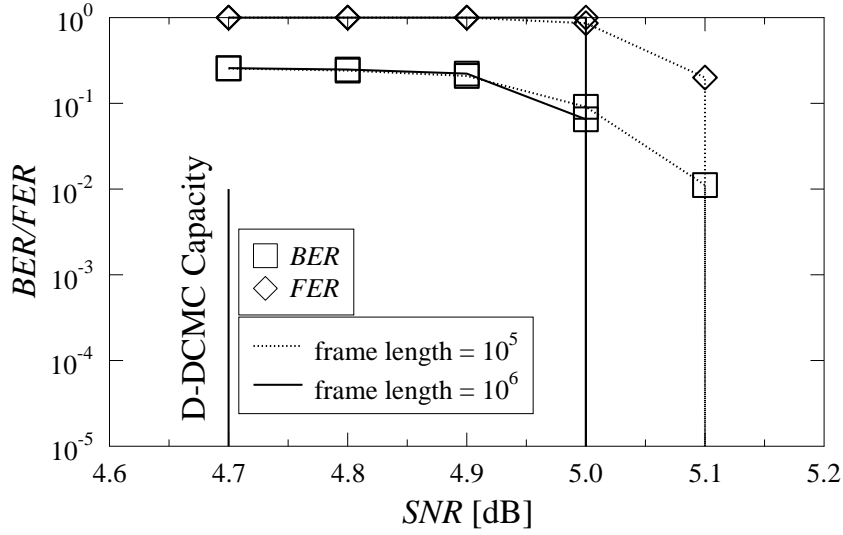


Figure 2.31: The performance of the proposed IrCC-URC-MSDD-aided-DQPSK scheme in the small-scale Rayleigh fading channel with $f_d = 0.03$.

It is expected that by allocating each encoded frame into subframes [165, 166], the diversity degree of the transmission link is increased, thereby improving the performance of the transmission link over the block fading channel. Let us continue by employing IrCC-URC-MSDD-aided-DBPSK coding scheme, in order to demonstrate the benefit of the employment of subframes. More specifically, it can be seen in Figure 2.33 that while the number N_{sub} of the sub-frames is increasing from $N_{sub} = 1$ to $N_{sub} = 10^4$, the performance of the IrCC-URC-MSDD-aided-DBPSK scheme recorded for transmission over a channel, where both the block shadow fading and the small-scale Rayleigh fading are taken into consideration, approaches that of the IrCC-URC-MSDD-aided-DBPSK scheme communicating over the small-scale Rayleigh fading channel.

2.5 Non-Coherent versus Coherent Near-Capacity Schemes

In order to answer the dilemma about whether the coherent system or non-coherent system would be favoured in a given scenario, we examine the effect of channel estimation error on the performance of the coherent system. Let us define θ as the normalised estimation accuracy, which can be determined by:

$$\theta = 100 \times \mathbb{E} \left[1 - \frac{||h| - |\hat{h}||}{|h|} \right], \quad (2.39)$$

where \hat{h} is the estimated value of the channel coefficient h . It should be noted that if we have $\frac{||h| - |\hat{h}||}{|h|} > 1$, the accuracy is equal to zero, $\theta = 0$. For the sake of readability, the estimated channel coefficient of \hat{h} is deemed to be formed by

$$\hat{h} = h + n_{est}, \quad (2.40)$$

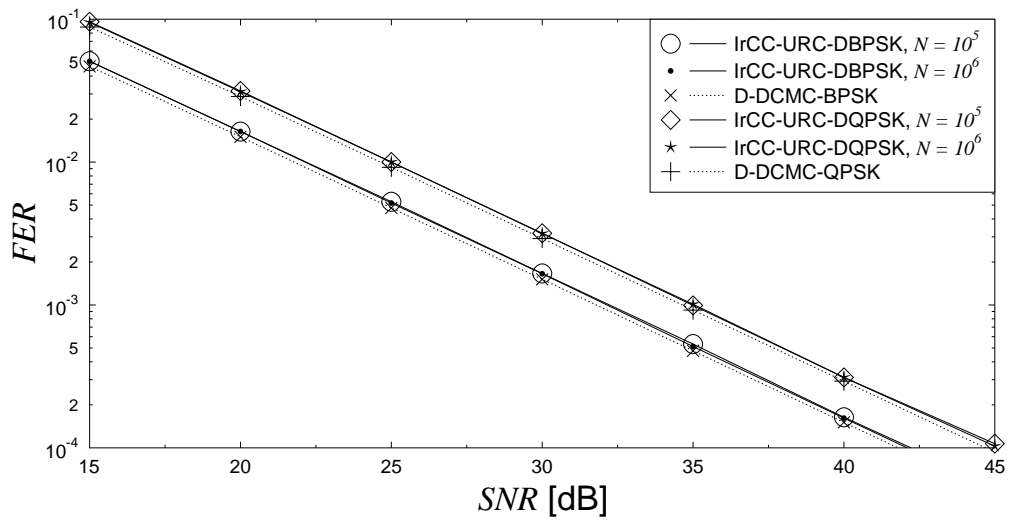


Figure 2.32: FER performance of IrCC-URC-MSDD-aided-DBPSK(DQPSK) in block Rayleigh fading channel.

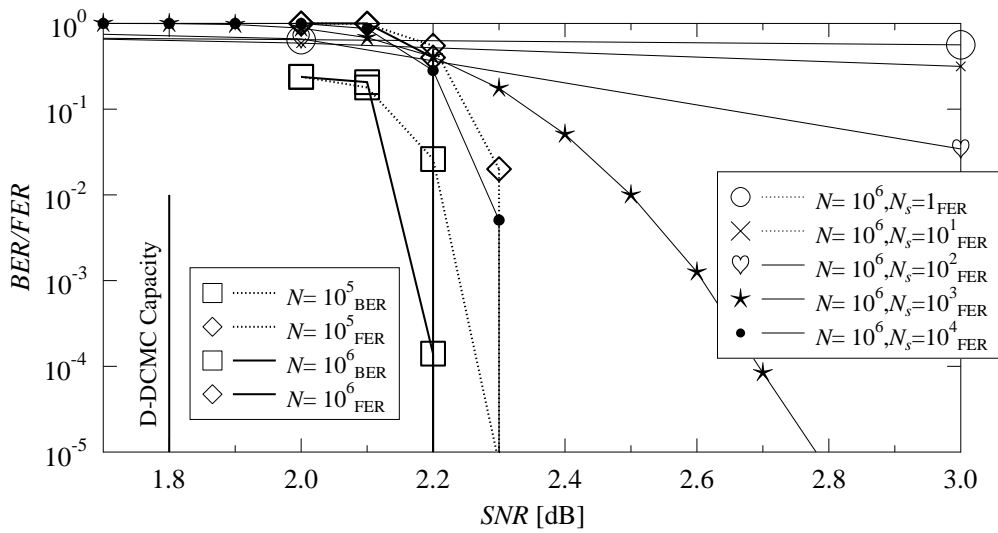


Figure 2.33: Performance of the proposed IrCC-URC-MSDD-aided-DBPSK scheme in the small-scale Rayleigh fading channel with $f_d = 0.03$ as well as in the block fading channel, the number of sub-frames ranging from $N_{sub} = 1$ to $N_{sub} = 10^4$.

where n_{est} is likened to the estimated noise springing from the inaccuracy of the channel estimator. We further consider the estimated noise of n_{est} as an AWGN process having a variance of $N_{0,est}/2$ per dimension at a nominal estimated Signal to Noise Ratio of SNR_{est} . Accordingly, as seen in Figure 2.34, the normalised channel estimation accuracy of θ given in (2.39) is plotted against different values of SNR_{est} .

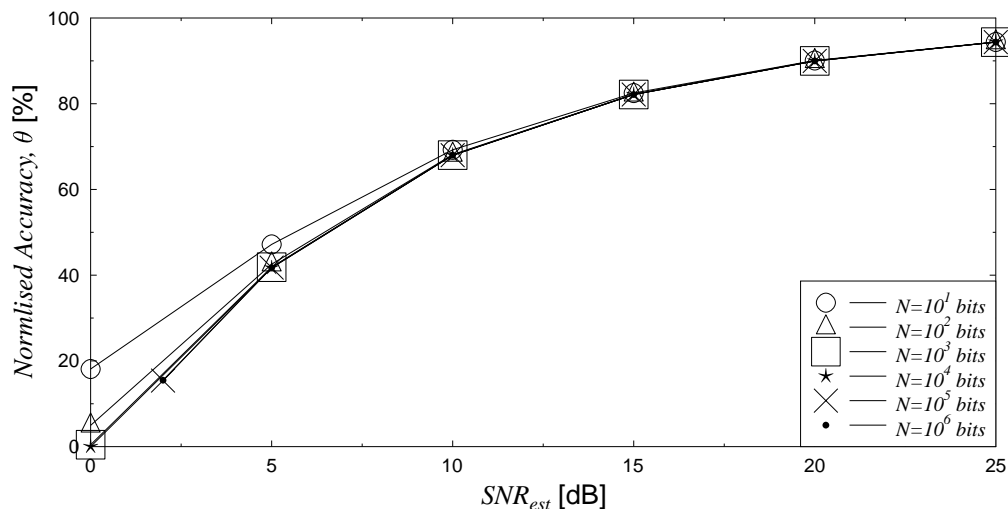


Figure 2.34: The normalised channel estimation accuracy of θ , when considering different frame lengths N ranging from $N = 10^1$ bits to $N = 10^6$ bits.

The benefit of introducing estimated Signal to Noise Ratio of SNR_{est} is that we can examine the performance's degradation of the coherent system employing a practical channel estimator, compared to the performance of the coherent system assuming that the channel state information is available at the receiver.

It can be inferred from Figure 2.34 that the value of SNR_{est} corresponding to a given value of the channel estimation accuracy can be calculated. For example, Table 2.8 lists the values of SNR_{est} associating with different values of normalised channel estimation accuracy, namely from 10% to 100%.

Employing the channel estimation noise conventionally corresponding to SNR_{est} given by Table 2.8, we can have the corresponding performance of the system, which is IrCC-URC-QPSK, when different levels of the channel estimation accuracy are supported by the channel estimator. As seen in Figure 2.35, the performance's degradation increases to about 5 dB when the accuracy reaches the threshold of 50%. A significant degradation of more than 20 dB in the system's performance is recorded, once the accuracy becomes smaller than 40%.

In order to provide a comparative picture about the pros-and-cons of the coherent and non-coherent system, the performance comparison of the IrCC-URC-QPSK scheme in different regimes, namely the non-coherent regime and the coherent regime taking into consideration of the channel

Normalised channel estimation accuracy, θ [%]	SNR_{est} [dB]
10%	1.676
20%	2.518
30%	3.554
40%	4.783
50%	6.276
60%	8.127
70%	10.571
80%	14.027
90%	20.015
100%	100.667

Table 2.8: SNR_{est} values corresponding to different values of the normalised channel estimation accuracy θ ranging from $\theta = 10\%$ to $\theta = 100\%$.

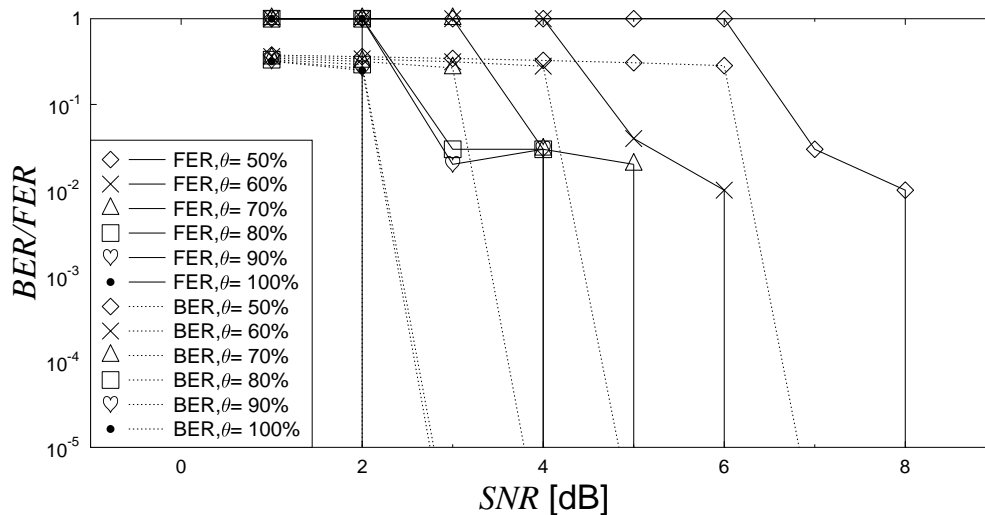


Figure 2.35: Performance of IrCC-URC-QPSK, with different accuracy levels of the normalised channel estimation, when communicating over the small-scale Rayleigh fading channel.

estimator, is characterised in Figure 2.35. In Figure 2.36, the comparison is presented for the IrCC-URC-QPSK based systems, all of which employ the same frame length of $N = 10^5$. It can be seen in Figure 2.36 that a degradation of 3.1 dB in FER-performance is exhibited, when we change from employing the coherent system relying on IrCC-URC-QPSK coding scheme to exploiting the non-coherent system basing on IrCC-URC-MSDD-aided-DQPSK coding scheme. As also seen in Figure 2.36, the performance of the system employing IrCC-URC-DQPSK coding scheme is equivalent to that of IrCC-URC-QPSK, provided that the accuracy of the channel estimator is capable of achieving the value of $\theta = 60\%$.

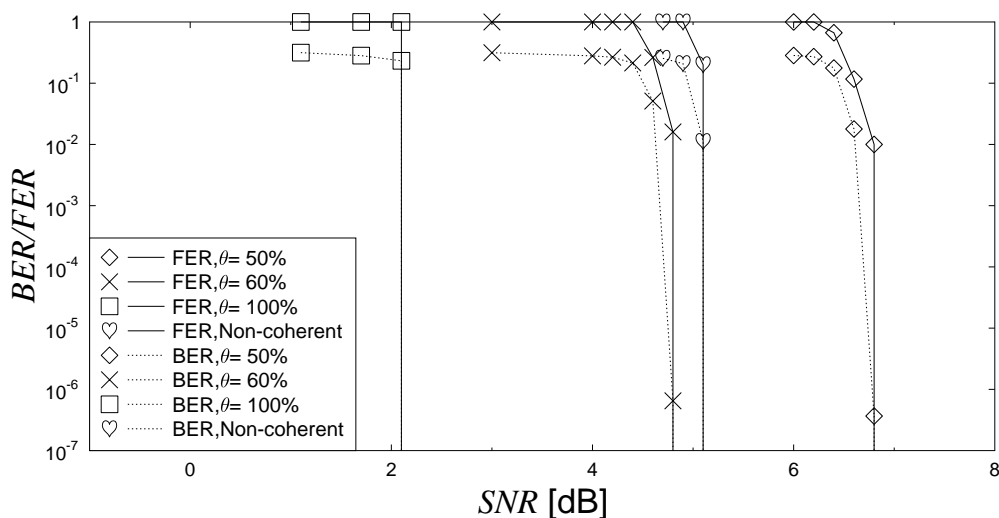


Figure 2.36: Comparison of the non-coherent versus coherent: IrCC-URC-QPSK scheme versus IrCC-URC-MSDD-aided-DQPSK, the frame length of $N = 10^5$, when communicating over the small-scale Rayleigh fading channel.

2.6 Chapter Summary

In this chapter, we have investigated the capacity and outage probability of the Continuous-input Continuous-output Memoryless Channel (CCMC), Discrete-input Continuous-output Memoryless Channel (DCMC) and Differential Discrete-input Continuous-output Memoryless Channel (D-DCMC). Both the small-scale and the block fading channels have been considered in our investigation. The frame-length was also taken into consideration when calculating the channel capacity and outage probability. The Extrinsic Information Transfer (EXIT) chart is invoked for designing the near-capacity coding schemes of IrCC-URC-MPSK, IrCC-URC-DMPSK and IrCC-URC-STTC-MPSK. The comparison between non-coherent and coherent system was conducted, and channel estimation was also taken into consideration. In the following chapters, the near-capacity coding schemes readily designed in this chapter are employed for building up near-capacity relay-aided systems.

The outage probability of the DCMC and D-DCMC may be calculated based on the associated SNR_r value corresponding to a given transmission rate R . The SNR_r value may be determined by looking up the corresponding value on the capacity curve constructed by using Equation (2.16) or by employing EXIT charts. The employment of EXIT charts used for formulating the capacity curve may be described in the following steps:

- EXIT curves pertaining to a given modulation scheme are generated for different SNR_r values.
- A single point on the capacity curves is determined by computing the area under the EXIT curve and its corresponding SNR_r .

A three stage near-capacity coding arrangement relying on Irregular Convolutional Codes (IrCC) may be designed by carrying out the following steps:

- Optimise the inner-most two-stage coding arrangement by finding the most appropriate number of iterations associated with the affordable complexity.
- Create the EXIT curve of the amalgamated inner decoder, which has been optimised, for different SNR_r values.
- Fix the overall coding rate of the IrCC encoder and then employ the EXIT curve matching algorithm for generating the optimised weighting coefficients α_i . The number of IrCC component codes used was either 17 or 36.

Distributed Three-Stage Concatenated Single-Antenna Aided Cooperation

In this chapter, the near capacity coding schemes designed in Chapter 2 are employed for constructing a distributed three stage coding scheme, which is composed of Distributed Concatenated Irregular Convolutional Code, Unity-Rate Code and Space-Time Trellis Code (DC-IRCC-URC-STTC). The system was designed for supporting a cooperative single-antenna relay aided system, as also seen in the thesis structure presented in Figure 1.16. More specifically, we consider two typical scenarios corresponding to the availability/unavailability of the signals from the source node at the destination node. In the first case the source to destination link is weak and hence it is negligible, while in the second scenario the availability of the source-to-destination link is taken into consideration during the decoding process at the destination.

3.1 Relay aided MIMO

The ultimate aim of designing a wireless communication system is to provide reliable high data rate links. MIMO systems provide a linearly increasing capacity as a function of the transmit power, provided the extra power is assigned to additional antennas [67]. STTCs [68] and STBCs [72], which are joint coding and transmit-receive diversity aided MIMO systems, constitute efficient techniques of communicating over fading channels [31], as detailed in Section 1.1.1 and Section 1.1.2, respectively. However, it is impractical to allocate multiple antennas to a shirt-pocket-sized mobile unit. Cooperative communication systems, which have recently attracted substantial research efforts [7, 8, 34, 171–173], are capable of creating a Virtual MIMO (VMIMO) system from multiple single-antenna relays. Depending on the type of the relays, the set of algorithms developed for cooperative communication can be categorised into two main groups, namely Amplify-and-Forward (AF) as well as Decode-and-Forward (DF) techniques [7, 8, 34, 171–173].

In a nutshell, a near-capacity three component IrCC-URC-STBC scheme was designed in [161],

which requires multiple antennas at both the transmitter and receiver sides. We note however that STTCs are capable of attaining a coding gain in addition to their spatial diversity gain, while the STBCs of [161] can only achieve a spatial diversity gain [45], but no coding gain.

Against this background, the novel contribution of this chapter is that we amalgamate the ideas of distributed space time coding [7,8] and near-capacity channel coding with the cooperative DF approach employing multiple single-antenna relays and use our Irregular Convolutional Coded Unity Rate Coded Space Time Trellis Code (IrCC-URC-STTC) coding arrangement to design a near-capacity coding scheme for single-antenna aided cooperative relaying systems. In other words, our objective is to design a near-capacity coding scheme for optimising the overall system and for devising the algorithms for finding relays for cooperation in the most appropriate locations in order to provide the best possible performance.

3.2 Link Configuration in the Absence of the SD Link

This section is dedicated to the characterisation of the above-mentioned first scenario, in which a source node (S) and a destination node (D) are communicating through two relay nodes (R) due to the low quality of the signal transmitted from the S node at the D node. Hence the SD link is often assumed to be unavailable [174].

3.2.1 System Model in the Absence of the SD Link

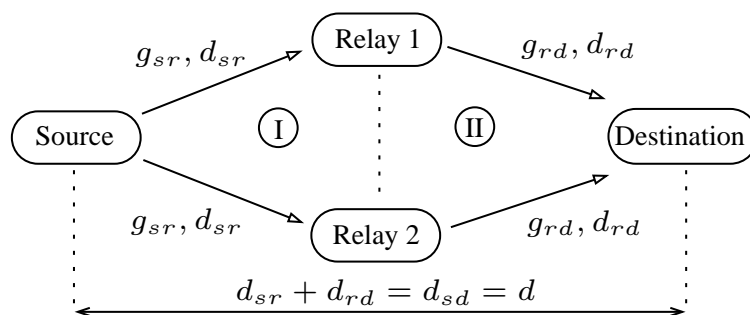


Figure 3.1: The model of the distributed coding system in the absence of the source-destination link.

Let us now consider the system model depicted in Figure 3.1, where the S node and the D node are connected via two R nodes. It should be noted that due to the constraint of having a single antenna at the S , D and R node, at least two R nodes should be employed for forming a VMIMO system, in order to exploit the benefits of MIMO systems. A transmission session of the system detailed in Figure 3.1 is accomplished in two transmission periods, namely the first transmission period is for the transmission from the S node to the R node and the other is for the transmission from the R nodes to the D node.

More specifically, during the first transmission period, the S node transmits its coded frame to the R nodes. Then, after decoding and re-encoding the signals received from the S node, the two R nodes transmit the resultant coded frame to the D node during the second transmission period. At the destination, the signals received from the two single-antenna aided relays are combined, detected and decoded, in order to recover the information transmitted from the S node. Although the signals are transmitted from two separate R nodes having a single antenna, these signals are treated, as if they came from a single relay having two transmit antennas. Naturally, the two relays are required to collaborate, which is further elaborated on Section 3.2.2, where the structure of the distributed encoder and decoder is described.

Let us now consider the channel model of the system. According to [169,171], the power-gain (or geometrical pathloss reduction), g_{sr} is expressed as a ratio or as $G_{sr}(\text{dB})$, which is experienced by the source-to-relay link with respect to the source-to-destination link as a benefit of its reduced distance and path loss, which is formulated as:

$$g_{sr} = \left(\frac{d_{sd}}{d_{sr}} \right)^\alpha, \quad (3.1)$$

where a free space pathloss exponent of $\alpha = 2$ was considered, while d_{sd} represents the distance between the S node and the D node. Finally, d_{sr} indicates the distance from the S node to the R node, as seen in Figure 3.1.

Similarly, the relay-to-destination link's power-gain, g_{rd} expressed as a ratio or $G_{rd}(\text{dB})$, with respect to the source-to-destination link can be formulated as:

$$g_{rd} = \left(\frac{d_{sd}}{d_{rd}} \right)^\alpha, \quad (3.2)$$

where d_{rd} is used for representing the distance from the R node to the D node, as illustrated in Figure 3.1.

Naturally, the power-gain of the source-to-destination link with respect to itself is unity, i.e. $g_{sd} = 1$. For the sake of simplicity, we may stipulate another assumption, namely that the R nodes are located on the straight line from the S node to the D node, which we have:

$$d_{sd} = d_{sr} + d_{rd} = d, \quad (3.3)$$

where d is used as an alternative of d_{sd} for the sake of brevity. Substituting Equation (3.3) into Equation (3.1) and Equation (3.2), it can be inferred that

$$g_{rd} = \frac{g_{sr}}{(\sqrt{g_{sr}} - 1)^2}. \quad (3.4)$$

Accordingly, the relation between the link's power gain and the associated position of the relay is characterised in Figure 3.2, where typical values of the free space pathloss exponent, namely $\alpha = 2, 3, 4$ are investigated.

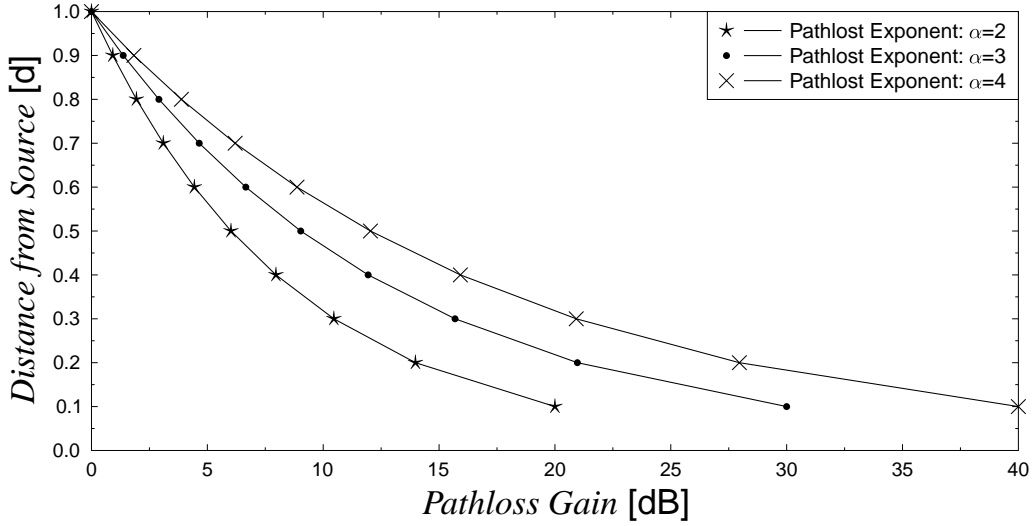


Figure 3.2: The link's power gain versus relay's position compared in different free space pathloss exponents, namely $\alpha = 2, 3, 4$.

Let us take into account the link's power-gain of Equation (3.1) and Equation (3.2) by defining SNR_t as the ratio of the power transmitted from the transmitter to the noise power encountered at the receiver¹. Following the approach in [169, 171], where the noise power of N_0 is assumed to be constant, we have:

$$SNR_{t(source)} = SNR_{t(relay)} = SNR_t, \quad (3.5)$$

provided that the transmit power at the source equals that at the relays. Note that $SNR_{t(source)}$ and $SNR_{t(relay)}$ represent the value of SNR_t for the source and relay, respectively. Furthermore, we define SNR_r as the ratio of the received power to the noise power at the receiver as:

$$SNR_r = G + SNR_t, \quad (3.6)$$

where $G(\text{dB})$ is the power gain of the link. According to Equation (3.6) and Equation (3.5) we arrive at:

$$SNR_{r(relay)} - G_{sr} = SNR_{r(dest.)} - G_{rd}, \quad (3.7)$$

where $SNR_{r(relay)}$ and $SNR_{r(dest.)}$ are the receiver's SNRs at the relays and the destination, respectively.

According to the system model portrayed in Figure 3.1, the signals propagating in the system may be described by firstly assuming that $i \in \{1, \dots, M_r\}$ with M_r being the number of relay nodes, while $k \in \{1, \dots, N_s\}$ with N_s being the number of symbols per frame transmitted from the

¹This definition is unconventional, because it relates physical quantities measured at different locations. However, it is convenient for illustrating the benefit the geometrical pathloss reduction.

S node. Then, the k^{th} received signal at the i^{th} relay node during the first transmission period can be formulated as:

$$y_{r_i,k} = \sqrt{g_{sr_i}} h_{sr_i,k} x_k + n_{r_i,k}, \quad (3.8)$$

where $h_{sr_i,k}$ is the complex-valued Rayleigh fading coefficient between the S node and the i^{th} R node, which is associated with the k^{th} symbol instant, x_k , of the symbol sequence x transmitted from the S node, while $n_{r_i,k}$ is the corresponding AWGN process having a variance of $N_0/2$ per dimension. Likewise, the l^{th} received symbol at the D node during the second transmission period can be expressed as:

$$y_{d,l} = \sqrt{g_{r_1d}} h_{r_1d,l} x_{r_1,l} + \sqrt{g_{r_2d}} h_{r_2d,l} x_{r_2,l} + n_{d,l}, \quad (3.9)$$

where $l \in \{1, \dots, N_r\}$; N_r is the number of symbols per frame transmitted from the R node; $h_{r_i,d,l}$ is the complex-valued Rayleigh fading coefficient between the i^{th} r node and the D node, which is associated with the l^{th} instant, $x_{r_i,l}$, of the symbol sequence x_{r_i} transmitted by Relay i ; $n_{d,l}$ is the AWGN having a variance of $N_0/2$ per dimension.

3.2.2 Distributed Concatenated IrCC, URC and STTC

The distributed coding scheme used for the system model portrayed in Figure 3.1 is presented in Figure 3.3. In the DC-IrCC-URC-STTC coding scheme depicted in Figure 3.3, a two-stage encoder constituted by an Irregular Convolutional Code and Unity-Rate Code (IrCC-URC) is employed at the S node. By contrast, at both the two R nodes and D node, the three-stage coding scheme constituted by the IrCC-URC-STTC is employed. It should be noted that the collaboration of the two R nodes has to guarantee that at any instant only the signals of a single STTC component of the single-antenna R nodes is transmitted. Thus, the signals received at the D node are a combination of the signals received from the two relays during the second transmission period. Then, the signals received at the D node are treated, as if they arrived from a single relay transmitter equipped with two co-located transmit antennas. In our investigation, we will employ both QPSK and 8PSK modulation for the two-stage IrCC-URC coding scheme of the S node, while only QPSK modulation is used for the three-stage IrCC-URC-STTC, in order to highlight benefits of our EXIT chart assisted design approach.

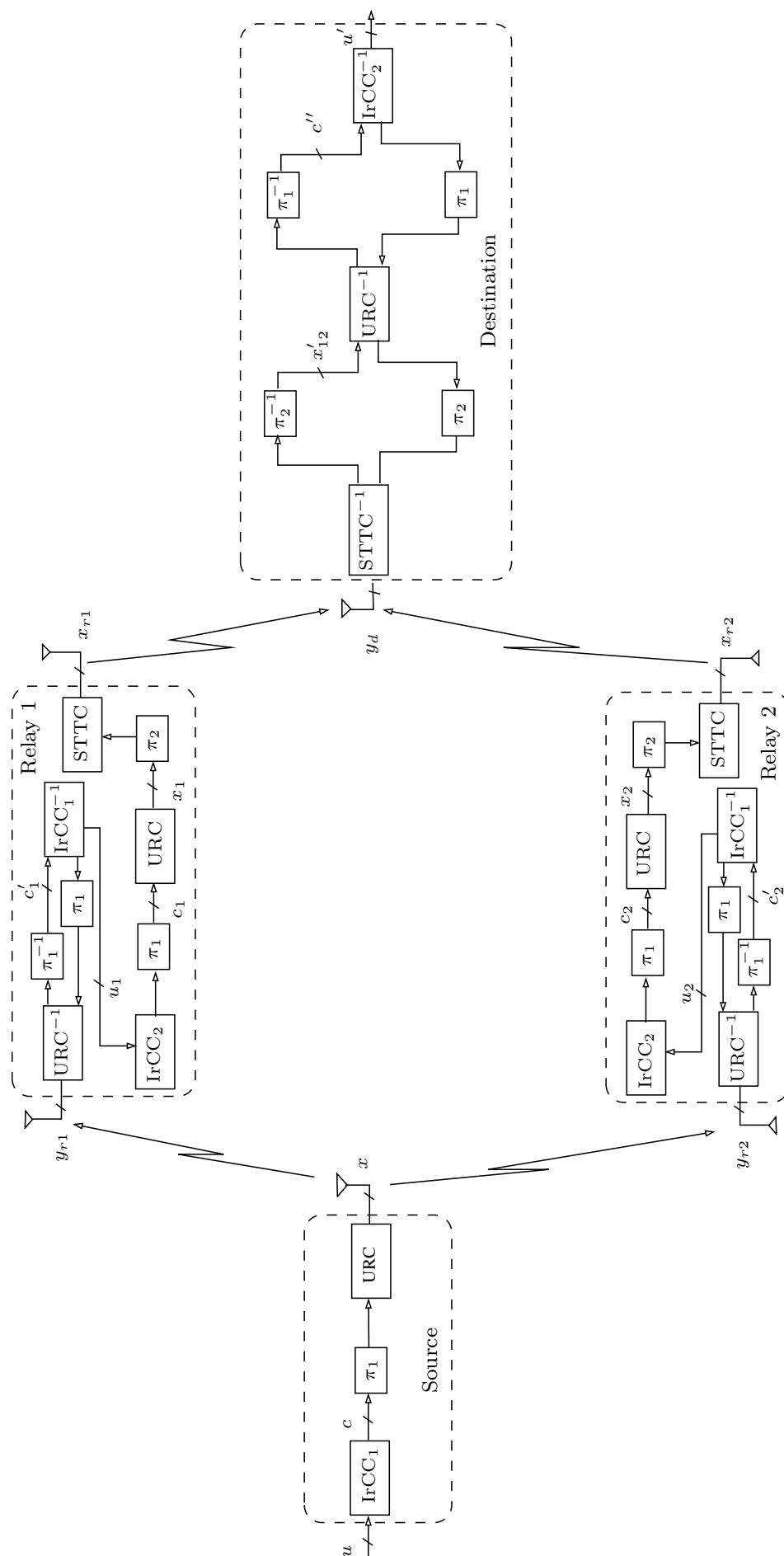


Figure 3.3: The block diagram of the Distributed Concatenated Irregular Convolutional Code, Unity-Rate Code and Space-Time Trellis Code scheme for the system model presented in Figure 3.1. This scheme relies on the IrCC-URC-STTC-MPSK arrangement detailed in Section 2.3.2 and on the Irregular Convolutional Coded Unity Rate Code M-ary Phase Shift Keying (IrCC-URC-MPSK) arrangement presented in Section 2.3.3.

As seen in Figure 3.3, the information bit sequence u is encoded by the IrCC encoder at the S node for producing the coded sequence c , before passing c through the interleaver π_1 . The interleaved bit sequence is encoded by the URC encoder and then modulated using 8PSK or QPSK, in order to form the transmitted symbol sequence x . The signals y_{r1} and y_{r2} received at the both relays, as presented in Equation (3.8), are iteratively decoded by the IrCC-URC decoders, as seen in Figure 3.3, in order to estimate the original information bit sequences, u_1 and u_2 , at R node 1 and 2, respectively. Then the estimated bit sequences of u_1 and u_2 are passed through the IrCC-URC-STTC encoding process relying on the pair of interleavers, π_1 and π_2 , which are located between the IrCC encoder and URC encoder as well as between the URC encoder and the STTC encoder, respectively. These two interleavers facilitate the provision of hitherto in exploited extrinsic information for the iterative decoding process at the destination, where the iterations exchanging extrinsic information between the STTC decoder and the URC decoder are performed I times, before one of J times iteration between the URC decoder and the IrCC decoder is carried out, as detailed in Section 2.3.2. In other words, once I inner iterations are accomplished, one iteration of J outer iterations is triggered before passing the information back to the inner iterations. This process is repeated, until all the affordable number of J outer iterations are performed, as seen in the destination block of Figure 3.3.

Then, QPSK modulation is employed at the output of the R node's STTC encoder. Note that the sequences transmitted by each of the relays, namely x_{r1} and x_{r2} presented in Equation (3.9), are created by choosing only one predefined output of the two-antenna 4-state STTC encoder of [68]. The sequence received at the D node, namely y_d given in Equation (3.9), is then subjected to the inverse process: y_d is demodulated, and finally the resultant sequence is decoded by two iterative decoders, namely by the URC-STTC decoder and the IrCC-[amalgamated-URC-STTC] decoder of Figure 3.3. The decoded information bit sequence u' seen in Figure 3.3 is compared to the original one for evaluating the performance of the system.

The URC, IrCC and STTC component codes have the code rates of R_{URC} , R_{IrCC} and R_{STTC} , respectively. Thus, the code rates of the concatenated coding arrangements, namely of the IrCC-URC and IrCC-URC-STTC can be expressed as:

$$R_{IrCC-URC} = R_{IrCC} \times R_{URC}, \quad (3.10)$$

and

$$R_{IrCC-URC-STTC} = R_{IrCC} \times R_{URC} \times R_{STTC}. \quad (3.11)$$

The overall throughput of the proposed two-hop cooperative system can be calculated by:

$$\eta = \frac{N_i}{N_s + N_r} [BPS], \quad (3.12)$$

where N_i is the number of information bits transmitted within a duration of $(N_s + N_r)$ symbol periods, while N_s and N_r are the number of symbols transmitted by the S node and the R node within

a transmission session, respectively. In what follows, a numerical example is presented for demonstrating how the parameters of the system are determined by Equation (3.10), Equation (3.11) and Equation (3.12)

Example 3.1. *Let us assume that either 8PSK or QPSK is used for the source-relay transmission, while QPSK is employed for the transmission between the R nodes and D node. In addition, the URC, IrCC and STTC component codes have the code rates of $R_{URC} = 1.0$, $R_{IrCC} = 0.5$ and $R_{STTC} = 1.0$, respectively.*

Accordingly, the number of symbols transmitted by the S node may be calculated by:

$$N_s = \frac{N_i}{R_{IrCC-URC} \times \log_2 L'} \quad (3.13)$$

where L is the number of modulation levels, which is equal to $L = 4$, when a QPSK modulation scheme is used. As a result of employing QPSK modulation, substituting Equation (3.10) into Equation (3.13), we may obtain

$$\begin{aligned} N_s &= \frac{N_i}{0.5 \times 1.0 \times \log_2 4'} \\ &= N_i. \end{aligned} \quad (3.14)$$

Likewise, N_r that is the number of symbols transmitted by the R node, which can be computed as:

$$N_r = \frac{N_i}{R_{IrCC-URC-STTC} \times \log_2 L}. \quad (3.15)$$

It should be noted that we calculate N_r as if we had a single relay having two co-located antennas. Since QPSK modulation is employed for the relay-destination link, we still have $L = 4$. Hence, substituting Equation (3.11) into Equation (3.15) results in the following value of N_r :

$$\begin{aligned} N_r &= \frac{N_i}{R_{IrCC-URC-STTC} \times \log_2 L'} \\ &= \frac{N_i}{0.5 \times 1.0 \times 1.0 \times \log_2 4'} \\ &= N_i. \end{aligned} \quad (3.16)$$

Then, substituting Equation (3.17) and Equation (3.14) into Equation (3.12) leads to the system's overall throughput of η as:

$$\begin{aligned} \eta &= \frac{N_i}{N_s + N_r} [BPS], \\ &= \frac{N_i}{N_i + N_i} [BPS], \\ &= 0.5 [BPS]. \end{aligned} \quad (3.17)$$

Similarly, when an 8PSK modulation scheme is used for the source-relay link and QPSK is applied for the relay-destination link, the above steps may be replicated for obtaining the corresponding system's overall throughput of $\eta = 0.6[BPS]$.

Note that once the system's overall throughput has been calculated, as demonstrated in Example 3.1, the relationship between the E_b/N_0 and SNR values of the system can be formulated as:

$$\frac{E_b}{N_0} = \frac{SNR}{\eta}. \quad (3.18)$$

The relationship stipulated by Equation (3.18) is necessary for the sake of a fair performance comparison of the different systems having different throughputs caused by using different parameters.

3.2.3 System Capacity and Relay Selection

In this section, we first derive the bounds for relay channels' DCMC capacity corresponding to the capacity of our DC-IrCC-URC-STTC scheme. Then the near-capacity coding arrangements designed in Section 2.3 are applied for the appropriate transmission links of the DC-IrCC-URC-STTC system. Furthermore, the results of our EXIT-chart based design are employed for choosing relays, in order to optimise the system's BER-performance.

3.2.3.1 Relay Channel Capacity

According to [173], the achievable CCMC capacity of a full duplex relay aided system can be calculated as follows:

$$C_{CCMC}^{relay} \geq \max_{p(X_1, X_2)} \min\{I(X_1; Y_2 | X_2), I(X_1, X_2; Y_3)\}, \quad (3.19)$$

where X_1, X_2, Y_2 and Y_3 are the signals transmitted from the S node and R node, as well as the signals received at the R node and the D node, respectively. Furthermore, $p(X_1, X_2)$ is the joint probability of signals transmitted from the S and R nodes. Applying the above general formulas to our half-duplex system, and assuming that the source-destination link is not considered, while a pair of relays is viewed as a single equivalent relay having two transmit antennas, we can formulate the relay's achievable DCMC capacity as:

$$C_{DCMC}^{relay} \geq \max_{p(X, X_r)} \min \left\{ \frac{N_s}{N_s + N_r} \times E[I(X; Y_r)], \frac{N_r}{N_s + N_r} \times E[I(X_r; Y_d)] \right\}, \quad (3.20)$$

where η is calculated from Equation (3.12), $X = [x_1, x_2, \dots, x_{N_s}]$ represents the signals transmitted from the s node with x_k formulated in Equation (3.8), while $X_r = [x_{r_1,1}, x_{r_2,1}, \dots, x_{r_1, N_r}, x_{r_2, N_r}]$ are the signals transmitted from the equivalent twin-antenna aided relay node with $x_{r_i, l}$ formulated in Equation (3.9). Furthermore, $Y_r = Y_{ri} = [y_{r_i,1}, \dots, y_{r_i, N_s}]$ and $Y_d = [y_{d,1}, \dots, y_{d, N_r}]$ are the signals received at the equivalent relay node and the D node, with $y_{r_i, k}$ and $y_{d, l}$ calculated from Equation (3.8) and Equation (3.9), respectively.

3.2.3.2 Relay Selection

In order to allow our coding scheme detailed in Figure 3.3 to attain the best possible performance, a pair of appropriate relays should be utilised. Without any loss of generality, we can assume that a sufficiently high number of relays are roaming between the source and destination. For the sake of employing appropriate active relays, one can either choose two relays at an appropriate position or equivalently choose two relays at an arbitrary position, provided that accurately controlled transmit powers are used both at the S node and at the two R nodes. These two strategies have the same influence on the system, since they result in the same received power.

Without any loss of generality, the first strategy is invoked by adopting two approaches, in order to choose the activated ones from the set of available relays. The first approach is straightforward. By contrast, our second approach relies on a more sophisticated novel proposition, namely on ensuring that the appropriately shaped EXIT tunnel of the system remains open:

1. Based on the first approach, we can simply pick two arbitrary relays that are about half-way between the S node and the D node. This approach can be generalised by picking two arbitrary relays that are close to each other and they both have a similar distance from both the S node and D node.
2. The more sophisticated EXIT-chart based approach appoints the optimal relays, which are those that facilitate the creation of an open EXIT tunnel, as presented in Section 2.3.2.1 and Section 2.3.3.1, leading to the (1,1) point at sufficiently high SNR_r values at both the S node and D node, provided that the SNR_t value is also sufficiently high.

Denoting the SNR difference between the BER turbo-cliffs of our concatenated coding arrangements, namely those of the IrCC-URC and the IrCC-URC-STTC arrangements as A (dB) or a in terms of their ratio and using Equation (3.7), we have :

$$A = SNR_{r(relay)} - SNR_{r(dest.)} = G_{sr} - G_{rd} . \quad (3.21)$$

In other words, satisfying Equation (3.21) means that the relay's position facilitates the creation of an open EXIT chart tunnel at both the R and D nodes simultaneously. As a result, BER/FER of both the source-relay link and of the relay-destination link becomes vanishingly low at the same SNR_t value. Note that the relationship between A and a is simply:

$$a = 10^{\frac{A}{10}} . \quad (3.22)$$

Combining Equations 3.1, 3.2, 3.4 and 3.21, we arrive at the optimal relay-position conditions as follows:

$$\begin{aligned} d_{sr} &= \frac{d}{(1 + \sqrt{a})}, d_{rd} = \frac{d \times \sqrt{a}}{(1 + \sqrt{a})}, \\ g_{sr} &= (1 + \sqrt{a})^2, g_{rd} = \frac{(1 + \sqrt{a})^2}{a}. \end{aligned} \quad (3.23)$$

Let us continue to use the numerical parameters of the system considered in Example 3.1, in order to illustrate our novel proposition stipulated by Equation (3.23) with the aid of the following example.

Example 3.2. *Let us again consider the illustrative system context described in Example 3.1. In this system, either 8PSK or QPSK is used for the source-relay transmission while QPSK is employed for the transmission between the R nodes and D node. The further details of the illustrative system, which is generalised in Figure 3.3, are that the URC, IrCC and STTC component codes have the code rates of $R_{URC} = 1.0$, $R_{IrCC} = 0.5$ and $R_{STTC} = 1.0$, respectively.*

Following Equation (3.23), we can look up in Figure 2.15, Figure 2.20 and Figure 2.23 the decoding convergence SNR points of the corresponding EXIT charts, which are the SNR_r values associated with the BER turbo cliff of the corresponding coding scheme, in order to infer to the value of A (or a). As a result, we can find the value of $A = 0.5$ dB and $A = 3.7$ dB for the cases of using QPSK and 8PSK, respectively, as summarised in Table 3.1 and Table 3.2.

Coding Schemes	Convergent Point, SNR_r [dB]
IrCC-URC-STTC-QPSK	2.3
IrCC-URC-QPSK	2.8
IrCC-URC-8PSK	6.0

Table 3.1: Convergence-SNRs extracted from EXIT charts, namely of the IrCC-URC-STTC-QPSK scheme presented in Figure 2.15, of the IrCC-URC-QPSK scheme given in Figure 2.20 and of the IrCC-URC-8PSK scheme characterised in Figure 2.23. These EXIT charts were obtained in a Rayleigh small-scale fading scenario.

By substituting the values of A into Equation (3.23), we can infer the optimal position of the relays, which are detailed in Table 3.2. Accordingly, the optimal position of the relays results in $g_{sr} = 4.24$ and $g_{rd} = 3.77$ for the QPSK case and $g_{sr} = 6.41$ and in $g_{rd} = 2.73$ for the 8PSK. The corresponding distances, namely d_{sr} and d_{rd} , are evaluated from Equation (3.1) and Equation (3.2), which become $0.48d$ as well as $0.52d$ for QPSK and $0.39d$ as well as $0.61d$ for 8PSK, respectively.

Distributed Coding Scheme		A (Convergence SNR Difference)	Optimal Position
Source-Relay	Relay-Destination		
IrCC-URC-QPSK	IrCC-URC-STTC-QPSK	0.5	$d_{sr} = 0.48d, d_{rd} = 0.52d$
IrCC-URC-8PSK	IrCC-URC-STTC-QPSK	3.7	$d_{sr} = 0.39d, d_{rd} = 0.61d$

Table 3.2: Optimal positions of the relays.

3.2.4 Relay Positioning and its Power Gain

In this section, we characterise the achievable BER versus E_b/N_0 performance corresponding to the two different relay-selection approaches, in order to verify the results of our EXIT-chart aided design provided in Section 3.2.3. Although perfect relaying is not required for the success of our coding scheme, we produce benchmark results for the perfect-relaying scenario, where no errors are imposed by the source-relay link, in order to specify the achievable upper bound performance. Note that the term ‘perfect relay’ implies that there are no errors occurring on the source-to-relay transmission links, while the term ‘practical relay’ indicates that the quality of the source-to-relay transmission link reflects the performance of the channel coding scheme used. Moreover, we assume that the knowledge of the relays’ position is available. It was suggested by [175] that the AF regime should be used when the relay position is close to the D node, while DF regime should be employed when activating relays close to the S node. This is because close to the D node a DF-based is likely to inflict severe error-propagation, whilst closer to the S node it is capable of flawlessly reproducing the original signal of the S node. Accordingly, we investigate the eight configurations of the system portrayed in Figure 3.3. These configurations listed in Table 3.3 are different in terms of the position and type of relays activated as well as in the modulation scheme used for the source-to-relay transmission links, which are summarised as follows:

1. **Configuration 1:** A pair of relays located at the half-way position is activated, which are assumed to be capable of perfect relaying. The IrCC-URC-QPSK scheme of Section 2.3.3 and IrCC-URC-STTC-QPSK of Section 2.3.2 are employed for the source-to-relay and relay-to-destination links, respectively.
2. **Configuration 2:** A pair of relays located at the half-way position is activated and the source-to-relay transmission links are supported by practical error-prone relaying. The IrCC-URC-QPSK and IrCC-URC-STTC-QPSK schemes are employed for the source-to-relay and relay-to-destination links, respectively.
3. **Configuration 3:** A pair of relays located at the half-way position is activated, which are assumed to be capable of perfect relaying. The IrCC-URC-8PSK and IrCC-URC-STTC-QPSK schemes are employed for the source-to-relay and relay-to-destination links, respectively.
4. **Configuration 4:** A pair of relays located at the half-way position is activated and the source-to-relay transmission links are supported by practical error-prone relaying. The IrCC-URC-8PSK and IrCC-URC-STTC-QPSK schemes are employed for the source-to-relay and relay-to-destination links, respectively.
5. **Configuration 5:** A pair of relays located at the optimal position is activated, which are assumed to be perfect relays. The IrCC-URC-QPSK and IrCC-URC-STTC-QPSK schemes are employed for the source-to-relay and relay-to-destination links, respectively.

6. **Configuration 6:** A pair of relays located at the optimal position is activated and the source-to-relay transmission links are supported by the practical relays. The IrCC-URC-QPSK scheme and IrCC-URC-STTC-QPSK are employed for the source-to-relay and relay-to-destination links, respectively.
7. **Configuration 7:** A pair of relays located at the optimal position is activated, which are assumed to be perfect relays. The IrCC-URC-8PSK and IrCC-URC-STTC-QPSK schemes are employed for the source-to-relay and relay-to-destination links, respectively.
8. **Configuration 8:** A pair of relays located at the optimal position is activated and the source-to-relay transmission links are supported by practical error-prone relays. The IrCC-URC-8PSK and IrCC-URC-STTC-QPSK schemes are employed for the source-to-relay and relay-to-destination links, respectively.

Configuration	Position of relays	Type of relays	Scheme in use
1	Half way	Perfect	$S \rightarrow R$: IrCC-URC-QPSK $R \rightarrow D$: IrCC-URC-STTC-QPSK
2	Half way	Practical	$S \rightarrow R$: IrCC-URC-QPSK $R \rightarrow D$: IrCC-URC-STTC-QPSK
3	Half way	Perfect	$S \rightarrow R$: IrCC-URC-8PSK $R \rightarrow D$: IrCC-URC-STTC-QPSK
4	Half way	Practical	$S \rightarrow R$: IrCC-URC-8PSK $R \rightarrow D$: IrCC-URC-STTC-QPSK
5	Optimal	Perfect	$S \rightarrow R$: IrCC-URC-QPSK $R \rightarrow D$: IrCC-URC-STTC-QPSK
6	Optimal	Practical	$S \rightarrow R$: IrCC-URC-QPSK $R \rightarrow D$: IrCC-URC-STTC-QPSK
7	Optimal	Perfect	$S \rightarrow R$: IrCC-URC-8PSK $R \rightarrow D$: IrCC-URC-STTC-QPSK
8	Optimal	Practical	$S \rightarrow R$: IrCC-URC-8PSK $R \rightarrow D$: IrCC-URC-STTC-QPSK

Table 3.3: Configurations of the system presented in Figure 3.3, corresponding to different modulation schemes employed for transmission from the S node to the R nodes, as well as the position and type of the relays in use.

As shown in Figure 3.4 and Figure 3.5, when having access to relays at the half-way position, a 3.0 dB E_b/N_0 improvement is attained for QPSK case, while a 2.0 dB E_b/N_0 improvement is achieved for 8PSK, when we compare the E_b/N_0 values required for having a BER of 10^{-5} with and without the relays. Quantitatively, observe from Figure 3.4 and Figure 3.5 that E_b/N_0 values of -0.3 dB, 2.7 dB are required for QPSK case and 0.2 dB, 2.2 dB for 8PSK, respectively. Note

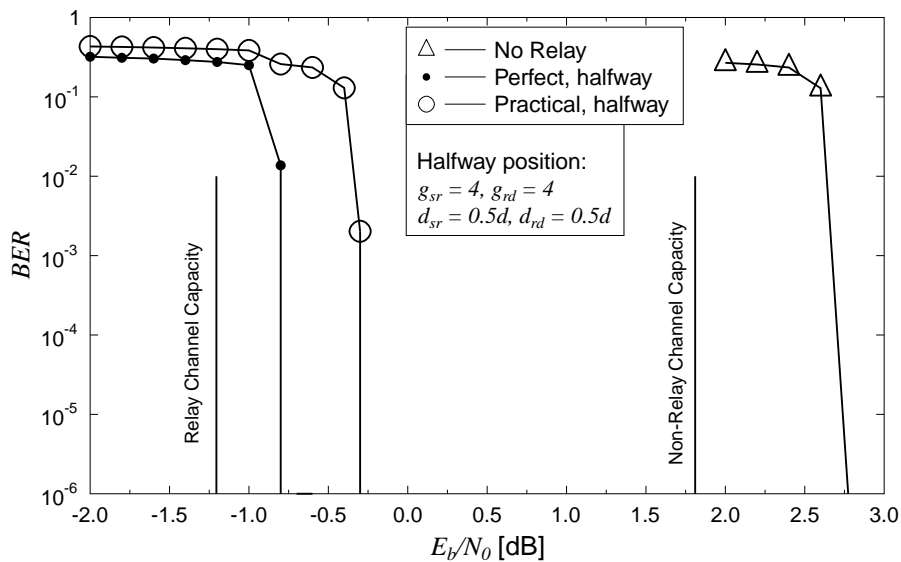


Figure 3.4: BER-performance comparison of the distributed coding aided system of Figure 3.3, when operating in different configurations activating the R nodes located half-way between the S node and the D node, namely the configuration 1 and 2 given in Table 3.3 for a Rayleigh small-scale fading scenario.

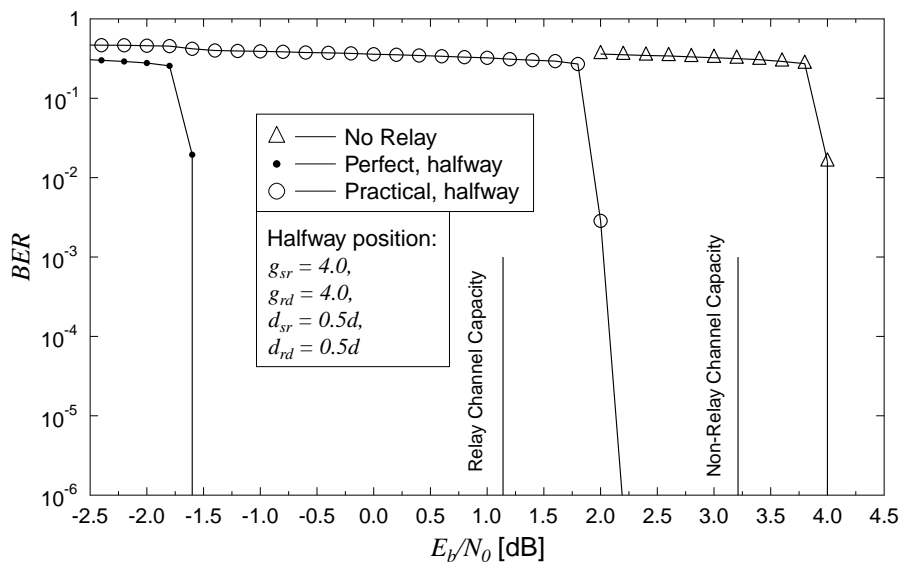


Figure 3.5: BER-performance comparison of the distributed coding aided system of Figure 3.3, when activating the R nodes located half-way between the S node and the D node, which corresponds to the configuration 3 and 4 listed in Table 3.3, where the 8PSK modulation scheme is employed for the transmission link spanning from the S node to the R nodes. A Rayleigh-distributed small-scale fading scenario is considered for all the transmissions in the system.

in Figure 3.4 that the idealistic perfect relay scheme operates beyond the realistic relay channel's capacity, which was calculated by evaluating the area under our realistic system's inner decoder's EXIT curve, as detailed in Section 2.1.4. As seen in Figure 3.6 and Figure 3.7, selecting the relays in the vicinity of the optimal position defined by Equation (3.23) has the potential of providing either a 3.2 dB E_b/N_0 improvement or a 4.0 dB E_b/N_0 improvement at a BER of 10^{-5} in comparison to the scenario dispensing with relaying, which is either 0.2 dB or 2.0 dB better than that of relaying having the relays at about the mid-way position corresponding to the cases of QPSK and 8PSK. Note that the performance gain of selecting relays at the optimum location, as opposed to using relays at the half-way location, will be higher when we have a higher value of A , which quantifies the difference between the two convergence SNR_r values given by Equation (3.21).

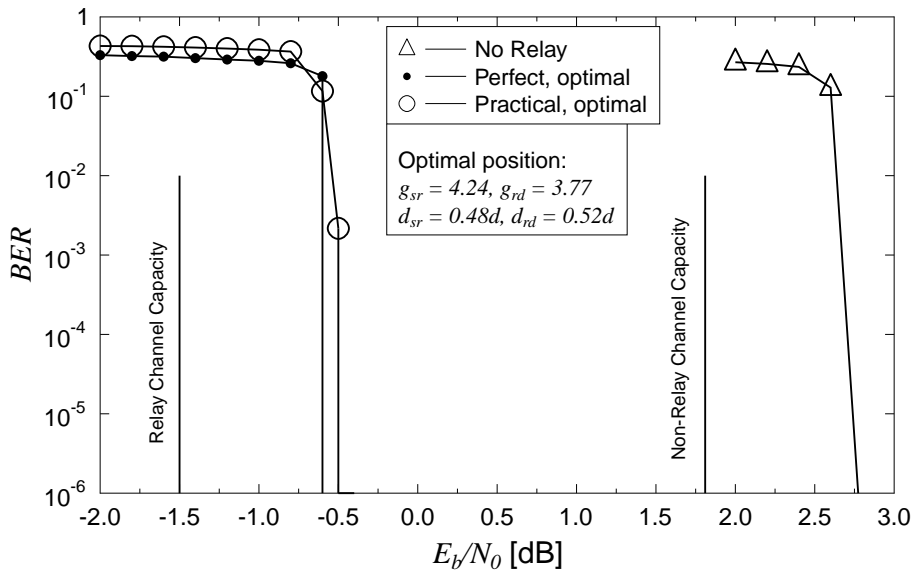


Figure 3.6: BER-performance comparison of the distributed coding aided system of Figure 3.3, when activating the R nodes nearby the optimal position determined by Equation (3.23). The scenarios considered corresponds to the configuration 5 and 6 listed in Table 3.3, where the QPSK modulation scheme is employed for the transmission link spanning from the S node to the R nodes, while all the transmissions in the system are affected by the Rayleigh-distributed small-scale fading.

As seen in Figure 3.4, the performance of the practical relay scheme, which may impose error-propagation owing to its decision-errors, is either about 0.5 dB or 3.6 dB from that of the idealised perfect relay scheme, which is due to the effects of error propagation imposed by the R nodes. More explicitly, the $SNR_{r(relay)}$ value is too low to achieve a sufficiently low BER, although the $SNR_{r(dest.)}$ is sufficiently high to attain a low BER, when the R nodes are located half-way between the S and D nodes. By definition, the optimal relay selection method aims for solving this problem by activating relays exactly at the optimal locations, so that the system may reach the $SNR_{r(relay)}$ and $SNR_{r(dest.)}$ values required for simultaneously achieving a low BER at both the R and D

nodes. According to Equation (3.23), the optimal relay nodes in the scheme considered are located at normalised positions of $0.48d$ and $0.39d$ closer to the S node, in order to achieve $g_{sr} = 4.24$, $g_{rd} = 3.77$ for QPSK case and $g_{sr} = 6.41$, $g_{rd} = 2.73$ for 8PSK case, respectively. The optimal relay-aided performance seen in Figure 3.6 and Figure 3.7 shows that the practical relaying scheme is now capable of operating a mere 0.1 dB and 0.2 dB away from the corresponding perfect relaying scheme for the cases of QPSK and 8PSK, respectively.

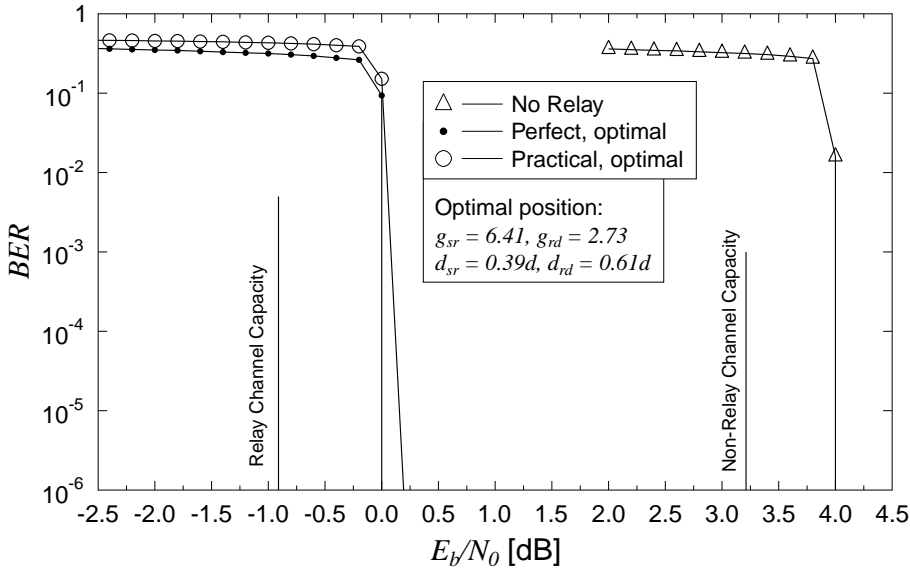


Figure 3.7: BER-performance of the distributed coding aided system pictured in Figure 3.3, when selecting R nodes nearby the optimal position determined by Equation (3.23). The scenarios considered corresponds to the configuration 7 and 8 mentioned in Table 3.3, where the 8PSK modulation scheme is chosen for the transmission link spanning from the S node to the R nodes, provided that all the transmissions in the system are carried out over Rayleigh-distributed small-scale fading channels.

Figures 3.4, 3.5, 3.6 and 3.7 also show that our coding scheme is capable of operating at 1.0 dB and 1.1 dB away from the relay realistic channel's capacity corresponding to the cases of mid-way relaying and optimal relaying for QPSK. These SNR-discrepancies are 5.0 dB and 1.1 dB for 8PSK. Note that the relay channel's capacity defined by Equation (3.20), when employing the relays near the optimal position stipulated by Equation (3.23), is always better than that of the relays roaming near the mid-way position. Equation (3.20) also suggests that there should be a different optimal position, when the objective function is that of maximising the relay channel's capacity. However, satisfying our optimal condition defined in Equation (3.23) always provides the best possible performance for our coding scheme, which is hence also better than that of the optimal position chosen for maximising the relay channel's capacity.

3.3 Distributed Coding Scheme with the Presence of SD Link

3.3.1 System Model in the Presence of the SD Link

In this section, we expand the model previously investigated in Section 3.2 by exploiting the weak signals transmitted from the S node during the first transmission period and received by the D node. As portrayed in Figure 3.8, the source node, the two relay nodes and the destination node use a single antenna for transmitting and receiving signals within the two transmission periods. During the first transmission period, the S node transmits its coded frame to both the R and D nodes. Then, after decoding and re-encoding the signals received from the S node, the R nodes transmit the resultant coded frame to the D node during the second transmission period. At the destination, the signals received during the two transmission periods are combined in order to recover the original signals. This regime is different from the system model used in Section 3.2.1, where the signals

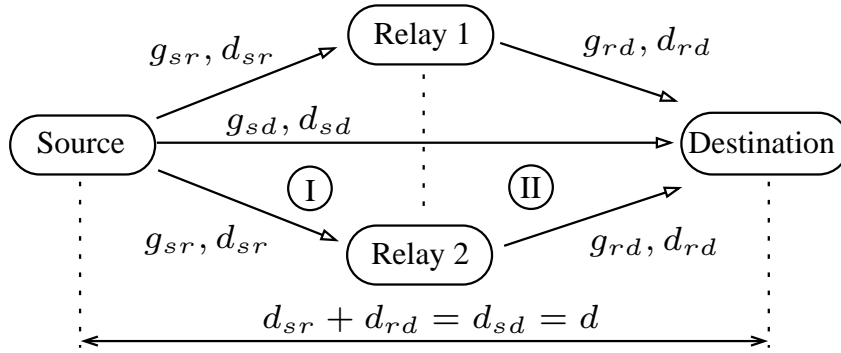


Figure 3.8: The system model of the distributed coding scheme, which is extended from the system model portrayed in Figure 3.1 by additionally taking into account the signals received from the source-destination link.

received at the D node comprise two components corresponding to the two transmission periods. The k^{th} and l^{th} symbols received at the D node during the first and second transmission period can be expressed as:

$$y_{d,k}^I = \sqrt{g_{sd}} h_{sd,k} x_k + n_{d,k}^I, \quad (3.24)$$

$$y_{d,l}^{II} = \sqrt{g_{r_1d}} h_{r_1d,l} x_{r_1,l} + \sqrt{g_{r_2d}} h_{r_2d,l} x_{r_2,l} + n_{d,l}^{II}. \quad (3.25)$$

3.3.2 Encoder and Decoder in the Presence of the SD Link

In the coding scheme illustrated in Figure 3.9, the weak signals received at the destination during the first transmission period are stored and then jointly and iteratively decoded with the aid of the signals received from the two relays during the second transmission period. Given this structure, we introduce two kinds of iterations within the decoder at the destination node, namely the inner

iterations referring to the iteration inside the decoders used during either the first or second transmission periods and the outer iteration implying the iteration between the two decoders used during two transmission periods.

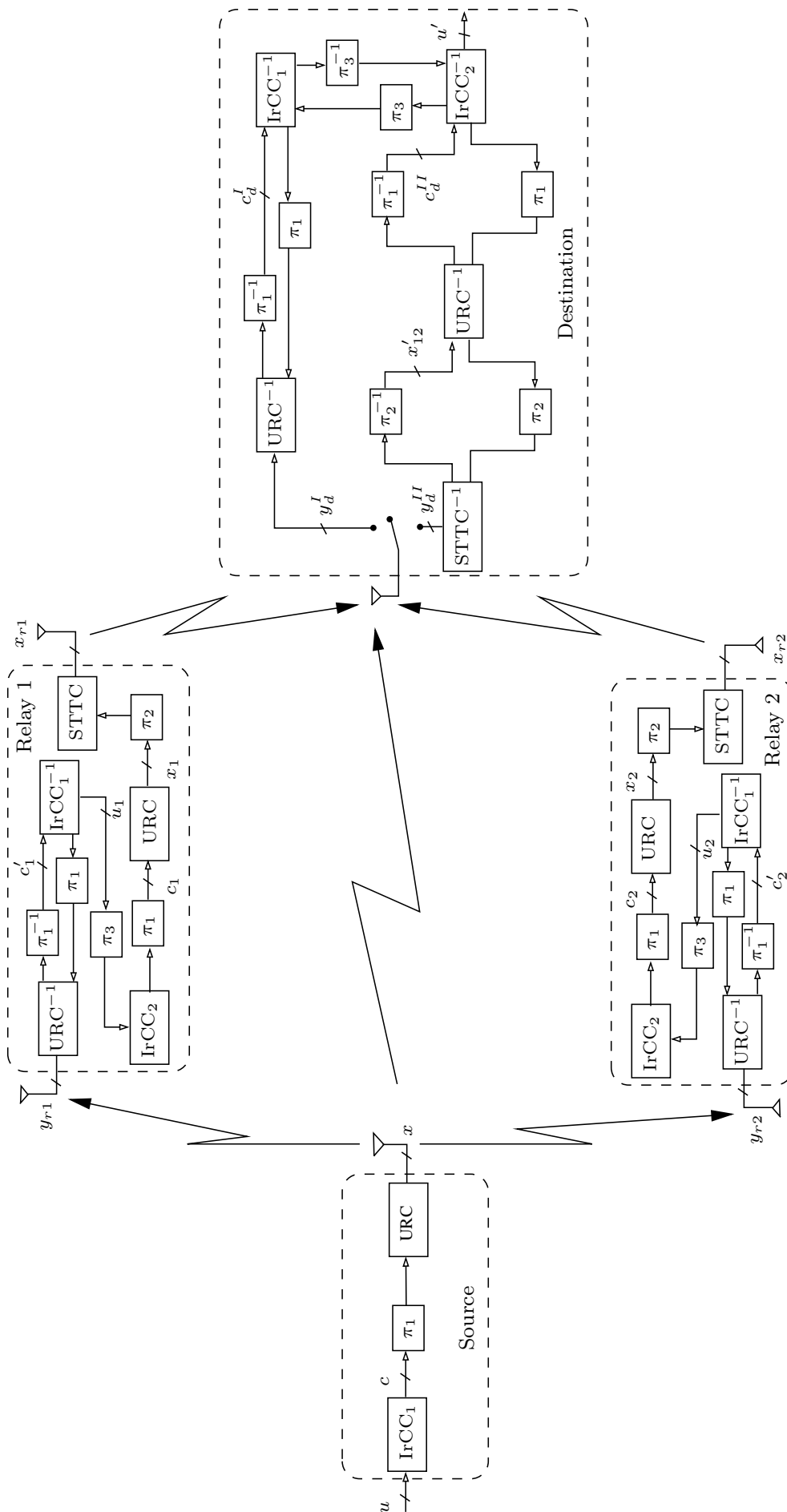


Figure 3.9: The block diagram of DCTS-IrCC-URC-STTC coding scheme in the presence of the source-destination link, which is developed from the scheme presented in Figure 3.3 by further taking into account the decoding process at the D node in the presence of the signals arriving from the S node.

3.3.3 Achievable Rate and Relaying Strategy

In this section, another novel method conceived for selecting relays is investigated. The relay-based achievable rate is also discussed. Additionally, EXIT charts are employed for determining the number of both inner and outer iterations during iterative decoding process.

3.3.3.1 Dynamically Selected Relays

In this section we compare two EXIT-chart based approaches involved for appointing relays in order to allow the DC-IrCC-URC-STTC coding scheme of Section 3.2 to attain its best possible performance.

1. The first EXIT-chart based approach was presented in Section 3.2.3.2.
2. The second EXIT-chart based approach dynamically selects the relays that are located at beneficial positions so that the SNR_r encountered at the relays is always close to but slightly above the SNR_r value required for attaining convergence to an infinitesimally low BER. For example, observe in Figure 2.20 that this was $\gamma = SNR_{r(relay)} = 2.8$ dB, when employing the IrCC-URC-QPSK scheme presented in Section 2.3.3. Moreover, the path gains and SNR values have to meet the following condition:

$$\begin{aligned} G_{SR} &= SNR_{r(relay)} - SNR_t \\ &= \gamma - SNR_t. \end{aligned} \quad (3.26)$$

Using Equations 3.1, 3.2, 3.4 and 3.26, we can calculate the positions of the relays, d_{sr} and d_{rd} , as well as the corresponding path gains, g_{sr} and g_{rd} , given a certain transmit power level by using the following formulas:

$$g_{sr} = 10^{(\gamma - SNR_t)/10}, \quad (3.27)$$

$$g_{rd} = \frac{10^{(\gamma - SNR_t)/10}}{(10^{(\gamma - SNR_t)/20} - 1)^2}, \quad (3.28)$$

$$d_{sr} = d \times 10^{-(\gamma - SNR_t)/20}, \quad (3.29)$$

$$d_{rd} = d \times \left(1 - 10^{-(\gamma - SNR_t)/20}\right). \quad (3.30)$$

As we can see in Figure 3.10 and Figure 3.11, the approach of dynamically selecting the relays at beneficial positions, so that the SNR_r encountered at the relays is always slightly above the turbo-cliff SNR improves the attainable performance, when E_b/N_0 is low. However, the dynamically selected relays offer the same performance as the relays located close to the optimal position when E_b/N_0 is sufficiently high. However, no error propagation is imposed by source-to-relay link, when employing dynamic relays. This property is essential for the EXIT-chart based analysis of the relay achievable rate and for designing the iterative decoder at the D node, when the signals received during both transmission periods are exploited by the iterative decoding process.

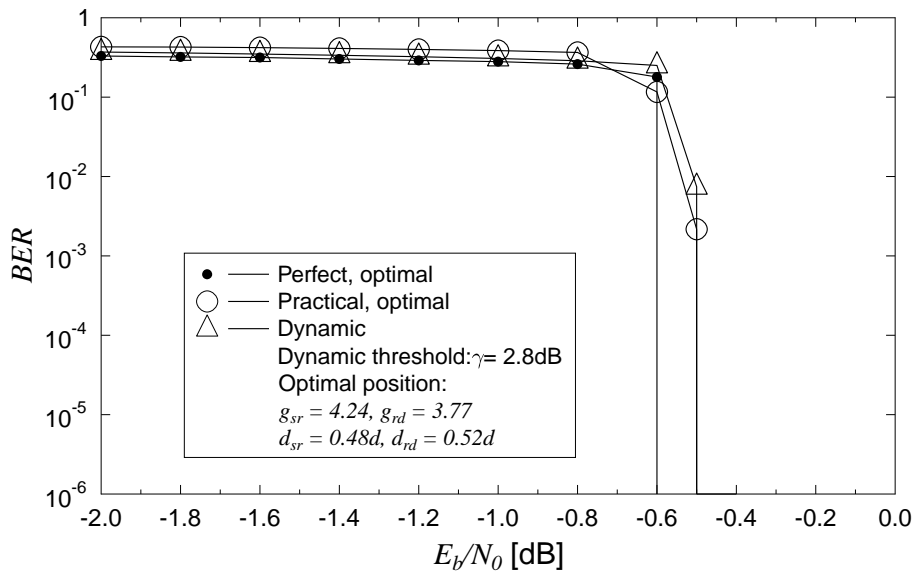


Figure 3.10: BER-performance of the system portrayed in Figure 3.3, when employing optimal relays defined by Equation (3.23) versus when using relays characterised by Equation (3.27), while all transmissions in the system are affected by the Rayleigh-distributed small-scale fading. QPSK modulation scheme was used for the source-relay transmission.

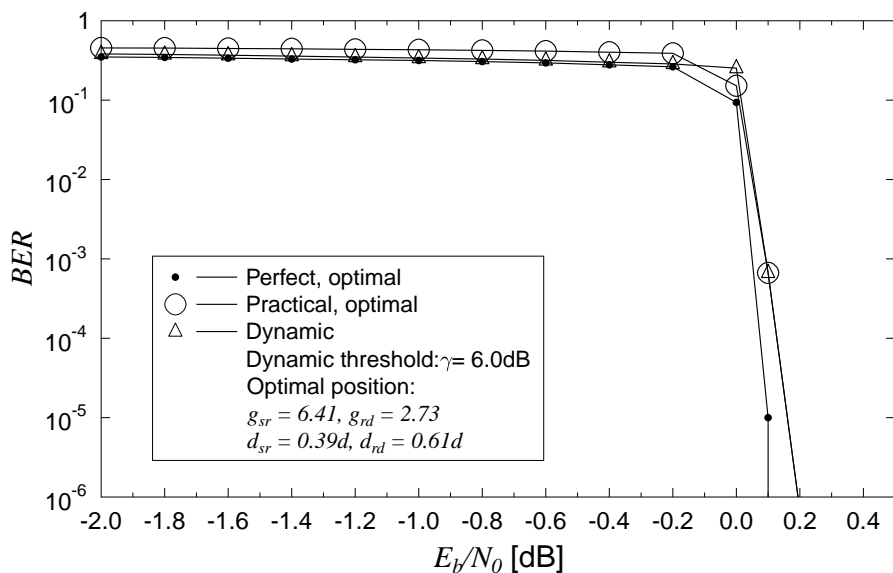


Figure 3.11: BER-performance of the system portrayed in Figure 3.3, when employing optimal relays defined by Equation (3.23) in comparison to using dynamic relays stipulated by Equation (3.27), where all transmissions in the system are affected by the Rayleigh-distributed small-scale fading. The source-relay transmission is relied on the 8PSK modulation scheme.

3.3.3.2 Relay Channel Capacity

According to [173], the upper bound and lower bound of the CCMC of a full duplex relay aided system can be calculated as follows:

$$C_{CCMC}^{relay} \leq \max_{p(X_1, X_2)} \min\{I(X_1; Y_2, Y_{3|X_2}), I(X_1, X_2; Y_3)\}, \quad (3.31)$$

$$C_{CCMC}^{relay} \geq \max_{p(X_1, X_2)} \min\{I(X_1; Y_{2|X_2}), I(X_1, X_2; Y_3)\}, \quad (3.32)$$

where X_1, X_2, Y_2 and Y_3 are the signals transmitted from the S node and R node, as well as the signals received at the R node and the D node, respectively. Furthermore, $p(X_1, X_2)$ is the joint probability of signals transmitted from the S and R nodes. The upper bound and lower bound of the CCMC capacity for a half duplex relaying can be calculated from Equation (3.31) and Equation (3.32) as follows:

$$C_{CCMC}^{relay} \leq \max_{p(X_1, X_2)} \min\{I(X_1; Y_2, Y_3), I(X_1, X_2; Y_3)\}, \quad (3.33)$$

$$C_{CCMC}^{relay} \geq \max_{p(X_1, X_2)} \min\{I(X_1; Y_2), I(X_1, X_2; Y_3)\}. \quad (3.34)$$

Let us now apply the Inequality (3.34) to our half duplex system presented in Section 3.3.1, and assume that the signals transmitted from the source during the second transmission period are available at the destination, and that a pair of relays is viewed as a single equivalent relay having two transmit antennas. Then, we can formulate the upper bound and lower bound of the relay channel's DCMC capacity as follows:

$$C_{CCMC}^{relay} \leq \max_{p(X_1, X_2)} \min\left\{\frac{N_s}{N_s + N_r} \times E[I(X; Y_d^I, Y_r)], \frac{N_s}{N_s + N_r} \times E[I(X; Y_d^I)]\right. \\ \left. + \frac{N_r}{N_s + N_r} \times E[I(X_r; Y_d^{II})]\right\}, \quad (3.35)$$

$$C_{CCMC}^{relay} \geq \max_{p(X_1, X_2)} \min\left\{\frac{N_s}{N_s + N_r} \times E[I(X; Y_r)], \frac{N_r}{N_s + N_r} \times E[I(X_r; Y_d^{II})]\right. \\ \left. + \frac{N_s}{N_s + N_r} \times E[I(X; Y_d^I)]\right\} \quad (3.36)$$

where $X = [x_1, x_2, \dots, x_{N_s}]$ represents the signals transmitted from the S node with x_k formulated in Equation (3.8), while $X_r = [x_{r1,1}, x_{r2,1}, \dots, x_{r1,N_r}, x_{r2,N_r}]$ are the signals transmitted from the equivalent twin-antenna based relay node with $x_{r_i,l}$ formulated in Equation (3.9). Furthermore, $Y_r = Y_{ri} = [y_{r_i,1}, \dots, y_{r_i,N_s}]$ are the signals received at the equivalent two-antenna based relay node with $y_{r_i,k}$ calculated from Equation (3.8). Furthermore, $Y_d^I = [y_{d,1}^I, \dots, y_{d,N_r}^I]$ and $Y_d^{II} = [y_{d,1}^{II}, \dots, y_{d,N_s}^{II}]$ are the signals received at the D node during the first and second transmission periods, where $y_{d,k}^I$ and $y_{d,l}^{II}$ can be calculated from Equation (3.24) and Equation (3.25), respectively. From Equation (3.35) and Equation (3.36), we can compute a range of diverse channel capacities pertaining to our systems as presented in Figure 3.12 and 3.13. Moreover, using these figures, we can calculate relay channel's capacity, as summarised in Table 3.4.

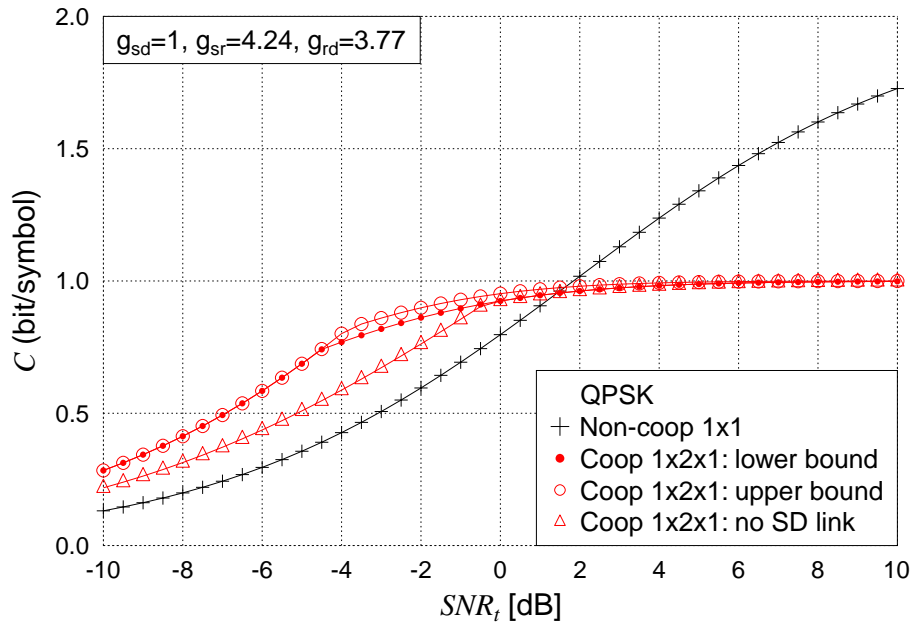


Figure 3.12: Optimal position based relay channel's capacity over the Rayleigh-distributed small-scale fading channel, when the QPSK modulation scheme is employed for source-relay transmission.

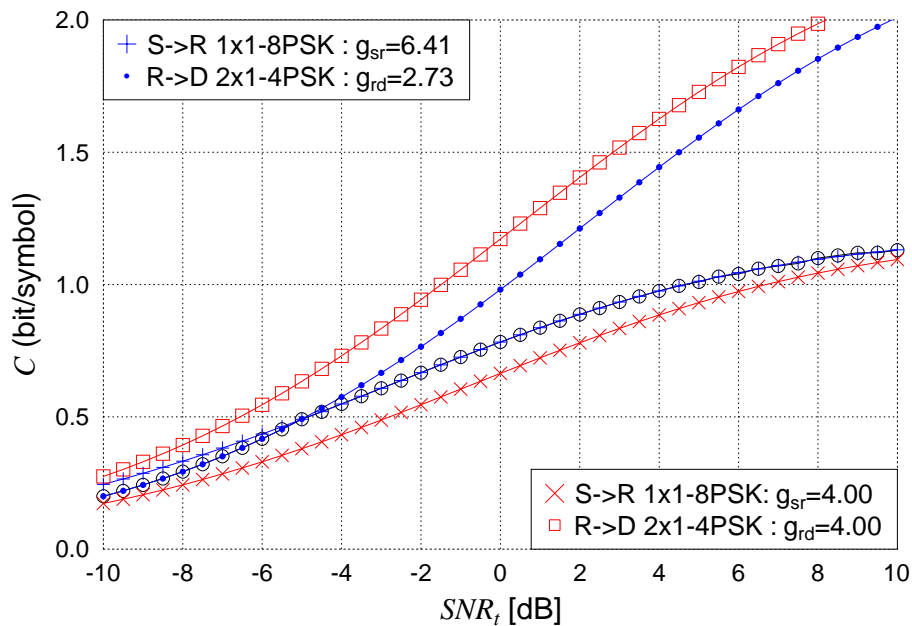


Figure 3.13: Optimal relay channel's capacity, when communicating over the Rayleigh small-scale fading channel, where the 8PSK modulation scheme is employed for source-relay transmission.

3.3.3.3 EXIT-chart for Determining the Number of Outer Iterations

As discussed in Section 3.3.3.1, no errors are imposed by the source-relay links, when dynamic relays are activated. This property guarantees the accuracy of our EXIT chart analysis. Hence, in this section, we calculate both the EXIT chart and the Monte-Carlo simulation based decoding trajectory using the dynamic relay appointment condition formulated in Equation (3.27) with $\gamma = 2.8$ dB. When the number of inner iterations between the URC and IrCC schemes within

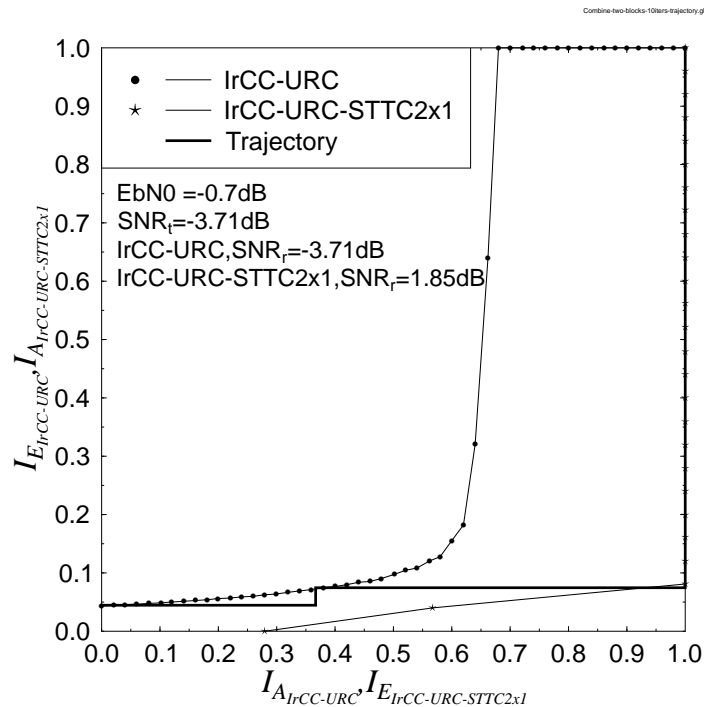


Figure 3.14: The EXIT matching of two amalgamated coding blocks, namely the block containing the IrCC-URC-QPSK scheme and the other relying on IrCC-URC-STTC-QPSK, with the number $I_{in} = 30$ of iterations between IrCC and URC.

the amalgamated coding block of Figure 3.8, namely between the IrCC-URC and Irregular Convolutional Coded Unity Rate Coded Space-Time Trellis Code employing two transmit antennas and one receive antenna (IrCC-URC-STTC2x1) is $I_{in} = 30$, we infer from Figure 3.14 that $I_{out} = 3$ outer iterations are required between the two amalgamated blocks for ensuring that the Monte-Carlo simulation based bit-by-bit decoding trajectory reaches the upper edge of the graph shown in Figure 3.14.

3.3.4 Optimal Relays versus Dynamic Relays

As seen in Figure 3.15, if $I_{out} = 3$ and $I_{in} = 30$ are applied to the decoder at the destination, an SNR improvement of 3.5 dB, 3.3 dB and 3.1 dB is achieved when employing dynamic, optimal and mid-way relays, respectively. Our simulation result also show that the BER performance matched

exactly the EXIT chart predictions presented in Section 3.3.3.3.

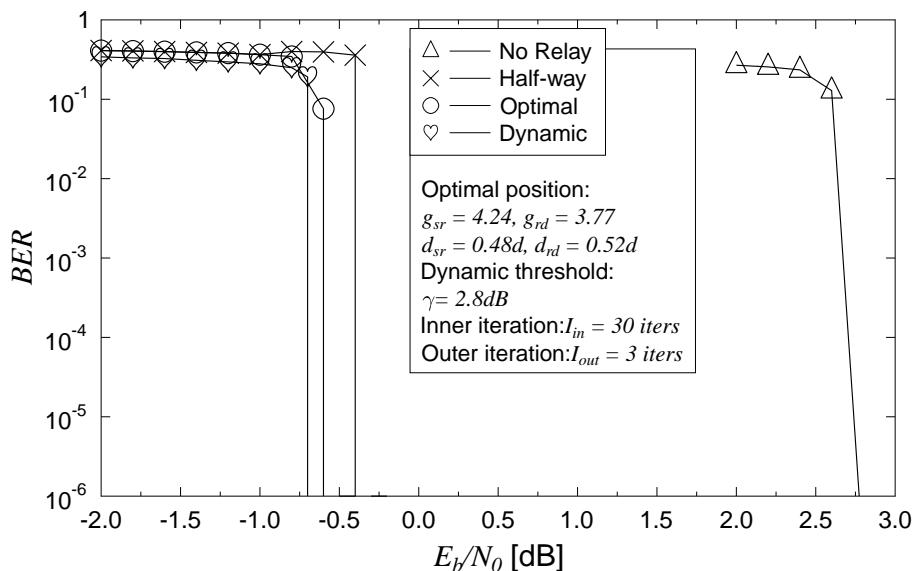


Figure 3.15: BER performance comparison in different position based scenarios, namely the scenario employing the mid-way relays, the scenario selecting the optimal relays and that activating the dynamic relays, when considering the presence of the signals transmitted from the S node at the D node. A Rayleigh channel was considered.

3.4 Chapter Summary

In this chapter, we have proposed a DC-IrCC-URC-STTC scheme for single-antenna based cooperative relaying. We formulated the associated design principles relying on EXIT charts for arbitrary three-stage concatenated cooperative systems. In order to ensure for our near-capacity coding scheme that it provides the best possible performance, we formulated and investigated an optimal condition for selecting the relays by ensuring that they are capable of maintaining an open EXIT chart tunnel both at the R and D nodes at the same value of SNR_r . The optimal relay scheme also mitigated the problem of potential error propagation often imposed by the relays, which was achieved by selecting relay nodes near the optimal locations for ensuring that the received SNR value required at the relay and destination nodes can be maintained simultaneously. Moreover, a dynamic method of relay-selection was proposed in Section 3.3.3.1, in order to make use of the signals transmitted from the source to the destination with the aid of the iterative decoding process used at the destination node in order to improve the achievable performance.

For the sake of convenient comparison, Table 3.4 summarised the channel capacity of different IrCC-URC-STTC based schemes.

Systems	Throughput (bit)	E_b/N_o (dB)	Distance (dB)
IrCC-URC-QPSK	1	1.8	1.0
IrCC-URC-8PSK	1.5	5.0	1.0
IrCC-URC-STTC2x1-QPSK	1	2.3	0.7
NON-SD Transmission QPSK			
DC-IrCC-URC-STTC2x1-QPSK-QPSK no-SD link (mid-way, perfect)	0.5	-1.22	0.5
DC-IrCC-URC-STTC2x1-QPSK-QPSK no-SD link (mid-way, actual)	0.5	-1.22	1.0
DC-IrCC-URC-STTC2x1-QPSK-QPSK no-SD link (optimal, perfect)	0.5	-1.5	0.9
DC-IrCC-URC-STTC2x1-QPSK-QPSK no-SD link (optimal, actual)	0.5	-1.5	1.1
DC-IrCC-URC-STTC2x1-QPSK-QPSK no-SD link (dynamic)	0.5	-1.4	1.0
NON-SD Transmission 8PSK			
DC-IrCC-URC-STTC2x1-8PSK-QPSK no-SD link (mid-way, perfect)	0.6	1.1	-2.5
DC-IrCC-URC-STTC2x1-8PSK-QPSK no-SD link (mid-way, actual)	0.6	1.1	1.1
DC-IrCC-URC-STTC2x1-8PSK-QPSK no-SD link (optimal, perfect)	0.6	-0.9	0.9
DC-IrCC-URC-STTC2x1-8PSK-QPSK no-SD link (optimal, actual)	0.6	-0.9	1.1
DC-IrCC-URC-STTC2x1-8PSK-QPSK no-SD link (dynamic)	0.6	-0.9	1.1
SD Transmission QPSK			
DC-IrCC-URC-STTC2x1-QPSK-QPSK SD link (mid-way, perfect)	0.5	-1.2	0.5
DC-IrCC-URC-STTC2x1-QPSK-QPSK SD link (mid-way, actual)	0.5	-1.2	1.0
DC-IrCC-URC-STTC2x1-QPSK-QPSK link (optimal, perfect)	0.5	-1.5	0.9
DC-IrCC-URC-STTC2x1-QPSK-QPSK SD link (optimal, actual)	0.5	-1.5	1.1
DC-IrCC-URC-STTC2x1-QPSK-QPSK SD link (dynamic)	0.5	-1.4	1.0

Table 3.4: Comparison of various distributed coding schemes in terms of their throughput and the distance between their performance curves and the corresponding DCMC capacity, when communicating over Rayleigh small-scale fading channels.

Near-Capacity Network Coding for Multi-User Cooperative Communications

In this chapter, we conceive multiple-user cooperative systems relying on the near-capacity coding schemes designed in Chapter 2. The chapter is commenced by deriving the upper and lower bounds for the FER performance of cooperative multi-user communications systems using network coding, in order to investigate idealised systems, where all the links are supported by perfect channel capacity-achieving codes operating right at the Continuous-input Continuous-output Memoryless Channel (CCMC) capacity. Then, our realistic near-capacity coding schemes are integrated into these multi-user cooperative systems for designing novel Near-Capacity Multi-user Network-coding (NCMN) based systems.

Aiming for characterising the NCMN based systems, the performance of the idealised multi-user systems operating right at Shannon's capacity is compared to that of the systems operating at the practically achievable capacity and to the realistic systems using our near-capacity channel coding scheme. In the NCMN based systems, both small-scale uncorrelated Rayleigh fading and slow fading channels are considered. In particular, near-capacity network coding schemes are studied along with the attainable capacity of the network coding systems.

Our design philosophy conceived for NCMN based systems may be invoked for arbitrary multi-user topologies using near-capacity channel codes having various throughputs.

4.1 From Network Coding to Generalised Dynamic Network Codes

Network coding is a recently introduced paradigm conceived for efficiently disseminating data in wireless networks, where the data flows arriving from multiple sources are combined for increasing

the throughput, for reducing the delay and/or for enhancing the robustness [176]. Similarly to the DF principle, the relay nodes store the incoming packets in their own buffer and transmit their linear combinations. The coefficients invoked for their linear combinations may be random numbers over a large finite field [42, 177] or from parity-check matrices of error control codes [47, 178]. The linear combination operation is typically performed over finite Galois Fields (GF) [47].

Dynamic Network Codes (DNCs) were recently proposed by Xiao and Skoglund [46], where each of the M users also acts as a relay for the other users. In this system, each user broadcasts a single Information Frame (IF) of its own both to the Base Station (BS) and to the other users during the first Time Slot (TS). Then, during the 2^{nd} to the $(M)^{th}$ TS, each user transmits $(M - 1)$ Parity Frames (PFs) to the BS. Each of these PFs consists of nonbinary linear combinations of the Information Frames (IFs) that it could successfully decode.

Generalised Dynamic Network Codes (GDNCs) were proposed in [47, 99] by interpreting the problem as being equivalent to that of designing linear block codes defined over $GF(q)$ for erasure correction. The authors of [47, 99] extended the original Dynamic Network Coding (DNC) concept by allowing each user to broadcast several (as opposed to a single) IFs of its own during the Broadcast Phase (BP), as well as to transmit several nonbinary linear combinations, which are also considered as PFs, during the Cooperative Phase (CP). A transmission session of Generalised Dynamic Network Code (GDNC) comprises two phases, namely the BP and the CP. In [46, 47, 99, 179], the range of diversity order in each system was estimated in order to roughly compare the expected performance of different systems. The FER performance of the GDNC scheme was determined in [47, 99] by calculating the rank of the matrix characterising GDNCs. This method, which we refer to as the Pure Rank Based Method (PRBM), always provides an optimistic estimate of the attainable FER performance of GDNCs.

4.2 Generalised Dynamic-Network Codes

In this section, we detail the formation of the cooperative multiple-user system portrayed in Figure 4.1, where M users cooperatively communicate with a common BS. A transmission session of the cooperative multiple-user system is conducted in two groups of phases, the Broadcast Phases (BPs) and the Cooperative Phases (CPs). The details of these phases are described as follows.

4.2.1 System Model

During the BPs, each user broadcasts k_1 number of its own IFs. An information frame (packet or message), namely $I_m(t), t = [m, M + m, \dots, (k_1 - 1)M + m]$ transmitted by User m , takes place during the specific broadcast phase $t, t = [m, M + m, \dots, (k_1 - 1)M + m]$, which is selected from the whole set of $k_1 M$ BPs. These $k_1 M$ BPs are comprised of k_1 groups of M BPs, where the k_1

groups are presented in Figure 4.1 by $(B_1) \dots (B_{k_1})$.

Then, during the Mk_2 CPs, each user transmits k_2 number of PFs, namely $\boxplus^1 m(t'), t' = [m, M + m, \dots, (k_2 - 1)M + m]$, containing nonbinary linear combinations of its own IFs and of the IFs transmitted by the other $(M - 1)$ users. The notation $\boxplus m(t')$ in Figure 4.1 denotes the parity frame transmitted by User m during the cooperative phase $k_2(m - 1) + t'$, and \boxplus represents the specific nonbinary linear combination, where the parity coefficients will be defined imminently in the context of Figure 4.1. Similar to the BPs, the Mk_2 CPs include k_2 groups of M CPs, where the k_2 groups are presented in Figure 4.1 by $(C_1) \dots (C_{k_2})$. Note that the number $(M - 2)$ is used for indicating a set of $(M - 2)$ links employed for transmitting IFs from either User m or User f to the other $(M - 2)$ users. The set of $(M - 2)$ links does not include the links used for transmitting IFs to the BS.

Moreover, it should be noted that a single phase is defined as a time period, in which a user performs a single transmission and the transmissions are conducted by M users via the appropriately created orthogonal channels either in the time-, frequency- or code-domain. We consider orthogonal channels in the time domain.

Example 4.1.

Let us consider a specific example of the general system model presented in Figure 4.1, where the system has $M = 2$ users and each user transmits $k_1 = 2$ IFs during the BPs as well as the $k_2 = 2$ PFs during CPs, respectively. In this system, there are $Mk_1 = 4$ BPs as well as $Mk_2 = 4$ CPs, and the details of the transmission phases are portrayed in Figure 4.2. The $Mk_1 = 4$ BPs are arranged in $k_1 = 2$ groups, namely B_1 and B_2 , corresponding to the $k_1 = 2$ IFs transmitted by each user during the BPs. By contrast, while the $Mk_2 = 4$ CPs are allocated to $k_2 = 2$ groups, namely C_1 and C_2 , which correspond to the $k_2 = 2$ PFs transmitted by each of the two users during the CPs. The arrangement of the broadcast and CPs seen in Figure 4.2 is summarised as follows

Broadcast phases

(B_1) Broadcast phase 1 : User 1 $\xrightarrow{I_1(1)}$ BS and User 2,

(B_1) Broadcast phase 2 : User 2 $\xrightarrow{I_2(2)}$ BS and User 1,

(B_2) Broadcast phase 3 : User 1 $\xrightarrow{I_1(3)}$ BS and User 2,

(B_2) Broadcast phase 4 : User 2 $\xrightarrow{I_2(4)}$ BS and User 1,

Cooperative phases

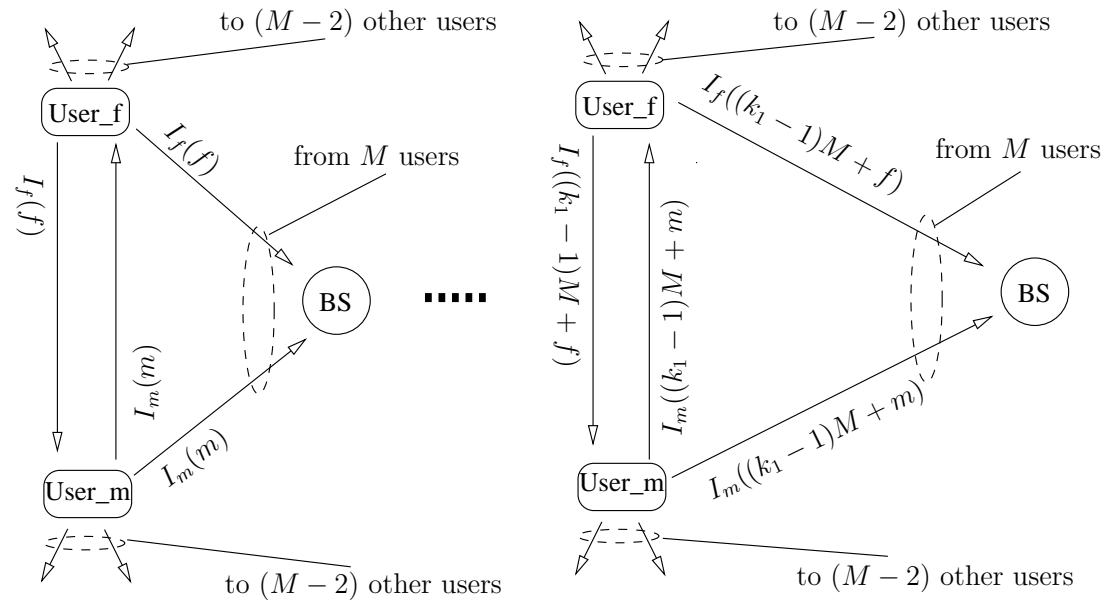
(C_1) Cooperative phase 1 : User 1 $\xrightarrow{\boxplus 1(1)=3I_1(1)+5I_2(2)+2I_1(3)+5I_2(4)}$ BS,

(C_1) Cooperative phase 2 : User 2 $\xrightarrow{\boxplus 2(2)=7I_1(1)+7I_2(2)+4I_1(3)+5I_2(4)}$ BS,

(C_2) Cooperative phase 3 : User 1 $\xrightarrow{\boxplus 1(3)=3I_1(1)+7I_2(2)+3I_1(3)+3I_2(4)}$ BS,

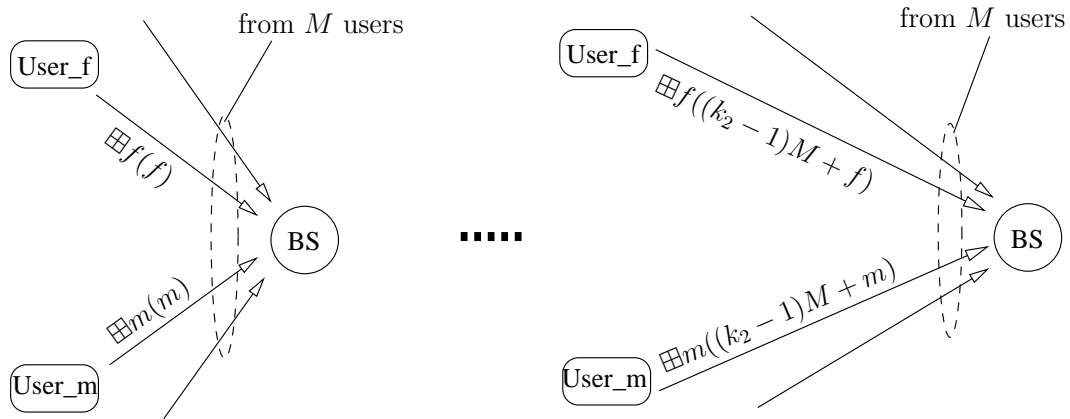
(C_2) Cooperative phase 4 : User 2 $\xrightarrow{\boxplus 2(4)=4I_1(1)+6I_2(2)+1I_1(3)+2I_2(4)}$ BS.

¹The \boxplus operation in this context was first introduced in [46, 179].



(B₁) Broadcast phases m and f

(B _{k_1}) Broadcast phases $(k_1 - 1)M + m$
and $(k_1 - 1)M + f$



(C₁) Cooperative phases m and f

(C _{k_2}) Cooperative phases $(k_2 - 1)M + m$
and $(k_2 - 1)M + f$

Figure 4.1: General model of the NCMN based system relying on M users.

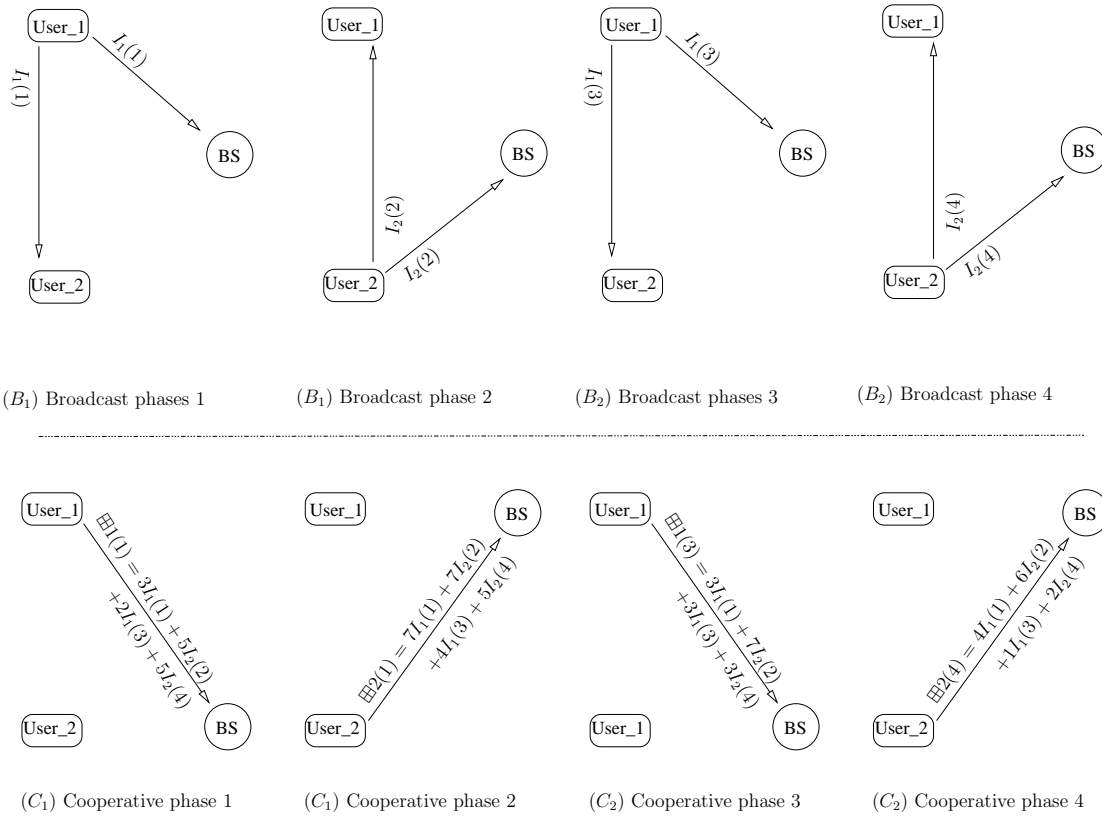


Figure 4.2: The model of the specific system supporting $M = 2$ users, where each user transmits $k_1 = 2$ IFs and $k_2 = 2$ PFs.

$$\mathbf{G}_{4 \times 8} = \left[\begin{array}{cccc|cccc} 1 & 0 & 0 & 0 & 3 & 7 & 3 & 6 \\ 0 & 1 & 0 & 0 & 5 & 7 & 7 & 4 \\ 0 & 0 & 1 & 0 & 2 & 4 & 6 & 1 \\ 0 & 0 & 0 & 1 & 5 & 5 & 3 & 2 \end{array} \right]. \quad (4.1)$$

4.2.2 Transfer Matrix

A transmission session of the system can be equivalently represented by the transfer matrix. The transfer matrix $\mathbf{G}_{k_1 M \times k_1 M + k_2 M}$ (or \mathbf{G} for shorthand) seen in Figure 4.5 comprising the identity matrix $\mathbf{I}_{k_1 M \times k_1 M}$ (or \mathbf{I} for shorthand) and the parity matrix $\mathbf{P}_{k_1 M \times k_2 M}$ (or \mathbf{P} for shorthand) represents a transmission session of the system, where all the frames transmitted during that session are successfully decoded. This transfer matrix can be derived from the appropriately selected systematic generator matrix G of an (n, k, d_{min}) linear block code [47] and [99], which is shown in Figure 4.3. The linear block code employed should be a Maximum Distance Separable (MDS) code for the sake of satisfying the maximum minimum distance bound [180]. The systematic generator matrix \mathbf{G} of the Reed Solomon (RS) codes constituting a well-known class of MDS codes is provided by the software application SAGE [181].

In Example 4.1, if all the frames transmitted within a session are successfully decoded, the

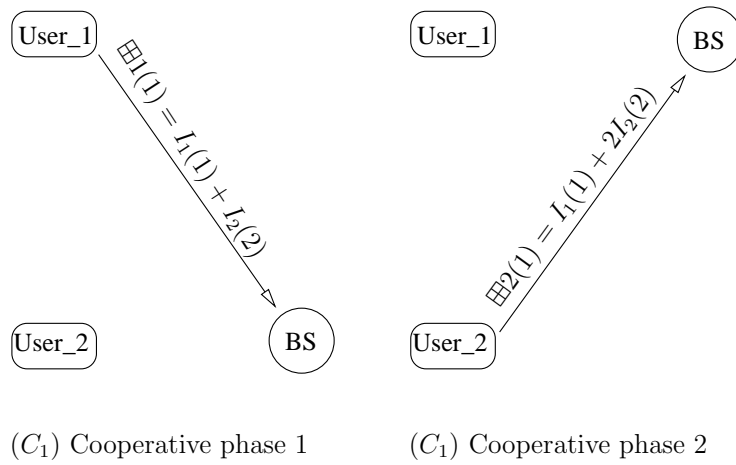
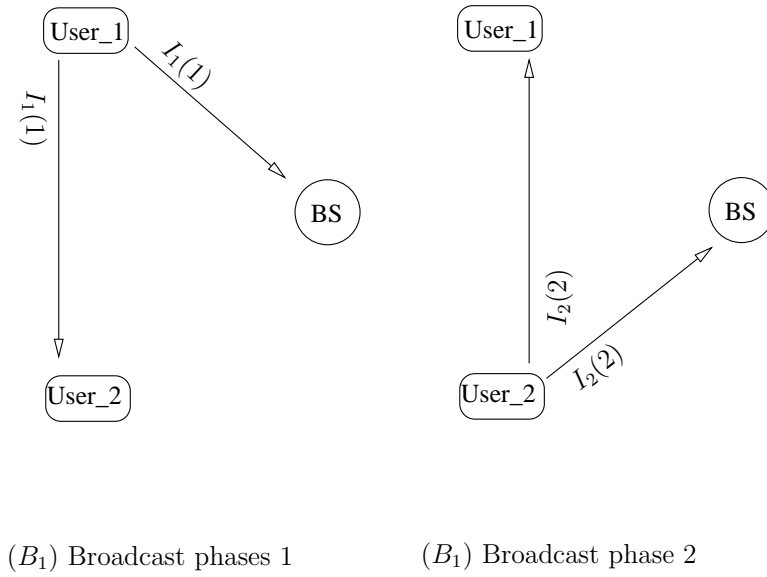


Figure 4.4: The model of the system supporting $M = 2$ users, where each user transmits $k_1 = 1$ IFs and $k_2 = 1$ PFs.

or User 2 during the cooperative phase C_1 or C_2 is successfully decoded at the BS, provided that the linear combining coefficient of the information frame $I_1(1)$ or $I_2(2)$ in this parity frame has a value of "1" or "1", respectively.

To elaborate further, the system might experience an actual transmission session containing $(k_1M + k_2M) = 4$ phases depending on the success or failure of a specific transmission attempt

as follows

Broadcast phases

$$\begin{aligned}
 (B_1) \quad & \mathbf{G}'_{2 \times 4}(1,3) = \mathbf{G}_{2 \times 4}(1,3), \\
 & [\text{User 1} \xrightarrow{=0} \text{BS}] : \mathbf{G}'_{2 \times 4}(1,1) = 0, \\
 & [\text{User 1} \xrightarrow{=1} \text{User 2}] : \mathbf{G}'_{2 \times 4}(2,4) = \mathbf{G}_{2 \times 4}(2,4), \\
 (B_2) \quad & \mathbf{G}'_{2 \times 4}(2,4) = \mathbf{G}_{2 \times 4}(2,4), \\
 & [\text{User 2} \xrightarrow{=0} \text{BS}] : \mathbf{G}'_{2 \times 4}(2,2) = 0, \\
 & [\text{User 2} \xrightarrow{=1} \text{User 1}] : \mathbf{G}'_{2 \times 4}(1,4) = \mathbf{G}_{2 \times 4}(1,4),
 \end{aligned}$$

Cooperative phases

$$\begin{aligned}
 (C_1) \quad & [\text{User 1} \xrightarrow{=0} \text{BS}] : \mathbf{G}'_{2 \times 4}(i,3) = 0, i = 1,2, \\
 (C_2) \quad & [\text{User 2} \xrightarrow{=1} \text{BS}] :,
 \end{aligned}$$

where ' \rightarrow ' represents the transmission direction, while ' $=0$ ' or ' $=1$ ' means that the frame is successfully/unsuccessfully recovered at the destination, respectively. We define $\mathbf{G}'_{2 \times 4}$ as the corresponding 'modified' transfer matrix, where the terminology 'modified' implies that the entries of $\mathbf{G}'_{2 \times 4}$ are modified from those of the original transfer matrix $\mathbf{G}_{2 \times 4}$ of Equation (4.2) according to the actual transmission session detailed in Equation (4.3). As a result, $\mathbf{G}'_{2 \times 4}$ is formed as

$$\mathbf{G}'_{2 \times 4} = \left[\begin{array}{cc|cc} 0 & 0 & 0 & 1 \\ 0 & 0 & 0 & 2 \end{array} \right], \quad (4.3)$$

where the diagonal elements '1' at the left of Equation (4.2) become '0' owing to the unsuccessful $[\text{User 1} \xrightarrow{=0} \text{BS}]$ and $[\text{User 2} \xrightarrow{=0} \text{BS}]$ transmissions in (4.3B₁) and (4.3B₂). The '0' elements in the third column of Equation (4.3) indicate the unsuccessful $[\text{User 1} \xrightarrow{=0} \text{BS}]$ transmission in (4.3C₁).

Let us now generalise this model. The transfer matrix $\mathbf{G}_{k_1 M \times k_1 M + k_2 M}$ (or \mathbf{G} for shorthand) in Figure 4.5 comprising the identity matrix $\mathbf{I}_{k_1 M \times k_1 M}$ (or \mathbf{I} for shorthand) and the parity matrix $\mathbf{P}_{k_1 M \times k_2 M}$ (or \mathbf{P} for shorthand) represents a transmission session of the system, where all the frames transmitted during that session are successfully decoded. Accordingly, the binary flag $I_m^{\text{Co}}(t)$ seen in Figure 4.5 represents the success or failure of decoding an information frame at the BS, namely $I_m(t)$, $t = [m, M + m, \dots, (k_1 - 1)M + m]$, transmitted by User m , $m \in \{1, \dots, M\}$, which is set during the specific broadcast phase t selected from the entire set of $k_1 M$ BPs according to:

$$I_m^{\text{Co}}(t) = \begin{cases} 1 & : \text{ If } I_m(t) \text{ is successfully recovered} \\ 0 & : \text{ Otherwise} \end{cases}. \quad (4.4)$$

The k_2 PFs transmitted by each of the M users contain nonbinary linear combinations of its own IFs with the successfully decoded IFs among $k_1(M - 1)$ IFs transmitted by the $(M - 1)$ other users. The variables $P_{m,s}(t)$ in Figure 4.5 correspond to the parity coefficient of the information frame $I_{t \bmod M}(t)$ contained in the s^{th} parity frame transmitted by User m during the cooperative

phase $[M(s - 1) + m]$, $s \in \{1, \dots, k_2\}$. The index r is determined by the rule that we get $r = M$ if we have $t \bmod M = 0$, otherwise we get $r = t \bmod M$. Let us denote the corresponding entry of $P_{m,s}(t)$ in the modified matrix \mathbf{G}' as $P'_{m,s}(t)$, which is determined by

$$P'_{m,s}(t) = \begin{cases} P_{m,s}(t) & : r = m \end{cases} . \quad (4.5)$$

Then, for the case that we have $r \neq m$, the entry $P'_{m,s}(t)$ is specified by

$$P'_{m,s}(t) = \begin{cases} P_{m,s}(t) & : \text{User } r \xrightarrow{=1} \text{User } m \\ 0 & : \text{User } r \xrightarrow{=0} \text{User } m \end{cases} . \quad (4.6)$$

The column $[M(s - 1) + m]$ of the parity matrix \mathbf{P} shown in Figure 4.5 contains the set of parity coefficients valid for the specific nonbinary linear combination, which forms the s^{th} parity frame transmitted by User m during the cooperative phase $[M(s - 1) + m]$. Hence, the entire column $P'_{m,s}(t)$ variables, $\forall t = [1, 2, \dots, k_1 M]$ will be set to zeros, if the BS could not successfully receive the s^{th} parity frame:

$$P'_{m,s}(t) = \begin{cases} P_{m,s}(t) & : [\text{User } m \xrightarrow{s^{\text{th}} \text{ parity frame} = 1} \text{BS}] \\ 0 & : \text{Otherwise, } \forall t = [1, 2, \dots, k_1 M] \end{cases} . \quad (4.7)$$

In brief, the modified transfer matrix \mathbf{G}' is formed by modifying the entries of the original transfer matrix \mathbf{G} based on Equation (4.4), Equation (4.6) and Equation (4.7) in turn.

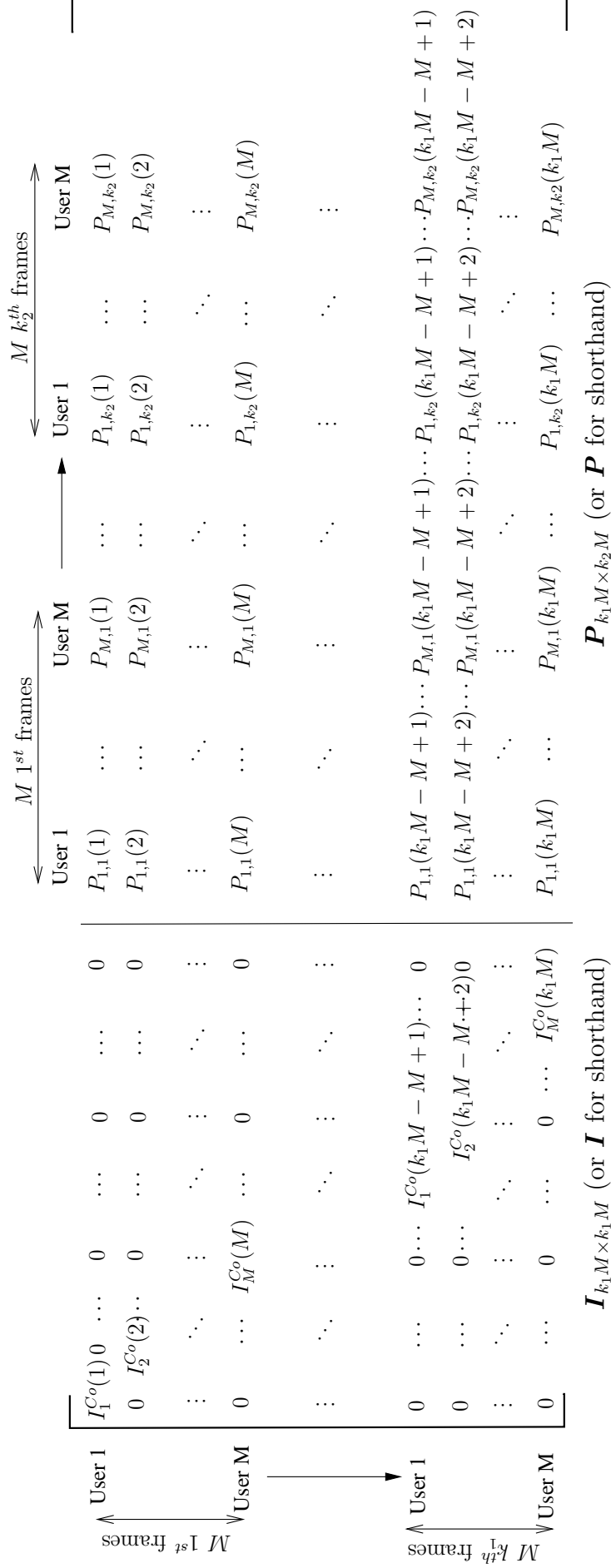


Figure 4.5: The transfer matrix $\mathbf{G}_{k_1 M \times k_1 M + k_2 M}$ (or \mathbf{G} for shorthand) illustrating a transmission session of the system having M users transmitting in $(k_1 M + k_2 M)$ phases, as presented in Figure 4.1.

4.3 Recovering of the Information Frames at the Base Station

Let us first consider a transmission session of the system described in Example 4.1, where the original transfer matrix $\mathbf{G}_{4 \times 8}$ is given by Equation (4.1). The actual transmission session results in a modified matrix $\mathbf{G}'_{4 \times 8}$ formulated as²

$$\mathbf{G}'_{4 \times 8} = \left[\begin{array}{cccc|cccc} 0 & 0 & 0 & 0 & 0 & 0 & 3 & 0 \\ 0 & 0 & 0 & 0 & 0 & 0 & 7 & 0 \\ 0 & 0 & 1 & 0 & 0 & 0 & 6 & 1 \\ 0 & 0 & 0 & 0 & 0 & 0 & 3 & 2 \end{array} \right]. \quad (4.8)$$

According to Figure 4.5, the modified matrix $\mathbf{G}'_{4 \times 8}$ consists of the two following sub-matrices

$$\mathbf{I}'_{4 \times 8} = \left[\begin{array}{cccc} 0 & 0 & 0 & 0 \\ 0 & 0 & 0 & 0 \\ 0 & 0 & 1 & 0 \\ 0 & 0 & 0 & 0 \end{array} \right], \quad (4.9)$$

$$\mathbf{P}'_{4 \times 8} = \left[\begin{array}{cccc} 0 & 0 & 3 & 0 \\ 0 & 0 & 7 & 0 \\ 0 & 0 & 6 & 1 \\ 0 & 0 & 3 & 2 \end{array} \right]. \quad (4.10)$$

If we denote the $k_1 M$ IFs transmitted by the two users as $\mathbf{X}_{4 \times 8} = \{I_1(1), I_2(2), I_1(3), I_2(4)\}$, we have

$$\mathbf{X}_{4 \times 8} \mathbf{I}'_{4 \times 8} = \mathbf{Y}_{I', 4 \times 8}, \quad (4.11)$$

$$\mathbf{X}_{4 \times 8} \mathbf{P}'_{4 \times 8} = \mathbf{Y}_{P', 4 \times 8}, \quad (4.12)$$

where $\mathbf{Y}_{I', 4 \times 8}$ and $\mathbf{Y}_{P', 4 \times 8}$ represent the signals received by the BS during the $k_1 M = 4$ BPs and $k_2 M = 4$ CPs, respectively. This implies that the BS knows the matrix $\mathbf{Y}_{I', 4 \times 8}$ and $\mathbf{Y}_{P', 4 \times 8}$, which may be presented by the following matrices of decimal numbers

$$\mathbf{Y}_{I', 4 \times 8} = \left[\begin{array}{cccc} 0 & 0 & 3 & 0 \end{array} \right], \quad (4.13)$$

$$\mathbf{Y}_{P', 4 \times 8} = \left[\begin{array}{cccc} 0 & 0 & 37 & 11 \end{array} \right]. \quad (4.14)$$

Accordingly, Equation (4.11) is equivalent to the following linear equation:

$$\begin{aligned} 0 \times I_1(1) + 0 \times I_2(2) + 1 \times I_1(3) + 0 \times I_1(4) &= 3, \\ I_1(3) &= 3, \end{aligned} \quad (4.15)$$

²It should be noted that all operations are conducted upon $\text{GF}(q)$. For the sake of readability, we present our numerical example in decimal numbers.

while Equation (4.12) may be represented by the following linear equations

$$3 \times I_1(1) + 7 \times I_2(2) + 6 \times I_1(3) + 3 \times I_1(4) = 37, \quad (4.16)$$

$$0 \times I_1(1) + 0 \times I_2(2) + 1 \times I_1(3) + 2 \times I_1(4) = 11. \quad (4.17)$$

Upon substituting Equation (4.15) into Equation (4.16) and Equation (4.17), we may eliminate the appearance of the $I_1(3)$, in order to arrive at

$$3 \times I_1(1) + 7 \times I_2(2) + 3 \times I_1(4) = 29, \quad (4.18)$$

$$2 \times I_1(4) = 8. \quad (4.19)$$

Observe at the left side of Equation (4.19) that there is a single term, i.e. $2 \times I_1(4)$. Hence, we can recover the information frame $I_1(4)$ as follows:

$$2 \times I_1(4) = 8,$$

$$I_1(4) = 4. \quad (4.20)$$

Similarly, we again substitute Equation (4.20) into Equation (4.18) for the sake of eliminating the appearance of $I_1(4)$, in order to obtain:

$$3 \times I_1(1) + 7 \times I_2(2) + 3 \times I_1(4) = 29,$$

$$3 \times I_1(1) + 7 \times I_2(2) = 17. \quad (4.21)$$

Again, observe in Equation (4.21) that instead of having a single term at the left of Equation (4.21), we have two additive terms. As a result, having an exhaustive search becomes impractical for a large set of possible values. This means that we cannot detect all the IFs. Hence, in our specific example the BS can only recover two out of the $Mk_1 = 4$ IFs, where the recovered frames are given by Equation (4.15) and Equation (4.20).

Generally, as the system proceeds through an actual transmission session, the corresponding modified transfer matrix \mathbf{G}' consisting of its identity matrix \mathbf{I}' and its parity matrix \mathbf{P}' is formed, where \mathbf{I}' is generated from Equation (4.4), while \mathbf{P}' is determined in turn by Equation (4.6) and Equation (4.7). The frames successfully received at the BS can be represented as

$$\mathbf{X}\mathbf{I}' = \mathbf{Y}_{I'}, \quad (4.22)$$

$$\mathbf{X}\mathbf{P}' = \mathbf{Y}_{P'}, \quad (4.23)$$

where $\mathbf{X} = \{I_1(1), I_2(2), \dots, I_M(k_1M)\}$ is a matrix representing the IFs transmitted by the M users during the transmission session of the system, while the matrices of $\mathbf{Y}_{I'}$ and $\mathbf{Y}_{P'}$ represent the frames successfully received at the BS during the BPs and CPs, respectively. In line with [47, 99], we assume that the BS is aware of how each parity frame was constructed, hence \mathbf{G}' is known at the

BS. Since the matrix \mathbf{I}' may be different from \mathbf{I} , the BS can certainly recover a set $\mathbf{X}_{I'}$ of frames, which is a subset of \mathbf{X} , from $\mathbf{Y}_{I'}$ as

$$\mathbf{X}_{I'} = \mathbf{Y}_{I'}. \quad (4.24)$$

Upon substituting $\mathbf{X}_{I'}$ given by Equation (4.23) into Equation (4.22), we arrive at:

$$(\mathbf{X} - \mathbf{X}_{I'}) \mathbf{P}' = \mathbf{Y}_{P'} - \mathbf{X}_{I'} \mathbf{P}'. \quad (4.25)$$

Then, a set $\tilde{\mathbf{X}}_{P'}$ of IFs is retrieved from Equation (4.25) by a two-step algorithm, which is based on the classic Gaussian elimination [182] algorithm. The following is the summary of the algorithm

1. Convert the matrix \mathbf{P}' of Equation (4.25) into an upper triangular matrix \mathbf{P}'_{UT} and change the matrix $\mathbf{Y}_{P'}$ correspondingly. Using the following algorithm steps:

```

i := 1
j := 1
while (i ≤ k2M and j ≤ k2M) do
  nonzero := i
  For k := i + 1 to k2M do
    if p' [k, j] ≠ 0 then
      nonzero := k
    end if
  end for
  if p' [nonzero, j] ≠ 0 then
    swap rows i and nonzero in both  $\mathbf{P}'$  and  $\mathbf{Y}_{P'}$ 
    divide each entry in row i by p' [i, j] in both  $\mathbf{P}'$  and  $\mathbf{Y}_{P'}$ 
    for u := i + 1 to k2M do
      subtract p' [i, j] * row i from row u in both  $\mathbf{P}'$  and  $\mathbf{Y}_{P'}$ 
    end for
    i := i + 1
  end if
  j := j + 1
end while;

```

2. Replace backwards in the matrix \mathbf{P}'_{UT} with the aid of the new version of $\mathbf{Y}_{P'}$ to determine $\tilde{\mathbf{X}}_{P'}$.

```

while    (a row having a single entry in  $\mathbf{P}'_{UT} := true$ ) do
        search for a row having a single entry in  $\mathbf{P}'_{UT}$ 
        if  $single-entry-row := found$  then
            calculate the corresponding frame
            replace this frame to all the row of  $\mathbf{P}'_{UT}$ 
        end if
        a row having single entry in  $\mathbf{P}'_{UT} := false$ 
end while;

```

Note that the variable *nonzero* used in the above-detailed algorithm represents the location of the entry that is not equal to zero.

Ultimately, the entire set of IFs recovered at the BS is given by $\tilde{\mathbf{X}}_{P'} \cup \mathbf{X}_{I'}$ out of the \mathbf{X} frames transmitted.

4.4 Pragmatic Method versus Rank-based Method

In this section, the method referred to as Purely Rank-Based Method (PRBM), which is a term used in Section 4.1 to refer to the method employed by the authors of [47, 99], is detailed. The results of the PRBM to those of our novel Pragmatic Algebraic Linear Equation Method (PALEM), which is capable of providing more accurate FER results for the characterisation of network codes than those provided by PRBM.

4.4.1 Purely Rank-Based Method

The FER performance of the system was determined in [47, 99] by calculating the rank of the modified matrix \mathbf{G}' , which always provides an optimistic estimate of the attainable FER performance of GDNCs. Let us characterise the system's performance estimated by the PRBM employed in [47, 99] by recalling Example 4.2, where the modified transfer matrix $\mathbf{G}'_{2 \times 4}$ has the form of

$$\mathbf{G}'_{2 \times 4} = \left[\begin{array}{cc|cc} 0 & 0 & 0 & 1 \\ 0 & 0 & 0 & 2 \end{array} \right]. \quad (4.26)$$

According to the prediction of the PRBM, the BS can recover $\text{Rank}(\mathbf{G}'_{2 \times 4}) = 1$ frame, where $\mathbf{G}'_{2 \times 4}$ is given in Equation (4.6). It is readily inferred from Equation (4.26) that

$$\mathbf{I}'_{2 \times 4} = \left[\begin{array}{cc} 0 & 0 \\ 0 & 0 \end{array} \right], \quad (4.27)$$

$$\mathbf{P}'_{2 \times 4} = \left[\begin{array}{cc} 0 & 1 \\ 0 & 2 \end{array} \right]. \quad (4.28)$$

Having the all-zero $\mathbf{I}'_{2 \times 4}$ of Equation (4.27) means that no IFs were received correctly by the BS before the end of the BPs. As a result of Equation (4.24), this leads to the all-zero matrix $\mathbf{Y}'_{I' 2 \times 4}$. Hence, the IFs presented by the matrix $\mathbf{X}_{2 \times 4} = \{I_1(1), I_2(2)\}$ may be recovered by relying on:

$$\mathbf{X}_{2 \times 4} \mathbf{P}'_{2 \times 4} = \mathbf{Y}_{P' 2 \times 4} \quad (4.29)$$

where the matrix $\mathbf{Y}_{P' 2 \times 4}$ represents the signals received at the BS during the CPs. Note that getting IFs, namely $I_1(1)$ and I_2 , from Equation (4.29) resembles determining two variables, namely $I_1(1)$ and $I_2(2)$, from the following equation

$$1 \times I_1(1) + 2 \times I_2(2) = Y, \quad (4.30)$$

where Y is known, provided that the value of $I_1(1)$ and $I_2(2)$ belongs to a set having a finite but extremely large number of elements. As a result, in fact the BS cannot recover any of two IFs, namely $I_1(1)$ and $I_2(2)$.

4.4.2 Pragmatic Algebraic Linear Equation Method

Based on the algorithms employed in the recovery of the frames at the BS as presented in Section 4.3, we proposed a new method that we refer to as the Pragmatic Algebraic Linear Equation Method (PALEM), which is capable of providing accurate FER performance results. The PALEM can be represented in form of the following three main steps:

1. Specify the rank of the transfer matrix \mathbf{G} and \mathbf{I}' : $\text{rank}(\mathbf{G}) = R_F, \text{rank}(\mathbf{I}') = R_{I'}$
2. Set all the specific variables that can be recovered with the aid of the matrix \mathbf{I}' in the entire modified transfer matrix \mathbf{G}' to zero for the sake of forming a new transfer matrix \mathbf{G}'' .
3. Let us now denote the number of recoverable variables by N_c , which is a function of $R_F, R_{I'}, R_{P''}$ and K_F , where $R_{P''}$ is the rank of the parity matrix \mathbf{P}'' , and K_F is the number of variables that can be recovered with the aid of the matrix \mathbf{P}'' . Hence, we have

$$N_c = \begin{cases} R_F & : R_{I'} + R_{P''} = R_F \\ R_{I'} + K_F & : R_{I'} + R_{P''} < R_F \end{cases}, \quad (4.31)$$

where K_F is calculated by using the following rules

$$K_F = \begin{cases} T_s & : \text{a single-term row found in } P''_{U,T} \\ 0 & : \text{otherwise} \end{cases}. \quad (4.32)$$

Note that T_s is the accumulated number of single-term rows found in $P''_{U,T}$ and its modified versions, where the modified version of $P''_{U,T}$ is formed by setting the entire column corresponding to the single term found to zero. For the sake of constructing a systematic search procedure, once a single term was found, T_s is incremented according to $T_s = T_s + 1$, and

the matrix $P''_{U,T}$ or its modified version is further updated for the next search step required for recovering the next variable. The search process is repeated, until no more single-term row can be found in the most recent matrix version, which was generated from $P''_{U,T}$.

Let us use the following example to describe how PALEM operates.

Example 4.3.

Let us continue to use the system detailed in Example 4.1, where again the original $\mathbf{G}_{4 \times 8}$ transfer matrix based system is represented as

$$\mathbf{G}_{4 \times 8} = \left[\begin{array}{cccc|cccc} 1 & 0 & 0 & 0 & 3 & 7 & 3 & 6 \\ 0 & 1 & 0 & 0 & 5 & 7 & 7 & 4 \\ 0 & 0 & 1 & 0 & 2 & 4 & 6 & 1 \\ 0 & 0 & 0 & 1 & 5 & 5 & 3 & 2 \end{array} \right]. \quad (4.33)$$

There might be an actual transmission session, which leads to a modified transfer matrix \mathbf{G}' of

$$\mathbf{G}'_{4 \times 8} = \left[\begin{array}{cccc|cccc} 0 & 0 & 0 & 0 & 0 & 0 & 3 & 0 \\ 0 & 0 & 0 & 0 & 0 & 0 & 7 & 0 \\ 0 & 0 & 1 & 0 & 0 & 0 & 6 & 1 \\ 0 & 0 & 0 & 0 & 0 & 0 & 3 & 2 \end{array} \right]. \quad (4.34)$$

Bearing in mind the structure of the matrix \mathbf{G}' , we have the corresponding identity matrix \mathbf{I}' and parity matrix \mathbf{P}' expressed in the following form:

$$\mathbf{I}' = \left[\begin{array}{cccc} 0 & 0 & 0 & 0 \\ 0 & 0 & 0 & 0 \\ 0 & 0 & 1 & 0 \\ 0 & 0 & 0 & 0 \end{array} \right]. \quad (4.35)$$

According to the PALEM, we have the following result:

1. We have the following ranks for \mathbf{G} and \mathbf{G}' : $\text{rank}(\mathbf{G}) = R_F = 4$, $\text{rank}(\mathbf{I}') = R_I = 1$;
2. Set all the specific variables that can be recovered with the aid of the matrix \mathbf{I}' in the entire modified transfer matrix \mathbf{G}' to zero for the sake of forming a new transfer matrix \mathbf{G}'' . Accordingly, we may obtain the new transfer matrix \mathbf{G}'' and its corresponding parity matrix \mathbf{P}'' as

$$\mathbf{G}''_{4 \times 8} = \left[\begin{array}{cccc|cccc} 0 & 0 & 0 & 0 & 0 & 0 & 3 & 0 \\ 0 & 0 & 0 & 0 & 0 & 0 & 7 & 0 \\ 0 & 0 & 0 & 0 & 0 & 0 & 0 & 0 \\ 0 & 0 & 0 & 0 & 0 & 0 & 0 & 2 \end{array} \right], \quad (4.36)$$

$$\mathbf{P}'' = \left[\begin{array}{cccc} 0 & 0 & 3 & 0 \\ 0 & 0 & 7 & 0 \\ 0 & 0 & 0 & 0 \\ 0 & 0 & 0 & 2 \end{array} \right]. \quad (4.37)$$

3. We can infer the upper triangular version $\mathbf{P}'_{U,T}$ of the transposed matrix \mathbf{P}'' as

$$\mathbf{P}'_{U,T} = \begin{bmatrix} -3 & -7 & 0 & 0 \\ 0 & 0 & 0 & 0 \\ 0 & 0 & 0 & 0 \\ 0 & 0 & 0 & 2 \end{bmatrix}. \quad (4.38)$$

From the matrix $\mathbf{P}'_{U,T}$, the next modified version $\mathbf{P}'''_{U,T}$ is formed as

$$\mathbf{P}'''_{U,T} = \begin{bmatrix} -3 & -7 & 0 & 0 \\ 0 & 0 & 0 & 0 \\ 0 & 0 & 0 & 0 \\ 0 & 0 & 0 & 0 \end{bmatrix}. \quad (4.39)$$

The matrices $\mathbf{P}'''_{U,T}$ and $\mathbf{P}'_{U,T}$ suggest that $K_F = T_s = 1$. This results in $N_c = R_I + K_F = 2$, since we have $R_I + R_{P''} = 3 < R_F = 4$, where $N_c = 2$ means that the BS can recover two IFs.

4.5 The System's Outage Probability

In this section the system's outage probability is formulated in order to facilitate the derivation of its bounds. For the sake of readability, we briefly summarise the main formulae, while the details of the derivations are presented in Appendix A.

Let $U_{m,t}$ be a set of user indices corresponding to the specific users that succeeded in correctly recovering an IF $I_m(t)$ transmitted by User m during TS t . Let us denote the number of members in the user set $U_{m,t}$ by $||U_{m,t}||$. Furthermore, let the complement set of $U_{m,t}$ be $U_{m,t}^*$. We always have $||U_{m,t}^*|| = M - ||U_{m,t}||$, $1 \leq ||U_{m,t}|| \leq M$. Then, according to [46, 47, 99, 179, 183], there exist at least $(k_1||U_{m,t}|| + k_2||U_{m,t}||)$ frames, which contain the IFs transmitted by all the users in the set $U_{m,t}$. Accordingly, an outage is declared for the IF $I_m(t)$, when the direct transmission $I_m(t)$ and at least $||U_{m,t}||k_2$ out of the remaining $(k_1||U_{m,t}|| - 1 + ||U_{m,t}||k_2)$ received frames are in outage. This occurs with a probability of [47, 99]

$$P_{o,m}(U_{m,t}^*) = \sum_{q=0}^Q \underbrace{\binom{Q+K}{K+q}}_{=T_{o,m}(q)} \frac{P_e^{K+q+1}}{(1-P_e)^{q-Q}}, \quad (4.40)$$

where $\binom{n}{k}$ is the binomial coefficient, while we have

$$Q = k_1||U_{m,t}|| - 1, \quad (4.41)$$

$$K = k_2||U_{m,t}||, \quad (4.42)$$

provided that P_e is the outage probability of the single link, which is defined in [152] for the CCMC scenario.

Note that there might be more than $(k_1||U_{m,t}|| + k_2||U_{m,t}||)$ frames [46,47,99,179,183], which contain the IFs transmitted by all users of the set $U_{m,t}$. If the availability of those extra frames is taken into account, we will arrive at the true outage probability $P_{o,m}^{True}(U_{m,t}^*)$ for the IF $I_m(t)$, which always satisfies

$$P_{o,m}^{True}(U_{m,t}^*) \leq P_{o,m}(U_{m,t}^*). \quad (4.43)$$

Notably, $P_{o,m}^{True}(U_{m,t}^*)$ is the outage probability for a given $U_{m,t}^*$. The system's total outage probability P_o for all possible sets of $U_{m,t}^*$ can be calculated by [99]

$$P_o = \sum_{||U_{m,t}^*||=0}^{M-1} \frac{P_e^{||U_{m,t}^*||}}{(1 - P_e)^{||U_{m,t}^*||-M+1}} P_{o,m}^{True}(U_{m,t}^*), \quad (4.44)$$

where $\frac{P_e^{||U_{m,t}^*||}}{(1 - P_e)^{||U_{m,t}^*||-M+1}}$ is the probability of $||U_{m,t}^*||$ out of $(M - 1)$ inter-user channels in time slot t being in outage.

4.5.1 The Upper Bound of the Outage Probability

In this section, by focusing on the low $P_e \ll 1$ region, we first approximate the term $T_{o,m}(q)$ of Equation (4.40). Having approximated the term $T_{o,m}(q)$ of Equation (4.40) leads to the upper-approximation of the $P_{o,m}(U_{m,t}^*)$ given by Equation (4.40), which is further employed for evaluating the probability $P_{o,m}^{True}(U_{m,t}^*)$ by utilising Inequality (4.43). Then, the approximation of $P_{o,m}^{True}(U_{m,t}^*)$ is deployed for formulating the upper bound of the outage probability P_o of Equation (4.44).

Let begin by considering the ratio of two successive terms in Equation (4.40), namely that of $T_{o,m}(j)$ and $T_{o,m}(j + 1)$, which may be expressed as:

$$R_{o,m}(j) = \frac{T_{o,m}(j + 1)}{T_{o,m}(j)} = \frac{(Q - j)P_e}{(K + j + 1)(1 - P_e)}, \quad (4.45)$$

where $j \in \{0, \dots, Q - 1\}$. Then, we can infer that

$$R_{o,m}(Q - 1) \leq R_{o,m}(j) \leq R_{o,m}(0). \quad (4.46)$$

By exploiting a series expansion [184], we can rewrite Equation (4.40) as

$$P_{o,m}(U_{m,t}^*) = T_{o,m}(0) \frac{1 - [R_{o,m}(j)]^Q}{1 - R_{o,m}(j)}. \quad (4.47)$$

Substituting Inequality (4.46) in Equation (4.47) leads to the upper and lower approximation of the probability $P_{o,m}(U_{m,t}^*)$, where the upper-approximation (lower-approximation) is used for deriving the upper bound (lower bound) of the outage probability P_o of Equation (4.44). Note that the term $T_{o,m}(0)$ can be obtained from Equation (4.40), while the terms, namely $R_{o,m}(0)$ and $R_{o,m}(Q - 1)$, can be calculated by using Equation (4.45). As a result accomplishing the substitutions, we arrive at

$$P_{o,m}(U_{m,t}^*) \leq \frac{\binom{Q+K}{K}}{P_e^{-(K+1)}} \underbrace{\frac{(\beta P_e)^{Q+1} - (1 - P_e)^{Q+1}}{(\beta P_e + P_e - 1)}}_{=M_u}, \quad (4.48)$$

$$P_{o,m}(U_{m,t}^*) \geq \frac{\binom{Q+K}{K}}{P_e^{-(K+1)}} \underbrace{\frac{(\alpha P_e)^{Q+1} - (1 - P_e)^{Q+1}}{(\alpha P_e + P_e - 1)}}_{=M_t}, \quad (4.49)$$

where we have $\beta = Q/(K + 1)$ and $\alpha = 1/(K + Q)$. Let us now consider the scenario of $P_e \ll 1$. The term M_u of Equation (4.48) may be simplified to:

$$M_u < \underbrace{\frac{1 - P_e}{1 - P_e - \frac{B}{F+1}P_e}}_{=M_u^{\max}}, \quad (4.50)$$

where we have $B = (Mk_1 - 1)$ and $F = Mk_2$. Then, the Inequality (4.48) becomes

$$P_{o,m}(U_{m,t}^*) < \underbrace{\left(\frac{Q+K}{K}\right) P_e^{K+1} M_u^{\max}}_{=P_{o,m}^{\max}(U_{m,t}^*)}. \quad (4.51)$$

By combining Equation (4.43), Equation (4.44) and Equation (4.51), we can infer that

$$P_o < \sum_{\|U_{m,t}^*\|=0}^{M-1} \left(\frac{Q+K}{K}\right) \underbrace{\frac{P_e^{K+1+\|U_{m,t}^*\|}}{(1 - P_e)^{\|U_{m,t}^*\|-M+1}} M_u^{\max}}_{=T_o^{\text{Upper}}(\|U_{m,t}^*\|)}. \quad (4.52)$$

Let us then exploit the fact that $\binom{Q+K}{K} \leq \binom{B+F}{F}$ and focus our attention on the case, where we have $\|U_{m,t}^*\| = M - 1$, in order to further approximate Equation (4.52) as

$$P_o < \underbrace{\frac{\binom{Q+K}{K} - \binom{B+F}{F}}{\left[T_o^{\text{Upper}}(\|U_{m,t}^*\|)\right]^{-1} \big|_{\|U_{m,t}^*\|=M-1}}_{=\Omega} + \sum_{\|U_{m,t}^*\|=0}^{M-1} \binom{B+F}{F} T_o^{\text{Upper}}(\|U_{m,t}^*\|). \quad (4.53)$$

Let us consider the ratio R_o of $T_o^{\text{Upper}}(i)$ and $T_o^{\text{Upper}}(i + 1)$ in Equation (4.53), which allows us to arrive at the following result

$$R_o = \frac{T_o^{\text{Upper}}(i)}{T_o^{\text{Upper}}(i + 1)} = \frac{1 - P_e}{P_e^{1-k_2}}, i \in \{0, \dots, M - 2\}. \quad (4.54)$$

Similar to the manner of formulating $P_{o,m}(U_{m,t}^*)$ in Equation (4.47) from Equation (4.40) and Equation (4.45), Inequality (4.53) can be expressed as

$$P_o < \underbrace{\Omega + \binom{B+F}{F} P_e^{M+k_2} M_u^{\max} \left[\frac{(R_o)^M - 1}{R_o - 1} \right]}_{=P_o^{\text{Upper}}}. \quad (4.55)$$

Hence, we define the strict upper bound of the system's outage probability as:

$$P_o^{\text{Upper}} = \Omega + \binom{B+F}{F} P_e^{M+k_2} M_u^{\max} \left[\frac{(R_o)^M - 1}{R_o - 1} \right], \quad (4.56)$$

where the terms of Ω , R_o and M_u^{\max} are defined in Equation (4.53), Equation (4.54) and Equation (4.55), respectively.

4.5.2 The Lower Bound of the Outage Probability

In contrast to the upper-bound-related assumption of Inequality (4.49), here we assume that the Inequality (4.48) is known in order to further approximate the probability $P_{o,m}^{True}(U_{m,t}^*)$ of Equation (4.44). Then, the approximation is employed for formulating the upper bound of the outage probability P_o given by Equation (4.44).

It may be inferred from Equation (4.44) that

$$P_o > \frac{P_e^{||U_{m,t}^*||}}{(1 - P_e)^{||U_{m,t}^*|| - M + 1}} P_{o,m}^{True}(U_{m,t}^*)|_{||U_{m,t}^*||=0}. \quad (4.57)$$

Note that we always have $P_{o,m}^{True}(U_{m,t}^*)|_{||U_{m,t}^*||=0} = P_{o,m}(U_{m,t}^*)|_{||U_{m,t}^*||=0}$, which can be taken into account in Equation (4.40), yielding:

$$P_{o,m}^{True}(U_{m,t}^*)|_{||U_{m,t}^*||=0} = \sum_{b=0}^B \binom{B+F}{F+b} \frac{P_e^{F+b+1}}{(1 - P_e)^{b-B}}. \quad (4.58)$$

Note that having $||U_{m,t}^*|| = 0$ makes Q of Equation (4.41) and K of Equation (4.42) become:

$$\begin{aligned} Q|_{||U_{m,t}^*||=0} &= k_1 M - 1, \\ &= B, \end{aligned} \quad (4.59)$$

$$\begin{aligned} K|_{||U_{m,t}^*||=0} &= k_2 M, \\ &= F. \end{aligned} \quad (4.60)$$

By considering B and F in Equation (4.58) as the special case of Q and K in Equation (4.49), respectively, we can use Equation (4.49) to obtain:

$$P_{o,m}^{True}(U_{m,t}^*)|_{||U_{m,t}^*||=0} \geq \binom{B+F}{F} P_e^{F+1} M_l^{\min}, \quad (4.61)$$

where we have

$$\begin{aligned} M_l^{\min} &= M_l|_{Q=B, K=F} \\ &= \frac{\left(\frac{P_e}{B+F}\right)^{B+1} - (1 - P_e)^{B+1}}{\frac{P_e}{B+F} + P_e - 1}. \end{aligned} \quad (4.62)$$

Upon substituting Equation (4.61) into Equation (4.57), we arrive at

$$P_o > \underbrace{\binom{B+F}{F} P_e^{F+1} \frac{M_l^{\min}}{(1 - P_e)^{1-M}}}_{= P_o^{Lower}}. \quad (4.63)$$

Hence, we define the strict lower bound of P_o as:

$$P_o^{Lower} = \binom{B+F}{F} P_e^{F+1} \frac{M_l^{\min}}{(1 - P_e)^{1-M}}, \quad (4.64)$$

where the term M_l^{\min} is given in Equation (4.62).

4.6 System Parameters

4.6.1 System Diversity Order

As mentioned in Section 4.2.1, each of the M users broadcasts the k_1 IFs to the other $M - 1$ users during BPs. Then, during CPs each of M users transmits the k_2 IFs to the BS. If all the inter-user transmissions are successful, all the PFs formed by a user are linearly independent combination of the IFs, which were successfully received during BPs. As a result, an IF is conveyed to the BS by $(Mk_2 + 1)$ independent paths, which leads to the diversity order of $(Mk_2 + 1)$. By contrast, the unsuccessful inter-channel transmissions may lead to the case where some of the PFs transmitted by a user are not linearly independent combinations of the IFs. The worst case is when each of the other $(M - 1)$ user is able to produce only a single linearly independent combination (PF), while the user itself is always capable of constructing k_2 linearly independent combinations. As a result of such worst case, there are $(M + k_2)$ independent paths for carrying the IF to the BS, which induces the diversity order of $(M + k_2)$. In line with the above-mentioned analysis, it was proved in [99, 179] that the diversity order D of the system is bounded by

$$M + k_2 \leq D \leq Mk_2 + 1. \quad (4.65)$$

The authors of [46, 47, 99, 179] formulated the diversity order D in Equation (4.64) as follows

$$D = \lim_{SNR \rightarrow \infty} \frac{-\log_2 P_o}{\log_2 SNR}, \quad (4.66)$$

where SNR is the signal to noise power ratio, while P_o was estimated on the basis of the best and worst cases instead of using P_e , assuming that $P_e \approx (2^R - 1)/SNR$ is the outage probability of the transmission link relying on a 'perfect capacity-achieving' code, which operates exactly at the CCMC channel capacity having a transmission rate of R .

Similarly, we may infer from the P_o^{Upper} defined in Equation (4.56) that the most influential term is $P_e^{M+k_2}$. Likewise, it can be seen in the P_o^{Lower} formula given in Equation (4.64) that the term having most significant influence is $P_e^{F+1} = P_e^{Mk_2+1}$. Hence, by using the most influential terms of P_o^{Upper} and P_o^{Lower} instead of P_o in Equation (4.66), it may be seen that the upper and lower bounds of the probability P_o are in harmony with the estimated diversity order given by Equation (4.64).

4.6.2 System Parameter Sets

Let us assume that all the links in the system have the same information rate R [47, 99]. For notational convenience, we characterise the system by using the set of parameters $(R, M, k_1, k_2, \mathbf{G}, R_{NCMN}, D_{NCMN})$, where the system's overall information rate R_{NCMN} is calculated as:

$$R_{NCMN} = R_{info}R = \frac{k_1 R}{k_1 + k_2}, \quad (4.67)$$

provided that the network coding information rate R_{info} is expressed as [47, 99]

$$R_{info} = \frac{k_1}{k_1 + k_2}. \quad (4.68)$$

We then define E_b/N_0 as the energy per bit to noise power spectral density ratio, which can be computed in our system as:

$$E_b/N_0 = \frac{SNR}{R_{NCMN}} = SNR \frac{k_1 + k_2}{k_1 R}. \quad (4.69)$$

For ease of readability, we summarise all these parameters in Table 4.1.

Parameters	Description
R [BPS]	Information rate calculated in Bit Per Symbol (BPS) for all the links in the system
R_c	The code rate of the IrCC encoder as described in Section 2.3
K [iteration]	The number of inner iterations described in Section 2.3
J [iteration]	The number of outer iterations described in Section 2.3
N [bit]	The number of information bits in a frame
M [user]	The number of users in the system
k_1 [frame]	The number of IFs transmitted by each of the M users during BPs within a transmission session
k_2 [frame]	The number of PFs transmitted by each of the M users during the CPs within a transmission session
\mathbf{G}	Original transfer matrix corresponding to the case where all the frames transmitted within a transmission session are successfully decoded
R_{info} [BPS]	The network code's information rate defined by Equation (4.68)
R_{NCMN} [BPS]	The system's overall information rate defined by Equation (4.67)
D_{NCMN}	Diversity order of the system determined by Equation (4.64)

Table 4.1: The main parameters of the system.

4.7 Network Coding Design

4.7.1 Cooperative System Approach

According to [173], the upper bound and lower bound of achievable rate in a full duplex relay aided CCMC can be calculated as follows:

$$C_{CCMC}^{relay-full} \leq \max_{p(X_1, X_2)} \min\{I(X_1; Y_2, Y_3|X_2), I(X_1, X_2; Y_3)\}, \quad (4.70)$$

$$C_{CCMC}^{relay-full} \geq \max_{p(X_1, X_2)} \min\{I(X_1; Y_2|X_2), I(X_1, X_2; Y_3)\}, \quad (4.71)$$

where X_1, X_2, Y_2 and Y_3 are the signals transmitted from the user considered and the other users, as well as the signals received at the other users and the BS, respectively. Furthermore, $p(X_1, X_2)$ is the joint probability of signals transmitted from the user considered and from the other $(M - 1)$ users. The upper bound and lower bound of a half duplex CCMC can be computed from Equation (4.70) and Equation (4.71) by:

$$C_{CCMC}^{relay-half} \leq \max_{p(X_1, X_2)} \min\{I(X_1; Y_2, Y_3), I(X_1, X_2; Y_3)\}, \quad (4.72)$$

$$C_{CCMC}^{relay-half} \geq \max_{p(X_1, X_2)} \min\{I(X_1; Y_2), I(X_1, X_2; Y_3)\}. \quad (4.73)$$

In order to take into account Equation (4.72) and Equation (4.73) in the system model of Figure 4.1, we assume that M users (sources) communicate with M relays and the BS (destination). This model is detailed in Figure 4.6.

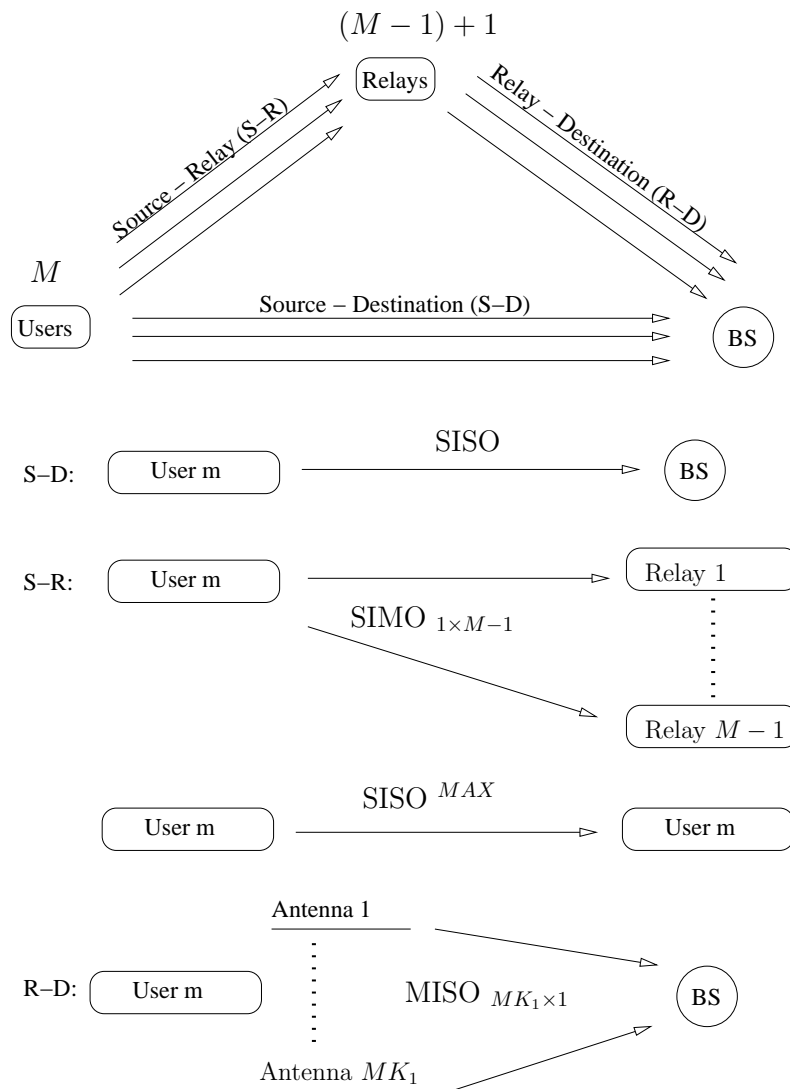


Figure 4.6: Equivalent system model for capacity calculation employing the cut-through theory approach used in Chapter 3.

1. In the Source-Destination (S-D) link, each of the M users transmits k_1 frames to the BS during the BPs, thus the capacity of the S-D link may be calculated as:

$$\begin{aligned} C_{S-D} &= \frac{Mk_1}{M(k_1 + k_2)} C_{SISO}, \\ &= \frac{k_1}{k_1 + k_2} C_{SISO}, \end{aligned} \quad (4.74)$$

where C_{SISO} represents the capacity of the Single-Input Single-Output (SISO) channel considered.

2. In the Source-Relay (S-R) link seen in Figure 4.6 each of the M users broadcasts to $(M - 1)$ other users acting as $(M - 1)$ relays as well as transmitting to itself, which is considered as a *special* relay. The capacity of the S-R link may then be formulated as:

$$\begin{aligned} C_{S-R} &= \frac{Mk_1}{M(k_1 + k_2)} C_{SISO_{1 \times M-1}} + \frac{Mk_1}{M(k_1 + k_2)} C_{SISO^{MAX}}, \\ &= \frac{k_1}{k_1 + k_2} C_{SISO_{1 \times M-1}} + \frac{k_1}{k_1 + k_2} C_{SISO^{MAX}}, \end{aligned} \quad (4.75)$$

where $C_{SISO_{1 \times M-1}}$ represents the capacity of the SISO channel, while $SISO^{MAX}$ is the maximum capacity of the SISO channel within the SNR range considered.

3. In the Relay-Destination (R-D) link also seen in Figure 4.6, each of the M users now plays a role as a relay transmitting k_2 PFs. The transmission of a parity frame may in fact be equivalently deemed to be the transmission of multiple signal replicas of a Multi-Input Multi-Output (MIMO) channel, where the number of transmit antennas is equal to the number of IFs contained in the parity frame. Thus, we can formulate the capacity of the R-D links as follows:

$$\begin{aligned} C_{R-D} &= \frac{Mk_2}{M(k_1 + k_2)} C_{MISO_{Mk_1 \times 1}}, \\ &= \frac{k_2}{k_1 + k_2} C_{MISO_{Mk_1 \times 1}}. \end{aligned} \quad (4.76)$$

Applying Equation (4.73) to our half duplex DCMC system presented in Section 4.2.1, given that the single links in the system are supported by links operating exactly at the DCMC capacity C_{DCMC} , we may formulate the upper bound and lower bound of the achievable rate of the relay channel as follows [173, 185]:

$$\begin{aligned} C_{DCMC}^{coop} &\geq \min\{C_{S-R}, C_{S-D} + C_{R-D}\}, \\ &\geq \min\left\{\frac{k_1}{k_1 + k_2} C_{SISO_{1 \times M-1}} + \frac{k_1}{k_1 + k_2} C_{SISO}^{MAX}, \right. \\ &\quad \left. \frac{k_1}{k_1 + k_2} C_{SISO} + \frac{k_2}{k_1 + k_2} C_{MISO_{Mk_1 \times 1}}\right\}, \\ &\geq \min\{R_{info} C_{SISO_{1 \times M-1}} + R_{info} C_{SISO}^{MAX}, \\ &\quad R_{info} C_{SISO} + (1 - R_{info}) C_{MISO_{Mk_1 \times 1}}\}, \end{aligned} \quad (4.77)$$

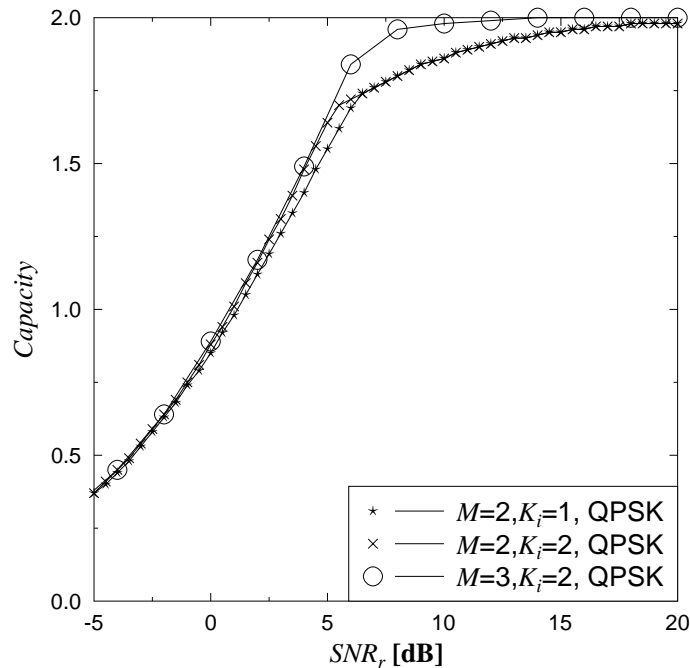


Figure 4.7: Channel capacity of network coding aided systems supporting M users.

where the system's overall information rate $R_{info} = k_1 / (k_1 + k_2)$ was introduced in Table 4.1. The channel capacity can be calculated based on Equation (4.77). As seen in Figure 4.7, given an information rate $R_{info} = k_1 / (k_1 + k_2)$, the channel capacity can be improved by increasing both k_1 and k_2 as well as increasing the number of users actively cooperating in the system.

4.7.2 Network Coding Approach

Observing the R_{info} expression of Equation (4.67) and the D_{NCMN} formula of Equation (4.64), it becomes plausible that we may conceive different systems having the same network coding rate R_{info} , but different diversity orders of D_{NCMN} by independently adjusting k_1 , k_2 and M . In other words, using Equation (4.67) and Equation (4.64), we are able to design a network-coding system having the highest possible diversity order at a given overall normalised data rate of R_{NCMN} . A higher diversity order implies that the system is capable of achieving an improved FER performance.

In order to employ the generic design principles mentioned above, let us now consider specific systems having the parameters summarised in Table 4.2 for both coherent and non-coherent channel coding schemes. The systems employ the transfer matrices, namely the matrix $\mathbf{G}_{2 \times 4}$ given in Equation (4.2), the matrix $\mathbf{G}_{4 \times 8}$ and the matrix $\mathbf{G}_{6 \times 12}$, where the matrix $\mathbf{G}_{4 \times 8}$ was provided by [47,

99]:

$$\mathbf{G}_{4 \times 8} = \left[\begin{array}{cccc|cccc} 1 & 0 & 0 & 0 & 3 & 7 & 3 & 6 \\ 0 & 1 & 0 & 0 & 5 & 7 & 7 & 4 \\ 0 & 0 & 1 & 0 & 2 & 4 & 6 & 1 \\ 0 & 0 & 0 & 1 & 5 & 5 & 3 & 2 \end{array} \right], \quad (4.78)$$

while the matrix $\mathbf{G}_{6 \times 12}$ was given in [99]

$$\mathbf{G}_{6 \times 12} = \left[\begin{array}{cccccc|cccccc} 1 & 0 & 0 & 0 & 0 & 0 & 11 & 2 & 4 & 6 & 14 & 12 \\ 0 & 1 & 0 & 0 & 0 & 0 & 1 & 11 & 13 & 10 & 14 & 10 \\ 0 & 0 & 1 & 0 & 0 & 0 & 2 & 4 & 2 & 10 & 5 & 9 \\ 0 & 0 & 0 & 1 & 0 & 0 & 6 & 13 & 12 & 11 & 8 & 12 \\ 0 & 0 & 0 & 0 & 1 & 0 & 4 & 12 & 12 & 2 & 6 & 6 \\ 0 & 0 & 0 & 0 & 0 & 1 & 11 & 13 & 10 & 14 & 10 & 4 \end{array} \right]. \quad (4.79)$$

It should be noted that the meaning of the entries in the transfer matrix in general case is described in Figure 4.1, where the left side of the transfer matrix \mathbf{G} portrayed in Figure 4.5, which is also referred to as the identity matrix \mathbf{I} , represents the transmission in the system during BPs. The right side of the transfer matrix \mathbf{G} referred in Figure 4.5 to as the parity matrix \mathbf{P} reflects the transmissions in the system during CPs, where each column in the \mathbf{P} represents a PF transmitted during a corresponding CP. In particular, the use of the entries in $\mathbf{G}_{4 \times 8}$ of Equation (4.78) is illustrated in Example 4.1. Similarly, the usage of the entries in the transfer matrix $\mathbf{G}_{6 \times 12}$ for representing transmission phases, namely 6 BPs in 3 groups (B_1, B_2, B_3) and 6 CPs in 3 groups (C_1, C_2, C_3), can be summarised as follows:

Broadcast phases

$$(B_1) \text{ BP 1 : User 1 } \xrightarrow{I_1(1)} \text{BS and User 2,} \quad (4.80)$$

$$(B_1) \text{ BP 2 : User 2 } \xrightarrow{I_2(2)} \text{BS and User 1,} \quad (4.81)$$

$$(B_2) \text{ BP 3 : User 1 } \xrightarrow{I_1(3)} \text{BS and User 2,} \quad (4.82)$$

$$(B_2) \text{ BP 4 : User 2 } \xrightarrow{I_2(4)} \text{BS and User 1,} \quad (4.83)$$

$$(B_2) \text{ BP 5 : User 1 } \xrightarrow{I_1(5)} \text{BS and User 2,} \quad (4.84)$$

$$(B_2) \text{ BP 6 : User 2 } \xrightarrow{I_2(6)} \text{BS and User 1,} \quad (4.85)$$

Cooperative phases

$$(C_1) \text{ CP 1 : User 1 } \xrightarrow{\oplus(1)=11I_1(1)+1I_2(2)+2I_1(3)+6I_2(4)+4I_1(5)+11I_2(6)} \text{BS,} \quad (4.86)$$

$$(C_1) \text{ CP 2 : User 2 } \xrightarrow{\oplus(2)=2I_1(1)+11I_2(2)+4I_1(3)+13I_2(4)+12I_1(5)+13I_2(6)} \text{BS,} \quad (4.87)$$

$$(C_2) \text{ CP 3 : User 1 } \xrightarrow{\oplus(3)=4I_1(1)+13I_2(2)+2I_1(3)+12I_2(4)+12I_1(5)+10I_2(6)} \text{BS,} \quad (4.88)$$

$$(C_2) \text{ CP 4 : User 2 } \xrightarrow{\oplus(4)=6I_1(1)+10I_2(2)+10I_1(3)+11I_2(4)+2I_1(5)+14I_2(6)} \text{BS,} \quad (4.89)$$

$$(C_3) \text{ CP 5 : User 1 } \xrightarrow{\oplus(5)=14I_1(1)+14I_2(2)+5I_1(3)+8I_2(4)+6I_1(5)+10I_2(6)} \text{BS,} \quad (4.90)$$

$$(C_3) \text{ CP 6 : User 2 } \xrightarrow{\oplus(6)=12I_1(1)+10I_2(2)+9I_1(3)+12I_2(4)+6I_1(5)+4I_2(6)} \text{BS.} \quad (4.91)$$

As shown in Table 4.2, the transfer matrices are specifically selected for ensuring having fair comparisons. More specifically, we have the same parameter values such as the transmission rate $R = \{0.5, 1.0\}$, the number of users $M = 2$ and the network coding rate $R_{info} = 0.5$, when comparing the $\mathbf{G}_{2 \times 4}$ based system and the $\mathbf{G}_{4 \times 8}$ based system. Furthermore, the benefit of employing additional users in the system is highlighted by comparing the $\mathbf{G}_{2 \times 4}$ and $\mathbf{G}_{4 \times 8}$ based systems supporting $M = 2$ users to the $\mathbf{G}_{6 \times 12}$ based system supporting $M = 3$ users. Note that all the three systems detailed in Table 4.2 have the same overall rate of R_{NCMN} , provided that the same channel coding scheme is employed.

As a result, the more complex transfer matrix, for example the matrix $\mathbf{G}_{4 \times 8}$, supports a higher diversity order, for example $4 \leq D_{4 \times 8} \leq 5$ (as opposed to $3 \leq D_{2 \times 4} \leq 3$) as seen in Table 4.2, hence it is associated with a better detection reliability, but may impose a higher detection complexity at the BS. Similarly, it is expected that the system relying on the matrix $\mathbf{G}_{6 \times 12}$ associated with the diversity order of $5 \leq D_{6 \times 12} \leq 7$ outperforms the system employing the transfer matrix $\mathbf{G}_{4 \times 8}$ pertaining to a lower diversity order of $4 \leq D_{4 \times 8} \leq 5$.

4.7.3 Near Capacity Multi User Network Coding Aided Systems

The capacity of NCMN based systems can be characterised by capacity of the transmission link from a certain user in the system to the BS. This link in the NCMN based systems can be equivalently considered as an equivalent single-link model, where the equivalent transmission rate R_e of the link is computed as

$$R_e = R_{info}R, \quad (4.92)$$

where the information rate of R and the network-code's information rate of R_{info} are defined in Table 4.1. Then, the equivalent transmission rate of R_e is used for determining the capacity of the channel, which is detailed in Section 2.1.3 and Section 2.1.4 for the DCMC capacity and D-DCMC capacity, respectively. In what follows, two examples are invoked for detailing the calculation of the above-mentioned capacity of the NCMN based systems in two scenarios, namely in the coherent and the non-coherent based NCMN.

Example 4.4. *The coherent based NCMN system.*

Let us consider a specific example of a NCMN system having a network-coding information rate of $R_{info} = 0.5$. This system employs a channel coding scheme characterised by an information rate of $R = 0.5$ and by a coding rate of $R_c = 0.5$. The configuration of the system used in this example results in a μ number of modulated bits given by:

$$\begin{aligned} \mu &= \frac{R}{R_c} = \frac{0.5}{0.5}, \\ &= 1. \end{aligned} \quad (4.93)$$

Parameters	Coherent $G_{2 \times 4}$ system	Non-coherent $G_{2 \times 4}$ system
R [BPS]	1.5(8PSK), 1.0(QPSK), 0.5(BPSK)	1.0(DQPSK), 0.5(DBPSK)
R_c	0.5	0.5
I [iteration]	0	2
J [iteration]	30	30
N [bit]	$10^6, 10^5$	10^6
M [user]	2	2
k_1 [frame]	1	1
k_2 [frame]	1	1
G	$G_{2 \times 4}$	$G_{2 \times 4}$
R_{NCMN} [BPS]	0.75(8PSK), 0.5(QPSK), 0.25(BPSK)	0.5(DQPSK), 0.25(DBPSK)
D_{NCMN}	$3 \leq D_{2 \times 4} \leq 3$	$3 \leq D_{2 \times 4} \leq 3$
Parameters	Coherent $G_{4 \times 8}$ system	Non-coherent $G_{4 \times 8}$ system
R [BPS]	1.5(8PSK), 1.0(QPSK), 0.5(BPSK)	1.0(DQPSK), 0.5(DBPSK)
R_c	0.5	0.5
I [iteration]	0	2
J [iteration]	30	30
N [bit]	$10^6, 10^5$	10^6
M [user]	2	2
k_1 [frame]	2	2
k_2 [frame]	2	2
G	$G_{4 \times 8}$	$G_{4 \times 8}$
R_{NCMN} [BPS]	0.75(8PSK), 0.5(QPSK), 0.25(BPSK)	0.5(DQPSK), 0.25(DBPSK)
D_{NCMN}	$4 \leq D_{4 \times 8} \leq 5$	$4 \leq D_{4 \times 8} \leq 5$
Parameters	Coherent $G_{6 \times 12}$ system	Non-coherent $G_{6 \times 12}$ system
R [BPS]	1.5(8PSK), 1.0(QPSK), 0.5(BPSK)	1.0(DQPSK), 0.5(DBPSK)
R_c	0.5	0.5
I [iteration]	0	2
J [iteration]	30	30
N [bit]	$10^6, 10^5$	10^6
M [user]	3	3
k_1 [frame]	2	2
k_2 [frame]	2	2
G	$G_{6 \times 12}$	$G_{6 \times 12}$
R_{NCMN} [BPS]	0.75(8PSK), 0.5(QPSK), 0.25(BPSK)	0.5(DQPSK), 0.25(DBPSK)
D_{NCMN}	$5 \leq D_{6 \times 12} \leq 7$	$5 \leq D_{6 \times 12} \leq 7$

Table 4.2: The parameters of the NCMN systems relying on the transfer matrices, namely the $G_{2 \times 4}$, $G_{4 \times 8}$ and $G_{6 \times 12}$, on the IrCC-URC-MPSK scheme presented in Section 2.3.3 and on the IrCC-URC-DMPSK detailed in Section 2.3.4.

Having $\mu = 1$ BPS means that a modulation scheme relying on BPSK may be employed by each user in the system. Similar to the method invoked in Section 2.1.3 for determining the receive SNR value SNR_r corresponding to a given throughput of R , which is also considered as the information rate in this context, the capacity of the above-mentioned NCMN system is determined by following a similar approach, namely by finding the value of SNR_r . We define $SNR_e|_{R_e}$ as the equivalent SNR_r value corresponding to a given throughput of $R_e = R_{info}R = 0.25$. The $SNR_e|_{R_e}$ value is determined by identifying a point on the DCMC capacity curve generated from Equation (2.16), which is repeated here for the sake of convenience:

$$C^{DCMC}(\eta) = \eta - \frac{1}{2^\eta} \sum_{l=1}^{l=2^\eta} E \left[\log_2 \sum_{z=1}^{z=2^\eta} \exp(\psi_{l,z}) | X_l \right], \quad (4.94)$$

where $\eta = \log_2(L)$ is the asymptotic DCMC capacity, and L is the number of modulation levels. The expression of $E[A|X_l]$ represents the expectation of A conditioned on the L -ary signals X_l , whereas the formula for calculating $\psi_{l,z}$ is given by Equation (2.17).

As a result of having $\eta = 1$ and $R_e = 0.25$ in this example, the corresponding equivalent receive SNR value of $SNR_e|_{R_e} = -6.1$ dB may be found on the DCMC capacity curve, as seen in Figure 4.8a.

For the scenario when the NCMN system employs non-coherent modem schemes, EXIT charts may be invoked for estimating the NCMN system's capacity. Let us consider the following example for characterising our method.

Example 4.5. *Non-coherent detection based NCMN system.*

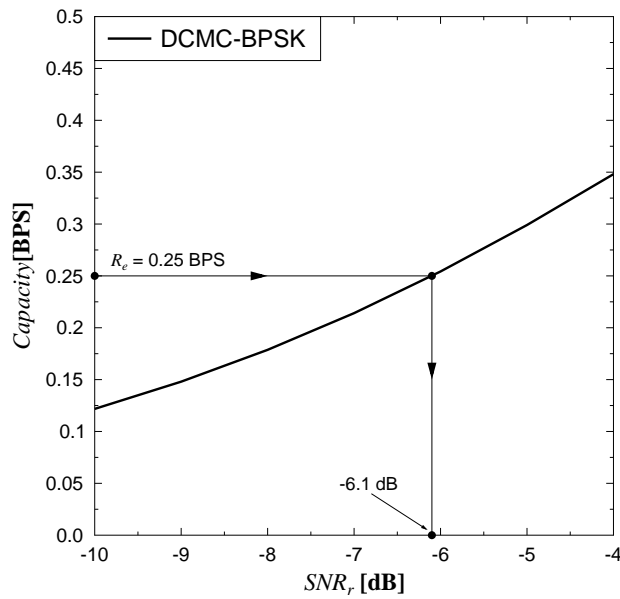
Let us now consider another NCMN system having a network-coding information rate of $R_{info} = 0.5$. Let us assume that this system relies on a non-coherent detection scheme associated with an information rate of $R = 1.0$ and with a coding rate of $R_c = 0.5$. Accordingly, the number of modulated bits can be calculated as:

$$\begin{aligned} \mu &= \frac{R}{R_c} = \frac{1.0}{0.5} \\ &= 2. \end{aligned} \quad (4.95)$$

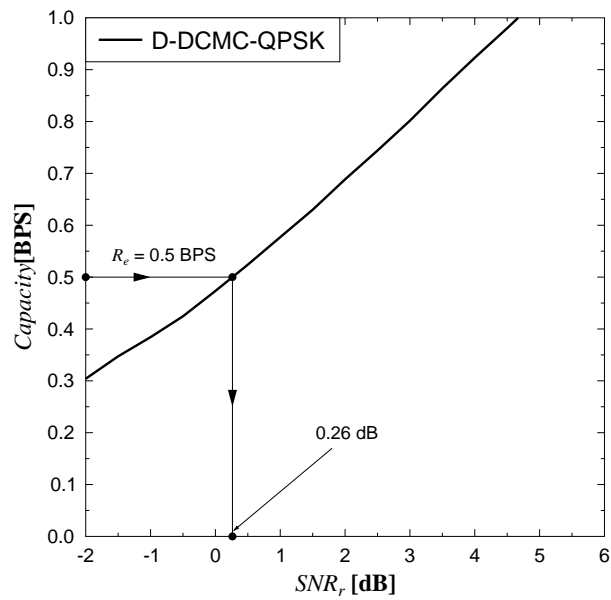
It can be inferred from the value of $\mu = 2$ BPS that a QPSK or 4QAM scheme, may be employed for each transmission link in the system. It should be noted that the capacity of the above-mentioned NCMN system determines the achievable capacity of a transmission link having a throughput of $R_e = R_{info}R = 1/2$ BPS.

In contrast to the method employed in Example 4.4, where Equation (4.94) was used for generating the capacity curve, as an alternative, we can exploit EXIT charts in order to estimate the capacity of our non-coherent system. More specifically, EXIT curves corresponding to different SNR_r values are generated. Then, the area under each EXIT curve is quantified for representing the maximum information rate that may be error-freely transmitted over the channel, when the associated SNR_r value is achieved at the receiver.

In order to determine the attainable system capacity, the corresponding throughput R_e is used for determining the equivalent receive SNR value $SNR_e|_{R_e}$, which is defined similarly in Exam-



(a) Coherent scheme, DCMC-BPSK.



(b) Non-coherent scheme, D-DCMC-QPSK.

Figure 4.8: Example of calculating the capacity of the network-coding based system relying on a coherent BPSK (non-coherent DQPSK) scheme having an information rate of $R = 0.5$ ($R = 1.0$) and a coding rate of $R_c = 0.5$, when communicating over fast Rayleigh fading channel.

ple 4.4. This $SNR_e|_{R_e}$ value may be used for representing the system capacity, as also mentioned in Example 4.4.

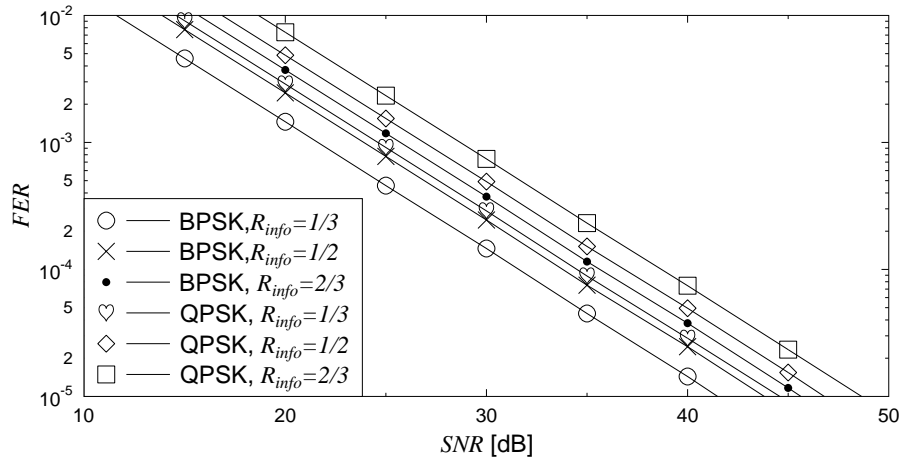
As a result of having $\eta = 1$ and $R_e = 0.5$ in this example, the corresponding equivalent receive SNR of $SNR_e|_{R_e} = 0.266$ dB may be found on the D-DCMC-QPSK capacity curve, as seen in Figure 4.8b. Then, this $SNR_e|_{R_e}$ value may be used as the achievable capacity for the system described in this example.

As a result, the equivalent achievable capacity of the NCMN system can be determined by applying the principle presented in Example 4.4 and Example 4.5. The results recorded for various configurations of the system are summarised in Table 4.3.

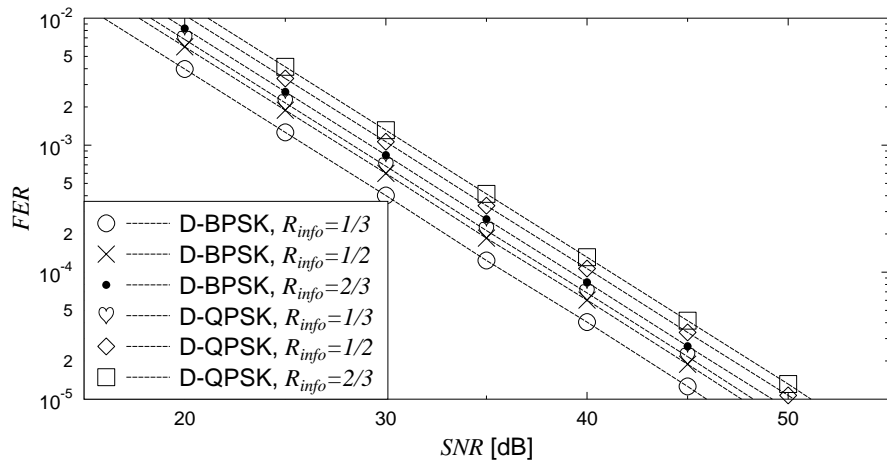
Network-Coding Rate R_{info}	$SNR_e _{R_e}$ [dB]	
	Coherent, $R_c = 0.5$	
	$\eta = 1$ BPS (BPSK)	$\eta = 2$ BPS (QPSK)
1/3	$R_e = 1/6, SNR_e _{R_e} = -8.375$	$R_e = 1/3, SNR_e _{R_e} = -5.403$
1/2	$R_e = 1/4, SNR_e _{R_e} = -6.101$	$R_e = 1/2, SNR_e _{R_e} = -3.120$
2/3	$R_e = 1/3, SNR_e _{R_e} = -4.293$	$R_e = 2/3, SNR_e _{R_e} = -1.305$
	Non-coherent, $R_c = 0.5$	
	$\eta = 1$ BPS (DBPSK)	$\eta = 2$ BPS (DQPSK)
1/3	$R_e = 1/6, SNR_e _{R_e} = -4.001$	$R_e = 1/3, SNR_e _{R_e} = -1.661$
1/2	$R_e = 1/4, SNR_e _{R_e} = -2.239$	$R_e = 1/2, SNR_e _{R_e} = 0.263$
2/3	$R_e = 1/3, SNR_e _{R_e} = -0.785$	$R_e = 2/3, SNR_e _{R_e} = 1.814$

Table 4.3: $SNR_e|_{R_e}$ values calculated on the basis of the principle illustrated in Example 4.4 and Example 4.5.

It should be noted that the values given in Table 4.3 may be considered as the achievable capacity of the corresponding NCMN systems, when communicating over fast fading channels. By contrast, when slow-fading channels are considered, we can obtain the achievable capacity of the NCMN systems by calculating the associated outage capacity, as detailed in Section 2.2. Accordingly, we have the different achievable capacity curves corresponding to various configurations of the NCMN system presented in Figure 4.9. Accordingly, the performance curves plotted in Figure 4.9 may be used as the performance of the NCMN system employing ideal/perfect coding schemes relying on coherent or non-coherent modem and operating at exactly DCMC or DDCMC capacity. When comparing the curves associated with the coherent detection and that pertaining to the non-coherent detection in Figure 4.9a and Figure 4.9b, the average of the distance between them is approximately 3 dB, which is similar to the corresponding distance in the fast fading environment presented in Section 2.1 and to that in the quasi-static fading environment detailed in Section 2.2.



(a) Coherent schemes, namely BPSK and QPSK schemes



(b) Non-coherent schemes, namely DBPSK and DQPSK schemes

Figure 4.9: Outage capacity of the NCMN system relying on the *coherent* and *non-coherent* schemes, when communicating over wireless channels influenced by both the fast Rayleigh and block Rayleigh fading. A coding rate of $R_c = 0.5$ was used in conjunction with various network coding rates, namely $R_{info} = 1/3, 1/2, 2/3$.

4.8 Pure Rank, Pragmatic Algebraic and SIMULATION Methods

In Section 4.4, we have illustrated the optimistic performance obtained by the PRBM of Section 4.4.1 in contrast to those attained by the PALEM of Section 4.4.2 through the numerical examples. More specifically, by numerical examples, we have proved that the PRBM results in optimistic decisions on evaluating the system's performance. By contrast, the PALEM always reflects accurately the system's performance. Hence, it was concluded in Section 4.4.2 that the PALEM is capable of accurately determining the system performance. However, the difference in the performance of the system when employing the PRBM and PALEM is an open issue, which has yet been characterised by the end of Section 4.4. In this section, we further substantiate the difference in the system's performance, as a result of employing the PRBM and PALEM.

In order to compare the results suggested by the two methods, we examine the NCMN based systems, namely the coherent $\mathbf{G}_{2 \times 4}$ system and the coherent $\mathbf{G}_{4 \times 8}$ system, as specified in Table 4.2. More specifically, Figure 4.10 characterises the performance of the NCMN based systems and substantiates our analysis provided in Section 4.4, where the performance found with the aid of the PRBM of Section 4.4.1 was always superior, but optimistic in comparison to that obtained by the actual simulations. More explicitly, it is shown in Figure 4.10 that the deviation between the performance curves obtained by actual Monte-Carlo simulations and those suggested by PRBM was found to be in the range of 0.3 dB to 0.5 dB at an FER of 10^{-4} .

As expected, the estimate of the system's performance obtained by the PALEM of Section 4.4.2 is similar to those provided by Monte-Carlo simulations, as seen in Figure 4.10. Moreover, as seen in Figure 4.11, for the non-coherent systems, performance suggested by both the Monte-Carlo simulations and PALEM is identical, which again confirmed the analysis presented in Section 4.4.2. As a result, the less complex PALEM may be used for replacing the Monte-Carlo simulations in evaluating the NCMN system's performance.

4.9 Performance Bounds of the Systems

In this section, we first compare the upper and lower bounds derived in Section 4.5 to our numerical results. The results associated with the $\mathbf{G}_{2 \times 4}$ -based and $\mathbf{G}_{4 \times 8}$ -based systems of [47, 99] are also presented for direct comparison with our results. Then, the upper and lower bounds are further examined in the NCMN based systems relying on the realistic IrCC-URC-MPSK(IrCC-URC-DMPSK) coding schemes detailed in Section 2.3.3 (Section 2.3.4).

Specifically, we consider the $\mathbf{G}_{2 \times 4}$ -based system represented by ($R = 0.5, M = 2, k_1 = 1, k_2 = 1, \mathbf{G}_{2 \times 4}, R_{info} = 0.5, 3 \leq D_{2 \times 4} \leq 3$) and the $\mathbf{G}_{4 \times 8}$ -based one characterised by ($R = 0.5, M = 2, k_1 = 2, k_2 = 2, \mathbf{G}_{4 \times 8}, R_{info} = 0.5, 4 \leq D_{4 \times 8} \leq 5$), as seen in Table 4.2. The two systems of our choice are comparable, since they have the same R, M and R_{info} values. Hence, both

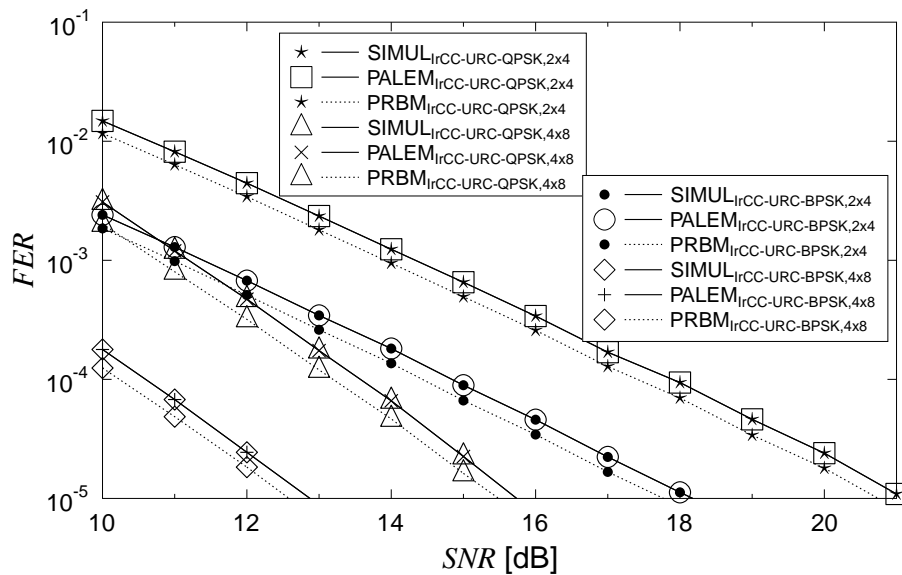


Figure 4.10: FER versus SNR performance of the $G_{2 \times 4}$ and $G_{4 \times 8}$ based systems employing the realistic IrCC-URC-BPSK and IrCC-URC-QPSK schemes instead of assuming a perfect capability-achieving code, when communicating over wireless channels influenced by both the fast Rayleigh and block Rayleigh fadings. The specifics of the schemes are summarised in Table 4.2

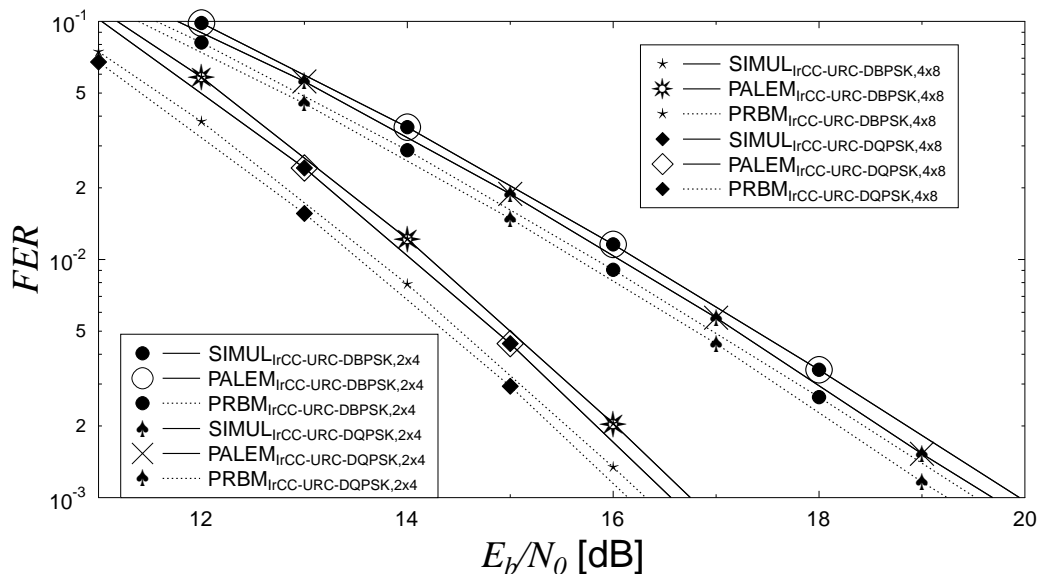


Figure 4.11: FER performance of the non-coherent $G_{2 \times 4}$ and $G_{4 \times 8}$ systems employing the IrCC-URC-MSDD-aided-DMPSK, when communicating over wireless channels influenced by both the fast Rayleigh and block Rayleigh fadings, where the details of the systems are presented in Table 4.2.

systems are supported by an ideal/perfect channel coding scheme operating exactly at the CCMC capacity and having a data rate $R = 0.5^3$. As detailed in Table 4.2, the more complex transfer matrix $\mathbf{G}_{4 \times 8}$ [47, 99] has a higher diversity order of $4 \leq D_{4 \times 8} \leq 5$ (as opposed to $3 \leq D_{2 \times 4} \leq 3$), hence it is associated with a higher detection complexity at the BS. The differences in the diversity order are also reflected by the different slope of both the bounds and of the performance curves, as seen in Figure 4.12.

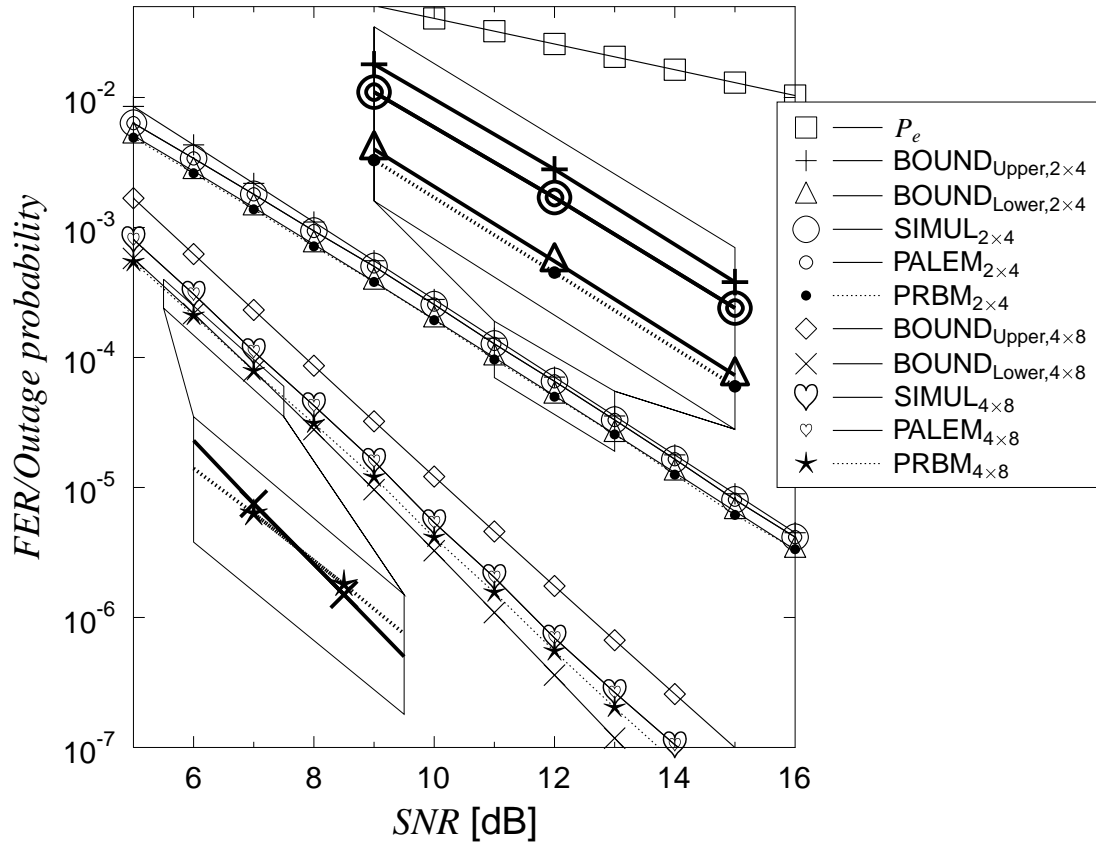


Figure 4.12: The outage probability bounds and FER performance of the $\mathbf{G}_{2 \times 4}$ and $\mathbf{G}_{4 \times 8}$ systems employing an ideal/perfect channel coding scheme operating at the CCMC capacity and having a data rate of $R = 0.5$, when communicating over wireless channels influenced by both the fast Rayleigh and block Rayleigh fading.

It can be seen in Figure 4.12 that the system's performance curves obtained from both the Monte-Carlo simulations and the PALEM of Section 4.4.2 are identical, which validates the analysis presented in Section 4.4 and the results presented in Section 4.8. The PRBM of Section 4.4.1 always suggests a superior performance in comparison to the actual performance obtained by sim-

³The data rate $R = 0.5$ is chosen for fairly comparing our results with the results presented in [47, 99], where the data rate $R = 0.5$ was also selected for the ideal/perfect channel coding scheme operating at the CCMC capacity

ulations, as demonstrated by the specific example of Section 4.4.2. Observe furthermore in Figure 4.12 that the system's actual FER performance curve is always between the upper bound and lower bound. The PRBM-based performance estimate in fact violates the strict lower bounds at low SNRs.

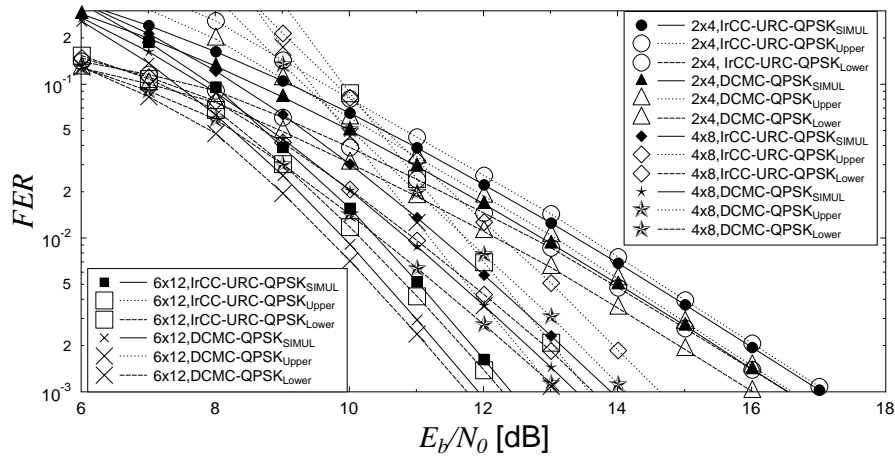
We then apply the upper and lower bound for the coherent based NCMN systems employing the realistic IrCC-URC-MPSK coding schemes presented in Section 2.3.3. It is substantiated in Figure 4.13 that the system's actual FER performance curves are always between their upper bound and lower bound. Thus, the upper and lower bounds may be used for estimating the performance of other NCMN systems, without extremely time-consuming simulations. This is particularly beneficial, when a large transfer matrix is employed. Similarly, for NCMN systems relying on the realistic non-coherent schemes detailed in Section 2.3.4, the FER-performance curves seen in Figure 4.14 substantiate that the system's actual FER performance curves are again always between their upper and lower bounds. This again suggested that the performance of NCMN systems can be accurately characterised by the upper and lower bounds, rather than by extremely time-consuming simulations. The convenience of using the bounds becomes particularly remarkable, when a large transfer matrix is employed.

Hence, by combining the results of the channel coding design presented in Section 2.3, the bounds of the system's outage probability can be further exploited for estimating the approximate performance of the NCMN system without Monte-Carlo simulations, which would be very time-consuming. The the system performance results estimated by the upper and lower bounds are presented subsequently in Section 4.10.

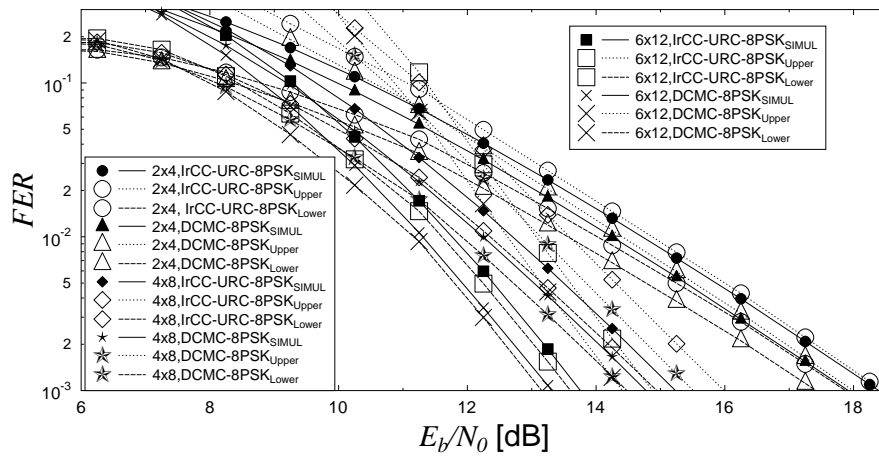
4.10 Near-capacity Coherent/Non-coherent based System

In this section, the performance of the NCMN based systems are compared to highlight the benefits of network coding. Near-capacity results are then presented from different perspectives, namely the distance between the FER-performance of our systems relying on a perfect capacity-achieving channel coding scheme and that of the systems employing our coherent realistic coding scheme of IrCC-URC-MPSK. Additionally, the system capacity curves, which are defined and calculated in Section 4.7.3 are benchmarked against the system's FER-performance, in order to highlight how our system may be improved. Moreover, the performance of the coherent based systems when considering errors induced by channel estimators is compared to that of the non-coherent systems for suggesting the scenarios, where the coherent or non-coherent based systems are duly selected.

Again, we consider the $\mathbf{G}_{2 \times 4}$ and $\mathbf{G}_{4 \times 8}$ based systems employing the IrCC-URC-BPSK(QPSK) coding schemes, which were designed in Section 2.3.3. More details pertaining to the two systems are summarised in Table 4.2. As a result, the FER versus SNR performance of the $\mathbf{G}_{2 \times 4}$ and $\mathbf{G}_{4 \times 8}$ based systems employing the IrCC-URC-BPSK(QPSK) scheme and the corresponding ide-

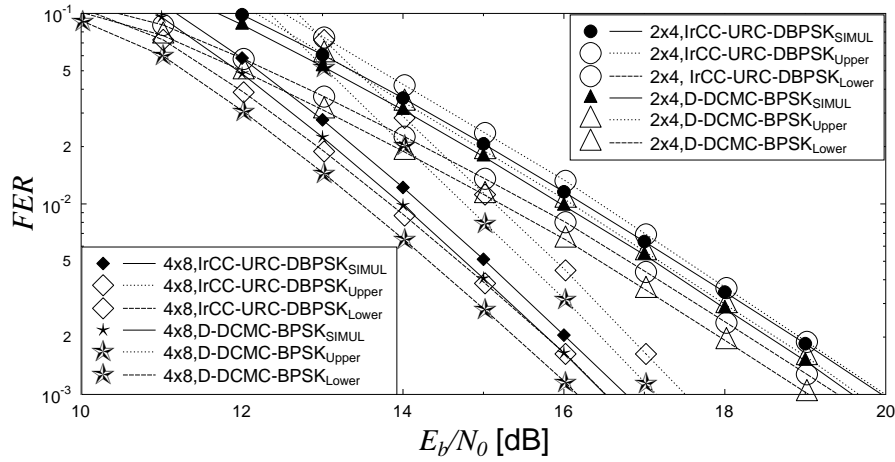


(a) QPSK modulation scheme

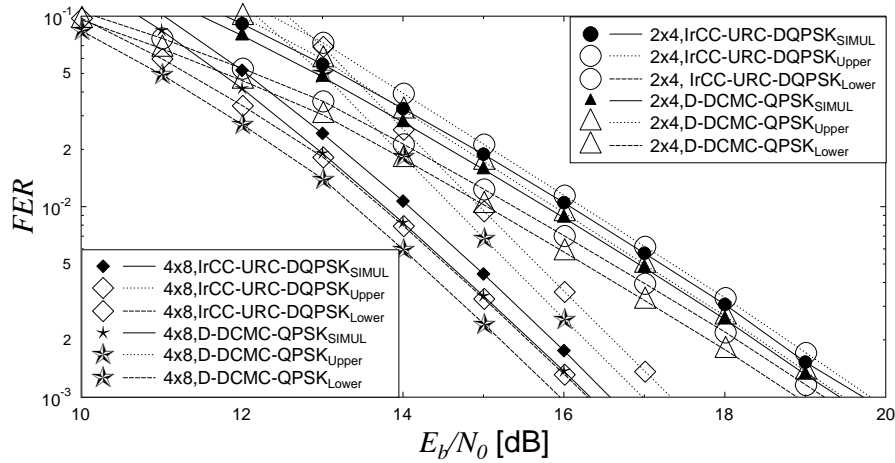


(b) 8PSK modulation scheme

Figure 4.13: FER performance comparison between $G_{2 \times 4}$, $G_{4 \times 8}$ and $G_{6 \times 12}$ based systems employing the IrCC-URC-QPSK(8PSK) scheme and idealised/perfect DCMC-QPSK(8PSK) channel coding schemes and their corresponding bounds, when communicating over wireless channels influenced by both the fast Rayleigh and block Rayleigh fading.



(a) DBPSK modulation scheme



(b) DQPSK modulation scheme

Figure 4.14: FER versus SNR performance of the $G_{2 \times 4}$ and $G_{4 \times 8}$ based systems employing the realistic channel coding scheme IrCC-URC-BPSK(QPSK) and idealised/perfect CCMC and DCMC channel coding schemes, when communicating over wireless channels influenced by both the fast Rayleigh and block Rayleigh fadings.

alised/perfect CCMC and DCMC channel coding schemes is shown in Figure 4.15. It can be seen from Figure 4.15 that the difference in the diversity order of the $G_{2 \times 4}$ and $G_{4 \times 8}$ based systems, as specified in Section 4.7, is reflected by the different slope of the performance curves. As a benefit, the $G_{4 \times 8}$ -based system outperforms the $G_{2 \times 4}$ -based system by about 4.2 dB to 4.4 dB at an FER of 10^{-4} in the cases of using the CCMC, DCMC, IrCC-URC-BPSK and IrCC-URC-QPSK channel coding schemes.

Another important result gleaned from Figure 4.15 is that the performance of the NCMN systems using idealised/perfect CCMC channel coding schemes represents the best-case performance bound of all NCMN system using realistic channel coding schemes, provided that those schemes have the same equivalent data rate R . Furthermore, the performance of the NCMN systems relying on idealised/perfect DCMC channel coding schemes set the best-case performance bounds of all NCMN system supported by realistic coding schemes, provided that those schemes invoke the same data rate R as well as the same modulation scheme.

Similar to the coherent scenario, it can also be seen from Figure 4.16 that the performance of the NCMN systems using the idealised/perfect D-DCMC capacity-achieving channel coding schemes, namely the D-DCMC-BPSK and D-DCMC-QPSK schemes, represents the best-case performance bound of all NCMN systems using realistic channel coding schemes, provided that those schemes employ the same modulation scheme as well as have the same equivalent data rate R .

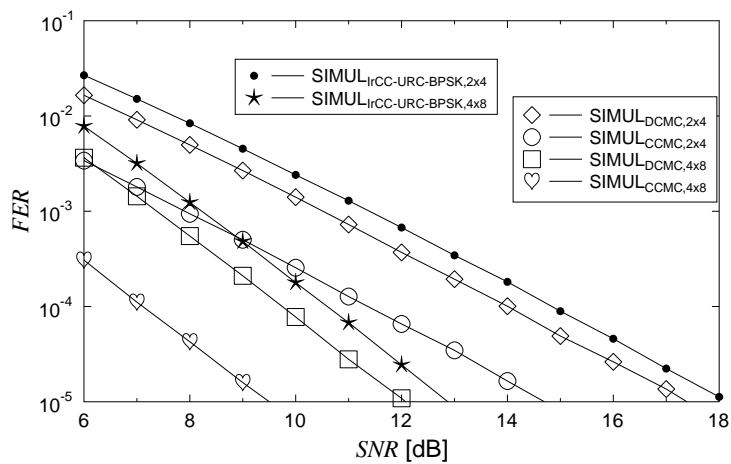
As regards to the distance between the performance curves associated with the realistic scheme and those pertaining to the idealised/perfect DCMC schemes, it can be seen in Figure 4.15 that the performance of the $G_{4 \times 8}$ and $G_{2 \times 4}$ -based systems using our IrCC-URC-BPSK(QPSK) scheme was within 0.8 dB from that of the corresponding systems relying on the assumption of using an idealised/perfect DCMC-achieving channel coding scheme at an FER of 10^{-4} . In the non-coherent systems, a similar distance ranging from 0.5 dB to 0.7 dB is exhibited in Figure 4.16.

4.10.1 Benefits of Network Coding

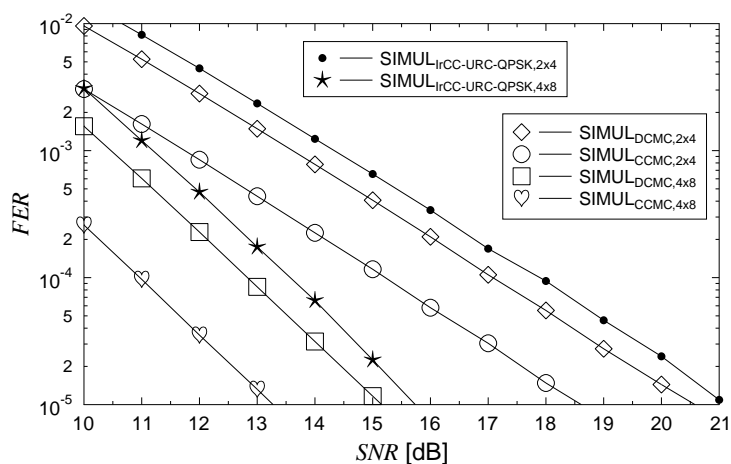
Regarding the benefits of network coding, the following questions may be posed:

1. What is the capacity of the NCMN systems?
2. How far is the performance of a NCMN system from its capacity?

Question 1 was partially answered in Section 4.7.3, where the capacity of the NCMN system was determined by considering network coding as a specific stage of the multi-stage coding scheme. In order to further elaborate on both questions, let us study Figure 4.17, where the FER -performance of the system employing various network coding schemes having the same network coding rate of $R_{info} = 1/2$ is plotted in comparison to its capacity given in Table 4.3. As seen in Figure 4.17, the more powerful the network coding, the closer the FER -performance of our system to its capacity,



(a) IrCC-URC-BPSK



(b) IrCC-URC-QPSK

Figure 4.15: FER versus SNR performance of the $G_{2 \times 4}$ and $G_{4 \times 8}$ based systems employing the realistic IrCC-URC-BPSK(QPSK) and the idealised/perfect CCMC and DCMC-achieving channel coding schemes, when communicating over wireless channels influenced by both the fast Rayleigh and block Rayleigh fading.

where the capacity is calculated by using the method detailed in Section 4.7.3. Indeed, we have to answer another provoking question about which powerful network code we should choose in order to have an FER-performance as close to capacity as desired. A straightforward solution is to simply increase the diversity order D_{NCMN} of our system. As seen in Table 4.2, the diversity orders of the $G_{2 \times 4}$, $G_{4 \times 8}$ and $G_{6 \times 12}$ based systems are $D_{2 \times 4} = 3$, $4 \leq D_{4 \times 8} \leq 5$ and $5 \leq D_{6 \times 12} \leq 7$, respectively. This means we can examine the performance of different network codes, until the appropriate network code is found. This however would require an extreme amount of simulation-related work.

Alternatively, we can invoke the performance bounds derived in Section 4.5, in order to explore the system's FER-performance for finding the most appropriate network code. More specifically,

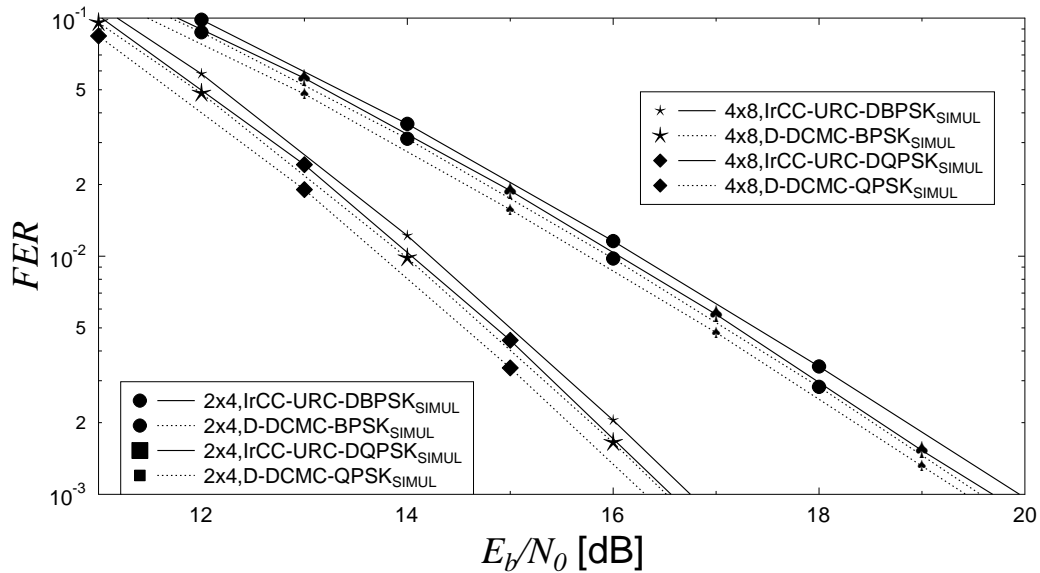


Figure 4.16: FER versus SNR performance of the $G_{2 \times 4}$ and $G_{4 \times 8}$ based systems employing the non-coherent IrCC-URC-DBPSK(DQPSK) scheme and idealised/perfect and D-DCMC channel coding schemes, when communicating over wireless channels influenced by both the fast Rayleigh and block Rayleigh fading.

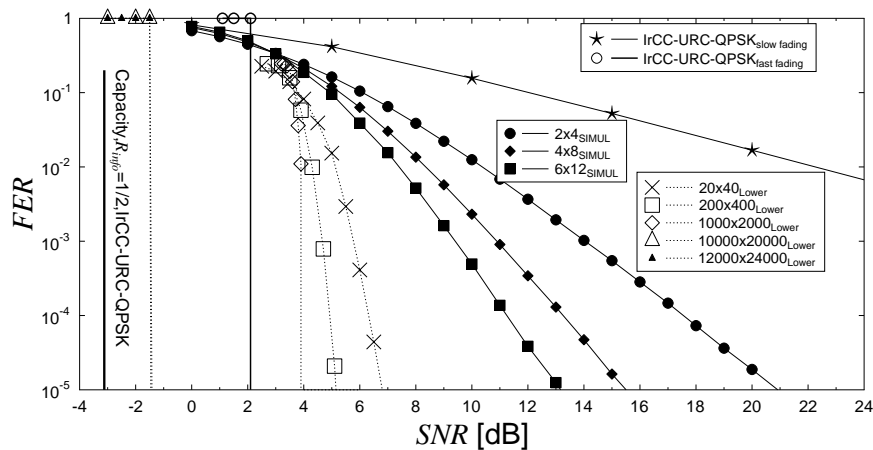


Figure 4.17: The FER performance of network coding based systems having $R_{info} = 1/2$ and employing the realistic IrCC-URC-QPSK channel coding scheme, when communicating over wireless channels influenced by both the fast Rayleigh and block Rayleigh fading.

it may be inferred from Equation (4.64) that the performance of the system approaches its lower bound more closely, when the SNR value increases. Hence, we can use the lower bound of the system performance for estimating its capacity, when employing large transfer matrices. More explicitly, it can be seen in Figure 4.17 that as the size of the transfer matrix increases from $\mathbf{G}_{2 \times 4}$ to $\mathbf{G}_{4 \times 8}$, $\mathbf{G}_{6 \times 12}$, $\mathbf{G}_{20 \times 40}$, $\mathbf{G}_{200 \times 400}$, $\mathbf{G}_{1000 \times 2000}$, $\mathbf{G}_{10000 \times 20000}$ and $\mathbf{G}_{12000 \times 24000}$, the distance from the NCMN system capacity having a network coding rate of $R_{info} = 1/2$ is reduced to 1.7 dB from 24.8 dB, where a further marginal improvement is exhibited when employing a transfer matrix having a larger size than the matrix $\mathbf{G}_{12000 \times 24000}$.

As regards to the benefits of network coding, it can be seen in Figure 4.17 that a significant system's performance improvement is exhibited, compared to the scenario operating without employing the network code. In particular, an FER-performance improvement of 21.6 dB, 25.1dB and 26.9 dB is demonstrated at a $FER = 10^{-5}$, when employing network-coding relying on the matrices $\mathbf{G}_{2 \times 4}$, $\mathbf{G}_{4 \times 8}$ and $\mathbf{G}_{6 \times 12}$, respectively, as seen in Figure 4.17. Furthermore, when a network code relying on a larger transfer matrix, say $\mathbf{G}_{12000 \times 24000}$ is used, a maximum improvement of approximately 44 dB may be expected in the context of our system.

It should be noted that as seen in Figure 4.17, the FER -versus- SNR performance of the system relying on the IrCC-URC-QPSK channel coding scheme may exceed the FER -versus- SNR performance of single link employing the IrCC-URC-QPSK scheme, when an appropriate network-code is used in the system. In particular, when a powerful network-code corresponding to a large transfer matrix of $\mathbf{G}_{10000 \times 20000}$ is employed in our system, the FER -versus- SNR performance reaches its limit. Once the limit of the system's performance is achieved, no further FER -versus- SNR performance improvement is attained, even if more complex network codes are invoked. The performance limit of the system is about 1.6 dB from the corresponding network-coding capacity, which was defined and calculated in Section 4.7.3.

4.10.2 Sub-frame Transmission for Approaching the Capacity

By observing the upper and lower bounds of Equation (4.56) and Equation (4.64), we notice that the performance of NCMN systems may be improved by reducing the P_e term, which means that the performance of each single link in the NCMN systems is improved. As presented in Section 2.4, the employment of subframes is capable of improving the single link transmission in slow fading scenarios. Moreover, in practical systems, such as the Long Term Evolution (LTE) and LTE-Advanced [165, 166] systems, each channel-encoded frame tends to be transmitted in N_{sub} sub-frames.

Let us continue to use the $\mathbf{G}_{2 \times 4}$ and $\mathbf{G}_{4 \times 8}$ based systems relying on the IrCC-URC-QPSK scheme for characterising the performance improvements obtained by activating the subframe-based operation at each transmission link of the systems. Figure 4.18 characterises the FER performance of the systems obtained by Monte-Carlo simulations, when the number of sub-frames

increases from $N_{sub} = 1$ to $N_{sub} = 10^3$. It should be noted that when the number of subframes exceeds $N_{sub} = 10^3$, no further improvement is seen in the system's performance. As observed in Figure 4.18, the $G_{4 \times 8}$ based system significantly outperforms the $G_{2 \times 4}$ based system, when N_{sub} is $N_{sub} \leq 10^2$. However, only a marginal difference is exhibited, when N_{sub} approaches $N_{sub} = 10^3$.

As shown in Figure 4.18, the performance of the $G_{2 \times 4}$ and $G_{4 \times 8}$ based systems converges to that of the single link transmission in the fast fading scenario. In other words, the performance of the single link transmission in the fast fading environment sets the best-possible bound for that of the network coding based systems in the context of our considerations. As a result, the combination of sub-frame based transmissions and network coding is capable of providing an approximately 19 dB (or 13 dB) performance improvement, when comparing the $G_{2 \times 4}$ (or $G_{4 \times 8}$) based systems employing either $N_{sub} = 1$ or $N_{sub} = 10^3$ sub-frames at an FER of 10^{-5} . Another important result gleaned from Figure 4.18 is that if either the network coding scheme used or the number of sub-frames N_{sub} is given, we can optimise one of these two parameters, so that the system achieves its best possible performance.

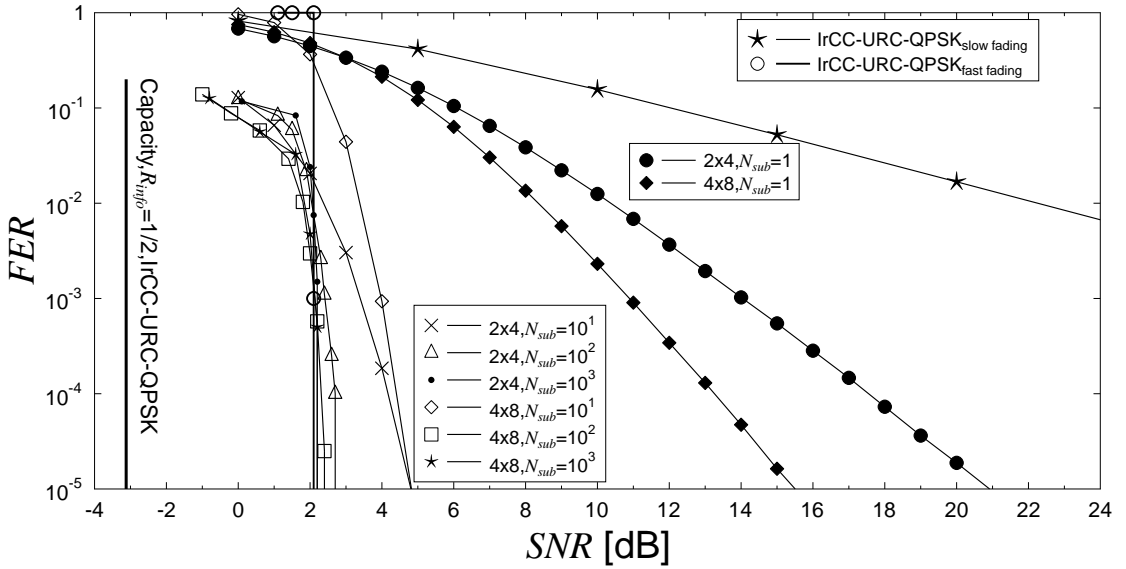


Figure 4.18: FER performance the $G_{2 \times 4}$ and $G_{4 \times 8}$ based systems employing the IrCC-URC-QPSK scheme, when employing the different number of sub-frames $N_{sub} = 1, 10^1, 10^2, 10^3$, when communicating over wireless channels influenced by both the fast Rayleigh and block Rayleigh fadings.

4.10.3 Non-coherent versus Coherent Systems

In this section, we compare the performance of NCMN systems relying on either the coherent scheme designed in Section 2.3.3 or the non-coherent scheme presented in Section 2.3.4. In order to make realistic comparison, the error imposed by the channel estimation used in the coherent sys-

tems is taken into consideration, when deciding whether the non-coherent or the coherent systems should be chosen.

As shown in Figure 2.36 of Section 2.5, the performance of the IrCC-URC-QPSK scheme is superior to that of the IrCC-URC-MSDD-aided-DQPSK scheme, when considering a fast Rayleigh fading scenario, provided that the accuracy probability of the channel estimation is $\theta \geq 60\%$ ⁴. Hence, we investigate the NCMN system's performance, when employing the IrCC-URC-QPSK scheme relying on a channel estimator having different accuracy, namely $\theta = 50\%, 60\%, 100\%$. Then, the performance of the NCMN system relying on the IrCC-URC-QPSK scheme taking into consideration the different levels of channel estimation accuracy is compared to that of the NCMN system employing the IrCC-URC-MSDD-aided-DQPSK scheme.

As seen in Figure 4.19, the coherent IrCC-URC-QPSK scheme outperforms the non-coherent IrCC-URC-MSDD-aided-DQPSK scheme, when the accuracy of the channel estimation is $\theta = 100\%$. However, the performance of the system relying on the non-coherent scheme becomes superior to that of the system relying on the coherent scheme, when the channel-estimator's accuracy becomes lower than $\theta = 60\%$. In conclusion, we can conceive an NCMN system capable of operating in both coherent and non-coherent modes. These modes may be switched by comparing the accuracy of the channel estimation with a pre-calculated threshold, say $\theta = 60\%$.

4.11 Augmenting Multiplexing and Diversity Capability of Network Coding

The NCMN system's performance can be further redeemed by looking at different perspectives of the network coding. In the *first perspective*, by investigating the system's multiplexing facet and the system's diversity facet, the network coding performance can be improved by enhancing diversity facet or by redeeming the multiplexing facet or in fact by combining individual measures, in order to attain a combined gain.

1. As regards to the diversity aspect, the performance of our system can be further improved by exploiting the broadcast nature of wireless communications. More specifically, a user can additionally listen to PFs transmitted by the other users during their CPs, in order for this user to acquire knowledge about the other users' IFs that were not received correctly due to the outages of inter-user transmissions occurring during the BPs. This approach was recently studied in [11] for the idealised simplifying scenario of two users in the context of a system assuming the employment of an idealised so-called perfect capacity-achieving channel code.

⁴According to our analysis in Section 2.5, the performance of the single link transmission relying on the IrCC-URC-QPSK schemes is superior to that of the transmission supported by the IrCC-URC-DQPSK scheme, when the accuracy of the channel estimator is in excess of $\theta = 60\%$. As a result, the threshold $\theta = 60\%$ of channel estimation may be used for switching the single link transmission from the coherent modem to the non-coherent modem, vice versa. Thus, it is expected that the same threshold of $\theta = 60\%$ may be employed for switching in the NCMN systems.

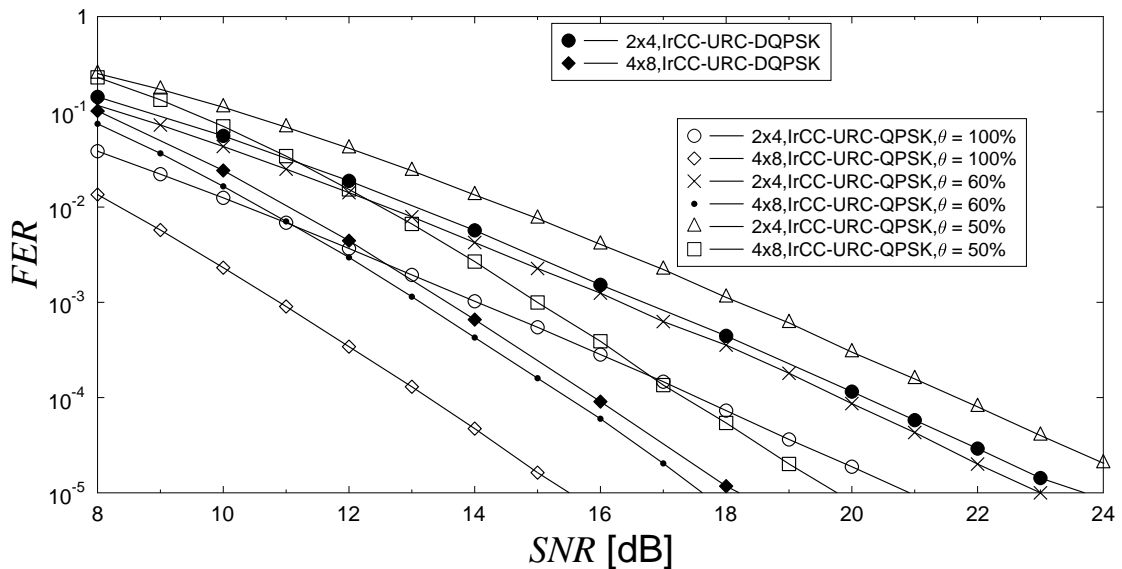


Figure 4.19: The performance of the systems operating in different scenarios, namely in the scenario employing non-coherent IrCC-URC-MSDD-aided-DQPSK scheme, in the case relying on the coherent IrCC-URC-QPSK with the aid of the channel estimator having different level of accuracy, i.e. $\theta = 50\%, 60\%, 100\%$, when communicating over wireless channels influenced by both the fast Rayleigh and block Rayleigh fadings.

Naturally, the realistic general case requires further investigations.

2. As regards to the multiplexing aspect, the general philosophy of the diversity versus multiplexing trade-off (DMT) is that the specific trade-off would rely on the particular channel conditions that the system experiences. When experiencing sufficiently high quality channels, the multiplexing gain of the system can be increased for example by reducing a number of the PFs transmitted. By contrast, an increased diversity may be achieved by increasing the number of PFs, when the channel conditions degrade. Furthermore, another mechanism may be invoked for the channel coding scheme, namely a channel coding scheme having a higher information rate R may be employed, when a good channel condition is encountered. This results in employing an adaptive channel coding scheme, which was also invoked in [186].

The *second perspective*, which is seen from the context of collaboration between channel coding and network coding. Channel coding and network coding may indeed be intrinsically further combined to improve the attainable system performance by adopting two options as follows.

1. The *first option* is that of implementing iterative decoding for exchanging extrinsic information between the channel code and network code. This idea has been studied in [187, 188] by performing iterative decoding with the aid of the PFs transmitted by a single relay, where network coding was performed. As a result, a significant performance improvement was

recorded. However, extending the iterative decoding scheme of [187, 188] to our scenario, while considering multiple-relays/users⁵ leads to an extremely high complexity. Hence it becomes impractical for joint channel-network code design. This conclusion is also suggested by a recent contribution presented in [189].

2. The *second option* advocates introducing an adaptive mechanism, which relies on a feedback flag directly reflecting the performance of the network coding scheme. This feedback flag can be employed to control the channel coding scheme, and vice versa, the feedback flag provided by the channel coding scheme may be utilised for controlling the operation of network coding. The authors of [12] applied this adaptive flag-controlled mechanism under the idealised simplifying assumption of using an ideal/perfect channel code.

In brief, the both perspectives as discussed above lead to the improved diversity aspect and the improved multiplexing aspect of the network coding, which is investigated in next chapter.

4.12 Chapter summary

In this chapter, the FER-performance upper and lower bounds of cooperative multi-user communications systems were derived. The system's FER-performance was also evaluated by Monte Carlo based simulations, in order to verify the accuracy of those bounds. These bounds guided our network coding design and assisted us in estimating the FER performance of the NCMN system without running extremely time-consuming Monte-Carlo simulations. More specifically, the lower bound may be used as the system's performance, when considering the high-SNR region

The capacity of NCMN systems was devised for the sake of benchmarking the performance of the NCMN system in different configurations. Additionally, the derived lower performance bounds was then employed for estimating the size of the transfer matrix required for attaining a given diversity order or for operating at a given distance from the benchmark system's capacity.

We proposed the detection model used for recovering the information frames at the Base Station. Accordingly, based on the algorithms employed for recovering the transmitted frames at the base station, we proposed a new method that we referred to as the Pragmatic Algebraic Linear Equation Method or PALEM. This method is capable of accurately characterising the system's FER performance. The system's performance estimated by our PALEM was compared to that obtained by the Pure Rank Based Method used in [47, 99]. Our proposed PALEM was shown to provide identical results in comparison to that suggested by Monte-Carlo simulations, while the PRBM always leads to optimistic system performance results.

Furthermore, we investigated the NCMN based systems using the IRCC-URC-MPSK scheme of Section 2.3.3 as well as employing IrCC-URC-DMPSK counterpart of Section 2.3.4. These

⁵In our scenario, each user itself plays a role as a relay. Hence, our the model has multiple-users and multiple-relays.

schemes approach their corresponding DCMC and D-DCMC capacities within approximately 1 dB at a FER of 10^{-5} . The performance of the NCMN systems relying on our realistic channel coding schemes, namely on the IrCC-URC-MPSK and IrCC-URC-DMPSK arrangement, was benchmarked against the corresponding NCMN based systems employing the idealised/perfect channel coding schemes operating at exactly the CCMC, DCMC and D-DCMC capacities.

The effect of errors imposed on the channel estimation is also taken into consideration, when comparing the non-coherent and coherent detection based systems. It was confirmed by our simulation results that the threshold $\theta = 60\%$ of the channel estimation accuracy may still be used for deciding whether coherent or non-coherent demodulation based schemes should be activated.

The employment of sub-frame transmissions was shown to be useful for approaching the system capacity, when the associated amount of delay is affordable in the system. The sub-frame transmission regime is capable of bringing the system's performance close to the performance of a single link in rapidly fading environments, when as many as $N_{sub} = 10^3$ sub-frames are used for conveying a transmission frame.

In the next chapter, a usage of measures conceived for improving the diversity gain of the system as well as for enhancing the multiplexing capability of the system, as suggested in Section 4.11, are investigated, in order to create a range of generalised NCMN systems.

Generalised Near-Capacity Multi-user Network-coding: Multilayer-and-Multimode Architecture

In this chapter, the Near-Capacity Multi-user Network-coding (NCMN) philosophy introduced in Chapter 4 is generalised for conceiving the concept of Generalised Near-Capacity Multi-user Network-coding (GNCMN), which has a multi-layer architecture and is capable of operating in multiple modes at each layer. More specifically, the GNCMN scheme is capable of closely approaching to its capacity by employing sub-frame based transmissions. As discussed in Section 4.11, both the multiplexing and diversity aspects of the GNCMN system can be improved by employing our adaptive network coding technique, as suggested in [12]. This scheme exploits the Parity Frames (PFs) transmitted during the Cooperative Phases (CPs) at each user for approaching the performance of full-diversity networking coding [11]. Moreover, a triple-layer coding scheme is devised for improving the achievable time diversity gain [190]. Additionally, with the aid of the feedback characterising the accuracy of the channel estimation presented in Section 2.5, the GNCMN becomes capable of activating either our coherent detection aided Irregular Convolutional Coded Unity Rate Coded M-ary Phase Shift Keying (IrCC-URC-MPSK) detailed in Section 2.3.3 or the non-coherent detection assisted Irregular Convolutional Coded Unity Rate Coded Differential M-ary Phase Shift Keying (IrCC-URC-DMPSK) arrangement described in Section 2.3.4. Having integrated the above-mentioned functionalities into our GNCMN system, we can then combine them appropriately, in order to achieve the combined benefits of amalgamating two or more of them.

5.1 Architecture of Generalised Near-Capacity Multi-user Network-coding System

The general architecture of the GNCMN system shown in Figure 5.1 can be structured into three coding layers, namely Channel Coding (CC), Network Coding 1 (NC1) and Network Coding 2 (NC2). In our triple-layer coding system, H frames of a user's information are processed in NC2, before feeding the Θ resultant encoded frames to NC1, as seen in Figure 5.1. In the NC1 layer, M users cooperatively transmit Mk_1 Information Frames (IFs) to the same destination node during a transmission session, where k_1 is the number of IFs transmitted by each of the M users during the transmission session. Once the frames to be transmitted have been constructed according to the processes performed at NC1 and NC2, each of the frames is encoded by the channel coding scheme, as shown in Figure 5.1.

5.1.1 Near-capacity Channel Coding

In the channel coding layer shown in Figure 5.1, we assume that all the links in the system are supported by channels having the same information rate R . As seen in Figure 5.1, the channel code of the GNCMN system is capable of operating either in a coherent mode, when a channel estimator is available or in a non-coherent mode, when system cannot afford incorporating a channel estimator. Moreover, the accuracy of the channel estimator is also taken into consideration, in order to introduce a more flexible switch-over mechanism. More specifically, the feedback characterising the accuracy of the channel estimator is exploited for determining, whether the coherent mode associated with high-quality channel estimation or the non-coherent mode should be activated.

In order to achieve an infinitesimally low BER in both the coherent and non-coherent modes, turbo detection may be employed at both the user's unit and the BS. Therefore, a recursive URC [164] having an infinite impulse response may be employed as an intermediate code, as seen in the channel coding section of Figure 5.1. If the user's unit and the BS can indeed afford the high decoding complexity imposed by a near-capacity IrCC scheme, then a near-capacity performance may be achieved by employing the three-stage IrCC-URC-MPSK coding arrangement of Figure 2.19 or IrCC-URC-DMPSK coding arrangement of Figure 2.27, as detailed in Section 2.3.3 or Section 2.3.4.

Additionally, the sub-frame transmission mode presented in Section 4.2.2 can also be used in both the coherent and non-coherent channel coding schemes. Once the sub-frame transmission is activated, the GNCMN system becomes capable of providing an adjustable diversity gain at the link level. Hence, the total diversity gain of the GNCMN system is constituted by three adjustable components, namely the diversity at the link-level, the diversity at the NC1 level and the diversity at the NC2 level. More specifically, the diversity obtained at the NC1 level can be adjusted by scaling the transfer matrix \mathbf{G} , as detailed in Section 4.2.2, while that of the NC2 level can be customised by

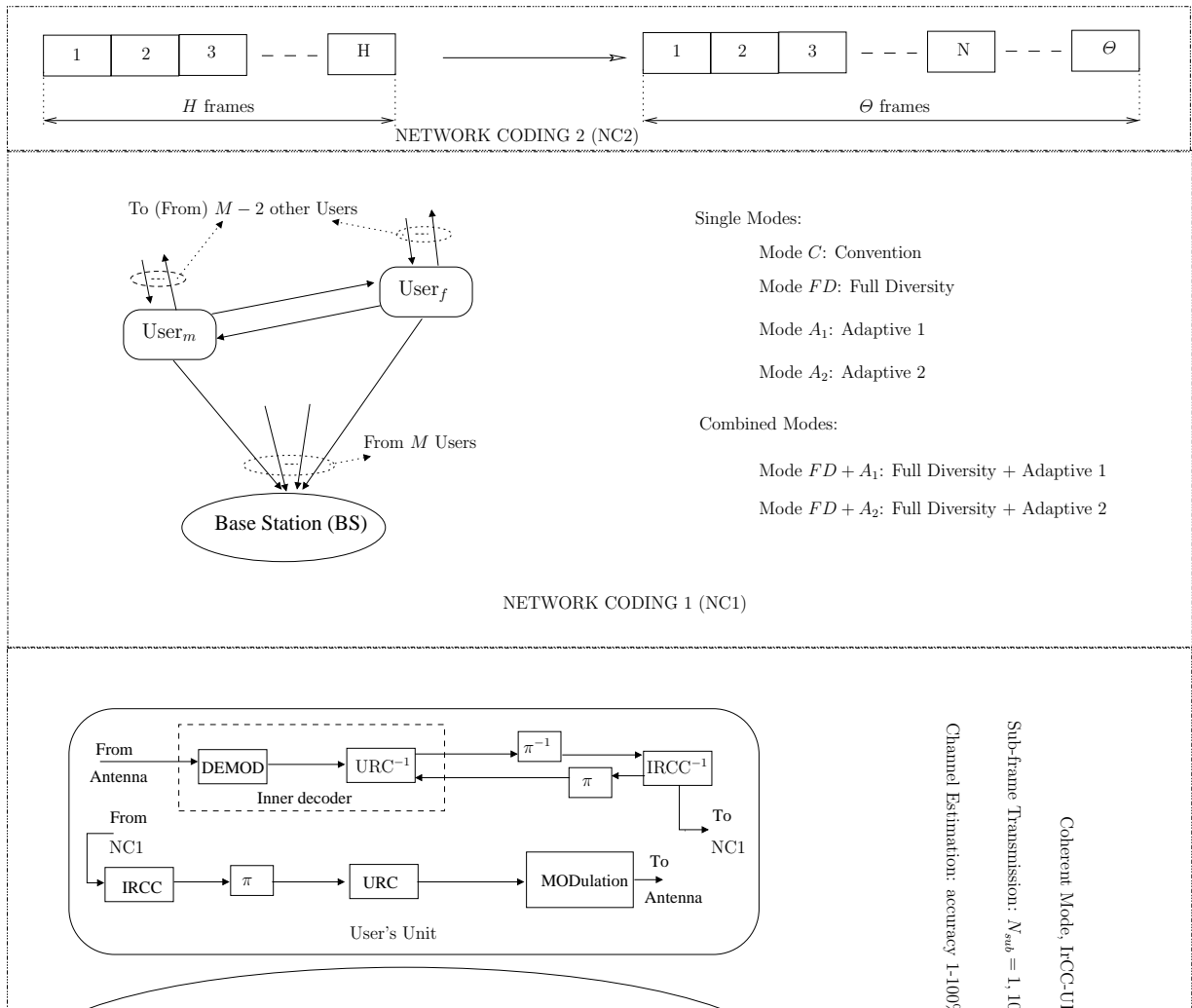


Figure 5.1: The architecture of the Generalised Near-Capacity Multi-user Network-coding system.

changing the number of the IFs N decoded, whereas that of the link-level can be manipulated by adjusting N_{sub} , namely the number of sub-frames in a transmitted frame, as detailed in Section 2.4.

5.1.2 Network Coding 1

As analysed in Section 4.11, both the diversity and multiplexing aspects of the network coding are improved in the GNCCMN system. As a result, the NC1 portrayed in Figure 5.1 is capable of operating in various regimes, which are determined by activating an appropriately selected set of the following four modes:

- The Conventional mode (C mode) is used for the default operation of NC1.
- The Full Diversity mode (FD mode) can be activated for improving the system's diversity gain.
- Two adaptive modes, namely modes A_1 and A_2 , can be chosen for improving the multiplexing gain of the system.

5.1.2.1 The Conventional mode

The C mode is the default mode for the normal operation of NC1. The operation principle of the C mode is detailed in Section 4.2 and Section 4.3. However, for the convenience of presenting other new modes, namely the FD mode, A_1 mode and A_2 mode, the operating principle of the C mode is briefly summarised in our example depicted in Figure 5.2. In the normal operation of the system portrayed in Figure 5.2, each of the $M = 2$ users transmits $k_1 = 1$ Information Frame (IF) during $Mk_1 = 2$ Broadcast Phases (BPs) (B_1 and B_2) and $k_2 = 2$ PFs during $Mk_2 = 4$ CPs (C_1, C_2, C_3 and C_4), respectively. Let us denote an IF transmitted by User m as $I_m(t), t = [m, M + m, \dots, (k_1 - 1)M + m]$, which takes place during the specific broadcast phase $t, t = [m, M + m, \dots, (k_1 - 1)M + m]$. Then, the arrangement of the BPs and CPs in Figure 5.2 can be summarised in the following transmission example:

Broadcast phases

$$\mathbf{G}'_{2 \times 6} = \mathbf{G}_{2 \times 6},$$

$$(B_1 U_2) : \text{User 1} \xrightarrow{=0} \text{User 2} \Rightarrow \mathbf{G}'_{2 \times 6}(1, i) = 0, i = [4, 6], \quad (5.1)$$

$$(B_1 B) : \text{User 1} \xrightarrow{=0} \text{BS} \Rightarrow \mathbf{G}'_{2 \times 6}(1, 1) = 0, \quad (5.2)$$

$$(B_2 U_1) : \text{User 2} \xrightarrow{=0} \text{User 1} \Rightarrow \mathbf{G}'_{2 \times 6}(2, i) = 0, i = [3, 5] \quad (5.3)$$

$$(B_2 B) : \text{User 2} \xrightarrow{=0} \text{BS} \Rightarrow \mathbf{G}'_{2 \times 6}(2, 2) = 0, \quad (5.4)$$

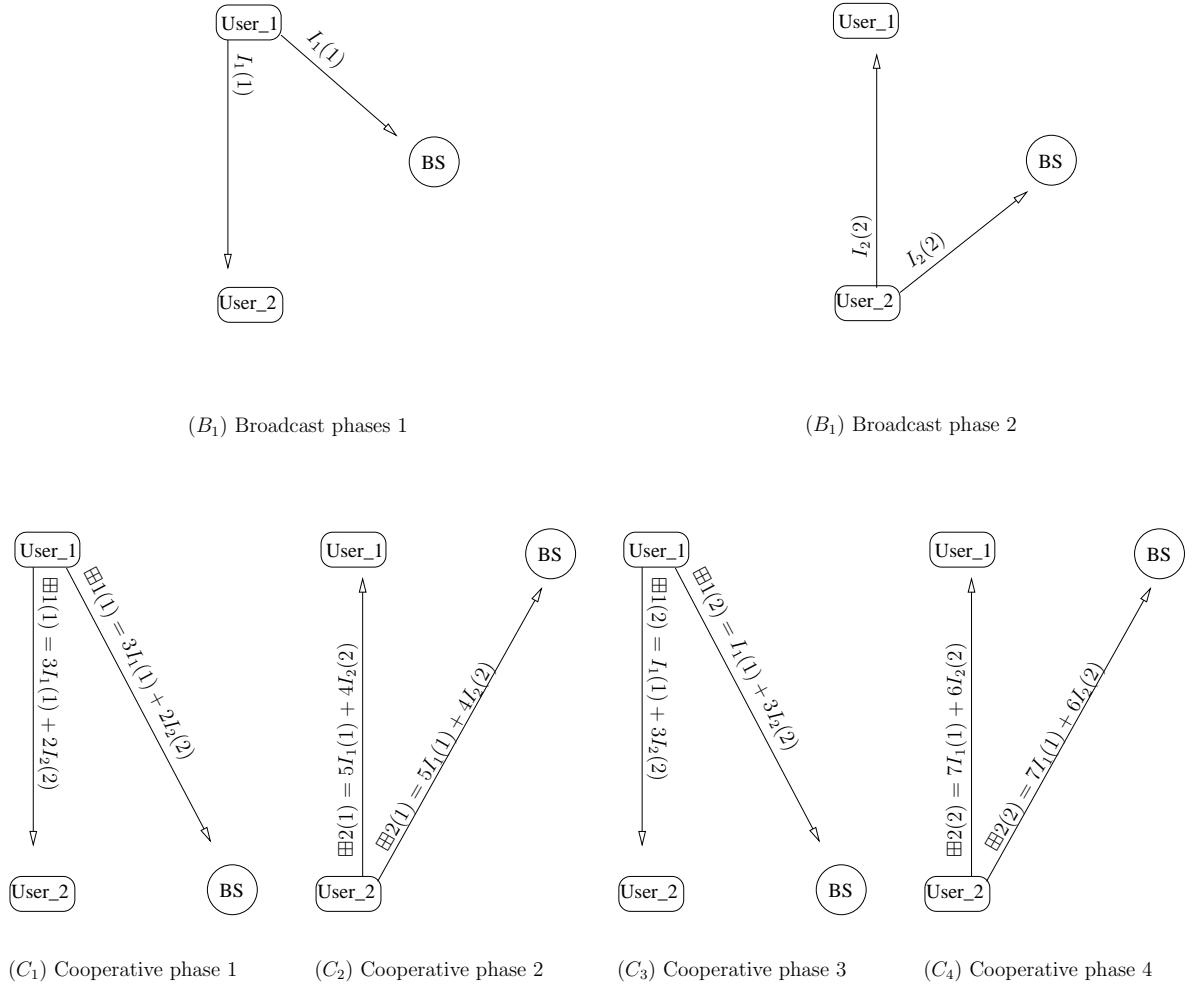


Figure 5.2: Model of NC1 of Figure 5.1, supporting $M = 2$ users, where each user transmits $k_1 = 1$ IF and $k_2 = 2$ PFs.

Cooperative phases

$$(C_1 U_2) : \text{User 1} \xrightarrow{=1} \text{User 2} \Rightarrow \text{NOT considered}, \quad (5.5)$$

$$(C_1 B) : \text{User 1} \xrightarrow{=1} \text{BS}, \Rightarrow \mathbf{G}'_{2 \times 6}(i, 3) \text{ unchanged}, i = 1, 2, \quad (5.6)$$

$$(C_2 U_1) : \text{User 2} \xrightarrow{=1} \text{User 1} \Rightarrow \text{NOT considered}, \quad (5.7)$$

$$(C_2 B) : \text{User 2} \xrightarrow{=0} \text{BS} \Rightarrow \mathbf{G}'_{2 \times 6}(i, 4) = 0, i = 1, 2, \quad (5.8)$$

$$(C_3 U_2) : \text{User 1} \xrightarrow{=0} \text{User 2} \Rightarrow \text{NOT considered}, \quad (5.9)$$

$$(C_3 B) : \text{User 1} \xrightarrow{=1} \text{BS} \Rightarrow \mathbf{G}'_{2 \times 6}(i, 5) \text{ unchanged}, i = 1, 2 \quad (5.10)$$

$$(C_4 U_1) : \text{User 2} \xrightarrow{=0} \text{User 1} \Rightarrow \text{NOT considered}, \quad (5.11)$$

$$(C_4 B) : \text{User 2} \xrightarrow{=0} \text{BS} \Rightarrow \mathbf{G}'_{2 \times 6}(i, 6) = 0, i = 1, 2. \quad (5.12)$$

Note that $B_k U$ (or $B_k B$) represents a user-to-User transmission (or a user-to-BS transmission) during the broadcast phase B_k , while $C_l U$ (or $C_l B$) indicates a user-to-User transmission (or a user-to-BS transmission) during the cooperative phase C_l . Additionally, the arrow ' \longrightarrow ' represents the transmission direction, while the variable $\boxplus i(j)$ seen in Figure 5.2 represents the j^{th} PF of User i ,

whereas the notation ‘(= 0)’ (or ‘(= 1)’) above the arrows of Equation (5.1)-Equation (5.12) indicates that the frame was unsuccessfully (or successfully) recovered at the receiver.

Employing our convention used in Section 4.2.2, if all the frames transmitted in a session are successfully received at both the $M = 2$ users and the BS, then the transmission session can be described by the following transfer matrix [99]:

$$\mathbf{G}_{2 \times 6} = \left[\begin{array}{cc|ccc} 1 & 0 & 3 & 5 & 1 & 7 \\ 0 & 1 & 2 & 4 & 3 & 6 \end{array} \right]. \quad (5.13)$$

Note that the transfer matrix $\mathbf{G}_{2 \times 6}$ is constructed from the generator matrix of Reed Solomon (RS) code formed over the Galois Field $GF(8)$. Please refer to Section 4.2.2 for more specifics of the transfer matrix.

As defined in Section 4.2.2, the modified transfer matrix $\mathbf{G}'_{2 \times 6}$ is used for representing an actual transmission session. Hence, the modified $\mathbf{G}'_{2 \times 6}$ has the entries modified with respect to those of the original transfer matrix $\mathbf{G}_{2 \times 6}$ of Equation (5.13) according to the success/failure of each transmission phase within an actual transmission session, as seen in Equation (5.1)-Equation (5.12). More specifically, according to the numerical example of the transmission session given in Equation (5.1)-Equation (5.12), the entries of $\mathbf{G}'_{2 \times 6}$ can be calculated by applying the general principles stipulated by Equation (4.4)-Equation (4.7), in order to lead to the modified matrix $\mathbf{G}'_{2 \times 6}$ as:

$$\mathbf{G}'_{2 \times 6} = \left[\begin{array}{cc|ccc} 0 & 0 & 3 & 0 & 1 & 0 \\ 0 & 0 & 0 & 0 & 0 & 0 \end{array} \right]. \quad (5.14)$$

For the generalised case, please refer to the Section 4.2.2 for the details of the transfer matrix $\mathbf{G}_{k_1 M \times (k_1 M + k_2 M)}$ (or \mathbf{G} for shorthand) and the modified transfer matrix $\mathbf{G}'_{k_1 M \times (k_1 M + k_2 M)}$ (or \mathbf{G}' for shorthand).

Accordingly, the NC1 information rate R_{info} is determined by Equation (4.68) as

$$R_{info} = \frac{k_1}{k_1 + k_2}. \quad (5.15)$$

5.1.2.2 The Full Diversity mode

In contrast to the C mode described in Section 5.1.2.1, where the inter-user transmissions during the cooperative phases are not taken into consideration, the GNCMN system in the FD mode is capable of exploiting the inter-user transmissions during cooperative phases, for improving inter-user transmissions in broadcast phases, as mentioned in Section 4.11. More specifically, if each user in our system is equipped with a network-coding decoder, which is identical to the network-coding decoder used at the BS, the user can decode all the IFs and PFs successfully received, in order to improve its knowledge about IFs transmitted by the other users. Then, the improved knowledge is exploited to construct the subsequent PFs transmitted by the user. The process of decode-and-update is repeatedly kicked off, as soon as the user receives a PF transmitted by another user in the

system. The decode-and-update process at a certain user is no longer required, as soon as all IFs transmitted by the other users during the broadcast phases are comprehensively known by the user.

Let us continue to consider the numerical example given in Equation (5.1)-Equation (5.12). It is worth noting that the transmissions in (C_1U_2) of Equation (5.5), (C_2U_1) of Equation (5.7), (C_3U_2) of Equation (5.9) and (C_4U_1) of Equation (5.11) are not utilised in the C mode. If a network coding decoder is invoked by each of the M users, the cooperative transmissions, namely (C_1U_2) of Equation (5.5) (C_2U_1) of Equation (5.7), (C_3U_2) of Equation (5.9) and (C_4U_1) of Equation (5.11), can be exploited for recovering the erroneous frames that were corrupted by the outage of the inter-user channels during BPs as follows.

- **Cooperative Phase 1, (C_1U_2)**

Cooperative phases

$$(C_1U_2) : \text{User 1} \xrightarrow{=0} \text{User 2} \quad \Rightarrow \text{CONSIDERED.} \quad (5.16)$$

At User 2, the entries of the contemporary modified matrix $\mathbf{G}'_{U_2,2 \times 6, C_1}$ for transmissions from User 1 to User 2 can be specified as

Broadcast phases

$$(B_1U_2) : \text{User 1} \xrightarrow{=0} \text{User 2} \quad \Rightarrow \mathbf{G}'_{U_2,2 \times 6, C_1} = \mathbf{G}_{2 \times 6}, \quad (5.17)$$

$$\Rightarrow \mathbf{G}'_{U_2,2 \times 6, C_1}(1, i) = 0, i = [4, 6], \quad (5.18)$$

$$\text{User 1} \xrightarrow{=1} \text{User 1} \quad \Rightarrow \mathbf{G}'_{U_2,2 \times 6, C_1}(1, i) \text{ unchanged}, i = [3, 5], \quad (5.19)$$

$$(B_2U_1) : \text{User 2} \xrightarrow{=0} \text{User 1} \quad \Rightarrow \mathbf{G}'_{U_2,2 \times 6, C_1}(2, i) = 0, i = [3, 5], \quad (5.20)$$

$$\text{User 2} \xrightarrow{=1} \text{User 2} \quad \Rightarrow \mathbf{G}'_{U_2,2 \times 6, C_1}(2, 2) = 1, \quad (5.21)$$

$$\Rightarrow \mathbf{G}'_{U_2,2 \times 6, C_1}(2, i) \text{ unchanged}, i = [4, 6], \quad (5.22)$$

and

Cooperative phases

$$(C_1U_2) : \text{User 1} \xrightarrow{=1} \text{User 2} \quad \Rightarrow \mathbf{G}'_{U_2,2 \times 6, C_1}(i, 3) \text{ unchanged}, i = [1, 2], \quad (5.23)$$

$$(C_2U_1) : \text{NOT transmitted yet} \quad \Rightarrow \mathbf{G}'_{U_2,2 \times 6, C_1}(i, 4) = 0, i = [1, 2], \quad (5.24)$$

$$(C_3U_2) : \text{NOT transmitted yet} \quad \Rightarrow \mathbf{G}'_{U_2,2 \times 6, C_1}(i, 5) = 0, i = [1, 2], \quad (5.25)$$

$$(C_4U_1) : \text{NOT transmitted yet} \quad \Rightarrow \mathbf{G}'_{U_2,2 \times 6, C_1}(i, 6) = 0, i = [1, 2]. \quad (5.26)$$

It is worth noting that in the broadcast phases, namely (B_1U_2) of Equation (5.17) and (B_2U_1) of Equation (5.20), we always have $\text{User } j \xrightarrow{=1} \text{User } j, j = [1, M]$. Accordingly, the modified matrix $\mathbf{G}'_{U_2,2 \times 6, C_1}$ can be obtained as

$$\mathbf{G}'_{U_2,2 \times 6, C_1} = \left[\begin{array}{cc|cccc} 0 & 0 & 3 & 0 & 0 & 0 \\ 0 & 1 & 0 & 0 & 0 & 0 \end{array} \right]. \quad (5.27)$$

Relying on $\mathbf{G}'_{U_2,2 \times 6, C_1}$, User 2 can recover IF $I_1(1)$ that could not be recovered owing to the inter-user outage occurring during the broadcast phase (B_1U_2) of Equation (5.17). It should be noted that after Cooperative Phase 1, User 2 has a comprehensive knowledge of all the IFs, namely $I_1(1)$ and $I_2(2)$. Since User 2 has the knowledge of all the IFs, no further detection process is needed for User 2. The comprehensive knowledge of the IFs is used for constructing the subsequent PFs transmitted by User 2 during the CPs of (C_2U_1) and (C_4U_1).

Let us denote the knowledge of User 2 about all IFs transmitted within the transmission session considered by $Y_2(\Gamma_{IF})$, where $\Gamma_{IF} = \{I_1(1), I_2(2)\}$ represents all the IFs transmitted within a transmission session, while $I_2(i)$ denotes the IF transmitted by User 2 during BP $i, i = [1, 2]$. As a result, having

$$Y_2(\Gamma_{IF}) = \{I_1(1), I_2(2)\}, \quad (5.28)$$

means that User 2 has a comprehensive knowledge of both IFs, namely of $I_1(1)$ and $I_2(2)$.

If the cooperative phase of (C_1U_2) detailed in (5.16) were not to be considered at User 2, the corresponding modified matrix $\mathbf{G}'_{U_2,2 \times 6}$ generated for transmissions to User 2 would be represented by:

$$\mathbf{G}'_{U_2,2 \times 6} = \left[\begin{array}{cc|cccc} 0 & 0 & 0 & 0 & 0 & 0 \\ 0 & 1 & 0 & 0 & 0 & 0 \end{array} \right]. \quad (5.29)$$

Relying on the modified matrix $\mathbf{G}'_{U_2,2 \times 6}$, User 2 would only be capable of recovering its own IF $I_2(2)$. This would lead to the knowledge $Y_2(\Gamma_{IF})$ of User 2 becoming:

$$Y_2(\Gamma_{IF}) = \{I_2(2)\}. \quad (5.30)$$

It can be readily inferred from (5.28) and (5.30) that exploiting the network decoder at each user can help improve the inter-user transmissions degraded by outage encountered in inter-user channels during broadcast phases.

- **Cooperative Phase 2, (C_2U_1)**

Let us now take into consideration the inter-user transmission during the cooperative phase C_2U_1 of Equation (5.24) as:

$$\begin{array}{c} \text{Cooperative phases} \\ (C_2U_1) : \text{User 2} \xrightarrow{=1} \text{User 1} \quad \Rightarrow \text{CONSIDERED.} \end{array} \quad (5.31)$$

Similar to the process of Cooperative Phase 1, the current modified matrix $\mathbf{G}'_{U_1,2 \times 6, C_2}$ generated for transmissions from User 2 to User 1 up to Cooperative Phase 2 is formed by its

corresponding entries, which are specified by:

Broadcast phases

$$\mathbf{G}'_{U_1,2 \times 6, C_2} = \mathbf{G}_{2 \times 6},$$

$$(B_1 U_2) : \text{User 1} \xrightarrow{=0} \text{User 2} \Rightarrow \mathbf{G}'_{U_1,2 \times 6, C_2}(1, i) = 0, i = [4, 6], \quad (5.32)$$

$$\text{User 1} \xrightarrow{=1} \text{User 1} \Rightarrow \mathbf{G}'_{U_1,2 \times 6, C_2}(1, 1) = 1, \quad (5.33)$$

$$\Rightarrow \mathbf{G}'_{U_1,2 \times 6, C_2}(1, i) \text{ unchanged}, i = [3, 5], \quad (5.34)$$

$$(B_2 U_1) : \text{User 2} \xrightarrow{=0} \text{User 1} \Rightarrow \mathbf{G}'_{U_1,2 \times 6, C_2}(2, 2) = 0, \quad (5.35)$$

$$\Rightarrow \mathbf{G}'_{U_1,2 \times 6, C_2}(2, i) = 0, i = [3, 5], \quad (5.36)$$

and by:

Cooperative phases

$$(C_1 U_2) : \text{User 1} \xrightarrow{=0} \text{User 2} \Rightarrow \mathbf{G}'_{U_1,2 \times 6, C_2} \text{ unchanged}, \quad (5.37)$$

$$(C_2 U_1) : \text{User 2} \xrightarrow{=1} \text{User 1} \Rightarrow \mathbf{G}'_{U_1,2 \times 6, C_2}(i, 4) \text{ unchanged}, i = [1, 2], \quad (5.38)$$

$$(C_3 U_2) : \text{NOT transmitted yet} \Rightarrow \mathbf{G}'_{U_1,2 \times 6, C_2}(i, 5) = 0, i = [1, 2], \quad (5.39)$$

$$(C_4 U_1) : \text{NOT transmitted yet} \Rightarrow \mathbf{G}'_{U_1,2 \times 6, C_2}(i, 6) = 0, i = [1, 2]. \quad (5.40)$$

Note that in the cooperative phase $(C_1 U_2)$ of Equation (5.37), the result of the transmissions from User 1 to User 2 has no effect on the entries of $\mathbf{G}'_{U_1,2 \times 6, C_2}$, since the detection process considered takes place at User 1. Note that the equivalent transmission from User 1 to User 1 is always successful, namely we have $\text{User 1} \xrightarrow{=1} \text{User 1}$, as specified in Equation (5.33) and Equation (5.34). As a result, the modified matrix $\mathbf{G}'_{U_1,2 \times 6, C_2}$ can be represented by

$$\mathbf{G}'_{U_1,2 \times 6, C_2} = \left[\begin{array}{cc|ccc} 1 & 0 & 3 & 0 & 0 & 0 \\ 0 & 0 & 0 & 4 & 0 & 0 \end{array} \right]. \quad (5.41)$$

Again, by employing the modified matrix $\mathbf{G}'_{U_1,2 \times 6, C_2}$ of (5.41), User 1 can recover all the IFs, namely $I_1(1)$ and $I_2(2)$. Hence, no further network decoding process is required at User 1, since a comprehensive knowledge of all IFs is extracted by User 1. Then, this comprehensive knowledge is used for forming the subsequent PF, which is broadcast during the cooperative phase $(C_3 U_2)$. Therefore, after the cooperative phase $(C_2 U_1)$, the knowledge $Y_1(\Gamma_{IF})$ of User 2 about all the IFs can be represented by:

$$Y_1(\Gamma_{IF}) = \{I_1(1), I_2(2)\}. \quad (5.42)$$

With the result of the network-decoding process both at User 1 and at User 2 in mind, we can now formulate the modified matrix $\mathbf{G}'_{2 \times 6, Full-Diversity}$ for transmissions to the BS in the case of having network-decoder at each user in the system. For the sake of brevity, the modified matrix

$\mathbf{G}'_{2 \times 6, \text{Full-Diversity}}$ is also denoted as $\mathbf{G}'_{2 \times 6, \text{FD}}$, which has entries specified as follows.

Broadcast phases

$$\mathbf{G}'_{2 \times 6, \text{FD}} = \mathbf{G}_{2 \times 6},$$

$$(B_1 U_2) : \text{User 1} \xrightarrow{=0} \text{User 2} \Rightarrow \mathbf{G}'_{2 \times 6, \text{FD}}(1, i) = 0, i = [4, 6], \quad (5.43)$$

$$(B_1 B) : \text{User 1} \xrightarrow{=0} \text{BS} \Rightarrow \mathbf{G}'_{2 \times 6, \text{FD}}(1, 1) = 0, \quad (5.44)$$

$$(B_2 U_1) : \text{User 2} \xrightarrow{=0} \text{User 1} \Rightarrow \mathbf{G}'_{2 \times 6, \text{FD}}(2, i) = 0, i = [3, 5] \quad (5.45)$$

$$(B_2 B) : \text{User 2} \xrightarrow{=0} \text{BS} \Rightarrow \mathbf{G}'_{2 \times 6, \text{FD}}(2, 2) = 0, \quad (5.46)$$

Cooperative phases

$$(C_1 U_2) : \text{User 1} \xrightarrow{=1} \text{User 2} \Rightarrow Y_2(\Gamma_{IF}) = \{I_1(1), I_2(2)\}, \quad (5.47)$$

\Rightarrow **Full knowledge achieved,**

$$Y_2(\Gamma_{IF}) = \{I_1(1), I_2(2)\} \Rightarrow \mathbf{G}'_{2 \times 6, \text{FD}}(1, i) = \mathbf{G}_{2 \times 6}(1, i), i = [4, 6], \quad (5.48)$$

$$(C_1 B) : \text{User 1} \xrightarrow{=1} \text{BS}, \Rightarrow \mathbf{G}'_{2 \times 6, \text{FD}}(i, 3) \text{ unchanged}, i = 1, 2,$$

$$(C_2 U_1) : \text{User 2} \xrightarrow{=1} \text{User 1} \Rightarrow Y_1(\Gamma_{IF}) = \{I_1(1), I_2(2)\}, \quad (5.49)$$

\Rightarrow **Full knowledge achieved,**

$$Y_1(\Gamma_{IF}) = \{I_1(1), I_2(2)\} \Rightarrow \mathbf{G}'_{2 \times 6, \text{FD}}(2, i) = \mathbf{G}_{2 \times 6}(2, i), i = [5], \quad (5.50)$$

$$(C_2 B) : \text{User 2} \xrightarrow{=0} \text{BS} \Rightarrow \mathbf{G}'_{2 \times 6, \text{FD}}(i, 4) = 0, i = [1, 2], \quad (5.51)$$

$$(C_3 U_2) : \text{User 1} \xrightarrow{=0} \text{User 2} \Rightarrow \text{No longer of interest}, \quad (5.52)$$

$$(C_3 B) : \text{User 1} \xrightarrow{=1} \text{BS} \Rightarrow \mathbf{G}'_{2 \times 6}(i, 5) \text{ unchanged}, i = [1, 2] \quad (5.53)$$

$$(C_4 U_1) : \text{User 2} \xrightarrow{=0} \text{User 1} \Rightarrow \text{No longer of interest}, \quad (5.54)$$

$$(C_4 B) : \text{User 2} \xrightarrow{=0} \text{BS} \Rightarrow \mathbf{G}'_{2 \times 6}(i, 6) = 0, i = [1, 2]. \quad (5.55)$$

Accordingly, we can obtain the modified transfer matrix of $\mathbf{G}'_{2 \times 6, \text{FD}}$ as

$$\mathbf{G}'_{2 \times 6, \text{FD}} = \left[\begin{array}{cc|ccc} 0 & 0 & 3 & 0 & 1 & 0 \\ 0 & 0 & 0 & 0 & 3 & 0 \end{array} \right]. \quad (5.56)$$

As seen from the modified matrix $\mathbf{G}'_{2 \times 6, \text{FD}}$ of Equation (5.56), the BS is now in a position to recover both IFs, namely $I_1(1), I_2(2)$, while with the aid of $\mathbf{G}'_{2 \times 6}$ given by Equation (5.14) only the IF of $I_1(1)$ is recovered in the C mode, when no network-decoder is provided at each user.

Let us now generalise the processes at each user operating in FD mode by firstly denoting $Y_l(\Gamma_{IF})$ as the knowledge of User l about all IFs transmitted within a certain transmission session, where $\Gamma_{IF} = \{I_1(1), I_2(2), \dots, I_M(k_1 M)\}$ represents the set of all the IFs in the transmission session, while $\Gamma_l(b)$ denotes the IF transmitted by User l during the b^{th} BP. Accordingly, the processes occurring at User l during Mk_2 CPs of a transmission session are represented by an algorithm having Mk_2 iterations, each of which is accomplished by conducting the following four sequences;

Sequence 1: Construct a modified transfer matrix \mathbf{G}' for all transmissions to User l in the system. The guidance for formulating the modified transfer matrix \mathbf{G}' can be found in Section 4.2.2.

Sequence 2: Apply the principle of the frame recovery described in Section 4.3, in order to recover all detectable IFs of the $(M - 1)k_1$ IFs;

Sequence 3: Update the knowledge $Y_l(\Gamma_{IF})$ of User l about all the $(M - 1)k_1$ IFs;

Sequence 4: Build a subsequent PF required to transmit in subsequently assigned CP by using the current knowledge $Y_l(\Gamma_{IF})$ of User l .

In brief, once the *FD* mode is activated, a user in the system can exploit the benefits of network coding and of the broadcast nature of wireless communications by exploiting the PFs transmitted by the other users, in order to improve inter-user communications. The improved inter-user transmissions amongst the M users would result in an improved diversity gain for the system. More specifically, due to the broadcast nature of wireless communications, all users in the system are capable of listening to the PFs destined to the BS. Naturally, each of the M users has to be equipped with a network coding decoder for decoding the PFs with the aid of its own IFs and by additionally using the IFs successfully received from the other users during the BPs. As a benefit of the additional decoding process, each user becomes capable of compensating for not knowing the IFs transmitted from the other $(M - 1)$ users, which is caused by outage of inter-user channels during the BPs. Once a user successfully receives a PF, the result of the decoding process at this particular user will provide updated knowledge about the IFs transmitted by the other users. The updated knowledge is then exploited during subsequent PFs transmitted by the user.

5.1.2.3 The Adaptive modes, A_1 mode and A_2 mode

In general, channel coding and network coding may indeed be intrinsically further combined to improve the attainable system performance by adopting two options. The *first option* is that of implementing iterative decoding for exchanging extrinsic information between the channel code and network code. This idea has been studied in [187, 188] by performing iterative decoding with the aid of the PFs transmitted by a single relay, where network coding was performed. As a result, a significant performance improvement was recorded. However, extending the iterative decoding scheme of [187, 188] to the scenario, where multiple-relays/users¹ are taken into consideration, leads to an extremely high complexity. Hence it becomes impractical for such joint channel-network code design. This conclusion is also suggested by a recent contribution presented in [189]. Alternatively, the inter-operation of channel- and network-coding may be exploited to provide an improved performance, as suggested in [12].

The *second option* advocates introducing an adaptive mechanism, which relies on a feedback flag directly reflecting the performance of the network coding scheme. This feedback flag can be

¹In our scenario, each user itself plays the role of a relay. Hence, our the model has multiple-users and multiple-relays.

employed to control the channel coding scheme, and vice versa, the feedback flag provided by the channel coding scheme may be utilised for controlling the operation of network coding. The authors of [12] applied this adaptive flag-controlled mechanism under the idealised simplifying assumption of using an ideal/perfect channel code.

In our system, we have opted for further developing this adaptive feedback flag based solution for the proposed near-capacity channel code, where each users will transmit a changeable number of PFs. The changeable number of PFs is calculated from the feedback flags sent from the base station (BS). The feedback flags indicate successful/unsuccessful transmission of the Information Frames (IFs) received at the BS. Additionally, the multiplexing gain of NC1 can be increased by reducing the number of transmitted PFs, as suggested by the analysis in Section 4.11. In line with [12], we assume that the BS is capable of sending back to the users a modest amount of information containing feedback flags. Then, the reduced number of PFs can be calculated by making use of the successful/unsuccessful IF feedback flags sent from the BS. More specifically, let us denote the number of PFs transmitted by User j in a transmission session by $k_{2,j}$. It was suggested in [12] that in order to increase the achievable multiplexing gain, the value of $k_{2,j}$ has to be adaptively adjusted for each transmission session according to two potential approaches.

In the *first adaptive* (A_1) mode, the diversity gain remains unaltered, while the value of $k_{2,j}$ is adaptively adjusted as

$$k_{2,j} = \begin{cases} 0 & : \text{ If } \Delta = 1 \\ k_2 & : \text{ Otherwise} \end{cases}, \quad (5.57)$$

where the feedback flag Δ is an acknowledgement bit sent by the BS to indicate the successful/unsuccessful reception of all the Mk_1 IFs transmitted by all the M users during their BPs. The value of Δ obeys the following rule:

$$\Delta = \begin{cases} 1 & : \text{ If } Mk_1 \text{ IFs successfully decoded} \\ 0 & : \text{ Otherwise} \end{cases}. \quad (5.58)$$

In the *second adaptive* (A_2) mode, the minimum diversity order of $D_{NCMN} = (M + k_2)$ is guaranteed, while the value of $k_{2,j}$ is adaptively adjusted as

$$k_{2,j} = \begin{cases} 0 & : \text{ If } \prod_{j=1}^M \Lambda_j = 1 \\ 1 & : \text{ Else if } \Lambda_j = 1 \\ k_2 & : \text{ Otherwise} \end{cases}, \quad (5.59)$$

where the feedback flag Λ_j is an acknowledgement bit sent by the BS to indicate the successful/unsuccessful reception of all the k_1 IFs transmitted by User j during his/her BPs. The value of Λ_j can be specified as:

$$\Lambda_j = \begin{cases} 1 & : \text{ If } k_1 \text{ IFs successfully decoded} \\ 0 & : \text{ Otherwise} \end{cases}. \quad (5.60)$$

As a result of applying the adaptive feedback-flag based mechanism, the average adaptive network code rate $R_{info,Adaptive}$ representing the R_{info,A_1} and the R_{info,A_2} can be calculated by

$$\begin{aligned} R_{info,A} &= \frac{E[\text{Number of IFs transmitted per session}]}{E[\text{Number of all frames transmitted per session}]}, \\ &= \frac{Mk_1}{Mk_1 + E[\sum_{j=1}^M k_{2,j}]} . \end{aligned} \quad (5.61)$$

The value $E[\sum_{j=1}^M k_{2,j}]_{A_1}$ (or $E[\sum_{j=1}^M k_{2,j}]_{A_2}$), when the system is supported by the A_1 mode (or the A_2 mode), can be computed as [12]

$$E[\sum_{j=1}^M k_{2,j}]_{A_1} = Mk_2 \left(1 - (1 - P_e)^{Mk_1}\right) , \quad (5.62)$$

$$E[\sum_{j=1}^M k_{2,j}]_{A_2} = Mk_2 \left(1 - (1 - P_e)^{Mk_1}\right) - \frac{M(k_2 - 1)}{(1 - P_e)^{-k_1}} \left(1 - (1 - P_e)^{(M-1)k_1}\right) , \quad (5.63)$$

where the probability P_e represents the outage probability of a single link in our system. Accordingly, the average adaptive network code rate corresponding to the two adaptive modes, namely the A_1 mode and the A_2 mode, becomes:

$$\begin{aligned} R_{info,A_1} &= \frac{Mk_1}{Mk_1 + Mk_2 \left(1 - (1 - P_e)^{Mk_1}\right)}, \\ &= \frac{k_1}{k_1 + k_2 \left(1 - (1 - P_e)^{Mk_1}\right)} \end{aligned} \quad (5.64)$$

and

$$\begin{aligned} R_{info,A_2} &= \frac{Mk_1}{Mk_1 + Mk_2 \left(1 - (1 - P_e)^{Mk_1}\right) - \frac{M(k_2 - 1)}{(1 - P_e)^{-k_1}} \left(1 - (1 - P_e)^{(M-1)k_1}\right)}, \\ &= \frac{k_1}{k_1 + k_2 \left(1 - (1 - P_e)^{Mk_1}\right) - \frac{(k_2 - 1)}{(1 - P_e)^{-k_1}} \left(1 - (1 - P_e)^{(M-1)k_1}\right)}. \end{aligned} \quad (5.65)$$

As a result of having improved average network code rates, namely the R_{info,A_1} and the R_{info,A_2} , we accordingly have the associated average multiplexing gain as:

$$\begin{aligned} \Omega_2 &= \frac{R_{info,A_2}}{R_{info}}, \\ &= \frac{k_1 + k_2}{k_1 + k_2 \left(1 - (1 - P_e)^{Mk_1}\right) - (1 - P_e)^{k_1} (k_2 - 1) \left(1 - (1 - P_e)^{(M-1)k_1}\right)} , \end{aligned} \quad (5.66)$$

where R_{info} is the network coding rate in the C mode given in Equation (4.68)

$$R_{info} = \frac{k_1}{k_1 + k_2} . \quad (5.67)$$

Additionally, we can infer from Equation (5.64) and Equation (5.65) that the average network coding rate R_{info,A_1} and R_{info,A_2} increase when the outage probability P_e decrease. Since we have

the outage probability $1 \geq P_e \geq 0$, the adaptive network coding rate formulated in Equation (5.64) and in Equation (5.65) can reach its maximum value, when the outage probability becomes zero $P_e = 0$. Thus, we have:

$$\begin{aligned} \text{Max} \{R_{info,A_1}\} &= R_{info,A_1}|_{P_e=0}, \\ &= 1 \end{aligned} \quad (5.68)$$

and

$$\begin{aligned} \text{Max} \{R_{info,A_2}\} &= R_{info,A_2}|_{P_e=0}, \\ &= 1. \end{aligned} \quad (5.69)$$

Having the average adaptive network coding rate reached its maximum value of 1 corresponds to the scenario where PFs are no longer required to be transmitted to the BS, provided that a sufficiently high SNR value is experienced by our system.

5.1.3 Network Coding 2

In order to enhance the reliability of our system, NC2 may be activated in order to form the triple-layer coding architecture depicted in Figure 5.1. In the NC2 layer, a random network code [42] is applied across the H IFs, namely across I_1, \dots, I_H , in order to generate the Θ network-coded frames of Z_1, \dots, Z_Θ , where $\Theta \geq H$. As a result, a linear combination of the H IFs having a length of N bits each forms a network-coded frame Z_j , $Z_j = \sum_{i=1}^H \alpha_{ij} I_i$, where scalars α_{ij} ($i \in [1, \dots, H]$ and $j \in [1, \dots, \Theta]$) may be chosen randomly and uniformly from a $GF(2^q)$. If the $GF(2^q)$ is sufficiently large, the expected number of successfully received frames required by the BS for successfully decoding the H IFs is approximately H [42, 191]. Thereafter, we assume that the reception of H network-coded frames at the BS is sufficient for the BS to recover H corresponding IFs. Accordingly, we define the conventional information rate of NC2 as:

$$R_{info2} = \frac{H}{\Theta}. \quad (5.70)$$

Bearing in mind the channel code rate R_c defined in Section 2.2.1 and the network code rate R_{info} of Equation (5.67), we can define the aggregate code rate of the GNCMN system as:

$$R_{GNCMN} = R \times R_{info} \times R_{info2}. \quad (5.71)$$

Once NC2 is activated in our system, the reception of H coded frames at the BS is sufficient for it to recover H IFs. Hence, an outage is declared, when the number of frames received at the BS is less than H , and this outage occurs with the probability of:

$$P_o^{NC2} = \sum_{i=0}^{H-1} \binom{\Theta}{i} (1 - P_o)^i P_o^{\Theta-i}, \quad (5.72)$$

where P_o is the outage probability of the system when NC2 is not in operation.

5.1.4 Parameters of the General Near-Capacity Multi-user Network-coding systems

For sake of readability, we summary the explanations for all the parameters of the GNCMN system in Table 5.1. It should be noted that the parameters belonging to the channel coding layer are identical to those listed in Table 4.1.

Accordingly, the values of the parameters described in Table 5.1 are listed in Table 5.2. Then, the different values of the parameters in Table 5.2 are employed for configuring different GNCMN systems investigated in the subsequent sections of this chapter.

5.2 Performance Bounds in the Full Diversity Mode and the Adaptive Modes

This section is dedicated for deriving the performance bounds associated with newly introduced modes, namely the *FD* mode presented in Section 5.1.2.2, the A_1 mode and the A_2 mode detailed in Section 5.1.2.3.

5.2.1 Full Diversity Performance Bounds

Let us again use the notations defined in Section 4.5 for conveniently deriving the performance's bounds of the NC1 system employing the *FD* mode, as presented in Section 5.1.2.2. For the sake of readability, those notations detailed in Section 4.5 are repeated here.

Let $U_{m,t} = \{u_{m,t}, u_{m,t} \in [1, \dots, M]\}$ for $\forall m \in \{1, \dots, M\}$ be a set of user indices corresponding to the specific users that are able to correctly recover an information frame $I_m(t)$ transmitted from User m during time slot t . Note that User m itself is always included in this set. Let us call $||U_{m,t}||$ the number of members in the set of users $U_{m,t}$, which is also the number of users that are capable of correctly detecting the information frame $I_m(t)$, and it is always true that

$$1 \leq ||U_{m,t}|| \leq M, \quad (5.73)$$

where we use $||A||$ to represent the cardinality of the set A .

We then again define the complement set of $U_{m,t}$ as $U_{m,t}^* = \{1, \dots, M\} \setminus U_{m,t}$ that comprises the indices of those users that cannot correctly recover the information frame $I_m(t)$. Hence we have

$$||U_{m,t}^*|| = M - ||U_{m,t}||. \quad (5.74)$$

Let P_e be the error probability of a single link corresponding to a given *SNR*. Assuming that all the links/users in the network employ the same channel coding scheme, the probability that $U_{m,t}^*$ users cannot recover the information frame $I_m(t)$ is approximately $P_e^{||U_{m,t}^*||}$, which is accurate at the high *SNR* region.

Parameters	Description
Layer	Channel Coding
R [BPS]	Information rate calculated in Bit Per Symbol (BPS) for all the links in the system and mentioned in Section 2.1
R_c	Code rate of IrCC encoder described in Section 2.3
K [iteration]	The number of inner iterations described in Section 2.3
J [iteration]	The number of outer iterations described in Section 2.3
N [bit]	The number of information bits in a frame
N_{sub} [bit]	The number of sub-frame in a transmitted frame, when activating the sub-frame transmission, which is detailed in Section 2.4
Layer	NC1
Operation mode	Operation modes of the NC1 comprise single modes, namely the C , FD , A_1 and A_2 modes. These single modes may be combined for forming the combined modes, namely the $FD + A_1$ and $FD + A_2$ modes, as detailed in Section 5.1.2
M [user]	The number of users supported by the NC1 layer, as defined in Section 4.2
k_1 [frame]	The number of IFs transmitted by each of M users during broadcast phases within a transmission session, as stipulated in Section 4.2.1 and Section 5.1.2
k_2 [frame]	The number of PFs transmitted by each of M users during cooperative phases within a transmission session, as stipulated in Section 4.2.1 and Section 5.1.2
\mathbf{G}	Original transfer matrix corresponding to the case where all the frames transmitted within a transmission session are successfully decoded. The details pertaining to the matrix \mathbf{G} are presented in Section 4.2.2 and Section 5.1.2
R_{info} [BPS]	The network-coding's information rate defined by Equation (4.68)
R_{NCMN} [BPS]	The system's overall information rate defined by Equation (4.67)
D_{NCMN}	Diversity order of the system determined by Equation (4.64)
Layer	NC2
H	The number of IFs at the input of the NC2, as mentioned in Section 5.1.3
Θ	The number of IFs at the output of the NC2, as mentioned in Section 5.1.3
R_{info2}	The coding rate of the NC2, which is defined by Equation (5.70)

Table 5.1: The descriptions of parameters employed in the General Near-Capacity Multi-user Network-coding system depicted in Figure 5.1.

Parameters	Channel Coding layer	
	Coherent	Non-coherent
R [BPS]	1.5(8PSK), 1.0(QPSK), 0.5(BPSK)	1.0(DQPSK), 0.5(DBPSK)
R_c	0.5	0.5
K [iteration]	0	2
J [iteration]	30	30
N [bit]	$10^6, 10^5$	10^6
N_{sub} [bit]	$1, 10, 10^1, 10^2, 10^3$	$1, 10, 10^1, 10^2, 10^3$
Parameters	NC1 layer	
Mode	$C, FD, A_1, A_2, FD + A_1, FD + A_2$	
\mathbf{G}	$\mathbf{G}_{2 \times 4}, \mathbf{G}_{4 \times 8}, \mathbf{G}_{6 \times 12}$	
M [user]	2	
k_1 [frame]	1($\mathbf{G}_{2 \times 4}$), 2($\mathbf{G}_{4 \times 8}$), 3($\mathbf{G}_{6 \times 12}$)	
k_2 [frame]	1($\mathbf{G}_{2 \times 4}$), 2($\mathbf{G}_{4 \times 8}$), 3($\mathbf{G}_{6 \times 12}$)	
R_{info}	0.5	
D_{NCMN}	$D_{2 \times 4} = 3, 4 \leq D_{4 \times 8} \leq 5, 5 \leq D_{6 \times 12} \leq 7$	
Parameters	NC2 layer	
H	10	
Θ	20	
R_{info2}	1/2	

Table 5.2: The parameters of the GNCMN system portrayed in Figure 5.1. The parameters comprise three groups representing the three layers, namely the CC layer, the NC1 layer and the NC2 layer.

Let us call $U_{m,t}(I)$ as the set of all IFs transmitted by the users in $U_{m,t}$ during the broadcast phases, including $I_m(t)$. Since each user broadcasts k_1 number of frames, we have:

$$||U_{m,t}(I)|| = k_1 ||U_{m,t}||. \quad (5.75)$$

There are at least $||U_{m,t}(I)|| + ||U_{m,t}||k_2$ packets [47, 179], which contain the information packets transmitted by all the users of $U_{m,t}$, where the $||U_{m,t}(I)||$ information packets are transmitted during the broadcast phases, while the $||U_{m,t}||k_2$ parity packets are transmitted during the cooperative phases.

It should be noted that due to the employment of the network coding by each user, the outage of inter-channel transmission during broadcast phases is compensated, as demonstrated by the numerical example in Section 5.1.2.2. As a result of the compensation, we can consider that the equivalent number $||U_{m,t}^{FD}||$ of users that can correctly recover the information frame $I_m(t)$ is greater than or

equal to the actual number $||U_{m,t}||$. Thus, we have:

$$||U_{m,t}^{FD}|| \geq ||U_{m,t}||, \quad (5.76)$$

$$||U_{m,t}^{*,FD}|| = M - ||U_{m,t}^{FD}||, \quad (5.77)$$

$$||U_{m,t}^{FD}(I)|| = k_1 ||U_{m,t}^{FD}||, \quad (5.78)$$

where $||U_{m,t}^{FD}(I)||$ is the equivalent set of all IFs transmitted by the users in $U_{m,t}^{FD}$, while $||U_{m,t}^{*,FD}||$ is the complement set of $||U_{m,t}^{FD}||$. Accordingly, an outage for the information packet $I_m(t)$ is declared when the direct transmission $I_m(t)$ and at least $||U_{m,t}^{FD}||k_2$ out of the remaining $||U_{m,t}^{FD}(I)|| - 1 + ||U_{m,t}^{FD}||k_2$ received packets are in outage, which occurs with a probability given by

$$P_{o,m}^{FD}(U_{m,t}^{*,FD}) = P_e \left[\frac{\sum_{i=0}^{||U_{m,t}^{FD}(I)||-1} (||U_{m,t}^{FD}(I)||-1+||U_{m,t}^{FD}||k_2) P_e^{||U_{m,t}^{FD}||k_2+i}}{||U_{m,t}^{FD}||k_2+i} \right], \quad (5.79)$$

It is suggested by [46,47,179,183] that there might be more than $(k_1||U_{m,t}^{FD}|| + k_2||U_{m,t}^{FD}||)$ frames, which contain the IFs transmitted by all users of the set $U_{m,t}^{FD}$. If we take into consideration the availability of those extra frames, the actual outage probability $P_{o,m}^{FD,Ac}(U_{m,t}^{*,FD})$ for the information frame $I_m(t)$ has to satisfy

$$P_{o,m}^{FD,Ac}(U_{m,t}^{*,FD}) \leq P_{o,m}^{FD}(U_{m,t}^{*,FD}). \quad (5.80)$$

Note that $P_{o,m}^{FD,Ac}(U_{m,t}^{*,FD})$ is the outage probability for a given value of $U_{m,t}^{*,FD}$. The system's total outage probability P_o^{FD} for all possible sets of $U_{m,t}^{*,FD}$ can be computed by

$$P_o^{FD} = \sum_{||U_{m,t}^{*,FD}||=0}^{M-1} \frac{P_e^{||U_{m,t}^{*,FD}||}}{(1 - P_e)^{||U_{m,t}^{*,FD}||-M+1}} P_{o,m}^{Ac}(U_{m,t}^{*,FD}). \quad (5.81)$$

Bearing in mind the equations of (5.76),(5.77) and (5.78), we can follow the manner conducted in Section 4.5, in order to come up with the upper bound as:

$$P_o^{FD} < \underbrace{\Omega + \binom{E+F}{F} P_e^{M+k_2} M_u^{\max} \frac{1 - R_o^M}{1 - R_o}}_{=P_o^{Upper,FD}}, \quad (5.82)$$

where we define $P_o^{Upper,FD}$ as the strict upper bound of the system's outage probability P_o^{FD} . The lower bound is specified by

$$P_o^{FD} > \underbrace{\binom{E+F}{F} P_e^{F+1} \frac{M_l^{\min}}{(1 - P_e)^{1-M}}}_{=P_o^{Lower,FD}}, \quad (5.83)$$

where we define $P_o^{Lower,FD}$ as the strict lower bound of P_o^{FD} . Note that we have:

$$P_o^{Upper,FD} = P_o^{Upper}, \quad (5.84)$$

$$P_o^{Lower,FD} = P_o^{Lower}, \quad (5.85)$$

where P_o^{Upper} and P_o^{Lower} are upper and lower bounds of the system's performance in the conventional mode, which are previously derived in Section 4.5. It should be noted that the outage probability corresponding to the maximum (minimum) diversity order of Equation (4.66) is employed for deriving the upper (lower) bound associated with the C mode and FD mode.

5.2.2 Adaptive System's Performance Bounds

This section is to present two approaches used for estimating the performance bounds of the system relying on the adaptive mechanism described in Section 5.1.2.3.

5.2.2.1 Adaptive Mode 1

It can be readily inferred from Equation (5.57) and Equation (5.58) that invoking the A_1 mode has no influence on the results of the detection process conducted at the BS. This is because none of PFs are transmitted when the BS already recovered all the IFs. As a result, with a given SNR value, the FER -versus- SNR performance of the systems remains unchanged when the A_1 mode is applied. This means that if a specific value of FER is given, the corresponding SNR values of $SNR|_{FER}$ and $SNR_{A_1|FER}$ on the FER -versus- SNR performance must comply with:

$$SNR|_{FER} = SNR_{A_1|FER}. \quad (5.86)$$

Let us then define $\Omega_{1|FER}$ as the multiplexing gain at an FER value when employing the A_1 mode. Naturally, the value of $\Omega_{1|FER}$ is shown by the difference between two values, namely $E_b/N_{0|FER}$ and $E_b/N_{0,A_1|FER}$, on the the FER -versus- E_b/N_0 performance curves corresponding to the C mode and the A_1 mode, which may be represented by

$$\begin{aligned} \Omega_1 &= \frac{E_b/N_{0|FER}}{E_b/N_{0,A_1|FER}}, \\ &= \frac{SNR|_{FER}}{\frac{R_{GNCMN}}{R_{GNCMN,A_1}}}, \end{aligned} \quad (5.87)$$

where R_{GNCMN} and R_{GNCMN,A_1} are the GNCMN system's code rates associated with the C mode and A_1 mode, respectively. Upon replacing Equation (5.71) and Equation (5.86) into Equation (5.87), we yield

$$\begin{aligned} \Omega_1 &= \frac{R_{GNCMN,A_1}}{R_{GNCMN}}, \\ &= \frac{R_{info2}R_{info,A_1}R}{R_{info2}R_{info}R}, \\ &= \frac{R_{info,A_1}}{R_{info}}. \end{aligned} \quad (5.88)$$

Additionally, by substituting R_{info} of Equation (5.15) and R_{info,A_1} of Equation (5.64) into Equation (5.88), we obtain the formula for calculating the multiplexing gain Ω_1 associated with the A_1

mode as

$$\begin{aligned}\Omega_1 &= \frac{R_{info,A_1}}{R_{info}}, \\ &= \frac{k_1 + k_2}{k_1 + k_2 \left(1 - (1 - P_e)^{Mk_1}\right)},\end{aligned}\quad (5.89)$$

As a benefit of Equation (5.86), we can formulate the performance bounds of the system operating in the A_1 mode by adding the multiplexing gain into the performance bounds of the conventional system, which are given in Equation (4.55) and Equation (4.63). Accordingly, the performance bounds of the system when activating the A_1 mode may be represented by

$$\Omega_1 P_o^{Lower} < P_o^{A_1} < \Omega_1 P_o^{Upper}, \quad (5.90)$$

where $P_o^{A_1}$ is the outage probability of the system employing the A_1 mode, while P_o^{Upper} and P_o^{Lower} is defined in Equation (4.55) and Equation (4.63), respectively.

5.2.2.2 Adaptive Mode 2

In contrast to the A_1 mode, it is suggested by Equation (5.59) and Equation (5.60) that upon introducing 0,1 or k_2 PFs, an increased multiplexing gain can be achieved at the cost of a decreased diversity gain. As a result of the decreased diversity gain, the condition given in Equation (5.86) is no more satisfied, thus the manner used for deriving the performance bounds associated with the A_1 mode cannot be utilised for formulating the performance bounds of the system operating in the A_2 mode. For the sake of brevity, we summarise the derivations in the following, while the details of the derivations are presented in Appendix C.

Bearing in mind the definitions and notations relating to Equation (5.73), Equation (5.74) and Equation (5.75). Let us additionally define $D_{m,t} = \{d_{m,t}, d_{m,t} \in [1, \dots, ||U_{m,t}|| - 1]\}$ as a set of user indices belonging to $U_{m,t}$ except for User m , provided that all the IFs transmitted by all users of $D_{m,t}$ have been successfully recovered by the BS by the end of BPs. Bearing Equation (5.59) and Equation (5.60) in mind, there are at least Γ frames containing the IF transmitted by all the users of $U_{m,t}$, where the value of Γ is specified by:

$$\Gamma = ||U_{m,t}|| (k_1 + k_2) + (1 - k_2) ||D_{m,t}||. \quad (5.91)$$

Accordingly, the outage probability for the information frame $I_m(t)$ may be calculated as:

$$P_m^{A_2}(U_{m,t}^*) = \sum_{i=0}^O \frac{\binom{O+S-||D_{m,t}||k_2+||D_{m,t}||}{S-||D_{m,t}||k_2+||D_{m,t}||+i}}{P_e^{-S-i-1} (1 - P_e)^{i-O}}, \quad (5.92)$$

where we define $O = ||U_{m,t}||k_1 - 1$ and $S = ||U_{m,t}||k_2$.

Having $||U_{m,t}|| - ||D_{m,t}|| \geq 1$ [12] would lead to an approximation of Γ , which would approximate $P_m^{A_2}(U_{m,t}^*)$ given by Equation (C.7) as:

$$P_m^{A_2}(U_{m,t}^*) \geq \overbrace{\sum_{i=0}^O \frac{\binom{O+S}{S+i} P_e^{O+i+1}}{(1-P_e)^{i+1-S}}}^{=P_m^{A_2,S}(U_{m,t}^*)} \quad (5.93)$$

$$P_m^{A_2}(U_{m,t}^*) \leq \sum_{i=0}^O \frac{P_e^{O+i+1}}{(1-P_e)^{O-i}} \cdot \underbrace{\left[\binom{O+k_2+\|U_{m,t}\|-1}{k_2+\|U_{m,t}\|-1+i} \right]^{-1}}_{=P_m^{A_2,G}(U_{m,t}^*)} \quad (5.94)$$

However, there might be more than Γ frames [46,47,99,179], which contain the IFs transmitted by all users of $U_{m,t}$. If the availability of those extra frames is taken into account, we will have

$$P_m^{A_2,Ac}(U_{m,t}^*) \leq P_m^{A_2}(U_{m,t}^*) \quad (5.95)$$

where $P_m^{A_2,Ac}(U_{m,t}^*)$ is the actual probability of the outage for the information frame $I_m(t)$. Notably, $P_m^{A_2,Ac}(U_{m,t}^*)$ is the outage probability for a given $U_{m,t}^*$. The system's outage probability for all possible $U_{m,t}^*$ can be calculated by

$$P^{A_2} = \sum_{\|U_{m,t}^*\|=0}^{M-1} \frac{P_e^{\|U_{m,t}^*\|} P_m^{A_2,Ac}(U_{m,t}^*)}{(1-P_e)^{\|U_{m,t}^*\|-M+1}} \quad (5.96)$$

By focusing our attention on the region corresponding to a low P_e or small $\|U_{m,t}^*\|$, Inequality (5.93) can be further approximated as

$$P^{A_2} > \underbrace{P^{A_2}|_{\|U_{m,t}^*\|=0}}_{=(1-P_e)^{M-1} P_m^{A_2,S}(U_{m,t}^*)|_{\|U_{m,t}^*\|=0}} \quad (5.97)$$

when we take into account that $P_m^{A_2,Ac}(U_{m,t}^*)|_{\|U_{m,t}^*\|=0} = P_m^{A_2,S}(U_{m,t}^*)|_{\|U_{m,t}^*\|=0}$. Additionally, upon substituting Inequality (5.94) and Inequality (5.95) into Equation (5.96), a further approximation can be derived as:

$$P^{A_2} \leq \sum_{\|U_{m,t}^*\|=0}^{M-1} \frac{P_e^{\|U_{m,t}^*\|} P_m^{A_2,G}(U_{m,t}^*)}{(1-P_e)^{\|U_{m,t}^*\|-M+1}} \quad (5.98)$$

Then, following a number of further steps commencing from Inequality (5.97) and Inequality (5.98), we arrive at:

$$P^{A_2,L} < P^{A_2} < P^{A_2,U} \quad (5.99)$$

where $P^{A_2,L}$ is given by:

$$P^{A_2,L} = P_o^{C,Lower} \quad (5.100)$$

while $P^{A_2,U}$ is calculated by:

$$P^{A_2,U} = \frac{\frac{P_e^K(1-P_e)}{1-P_e-\frac{O}{K}P_e}}{\left[\binom{k_1+k_2-1}{k_2} - \binom{O-1+K}{K-1} \right]^{-1}} + \frac{\frac{P_e^K(1-P_e)}{1-P_e-\frac{O}{K}P_e} \left[\frac{(R_{o,A_2})^{M-1}}{R_{o,A_2}-1} \right]}{\left[\binom{O+K-1}{K-1} \right]^{-1}} \quad (5.101)$$

where we have $R_{o,A_2} = 1 - P_e$ and $K = k_2 + M$.

Notably, the system's performance is also affected by the multiplexing gain Ω_2 . Similar to the definition of the multiplexing gain Ω_1 , we can define the multiplexing gain Ω_2 as:

$$\Omega_2 = \frac{R_{info,A_2}}{R_{info}}. \quad (5.102)$$

Since the average network-coding rate R_{info,A_2} associated with the A_2 mode is given by Equation (5.65) as

$$R_{info,A_2} = \frac{k_1}{k_1 + k_2 \left(1 - (1 - P_e)^{Mk_1}\right) - \frac{(k_2-1)}{(1-P_e)^{-k_1}} \left(1 - (1 - P_e)^{(M-1)k_1}\right)}, \quad (5.103)$$

we arrive at the multiplexing gain Ω_2 as:

$$\Omega_2 = \frac{k_1 + k_2}{k_1 + \frac{k_2}{[1 - (1 - P_e)^{Mk_1}]^{-1}} - \frac{(k_2-1)(1-P_e)^{k_1}}{[1 - (1 - P_e)^{(M-1)k_1}]^{-1}}}. \quad (5.104)$$

Then, the bounds of the system's performance reflecting both the achievable diversity gain and multiplexing gain can be represented by

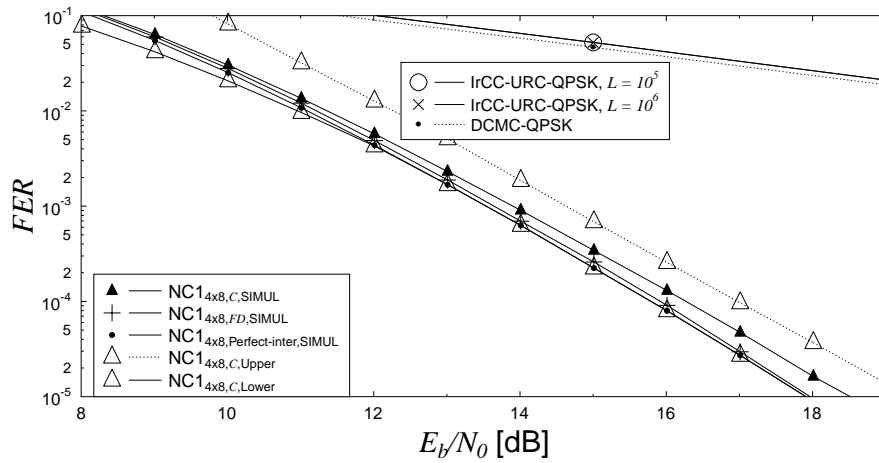
$$\underbrace{\Omega_2 P^{A_2,L}}_{=P_o^{A_2,Lower}} < \underbrace{\Omega_2 P^{A_2}}_{=P_o^{A_2}} < \underbrace{\Omega_2 P^{A_2,U}}_{=P_o^{A_2,Upper}} \quad (5.105)$$

where $P_o^{A_2}$ is the system's outage probability when A_2 is activated, while $P_o^{A_2,Lower}$ and $P_o^{A_2,Upper}$ are the corresponding lower and upper bounds of $P_o^{A_2}$, respectively. Finally, the probability $P^{A_2,L}$ and $P^{A_2,U}$ are given in Equation (5.100) and Equation (5.101), respectively.

5.2.3 The Bounds and Monte-Carlo based Performance

In this section, the bound of the system's performance derived in Section 5.2.1 and Section 5.2.2 are compared to the corresponding system's performance obtained by running Monte-Carlo simulations. Let us demonstrate our findings by studying the system employing $G_{4 \times 8}$ in the NC1 and relying on the coherent IrCC-URC-QPSK scheme in the CC layer. The sub-frame transmission having $N_{sub} = 1$ is activated for this comparison.

As seen in Figure 5.3a, the performance curve associated with the FD mode outperforms that associated with the C mode. The performance curve corresponding to the perfect inter-user transmission (Perfect-inter as denoted in Figure 5.3a) substantiates the analysis in Section 5.1.2.2 and Section 5.2.1. More specifically, the performance of the perfect inter-user transmission sets the limit for the performance of the system advocating the FD mode. Additionally, the lower performance bound for both performance of the system supported by either the C mode or the FD mode is established by approximating the outage probability in the perfect inter-user scenario, thus the upper bound of the system performance in both the C mode and the FD mode duly coincide to the performance of the system ideally having inter-user transmissions error-free, as manifested in



(a) The C and FD modes

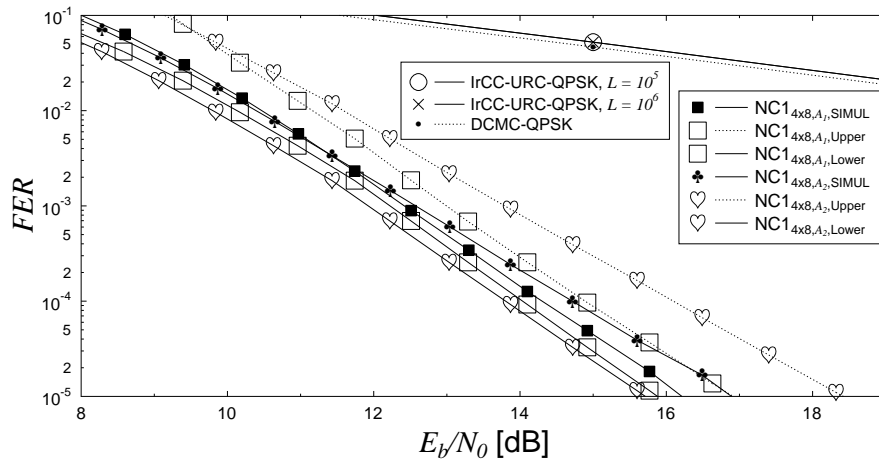
(b) The A₁ and A₂ modes

Figure 5.3: The performance bounds and the corresponding FER performance obtained by Monte-Carlo simulations for the GNCMN system relying on two layers of NC1 and CC, when considering the system employing the matrix $\mathbf{G}_{4 \times 8}$ in the NC1 and relying on the IrCC-URC-QPSK scheme in the CC layer, while NC2 is not. The sub-frame transmission is activated by choosing $N_{sub} = 1$. Both the block Rayleigh fading and the fast Rayleigh fading are considered, when a frame is transmitted in the $N_{sub} = 1$ subframe regime over the wireless channel.

Figure 5.3a. Importantly, the derivation of the performance bounds in Section 5.2.1 is verified by the performance curves pertaining to the C mode and the FD mode in Figure 5.3a.

As regards to the performance bounds associated with the A_1 mode and the A_2 mode, it can be seen in Figure 5.3b that the curves representing the system's performance obtained by simulations locate within their upper and lower bounds. This substantiates the derivation of the performance bounds for the A_1 and A_2 modes, as detailed in Section 5.2.2.1 and Section 5.2.2.1, respectively.

As regards to the benefit of utilising the single modes, namely the FD mode, the A_1 mode and the A_2 mode, as listed in Table 5.2, in comparison to the C mode, it is suggested by Figure 5.3 that the order of the better performance is the one associated with the C mode, the FD mode, the A_2 mode and the A_1 mode, respectively. It is also shown in Figure 5.3b that the performance of the system operating in the A_1 mode is superior to that of the system operating in the A_2 . The details regarding the advantageous performance of A_1 in comparison to the A_2 mode is further detailed in Section 5.3.

5.3 Multiplexing and Diversity Enhancement in the Network Coding 1

5.3.1 Diversity Gain in Full Diversity Mode

In the conventional scheme of [47,99] as detailed in Section 5.1.2.1, the inter-user communications only take place during the BPs. By contrast, as illustrated by a specific example in Section 5.1.2.2 for the FD mode, a user may exploit the benefits of network coding and of the broadcast nature of wireless communications during both the BPs and CPs. Explicitly, the PFs transmitted during the CPs can be additionally detected by the other users, in order to improve the inter-user communications. The improved inter-user transmissions amongst the M users would result in an improved diversity gain for the system. More specifically, due to the broadcast nature of wireless communications, all users in the system are capable of listening to the PFs destined to the BS. Naturally, each of the M users has to be equipped with a network coding decoder for decoding the PFs with the aid of its own IFs and by additionally using the IFs successfully received from the other users during the BPs. As a benefit of the additional decoding process, each user becomes capable of compensating for not knowing the IFs transmitted from the other $(M - 1)$ users, which is caused by outage of inter-user channels during the BPs.

Moreover, in the C mode, the system is potentially capable of approaching the full diversity, and this is reflected by the formula of Inequality (4.64) as:

$$M + k_2 \leq D \leq Mk_2 + 1. \quad (5.106)$$

However, achieving the maximum diversity order of $D = Mk_2 + 1$ is not guaranteed in all scenarios. Thus, the FD mode is employed for broadening scenarios, where the maximum diversity order

is achieved. These scenarios are corresponding to having a full knowledge of the IFs transmitted by the other users at the user under consideration. Therefore, having a full knowledge of the IFs of all the other users is the best scenario created by the *FD* mode. This best scenario is equivalent to the case, where all of the inter-user transmissions carried out during the BPs are successful. If this condition holds, our system always achieves its maximum diversity order given in [11] as:

$$D_{NCMN}^{Max} = Mk_2 + 1. \quad (5.107)$$

Hence, the system's performance associated with the idealised simplifying assumption of having perfect inter-user channels, where the inter-user channels are error free, sets a limit for the maximum attainable diversity gain of the near-full-diversity process.

5.3.2 Multiplexing and Diversity Gains from the Adaptive Mechanism

5.3.2.1 Maximum Adaptive Rate in Network Coding 1

Let us continue to consider the adaptive network code rate $R_{info,A}$ (either R_{info,A_1} given in Equation (5.64) or R_{info,A_2} formulated in Equation (5.64) may be calculated by

$$\begin{aligned} R_{info,A} &= \frac{E[\text{Number of IFs/session}]}{E[\text{Number of frames/session}]}, \\ &= \frac{Mk_1}{Mk_1 + E[\sum_{j=1}^M k_{2,j}]}. \end{aligned} \quad (5.108)$$

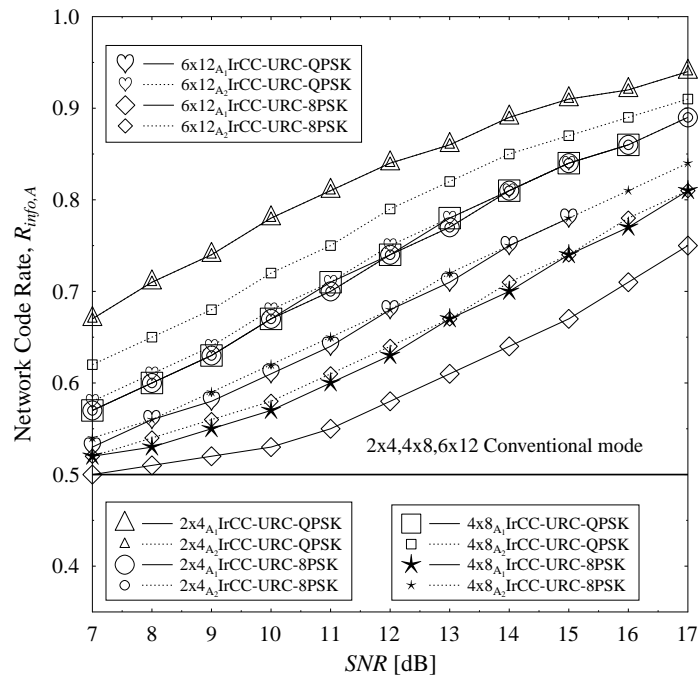
The value of the adaptive network coding rate $R_{info,A}$ given in Equation (5.108) increases when the *SNR* increases as seen in Figure 5.4. It can be also seen in Figure 5.4 that the A_2 mode can provide the improved network coding rate R_{info,A_2} in comparison to the R_{info,A_1} of the A_1 mode. Furthermore, we can infer from Equation (5.108) that the maximum value of the adaptive network coding rate can be calculated by:

$$\begin{aligned} \text{Max} \{R_{info,A}\} &= \text{Max} \left\{ \frac{Mk_1}{Mk_1 + E[\sum_{j=1}^M k_{2,j}]} \right\}, \\ &= 1, \end{aligned} \quad (5.109)$$

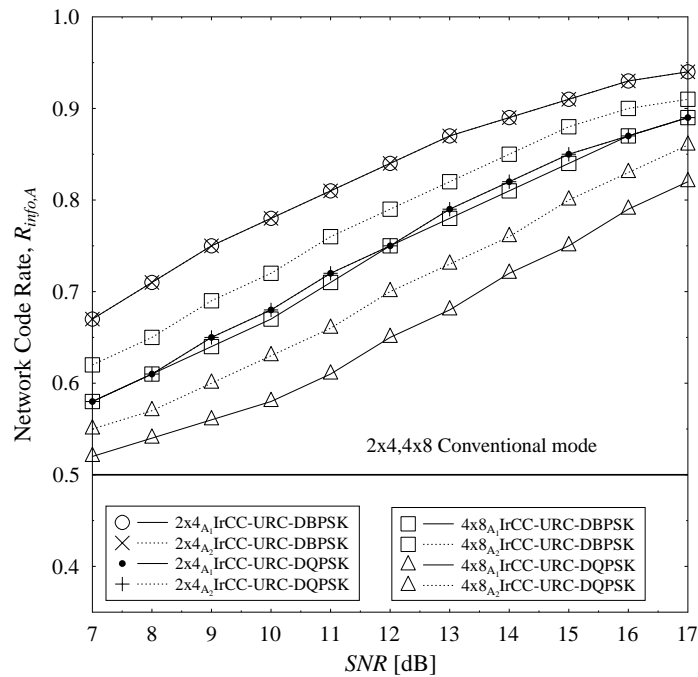
provided that the value of $E[\sum_{j=1}^M k_{2,j}]$ approaches zero. The condition of $E[\sum_{j=1}^M k_{2,j}] = 0$ would be satisfied, when PFs are no longer required to be transmitted to the BS, provided that a sufficiently high *SNR* value is experienced by our system.

5.3.2.2 Multiplexing Gain versus Diversity Gain in the Adaptive Network Coding

In order to investigate the relationship between the multiplexing aspect and the diversity aspect of our system, in this section we will first define in turn the multiplexing gain characterising the improved multiplexing of the system and then the diversity gain reflecting the improved diversity of the system. It should be noted that in order to have a fair comparison, the gains are compared in the same basis, for example *SNR* value of the system.



(a) Coherent IrCC-URC-MPSK schemes



(b) Non-coherent IrCC-URC-DMPK schemes.

Figure 5.4: Network coding rate $R_{info,A}$ of Equation (5.108) corresponding to various near-capacity schemes employed in the CC layer when the adaptive mechanism is applied in the NC1 layer relying on different transfer matrices, namely $\mathbf{G}_{2 \times 4}$, $\mathbf{G}_{4 \times 8}$ and $\mathbf{G}_{6 \times 12}$. Both the block Rayleigh fading and the fast Rayleigh fading are considered, when a frame is transmitted in the $N_{sub} = 1$ subframe regime over the wireless channel. The details of the systems are listed in Table 5.2.

Let us consider the multiplexing gains, namely Ω_1 of Equation (5.89) and Ω_2 of Equation (5.104), which can be repeated here as

$$\Omega_1 = \frac{k_1 + k_2}{k_1 + k_2 \left(1 - (1 - P_e)^{Mk_1}\right)}, \quad (5.110)$$

$$\Omega_2 = \frac{k_1 + k_2}{k_1 + \frac{k_2}{[1 - (1 - P_e)^{Mk_1}]^{-1}} - \frac{(k_2 - 1)(1 - P_e)^{k_1}}{[1 - (1 - P_e)^{(M-1)k_1}]^{-1}}}. \quad (5.111)$$

It can be readily seen in Equation (5.110) and Equation (5.111) that the values of Ω_1 and Ω_2 increase as the value of the single link outage probability P_e decreases, as a result of having increasing SNR value. When the value of P_e becomes vanishingly small due to benefiting from an extremely high SNR value, we have

$$\begin{aligned} \lim_{P_e \rightarrow 0} \Omega_1 &= \lim_{P_e \rightarrow 0} \left[\frac{k_1 + k_2}{k_1 + k_2 \left(1 - (1 - P_e)^{Mk_1}\right)} \right], \\ &= \frac{k_1 + k_2}{k_1}, \end{aligned} \quad (5.112)$$

and

$$\begin{aligned} \lim_{P_e \rightarrow 0} \Omega_2 &= \lim_{P_e \rightarrow 0} \left[\frac{k_1 + k_2}{k_1 + \frac{k_2}{[1 - (1 - P_e)^{Mk_1}]^{-1}} - \frac{(k_2 - 1)(1 - P_e)^{k_1}}{[1 - (1 - P_e)^{(M-1)k_1}]^{-1}}} \right], \\ &= \frac{k_1 + k_2}{k_1}, \end{aligned} \quad (5.113)$$

Accordingly, we define ϱ as the maximum value of the E_b/N_0 -improvement obtained by employing the adaptive feedback-flag based mechanism, which may be formulated as

$$\begin{aligned} \varrho &= \text{Max} \{10 \log (\Omega_1)\} [\text{dB}], \\ &= \text{Max} \{10 \log (\Omega_2)\} [\text{dB}], \\ &= 10 \log \left(\frac{k_1 + k_2}{k_1} \right) [\text{dB}]. \end{aligned} \quad (5.114)$$

If the matrix $G_{2 \times 4}$, the matrix $G_{4 \times 8}$ or the matrix $G_{6 \times 12}$ is used at the NC1, we have $k_1 = k_2 = 1$, $k_1 = k_2 = 2$ or $k_1 = k_2 = 3$, respectively, as listed in Table 5.2. As a result of replacing $k_1 = k_2 = 1$ or $k_1 = k_2 = 2$ or $k_1 = k_2 = 3$ into Equation (5.114), we may obtain the maximum value of the multiplexing gain as

$$\begin{aligned} \Omega_{1,2}^{\max} &= 10 \log \left(\frac{k_1 + k_2}{k_1} \right) [\text{dB}], \\ &= 3 [\text{dB}]. \end{aligned} \quad (5.115)$$

Hence, it is expected that the multiplexing gains, namely Ω_1 and Ω_2 , increasingly approaches the $\Omega_{1,2}^{\max} = 3$ dB, when increasing the SNR value applied in the GNCMN system employing the matrix $G_{2 \times 4}$, the matrix $G_{4 \times 8}$ or the matrix $G_{6 \times 12}$. As seen in Figure 5.5a presenting various gains

affecting the performance of the system relying on the IrCC-URC-QPSK scheme when activating the A_1 mode or the A_2 mode, both multiplexing gains, Ω_1 and Ω_2 increase along with the increase of the SNR value. The $\Omega_{1,2}^{\max} = 3$ dB sets an upper bound for both the multiplexing gains.

We deem that the diversity gain can be represented by changes in FER -versus- SNR performance of the system, when a new regime is employed in our system. The new regime can be the adaptive mechanism, the measure to approach the system's full-diversity or even a combination of the adaptive mechanism and the full-diversity measure. For example, when the adaptive mechanism is applied into our system, the changes in FER -performance of the system associating with a given SNR value reflects the effect of changing the number of PFs transmitted within transmission sessions on the FER -performance of the system. Furthermore, as analysed in Section 5.2.2.1 and Section 5.2.2.2, the attainable diversity gain may be characterised by the FER -versus- SNR performance of the system, when the adaptive mode is employed. More specifically, if either the A_1 or the A_2 mode is activated in our system, the attainable FER -performance of the system associated with a given SNR value directly reflects the effects of decreasing the number of PFs, as described in Equation (5.57)-Equation (5.60). Therefore, let us define the diversity gain Φ_1 and Φ_2 achieved in our system by applying the A_1 and A_2 mode, respectively:

$$\Phi_1 = SNR_C - SNR_{A_1}, \quad (5.116)$$

$$\Phi_2 = SNR_C - SNR_{A_2}, \quad (5.117)$$

where SNR_C , SNR_{A_1} and SNR_{A_2} denotes the SNR value required by the system using the C mode, A_1 mode and A_2 mode, respectively. It is worth noting that the SNR_C , SNR_{A_1} and SNR_{A_2} corresponding to a specific FER can be obtained with the aid of simulation results.

In the system supported by the A_1 mode, none of the PFs are transmitted, when the BS already recovered all the IFs, as detailed in Equation (5.57) and Equation (5.58). As a result, the FER -versus- SNR performance of the system remains unchanged at a given SNR value, when the A_1 mode is applied. Hence, the diversity gain Φ_1 corresponding to the system exploiting the A_1 mode is $\Phi_1 = 0$, as seen in Figure 5.5. Let us define the total-gain Σ_1 as the sum of the diversity gain and multiplexing gain in the case of employing the A_1 mode, which can be formulated as:

$$\Sigma_1 = \Omega_1 + \Phi_1, \quad (5.118)$$

where Ω_1 and Φ_1 are defined in Equation (5.110) and Equation (5.116), respectively. As a result of having a diversity gain of $\Phi_1 = 0$ for the A_1 mode, the total-gain Σ_1 is equal to the multiplexing gain Ω_1 , as also seen in Figure 5.5.

By contrast, introducing 0, 1 or k_2 PFs in the CPs of the A_2 mode detailed in Equation (5.59) and Equation (5.60) provides the improved multiplexing gain Ω_2 seen in Figure 5.5, which is also reflected by the network coding rate R_{info,A_2} plotted in Figure 5.4. As seen in Figure 5.5, although the system supported by the A_2 mode has the higher multiplexing gain Ω_2 , the overwhelming

degradation² of the related diversity gain Φ_2 results in an inferior total gain of Σ_2 , which is defined as:

$$\Sigma_2 = \Omega_2 + \Phi_2, \quad (5.119)$$

where Ω_2 and Φ_2 are defined in Equation (5.111) and Equation (5.117), respectively. Hence, it is expected that the system employing the A_1 mode outperforms the system invoking the A_2 mode in our investigations.

5.4 The Combined Modes in Network Coding 1

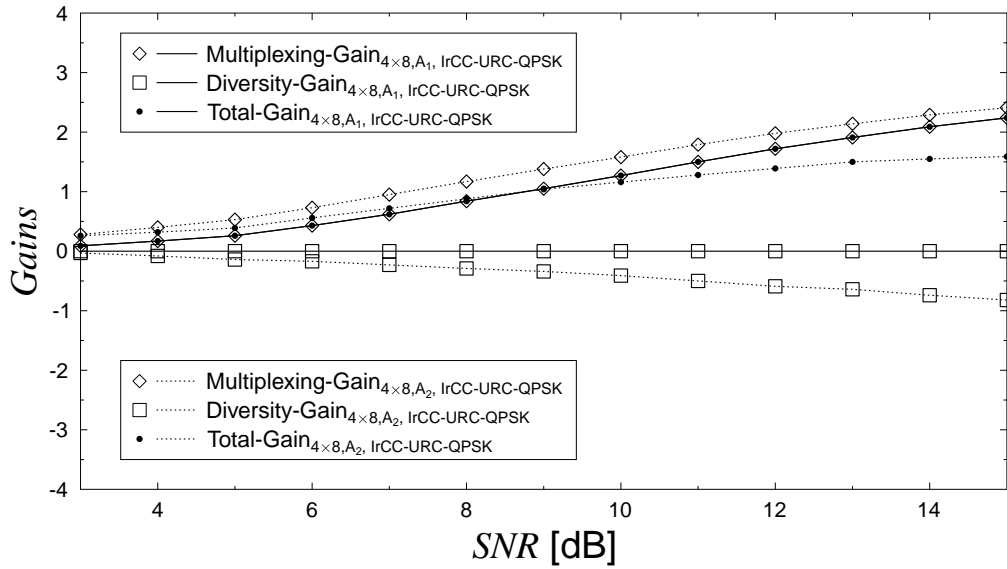
In order to study the benefit of employing the combined modes, namely the $(FD + A_1)$ mode and the $(FD + A_2)$ mode mentioned in Table 5.2, let us consider the GNCMN system comprising two layers, namely the CC layer and the NC1 layer. The parameters associated with the two layers are summarised in Table 5.2. Figure 5.6 and Figure 5.7 present our results related to a subset of the system parameters. More specifically, we consider the IrCC-URC-QPSK and IrCC-URC-8PSK coding schemes of Section 2.3.3 for the CC layer and employ the matrix $\mathbf{G}_{4 \times 8}$ and the $\mathbf{G}_{6 \times 12}$ of Section 4.7.2 in the NC1 layer.

As seen in Figure 5.6 and Figure 5.7, the FD mode helps to improve the system's performance in comparison to that of the system operating in the C mode. More specifically, as regards to the achievable diversity enhancement, the FER-performance curves of Figure 5.6 and Figure 5.7 substantiate the analysis provided both in Section 5.1.2.2 and in Section 5.3.1, demonstrating that the FER-performance of the system employing the FD mode is bounded by that of the idealised system relying on the idealised simplifying assumption of error-free inter-user channels, which is also referred to as the perfect inter-user scenario. The discrepancy is shown in Figure 5.6 and Figure 5.7 to be within 0.1 dB at an FER of 10^{-4} .

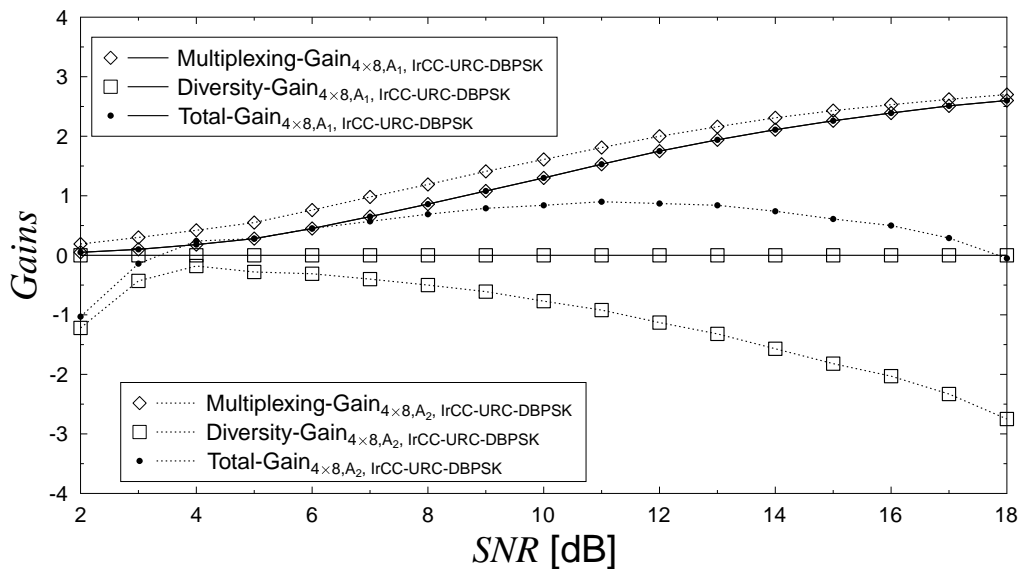
As regards to the achievable multiplexing gain analysed in Section 5.1.2.3 and Section 5.3.2, it is seen in Figure 5.6 and Figure 5.7 that the adaptive modes are capable of providing a significant E_b/N_0 -performance improvement in comparison to that of the system operating in the C mode. For instance, it is shown in Figure 5.6 that an average E_b/N_0 -performance improvement of 2.0 dB and 1.3 dB is recorded at an $FER = 10^{-4}$, when applying the A_1 mode and A_2 mode of the $\mathbf{G}_{4 \times 8}$ -based system, respectively. The attainable E_b/N_0 -improvement increases upon increasing the E_b/N_0 value and reaches its maximum of $\varrho = 10 \log(\frac{k_1+k_2}{k_1}) = 3$ dB, when the E_b/N_0 value becomes sufficiently high, as suggested by the analysis provided in Section 5.3.2.

As analysed in Section 5.3.2.2, although the less complex A_1 mode exhibits a lower multiplexing gain, it is capable of assisting the system in achieving a better FER performance than that of the system employing the A_2 mode, as seen in Figure 5.6 and Figure 5.7. This is because the

²The degradation in diversity gain Φ_2 is caused by introducing 0, 1 or k_2 PFs in the A_2 mode, rather than employing 0 or k_2 PFs in the A_1 mode as detailed in Equation (5.57)-Equation (5.60).



(a) Coherent IrCC-URC-QPSK scheme



(b) Non-coherent IrCC-URC-DBPSK scheme

Figure 5.5: The diversity-versus-multiplexing gain breakdown of the $G_{4 \times 8}$ based systems of Figure 5.1 relying the NC1 and CC layers, when considering both the A_1 mode and the A_2 mode at NC1 layer and activating the IrCC-URC-QPSK and IrCC-URC-DBPSK at the CC layer, as listed in Table 5.2. Both the block Rayleigh fading and the fast Rayleigh fading are considered, when a frame is transmitted in the $N_{sub} = 1$ subframe regime over the wireless channel. For the sake of brevity, the SNR-performance used for characterising the diversity gains in the A_1 and A_2 modes is presented in Section D.1.

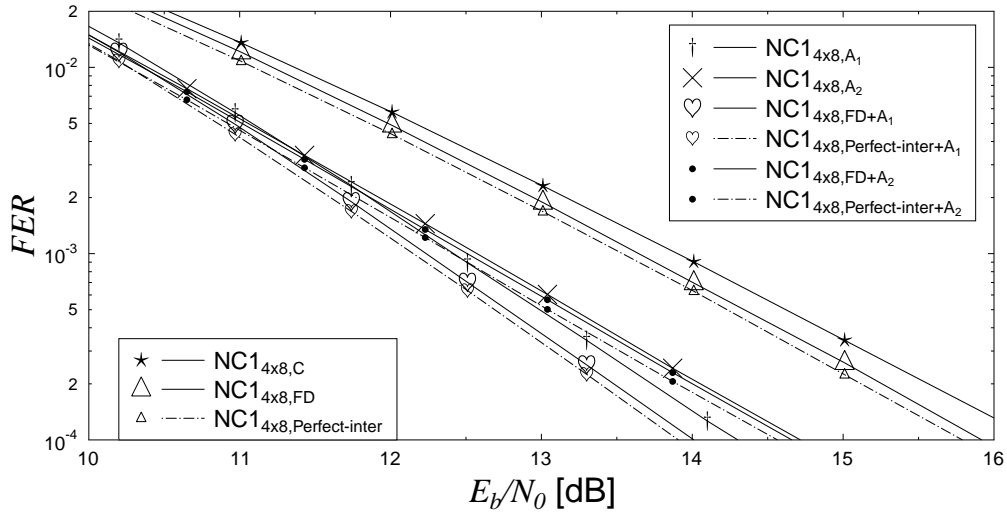
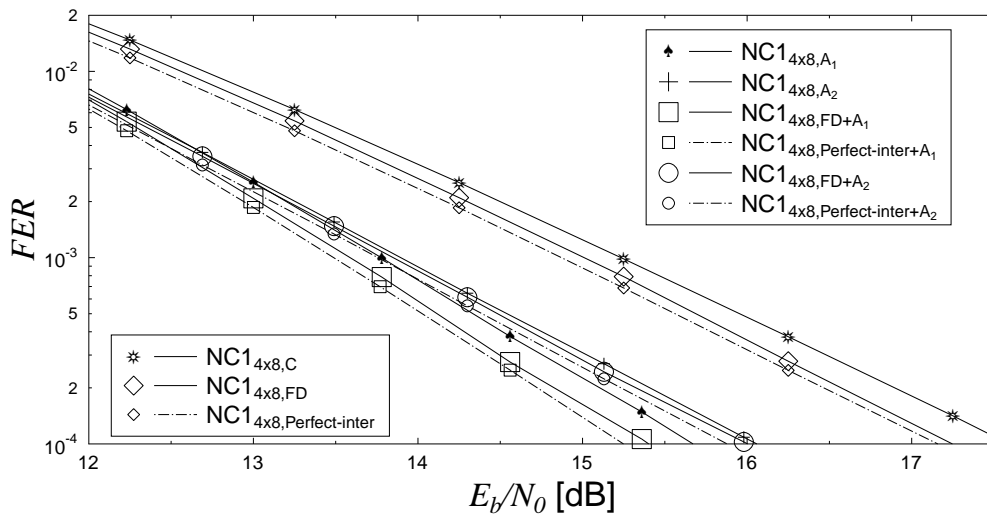
(a) $G_{4 \times 8}$, IrCC-URC-QPSK(b) $G_{4 \times 8}$, IrCC-URC-8PSK

Figure 5.6: FER performance of the system portrayed in Figure 5.1, relying on the NC1 and CC layers, where the $G_{4 \times 8}$ matrix is employed at the NC1 layer for operating in the full-diversity mode and adaptive mechanism, while the IrCC-URC-MPSK scheme is activated at the CC layer, as listed in Table 5.2. Both the block Rayleigh fading and the fast Rayleigh fading are considered, when a frame is transmitted in the $N_{sub} = 1$ subframe regime over the wireless channel.

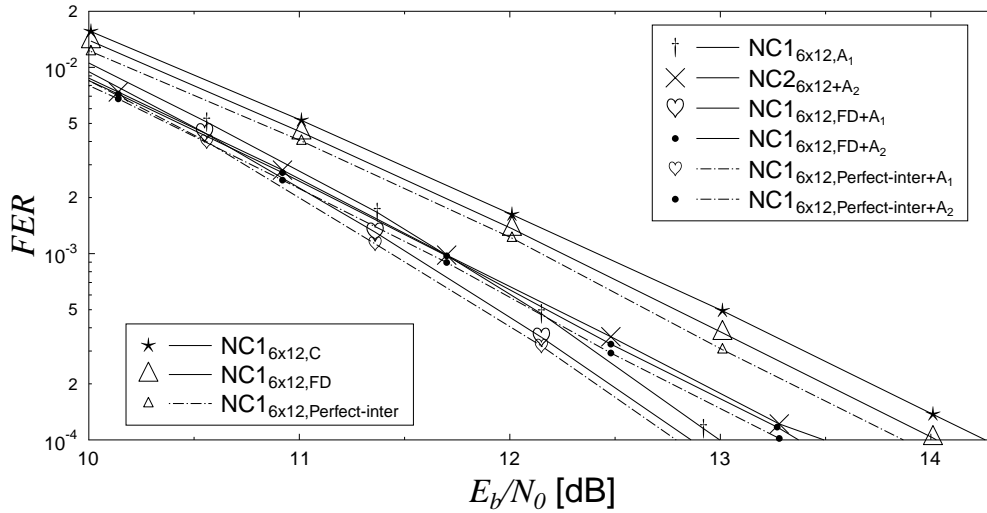
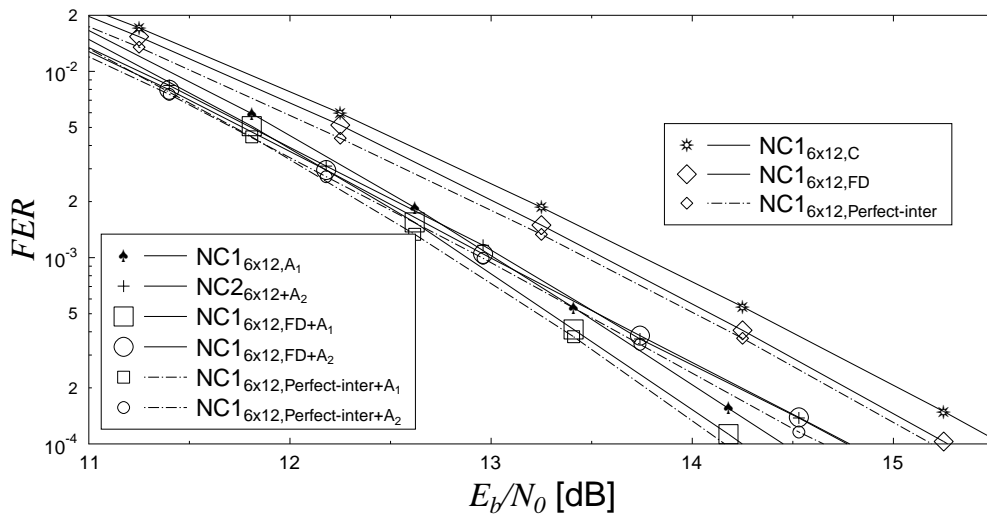
(a) $G_{6 \times 12}$, IrCC-URC-QPSK(b) $G_{6 \times 12}$, IrCC-URC-8PSK

Figure 5.7: FER performance of the system portrayed in Figure 5.1, relying on the NC1 and CC layers, where the $G_{6 \times 12}$ matrix is employed at the NC1 layer for operating in the full-diversity mode and adaptive mechanism, while the IrCC-URC-MPSK scheme is activated at the CC layer, as listed in Table 5.2. Both the block Rayleigh fading and the fast Rayleigh fading are considered, when a frame is transmitted in the $N_{sub} = 1$ subframe regime over the wireless channel.

superior multiplexing gain of the A_2 mode fails to compensate for the diversity-gain loss caused by transmitting less PFs. This result is in line with the conclusions presented in [12]. Furthermore, the superior performance supported by the A_1 mode remains undiminished, when the system activates simultaneously the adaptive mode (A_1 or A_2) and the FD mode, as seen in Figure 5.6 and Figure 5.7.

As expected, upon combining the adaptive modes, namely A_1 and A_2 with the FD mode, the system's performance can be increased further, as evidenced by Figure 5.6 and Figure 5.7. As shown in Figure 5.8 for example, where the matrix $G_{6 \times 12}(G_{4 \times 8})$ is employed at the NC1, while the IrCC-URC-QPSK scheme is activated at the CC layer having the sub-frame transmission $N_{sub} = 1$, a significant FER versus E_b/N_0 -performance improvement of approximately 30.0 dB (28 dB) can be achieved at an FER of 10^{-4} by activating the most appropriate mode, namely the $FD + A_1$ mode.

5.5 Gain by Network Coding 2

5.5.1 Design of Network Coding 2

As mentioned both in [191, 192] and in Section 5.1.3, the scalar of α_{ij} ($i \in [1, \dots, H]$) used in NC2 can be chosen from random coefficients defined over $GF(2^8)$, which is sufficiently large for providing the Θ number of virtually unlimited sets of α_{ij} , where the resultant Θ sets of α_{ij} form Θ vectors that are linearly independent of each other. According to [192], the coefficients α_{ij} may be obtained by obeying the constraints imposed by the specific structure of the Vandermonde matrix [193]. Then, the coefficient matrix may be pre-generated and be stored by the users as well as by the BS for encoding and decoding. Accordingly, the users only transmit the indices of the coefficient sets employed for encoding the IFs to be transmitted to the other users or the BS, as part of the session setup information, before transmitting actual data. As a result, no overhead pertaining to the random coefficients is transmitted during the actual communications session. In order to simply demonstrate the benefit of random network coding in the context of our system, we consider $\Theta = 20$, $H = 18$ and the fixed coding rate $R_{info2} = N/\Theta$ according to Equation (5.70), as summarised in Table 5.2.

5.5.2 Performance of the System assisted by Network Coding 2

Once NC2 is activated, the time diversity across $H = 18$ frames is exploited by scattering over $\Theta = 20$ encoded frames at the output of the NC2, in order to improve the system's performance. In fact, the system's performance is significantly improved by employing the NC2 scheme. More specifically, as shown in Figure 5.9a, a significant FER versus E_b/N_0 -performance improvement of approximately 34 dB can be achieved at an FER of 10^{-4} by activating the most appropriate modes of the triple-layer coding scheme presented in Figure 5.1. It should be noted that the ($FD +$

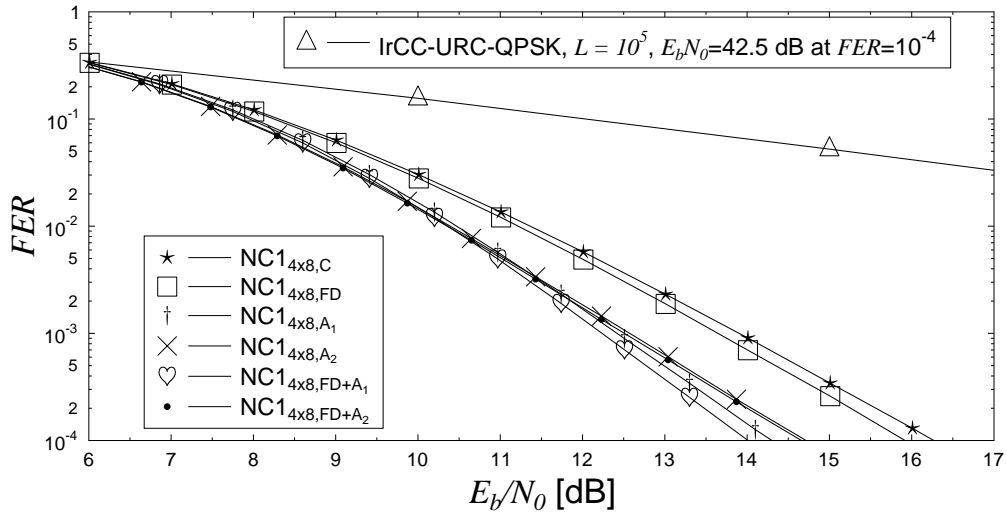
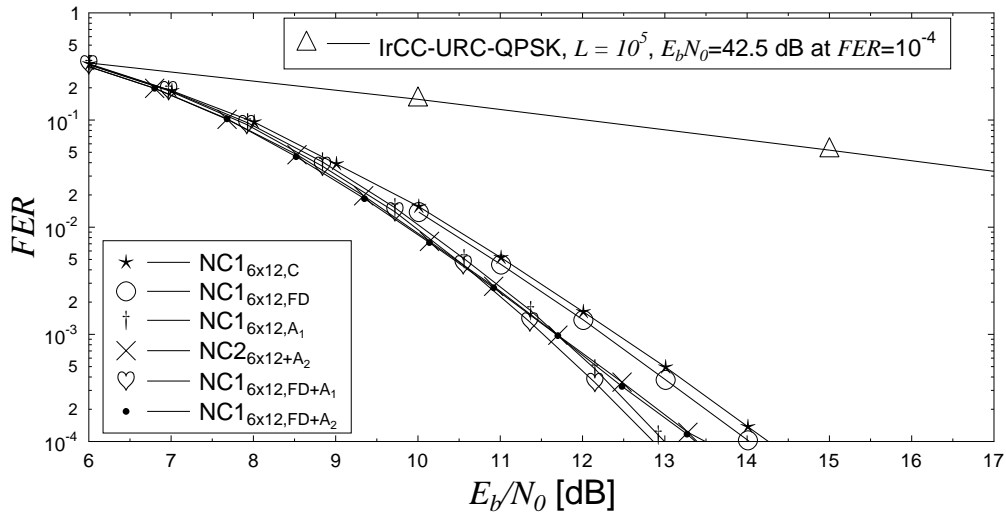
(a) $G_{4 \times 8}$ (b) $G_{6 \times 12}$

Figure 5.8: The performance gain of the system portrayed in Figure 5.1, relying on the NC1 and CC layers, obtained by selecting the appropriate modes in the NC1 layer, while the IrCC-URC-QPSK scheme is activated at the CC layer, as listed in Table 5.2. Both the block Rayleigh fading and the fast Rayleigh fading are considered, when a frame is transmitted in the $N_{sub} = 1$ subframe regime over the wireless channel.

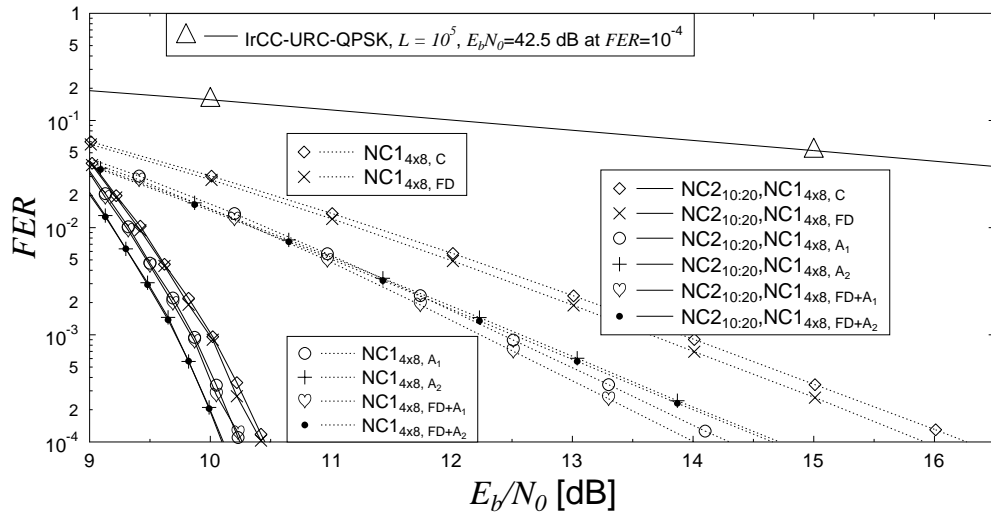
A2) mode is the most appropriate mode supporting the best performance of the system under investigation, as readily seen in Figure 5.9b, where the region having the FER range of 10^{-2} to 10^{-1} and the E_b/N_0 range of 8.25 dB to 10.00 dB in Figure 5.9a is magnified. The reason for this is that the system's performance supported by the different modes, namely the A_1 , A_2 , $FD + A_1$ and $FD + A_2$ modes, varies with respect to the others. More specifically, in the region characterised by Figure 5.9b, the order of the modes associated with the performance arranged from high to low is as follows: $FD + A_2$, A_2 , $FD + A_1$ and A_1 . By contrast, in the high E_b/N_0 region, say $E_b/N_0 \geq 13$ dB, the order of the modes associated with the performance arranged from high to low is given by $FD + A_1$, A_1 , $FD + A_2$ and A_2 . Hence, the appropriate mode supporting the best performance of the system may be selected by determining the operating region of the NC1.

In order to study the factor deciding the operating region of the NC1 layer as well as to investigate the most appropriate value of R_{info2} associated with the highest improvement of the system's performance, let us consider the performance of the different systems pertaining to different values of R_{info2} , as presented in Figure 5.10. As a result of reducing the network coding rate R_{info2} at the NC2 layer, the system's performance characterised in Figure 5.10 is improved. However, when the rate R_{info2} falls below the point corresponding to $R_{info2} = 10/20 = 1/2$, the performance of the system decreases, as seen in Figure 5.10. This may be interpreted by assuming that the point having $R_{info2} = 10/20 = 1/2$ is a threshold, where the gain provided by activating the NC2 reaches its maximum value. Thus, reducing the coding rate achieves no further network coding gain, while the multiplexing gain is reduced, which is determined by Equation (5.71).

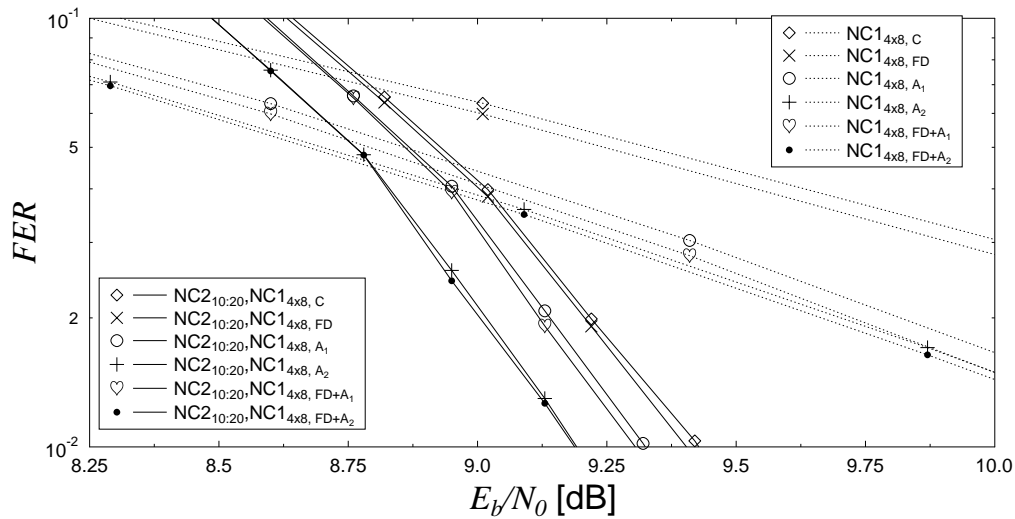
For further study, once the hardware capability of the GNCMN system allows us to support a higher value of H in the NC2, we may extend our scope for finding the optimal parameters of the NC2, namely the optimal value of H and Θ , in order to attain the best possible performance of the system, provided that the parameters of the CC and NC1 layers are given. For example, it is suggested by Figure 5.10 that the rate of $R_{info2} = 1/2$ is the optimal network coding rate in the scenario considered and that given $R_{info2} = 1/2$, the performance associated with higher values of the parameter Θ , say $\Theta = 200$, is better than that associated with the smaller value of $\Theta = 20$, when comparing Figure 5.10a and Figure 5.10b. Hence, it may be desirable to examine the optimal value of H and Θ , provided that the network coding rate $R_{info2} = 1/2$ remains unaltered.

In order to address the issue regarding the optimal value of the parameter H and Θ in the NC2 layer, we activate one of the modes in the NC1 relying on the matrix $\mathbf{G}_{4 \times 8}$, namely mode C, and employ the IrCC-URC-QPSK scheme in the CC layer relying on the sub-frame transmission associated with $N_{sub} = 1$. Then, the performance of the system is investigated for different values of Θ , namely for $\Theta = 2, 20, 2 \times 10^2, 2 \times 10^3, 2 \times 10^4, 2 \times 10^5$. Note that we fix the network coding rate to $R_{info2} = 1/2$ and assume that the parameter Θ and H are related by Equation (5.70) as

$$R_{info2} = \frac{H}{\Theta}. \quad (5.120)$$

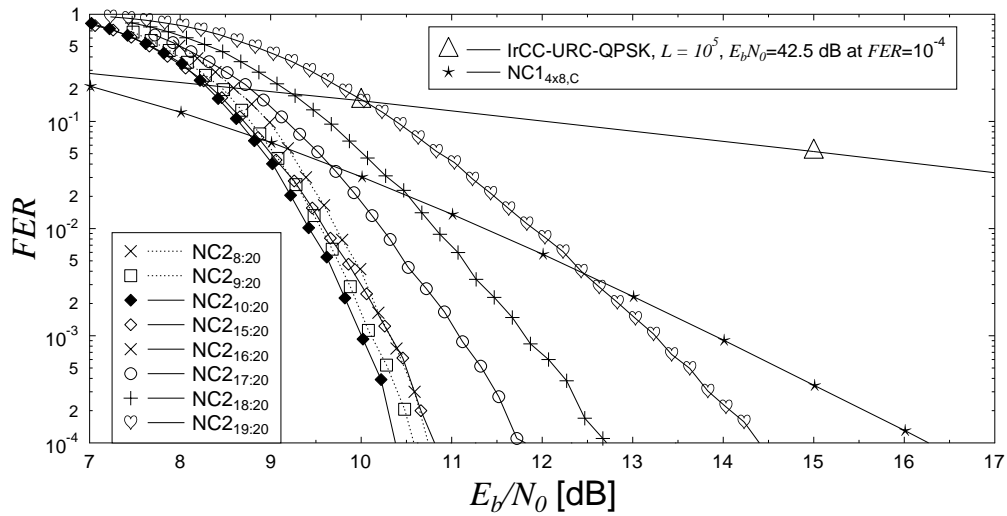


(a) Large range performance, namely FER values in a range from 10^{-4} to 1 and E_b/N_0 values in a range from 9 dB to 16.5 dB

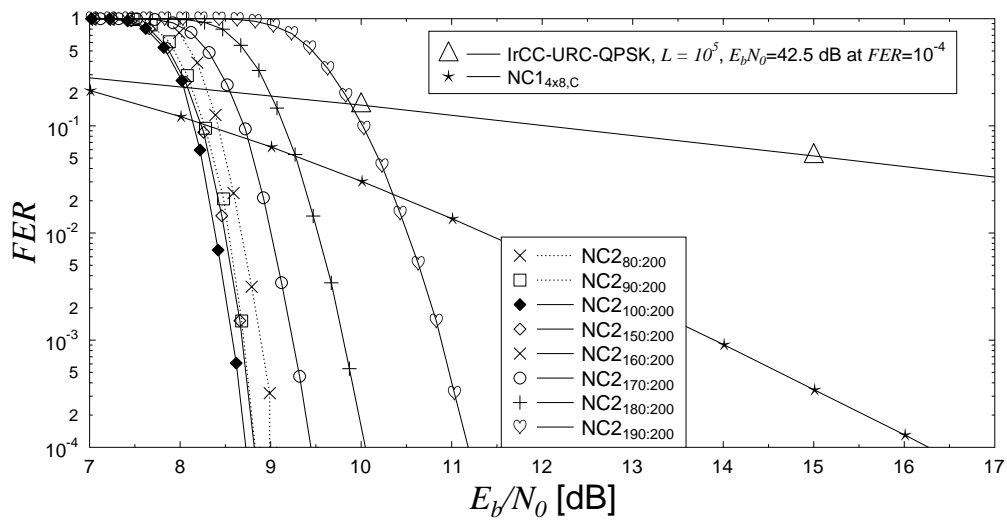


(b) Performance in low E_b/N_0 region, namely FER values in a range from 10^{-2} to 10^{-1} and E_b/N_0 values in a range from 8.25 dB to 10.00 dB

Figure 5.9: The benefit of employing the NC2 ($H = 10$ and $\Theta = 20$) in the GNCMN system portrayed in Figure 5.1, relying on the NC2, NC1 and CC layers, as listed in Table 5.2, when the matrix $G_{4 \times 8}$ is employed at the NC1 layer, while the IrCC-URC-QPSK activated at the CC layer for the $N_{sub} = 1$ sub-frame transmission over the wireless channel influenced by both the block Rayleigh and the fast Rayleigh fadings.



(a) NC2: $\Theta = 20$



(b) NC2: $\Theta = 200$

Figure 5.10: The performance of the GNCMN system portrayed in Figure 5.1, relying on the NC2, NC1 and CC layers, as listed in Table 5.2, when employing different values of R_{info2} at the NC2, while the matrix $G_{4 \times 8}$ is selected for operating in the C mode at the NC1 layer, whereas the IrCC-URC-QPSK scheme is used for transmitting in the $N_{sub} = 1$ sub-frame regime over wireless channels influenced by both fast Rayleigh and block Rayleigh fadings.

Thus, we have to investigate different values of Θ , in order to determine the optimal value of Θ and H associated with the best E_b/N_0 -versus- FER performance. It can be readily seen in Figure 5.11 that when the value of Θ increases from $\Theta = 2$ to $\Theta = 2 \times 10^4$, the E_b/N_0 -versus- FER performance of the system is improved. However, when the value of Θ becomes higher than $\Theta = 2 \times 10^4$, no further performance improvement is exhibited. Hence, we may deem $\Theta = 2 \times 10^4$ to be the optimal value for the system under investigation. As for the general case, the issue of finding the optimal value of Θ , provided that the other parameters of the system are given, is set aside for future work.

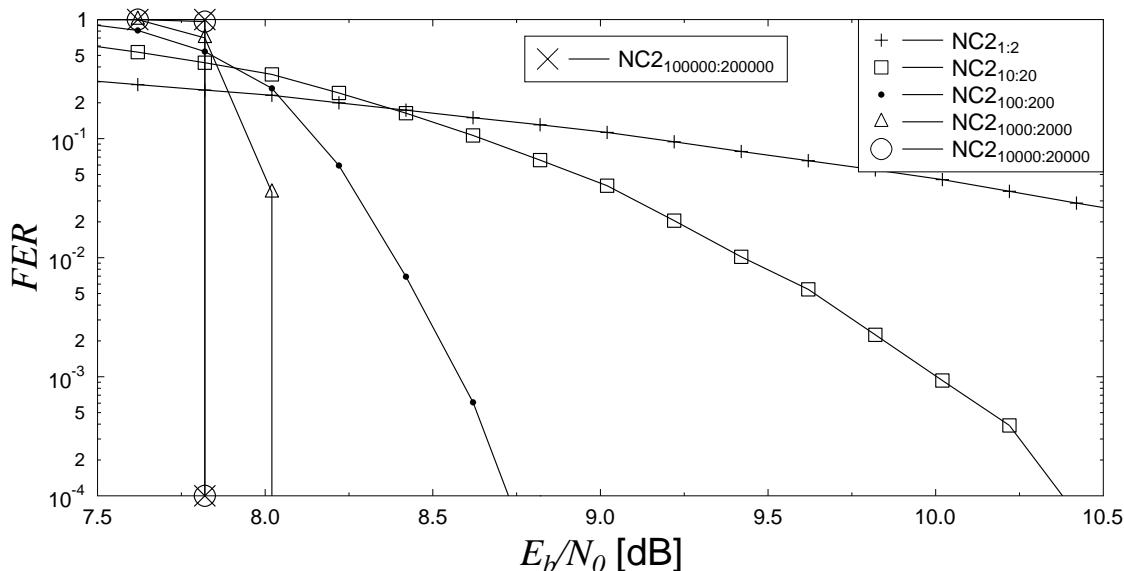


Figure 5.11: The performance of the GNCMN system portrayed in Figure 5.1, relying on the NC2, NC1 and CC layers, as listed in Table 5.2, corresponding to different values of Θ at the NC2 layer, namely $\Theta = 2, 20, 2 \times 10^2, 2 \times 10^3, 2 \times 10^4, 2 \times 10^5$, when the matrix $\mathbf{G}_{4 \times 8}$ along with the C mode is used at the NC1, while the IrCC-URC-QPSK is employed at the CC layer for supporting the $N_{sub} = 1$ sub-frame transmission over wireless channels influenced by both fast Rayleigh and block Rayleigh fadings.

5.6 Near Capacity System Performance

In this section, we first compare the performance of the system supported by the realistic channel coding scheme IrCC-URC-QPSK presented in Section 2.3.3 to that of the system relying on the ideal/perfect coding scheme operating exactly at the DCMC capacity detailed in Section 2.1.3, when activating various configurations at the NC1 and NC2. Then, we again use the method applied in Section 4.7.3 for determining the capacity of the GNCMN system, before addressing the issues of how to approach the capacity.

5.6.1 Achievable Capacity of the Ideal/Perfect Coding Scheme

Let us consider Figure 5.12, where the E_b/N_0 -versus- FER performance of the system employing the realistic IrCC-URC-QPSK scheme is plotted along with that of the system relying on the ideal/perfect channel coding scheme operating at the DCMC capacity. At the NC1, all the available modes, namely the C , A_1 , A_2 , $FD + A_1$ and $FD + A_2$ modes, are investigated, while the optimal coding rate $R_{info2} = 1/2$ determined in Section 5.5.2 is set at the NC2. It can be seen in Figure 5.12 that in all the cases plotted, the performance curves associated with the realistic IrCC-URC-QPSK scheme are approximately 1.0 dB apart from their corresponding performance curve supported by the ideal/perfect coding scheme at an $FER = 10^{-4}$. In other words, the FER-performance of the IrCC-URC-QPSK system is approximately 1.0 dB within its capacity, which is the performance of the system relying on the ideal/perfect coding scheme operating at the DCMC capacity.

5.6.2 Approaching the GNCMN capacity

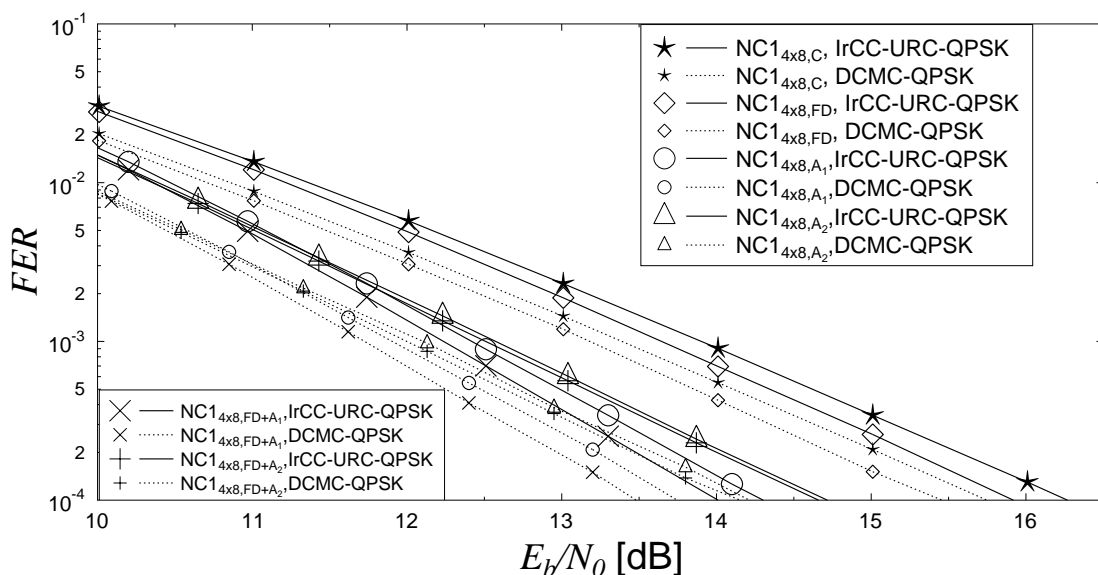
In contrast to the achievable capacity discussed in Section 5.6.1, we discussed metric, namely the system's capacity, in Section 4.7.3, where the estimate limit of the system's performance was investigated. Let us continue by employing the approach invoked in Section 4.7.3 for determining the GNCMN system's capacity. Accordingly, the capacity of the GNCMN based systems can be characterised by the transmission links capacity spanning from a certain user supported by the system to the BS. This link in the GNCMN based systems may be viewed as an equivalent single-link model, where the equivalent transmission rate R_e of the user-to-BS link in the GNCMN system can be formulated as

$$R_e = R_{info2}R_{info}R, \quad (5.121)$$

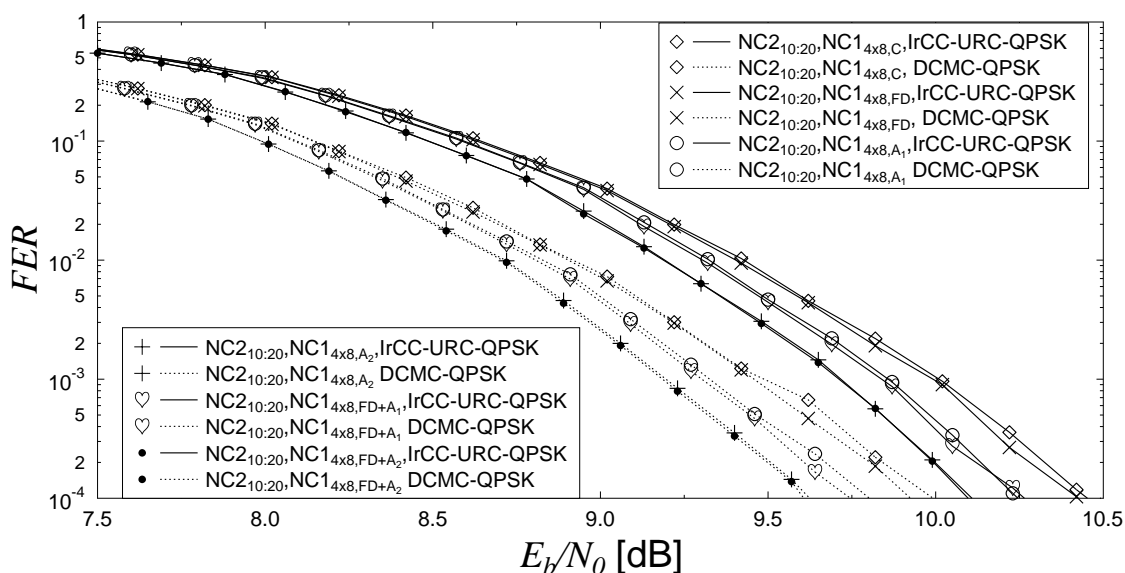
where R is the information rate of a single link in the GNCMN system, while the network-coding scheme's rate R_{info} of the NC1 and the network-coding arrangement's rate R_{info2} of the NC2 are described in Table 5.1. Then, the equivalent transmission rate R_e of Equation (5.121) may be used for determining the capacity of the channel, which is detailed in Section 2.1.3 and Section 2.1.4 in the case of the DCMC capacity and D-DCMC capacity, respectively. Let us invoke the following numerical example, in order to illustrate the method employed for determining the capacity of the GNCMN system.

Example 5.1 (The coherent detection based GNCMN system).

Let us consider a specific example of the GNCMN system having the parameters listed in Table 5.3. Accordingly, the network-coding's information rate of NC1 is $R_{info} = 0.5$. This system employs a channel coding scheme characterised by an information rate of $R = 0.5$ and by a coding rate of $R_c = 0.5$. The configuration of the system in this example results in the number of modulated bits



(a) Two layer architecture



(b) Three layer architecture

Figure 5.12: The performance of the GNCMN system portrayed in Figure 5.1, relying on the NC2, NC1 and CC layers, having parameters listed in Table 5.2, when comparing the two scenarios at the CC layer, namely that employing the realistic coding IrCC-URC-QPSK and that employing the corresponding ideal/perfect coding scheme operating at the DCMC capacity. The performance is recorded in various modes of the NC1 relying on the matrix $G_{4 \times 8}$, namely the C , A_1 , A_2 , $FD + A_1$ and $FD + A_2$ modes, while the R_{info2} at the NC2 is fixed at the optimal value of $R_{info2} = 1/2$, as determined in Section 5.5.2. Both the block Rayleigh fading and the fast Rayleigh fading are considered, when a frame is transmitted in the $N_{sub} = 1$ subframe regime over the wireless channel.

Parameters	CC layer	
	Coherent	Non-coherent
R [BPS]	1.0(QPSK)	1.0(DQPSK)
R_c	0.5	0.5
I [iteration]	0	2
J [iteration]	30	30
N [bit]	10^6	10^6
N_{sub} [bit]	1, 10, 10^2 , 10^3	1, 10, 10^2 , 10^3
Parameters	NC1 layer	
Mode	C, FD, A_1 , A_2 , FD + A_1 , FD + A_2	
\mathbf{G}	$\mathbf{G}_{2 \times 4}$, $\mathbf{G}_{4 \times 8}$, $\mathbf{G}_{6 \times 12}$	
M [user]	2	
k_1 [frame]	1($\mathbf{G}_{2 \times 4}$), 2($\mathbf{G}_{4 \times 8}$), 3($\mathbf{G}_{6 \times 12}$)	
k_2 [frame]	1($\mathbf{G}_{2 \times 4}$), 2($\mathbf{G}_{4 \times 8}$), 3($\mathbf{G}_{6 \times 12}$)	
R_{info}	0.5	
D_{NCMN}	$D_{2 \times 4} = 3, 4 \leq D_{4 \times 8} \leq 5, 5 \leq D_{6 \times 12} \leq 7$	
Parameters	NC2 layer	
H	10	
Θ	20	
R_{info2}	1/2	

Table 5.3: Parameters for an example of the GNCMN system portrayed in Figure 5.1.

expressed as follows:

$$\begin{aligned} \mu &= \frac{R}{R_c} = \frac{1.0}{0.5} \\ &= 2. \end{aligned} \tag{5.122}$$

Having $\mu = 2$ BPS means that the coherent (non-coherent) modulation scheme relying on QPSK (DQPSK) may be employed at each user in the system. Similar to the method invoked in Section 2.1.3 (Section 2.1.4) for determining the receive SNR value (SNR_r) corresponding to a given throughput R , which is also considered as the information rate in this context, the capacity of the above-mentioned GNCMN system may be equivalently determined by identifying the corresponding value of SNR_r .

For the convenience of presentation, we define $SNR_e|_{R_e}$ as the equivalent SNR_r value corresponding to a given throughput of R_e . According to Equation (5.121), the value of R_e in the numerical example can be determined by

$$\begin{aligned} R_e &= R_{info2} R_{info} R, \\ &= 0.5 \times 0.5 \times 1.0, \\ &= 0.25, \end{aligned} \tag{5.123}$$

where $R_{info} = 0.5, R_{info2} = 0.5$ and $R = 1.0$ are given in Table 5.3. Then, the $SNR_e|_{R_e}$ value is determined based on the DCMC capacity curve generated from Equation (2.16), which is repeated here for the sake of convenience as:

$$C^{DCMC}(\eta) = \eta - \frac{1}{2^\eta} \sum_{l=1}^{l=2^\eta} E \left[\log_2 \sum_{z=1}^{z=2^\eta} \exp(\psi_{l,z}) | X_l \right], \quad (5.124)$$

where $\eta = \log_2(L)$ is the asymptotic DCMC capacity and L is the number of modulation levels. The expression of $E[A|X_l]$ represents the expectation of A conditioned on the L -ary signals X_l , whereas the formula of calculating $\psi_{l,z}$ is given by Equation (2.17). For the non-coherent modulation scheme detailed in Section 2.1.4, the $SNR_e|_{R_e}$ value is determined on the D-DCMC capacity curve generated with the aid of EXIT charts, as presented in Section 2.3.4.

As a result of obtaining $R_e = 0.25$ in this example, the corresponding equivalent receive SNR value of $SNR_e|_{R_e} = -6.9$ dB ($SNR_e|_{R_e} = -2.73$ dB) may be found from the DCMC-QPSK (D-DCMC-QPSK) capacity curve, as seen in Figure 5.13. This $SNR_e|_{R_e}$ value can be benchmarked as the achievable capacity of the system in the configurations considered.

It should be noted that the value of the system's capacity is determined on an SNR basis. By contrast, when considering it on an E_b/N_0 basis, the equivalent coding rate $R_e = 0.25$ must be taken into account, in order to infer to the corresponding equivalent E_b/N_0 value in ratio as

$$E_b/N_0^R|_{R_e} = \frac{SNR_e^R|_{R_e}}{R_e}, \quad (5.125)$$

which can be presented in dB as:

$$E_b/N_0|_{R_e} = SNR_e|_{R_e} - 10 \times \log(R_e). \quad (5.126)$$

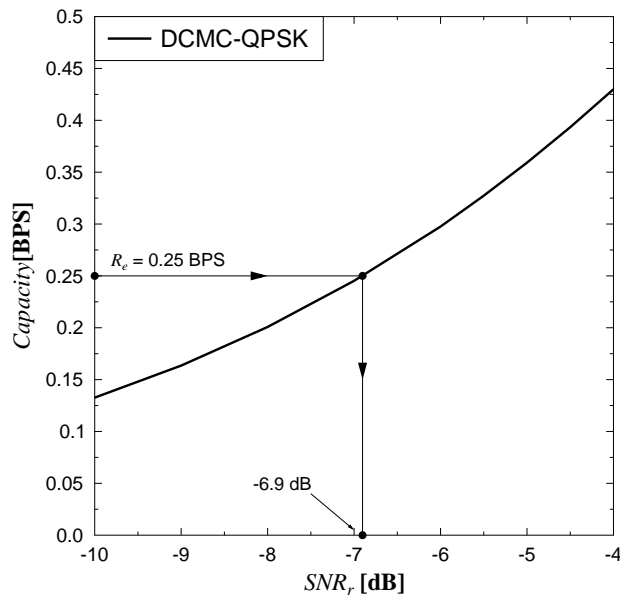
Accordingly, the value of $E_b/N_0|_{R_e}$ in the DCMC scenario is

$$\begin{aligned} E_b/N_0|_{R_e} &= SNR_e|_{R_e} - 10 \times \log(R_e), \\ &= -6.9 - 10 \times \log(0.25) \\ &= -0.88 \text{ dB}, \end{aligned} \quad (5.127)$$

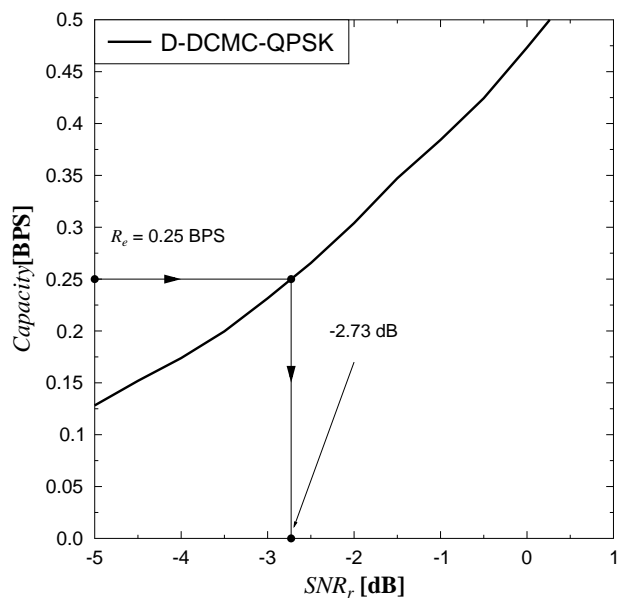
and that of the $E_b/N_0|_{R_e}$ in the D-DCMC scenario is

$$\begin{aligned} E_b/N_0|_{R_e} &= SNR_e|_{R_e} - 10 \times \log(R_e), \\ &= -2.73 - 10 \times \log(0.25), \\ &= 3.29 \text{ dB}. \end{aligned} \quad (5.128)$$

Having calculated the capacity of the GNCMN system, as demonstrated in Example 5.1, we can now consider the distance between the FER-performance curve of a GNCMN system and its capacity. It is worth noting that the distance must be compared at a vanishingly low value of FER, say at an $FER = 10^{-4}$. For example, Figure 5.14 characterises the distance between the system's capacity and the E_b/N_0 -versus-FER performance of the system employing $R_{info2} = 1/2$ at the NC2 and invoking the matrix $\mathbf{G}_{6 \times 12}$ at the NC1 activating the C as well as the FD modes and relying



(a) Coherent scheme, DCMC-QPSK



(b) Non-coherent scheme, D-DCMC-QPSK

Figure 5.13: Example for calculating the capacity of the network-coding based system relying on the coherent (non-coherent) channel coding scheme channel coding scheme having an equivalent information rate of $R_e = 0.25$, when communicating over fast Rayleigh fading channels.

on the IrCC-URC-QPSK scheme at the CC layer supported by $N_{sub} = 1$ frame transmission. Note that the value of $E_b/N_0 = -0.88$ dB calculated in Equation (5.127) is the system's E_b/N_0 limit. Accordingly, a relatively large gap of approximately 11 dB is exhibited at an $FER = 10^{-4}$. This leads to a question regarding which particular solution may be employed for reducing the gap of 11 dB.

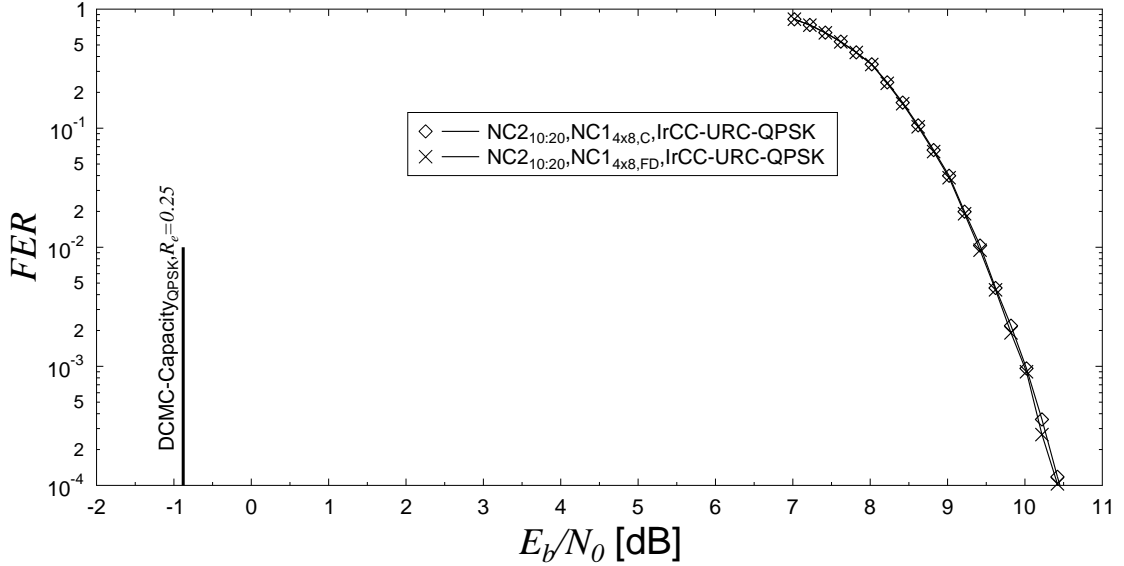


Figure 5.14: The E_b/N_0 -versus- FER performance of the GNCMN system portrayed in Figure 5.1, which comprises the NC2, NC1 and CC layers and has all parameters listed in Table 5.2. The system employs $R_{info2} = 1/2$ at the NC2, invokes the $G_{6 \times 12}$ matrix at the NC1 layer operating in the C and FD modes and relies on the IrCC-URC-QPSK scheme at the CC layer supported by $N_{sub} = 1$ frame transmission, when communicating over wireless channels influenced by both the fast Rayleigh and block Rayleigh fadings.

In order to answer the above-mentioned question, let us study Figure 5.1, where the GNCMN system comprising three layers, namely CC, NC1 and NC2, is characterised. Thus, a straightforward solution is to optimise each individual layer in a scenario, when the parameters of the other layers are given. More specifically:

- At the CC: The employment of sub-frames and our near-capacity coding design can be utilised for improving the system's performance;
- At the NC1: Selecting the appropriate transfer matrices, as detailed in Section 4.7, has the potential of enhancing the system's performance. Additionally, activating a suitable mode of the available ones, namely of the C , FD , A_1 , A_2 , $FD + A_1$ and $FD + A_2$ modes, may improve the system's performance;
- At the NC2: Applying the optimal network coding rate R_{info2} can help improve the system's

performance.

Hence, in the following sections, the above-mentioned issues of optimization at each layer are discussed in detail.

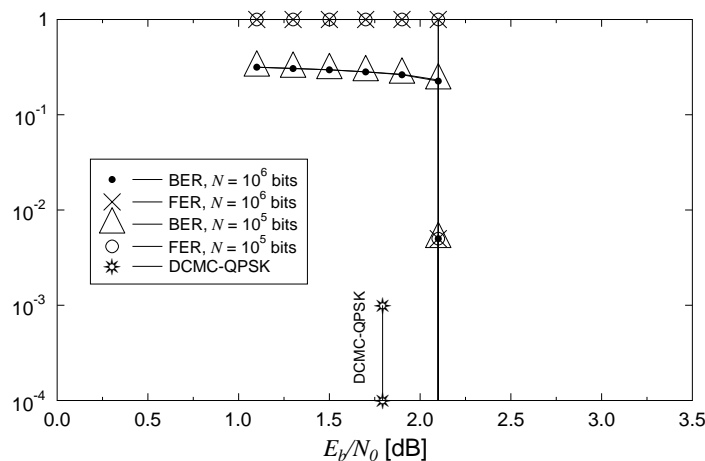
5.6.3 Potential Solutions at Channel Coding Layer

Let us continue to employ the IrCC-URC-QPSK scheme to demonstrate the benefits of the sub-frame transmission regime at the CC portrayed in Figure 5.1. Figure 5.15 characterises the performance of the IrCC-URC-QPSK scheme in the different fading scenarios, namely in the fast Rayleigh fading environment given Figure 5.15a and in the quasi-static block-fading Rayleigh environment presented Figure 5.15b. It is readily seen in Figure 5.15a that the performance of the system supported by the IrCC-URC-QPSK scheme is merely 0.5 dB away from the corresponding DCMC capacity, when the system operates in the environment influenced by the fast Rayleigh fading. By contrast, once the system encounters quasi-static Rayleigh block-fading, the system's performance is degraded substantially, as seen in Figure 5.15b. As a result, a significant gap of approximately 40 dB is seen, when comparing the system's performance seen in Figure 5.15b and the corresponding DCMC capacity in Figure 5.15a at an $FER = 10^{-4}$.

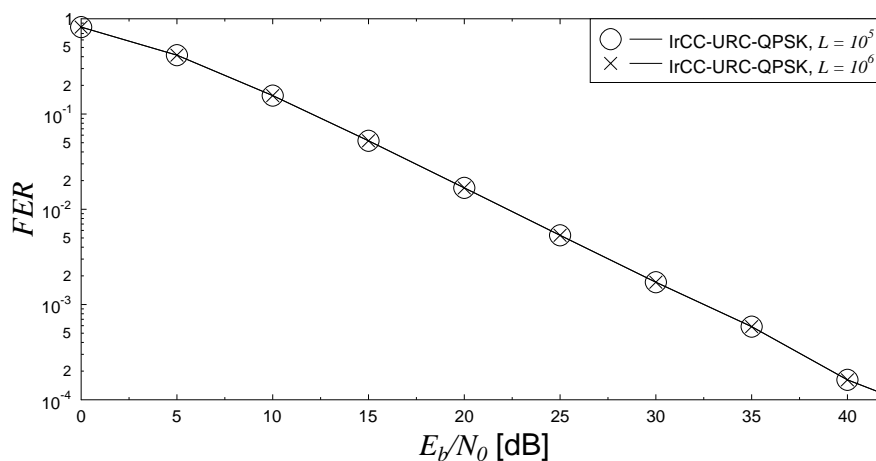
As a remedy, the sub-frame transmission regime detailed in Section 2.4 may be invoked at the CC layer for improving the system's performance in quasi-static Rayleigh block-fading environments. It can be seen in Figure 5.16 that the higher the number of sub-frames (N_{sub}) per transmission frame, the better the system's performance becomes. Particularly, if the system is designed to allow a transmission frame partitioned into $N_{sub} \geq 10^4$ sub-frames, the performance of the system supported by the IrCC-URC-QPSK scheme is capable of operating at a mere 0.5 dB from the corresponding DCMC capacity. It should be emphasised that when N_{sub} is higher than $N_{sub} = 10^4$, no further improvements are observed. It may be further inferred that once the system is permitted to partition a transmission frame into $N_{sub} = 10^4$ sub-frames, there is no need for employing the NC1 and NC2. If the NC1 and NC2 are still activated, the performance of the system would be degraded. This is because the FER-versus-SNR performance is no longer improved, but the multiplexing gain is reduced. However, in order to make the system capable of automatically adjusting its operational mode, the adaptive modes at both the NC1 and NC2 have to be activated. We will further discuss this issue later in Section 5.6.4 and Section 5.6.5

5.6.4 Solutions at the Network Coding 1 Layer

As discussed in Section 5.6.3, there is no need for employing the NC1, when the number of sub-frames used for conveying a transmission frame becomes as high as $N_{sub} = 10^4$. However, invoking a large number of sub-frames N_{sub} may result in an unaffordable delay incurred by a user. For example, a frame in the Long Term Evolution-Advanced (LTE-Advanced) standard is of 10ms du-



(a) The fast Rayleigh fading's influence on the performance of the IrCC-URC-QPSK scheme's performance



(b) The block Rayleigh fading's influence on the IrCC-URC-QPSK scheme's performance

Figure 5.15: The influence of the fast and block Rayleigh fadings on the performance of the IrCC-URC-QPSK scheme detailed in Section 2.3.3.

ration [84, 165]. Let us consider a scenario, in which the number of subframes is set to $N_{sub} = 10^4$ at the CC layer for transmitting a single transmission frame, while the fading coefficients remain constant during the time period of a frame length and vary independently frame by frame. In order to have a beneficial time diversity, each of the 10^4 sub-frames must be mapped to a single LTE-Advanced frame having a length of 10ms [84, 165]. In other words, 10^4 LTE-Advanced frames are used for conveying a single transmission frame, which is divided into $N_{sub} = 10^4$ sub-frames. Consequently, a transmission frame incurs a delay of $10^4 \times 10\text{ms} = 100\text{s}$, which is too high a delay for interactive communications. Hence, let us now consider a scenario employing $N_{sub} = 10$ sub-frames per transmission frame, which leads to a moderate delay of $10 \times 10\text{ms} = 100\text{ms}$. It should be noted that the employment of network coding can also lead to an additional delay, which is as much as k_1 frame lengths. For example, if the matrix $\mathbf{G}_{6 \times 12}$ is employed at the NC1, the delay becomes

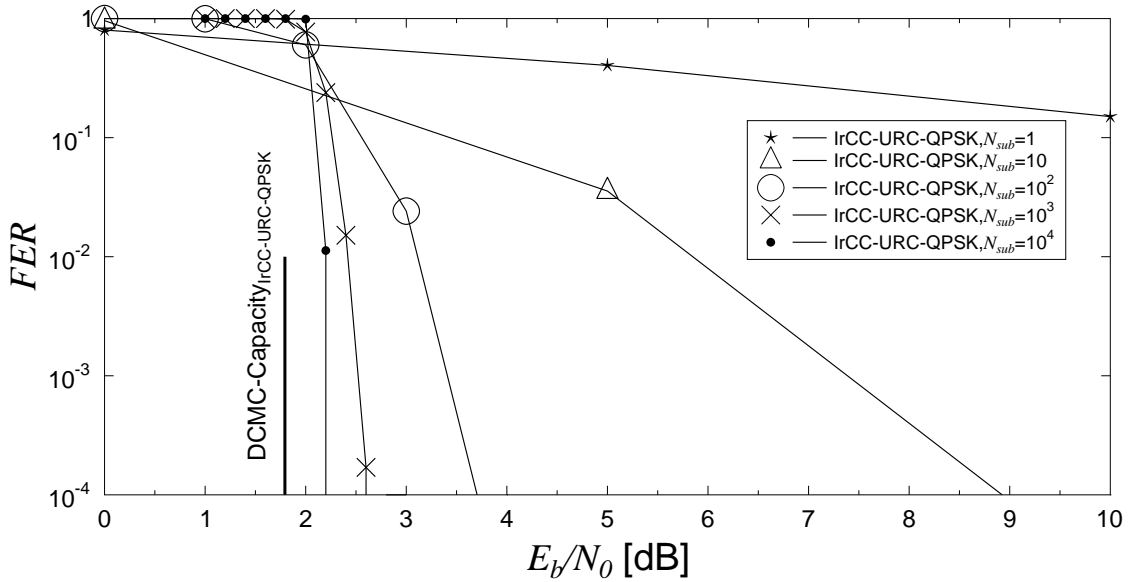


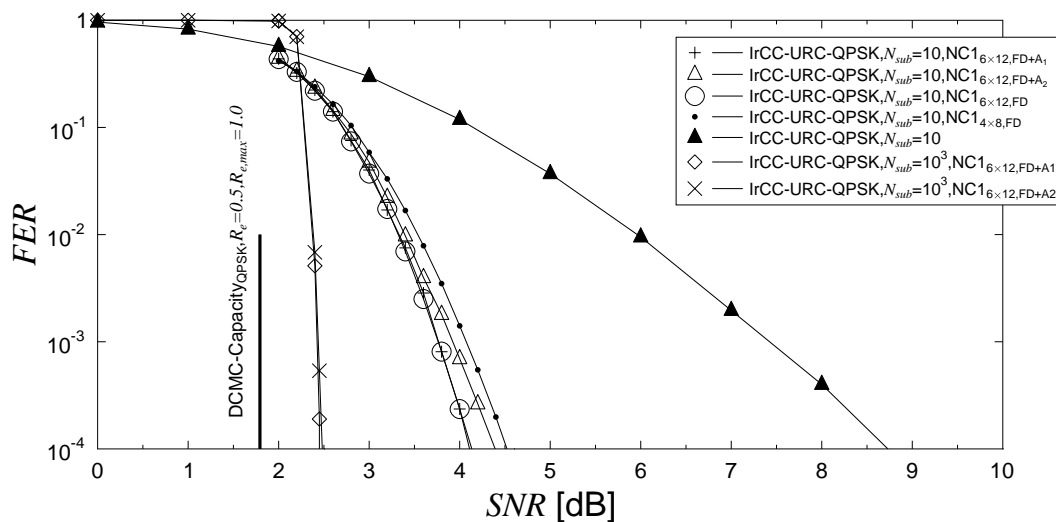
Figure 5.16: The benefit of employing different the sub-frames, namely $N_{sub} = 1, 10, 10^2, 10^3, 10^4$, in performance of the IrCC-URC-QPSK scheme detailed in Section 2.3.3, when communicating over a wireless channel influenced by both the fast Rayleigh and block Rayleigh fading.

$k_1 = 3$ times of the delay for a transmission frame, which is equal to $3 \times 100 = 300$ ms.

Having opted for $N_{sub} = 10$, let us now investigate the benefit of employing the NC1. As seen in Figure 5.17, the network coding significantly improves the attainable system performance. More specifically, the more powerful the network coding, the better performance in comparison to that of the system relying solely on sub-frame transmission, as seen in Figure 5.17b. At an $FER = 10^{-4}$, the distance to the E_b/N_0 value corresponding to the system's capacity having $R_e = 0.5$ from the performance curve of the system employing the $\mathbf{G}_{4 \times 8}$ and $\mathbf{G}_{6 \times 12}$ matrices is as low as 2.0 dB and 2.7 dB, respectively, as seen in Figure 5.17b. By contrast, that of the system solely supported by the $N_{sub} = 10$ -based transmission regime is approximately 7 dB, as seen in Figure 5.16. Hence, a gain of $(7-2.0=5)$ dB and $(7-2.7=4.3)$ dB may be achieved by employing the $\mathbf{G}_{4 \times 8}$ and $\mathbf{G}_{6 \times 12}$ matrices at the NC1 layer, respectively. Note that Figure 5.17a characterises the SNR-versus-FER performance of the system relying on the $\mathbf{G}_{4 \times 8}$ and $\mathbf{G}_{6 \times 12}$ matrices at the NC1 layer operating in the FD , $FD + A_1$ and $FD + A_2$ modes of Figure 5.1.

It should be noted that when the adaptive mechanism of Section 5.1.2.3 is applied at the NC1 layer by activating the A_1 and A_2 modes of Figure 5.1, the performance of the system may be improved beyond the SNR value associated with the capacity having $R_e = 0.25$ and approaches that associated with the capacity having $R_e = 0.5$, as seen in Figure 5.17b. This can be interpreted by considering Equation (4.95), which is repeated here as

$$R_e = R_{info}R. \quad (5.129)$$



(a) SNR-versus-FER performance

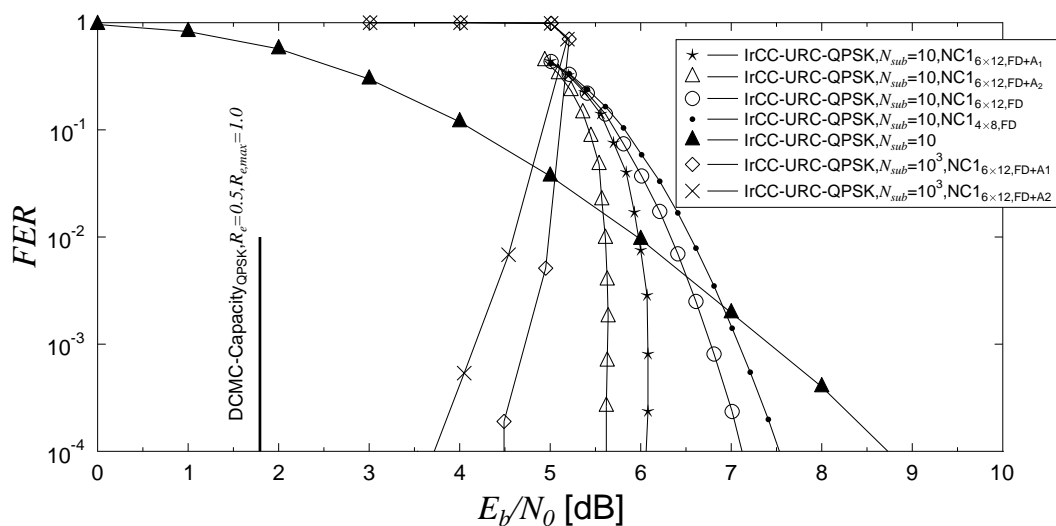
(b) E_b/N_0 -versus-FER performance

Figure 5.17: The benefit of employing the NC1 in the GNCMN system pictured in Figure 5.1. The system consists of the NC1 and CC layers having all the parameters listed in Table 5.2, where the $\mathbf{G}_{4 \times 8}$ and $\mathbf{G}_{6 \times 12}$ matrices are employed at the NC1 layer, while the IrCC-URC-QPSK scheme is activated at the CC layer for supporting the $N_{sub} = 10, 10^3$ sub-frame transmission regimes over wireless channels influenced by both the fast Rayleigh and block Rayleigh fadings.

Once the adaptive mechanism is employed, the coding rate R_{info} becomes $R_{info,A}$, as described in Section 5.3.2.1. Accordingly, when a sufficiently high E_b/N_0 value is encountered, the value of $R_{info,A}$ may approach its maximum of $R_{info,A} = 1$. As a result, upon integrating Equation (5.129) and Equation (5.109), the maximum value of R_e can be calculated as

$$\begin{aligned} R_{e,max} &= \underbrace{\text{Max} \{R_{info,A}\}}_{=1} R, \\ &= R. \end{aligned} \quad (5.130)$$

Since the IrCC-URC-QPSK scheme is employed at the CC, we have $R = 1$, which leads to

$$\begin{aligned} R_{e,max} &= R, \\ &= 1. \end{aligned} \quad (5.131)$$

Having $R_{e,max} = 1$ in Equation (5.131) is equivalent to having $R_n = 0.5$, as defined by Equation (2.21). Therefore, according to Table 2.1, we have the corresponding value of $SNR_e|_{R_{e,max}} = 1.78$ dB. Then, upon applying the formula of Equation (5.125), the corresponding $E_b/N_0|_{R_{e,max}}$ value displayed in Figure 5.17b can be calculated as

$$\begin{aligned} E_b/N_0|_{R_{e,max}} &= SNR_e|_{R_{e,max}} - 10 \times \log(R_{e,max}), \\ &= 1.78 - 10 \times \log(1) \\ &= 1.78 \text{ dB}. \end{aligned} \quad (5.132)$$

As a result of having an increased adaptive network coding rate $R_{info,A}$ upon increasing transmit power, the system experiences an increased multiplexing gain. Note that the multiplexing gain has no effect on the FER -versus- SNR performance of the system, as seen in Figure 5.17a. However, a substantially increased multiplexing gain ultimately leads to a considerably improved FER -versus- E_b/N_0 performance, as seen in Figure 5.17b. It is because values of increased multiplexing gain exceed the increment of the SNR values required to achieve the increased multiplexing gain. As a result, reduced E_b/N_0 values might actually be associated with a fixed or even increased SNR values owing to the changes in the coding rate, which potentially allows our system to provide an improved FER -versus- E_b/N_0 performance.

5.6.5 Solutions at the Network Coding 2 Layer

As demonstrated in Section 5.5, NC2 of Figure 5.1 has potential of further assisting the system in improving further its performance in some scenarios. In a delay-tolerant system that allows us to have a delay as high as N frame durations, NC2 is capable of facilitating approaching the achievable capacity, as determined in Example 5.1.

Let us illustrate the above-mentioned issue by considering the GNCMN system of Figure 5.1 relying on the IrCC-URC-QPSK scheme of Figure 2.19 and on the basis of $N_{sub} = 10$ sub-frame

transmission, while the $\mathbf{G}_{6 \times 12}$ matrix is employed at the NC1, where the $FD + A_1$ and $FD + A_2$ modes may be used for the sake of supporting the best attainable performance, as seen in Figure 5.17. Then, we investigate the benefit of employing the NC2 for the sake of approaching the system's capacity.

Parameters	CC layer	
	Coherent	
R [BPS]	1.0(QPSK)	
R_c	0.5	
I [iteration]	0	
J [iteration]	30	
N [bit]	10^6	
N_{sub} [bit]	10	
Parameters	NC1 layer	
Mode	$FD, FD + A_1, FD + A_2$	
\mathbf{G}	$\mathbf{G}_{2 \times 4}, \mathbf{G}_{4 \times 8}, \mathbf{G}_{6 \times 12}$	
M [user]	2	
k_1 [frame]	$3(\mathbf{G}_{6 \times 12})$	
k_2 [frame]	$3(\mathbf{G}_{6 \times 12})$	
R_{info}	0.5	
D_{NCMN}	$5 \leq D_{6 \times 12} \leq 7$	
Parameters	NC2 layer	
H	10	
Θ	20	
R_{info2}	1/2	
Mode	<i>Adaptive (Fixed)</i>	

Table 5.4: Parameters for an example of a GNCMN system used for illustrating the benefit of NC2.

Accordingly, Table 5.4 lists the parameters used in our investigations. It should be noted that NC2 is capable of operating in two modes

- The *Fixed* mode is the mode, when system has a fixed rate for the NC2. In other words, in the fixed mode, we always have $R_{info2} = H/\Theta$, which is equal to $R_{info2} = 1/2$, as listed in Table 5.4.
- The *Adaptive* mode may be activated, when the system can afford the delay of acquiring the feed-back information acknowledging the number of frames that are correctly recovered at the BS. Upon receiving the feed-back information from the BS, the users supported by the system may decide to refrain from transmitting the rest of the Θ encoded frames. Hence, the

adaptive rate at the NC2 may be expressed by:

$$R_{info2,A} = \frac{\Theta}{E[\text{Number of encoded frames transmitted}]}. \quad (5.133)$$

Note that when the system experiences an increasing value of SNR , we have

$$\lim_{SNR \rightarrow +\infty} E[\text{Number of encoded frames transmitted}] = \Theta. \quad (5.134)$$

Bearing Equation (5.134) in mind, the rate $R_{info2,A}$ of Equation (5.133) achieved in the high SNR region may be approximated as:

$$\begin{aligned} \text{Max} \{R_{info2,A}\} &= \frac{\Theta}{\Theta}, \\ &= 1. \end{aligned} \quad (5.135)$$

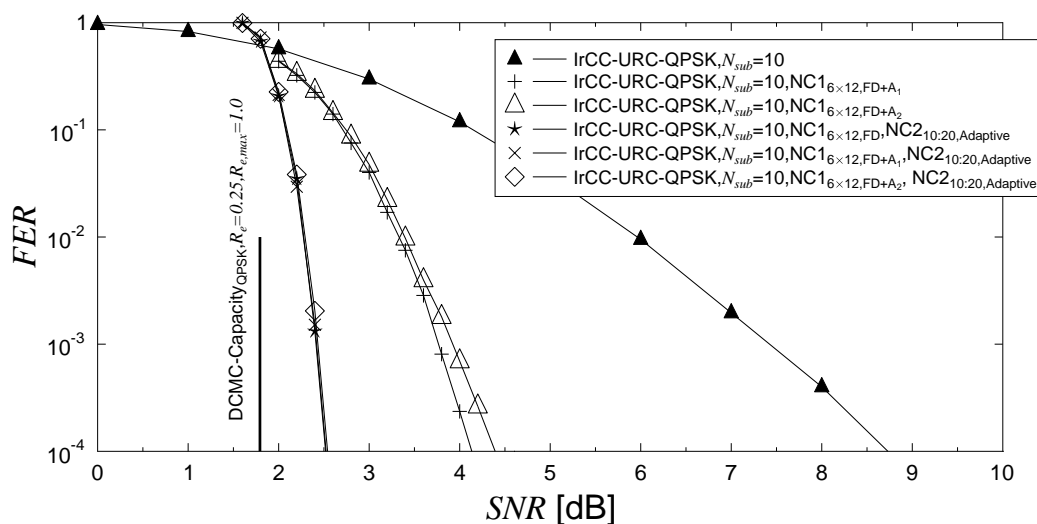
As seen in Figure 5.18, when the adaptive mode is activated at NC2, the performance of the system relying on the $G_{6 \times 12}$ matrix at the NC1 operating in the C mode tends to approach its capacity within a distance of 1.5 dB at an $FER = 10^{-4}$. When we further activate the adaptive mode at both the NC1 and NC2, namely the $FD + A_1$ and $FD + A_2$ modes at the NC1 and the adaptive mode at the NC2, it is expected that the performance curves closely approach their corresponding capacity, which is the one associated with the $R_e = 0.5$, as seen in Figure 5.18b. However, there is a distance of approximately 4.4 dB seen in Figure 5.18b, when we compare the capacity associated with $R_e = 0.5$ and the performance curve of the system employing the NC1 activating the $FD + A_1$ mode and the NC2 operating in the adaptive mode. We set aside for future study the issue of optimising the parameters in order to match the two adaptive modes at both the NC1 and NC2.

It is seen in Figure 5.18b that the increased aggregate multiplexing gain of both NC1 and NC2 requires reduced E_b/N_0 values for maintaining a fitted FER value. This is because the value of the aggregate multiplexing gain is higher than the increment of SNR value required to obtain the aggregate multiplexing gain. It should be noted that the increasing multiplexing gain has no impact on the FER -versus- SNR performance, where the effect of the adaptive mechanism employed at the NC1 is excluded, as seen in Figure 5.18a.

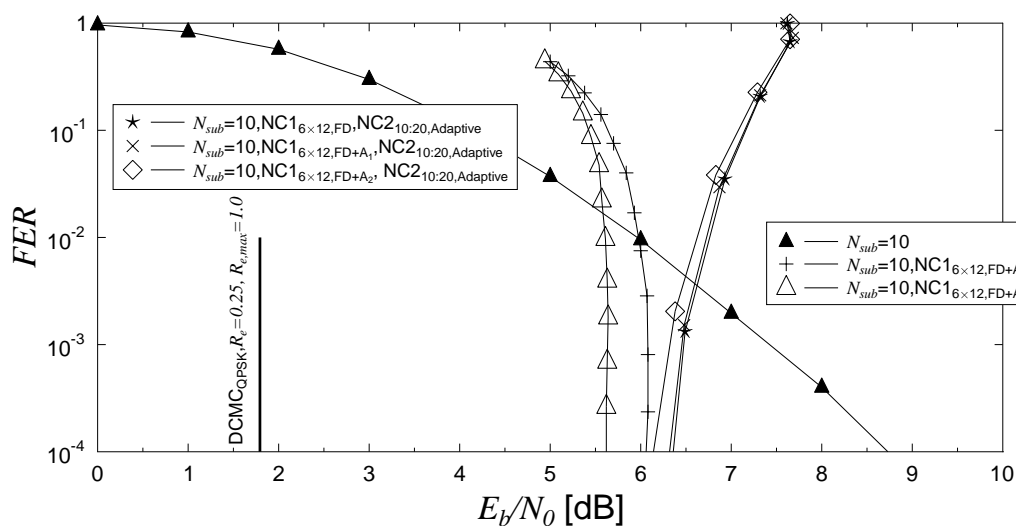
5.7 Coherent versus Non-coherent Systems

In this section, the dilemma regarding the employment of coherent versus non-coherent systems will be further discussed. As we can readily see from Section 5.1, which describes the system architecture, there is a large number of system parameters. Hence, we only used a small subset of legitimate configurations in order to support our observations pertaining to employment of the coherent or non-coherent scheme at the CC layer.

In Section 4.10.3, the performance of the Near-Capacity Multi-user Network-coding (NCMN) system is compared for different scenarios, namely for the case of employing the coherent IrCC-URC-QPSK scheme of Figure 2.19 when taking into consideration the accuracy of the channel



(a) SNR-versus-FER performance



(b) E_b/N_0 -versus-FER performance

Figure 5.18: The benefit of employing the NC2 in the GNCMN system pictured in Figure 5.1. The system comprise NC2, NC1 and CC layers having all the parameter listed in Table 5.4, where $H = 10$ and $\Theta = 20$ are employed at the NC2 layer operating in both the fixed and adaptive modes, while the $\mathbf{G}_{4 \times 8}$ and $\mathbf{G}_{6 \times 12}$ matrices are employed at the NC1 layer, whereas the IrCC-URC-QPSK scheme is activated at the CC layer for supporting the $N_{sub} = 10$ sub-frame transmission regime over wireless channels influenced by both the fast Rayleigh and block Rayleigh fadings.

estimation and the case of employing the non-coherent IrCC-URC-DQPSK scheme of Figure 2.27. We have considered different levels of channel estimation accuracy in Section 4.10.3. According to our analysis provided in Section 2.5, the performance of the single link transmission relying on the coherent IrCC-URC-QPSK scheme is superior to that supported by the non-coherent IrCC-URC-DQPSK scheme, provided that the accuracy of the channel estimator is better than $\theta = 60\%$, as defined in Section 2.5. Hence, it is expected that the same threshold of channel estimation, namely $\theta = 60\%$, is appropriate for the GNCMN system.

In order to substantiate our above-mentioned analysis, we investigate the performance of the GNCMN system employing the coherent IrCC-URC-QPSK scheme at the CC layer of Figure 5.1, when the accuracy of the channel estimator is $\theta = 50\%, 60\%, 100\%$. Then, the performance of the coherent detection based GNCMN system is compared to that of the non-coherent system relying on the IrCC-URC-DQPSK scheme. We chose the specific sub-sets of the parameters at the NC1 and NC2, which are summarised in Table 5.5.

Parameters	CC layer	
	Coherent	Non-coherent
R [BPS]	1.0(QPSK)	1.0(DQPSK)
R_c	0.5	0.5
I [iteration]	0	2
J [iteration]	30	30
N [bit]	10^6	10^6
N_{sub} [bit]	1	1
θ	50%,60%,100%	Not Applicable
Parameters	NC1 layer	
Mode	$FD + A_1, FD + A_2$	
\mathbf{G}	$\mathbf{G}_{6 \times 12}$	
M [user]	2	
k_1 [frame]	3	
k_2 [frame]	3	
R_{info}	0.5	
D_{NCMN}	$5 \leq D_{6 \times 12} \leq 7$	
Parameters	NC2 layer	
H	10	
Θ	20	
R_{info2}	1/2	
Mode	Fixed	

Table 5.5: Parameters for an example of a GNCMN system employed for characterising the threshold used for deciding whether coherent or non-coherent scheme is duly utilised.

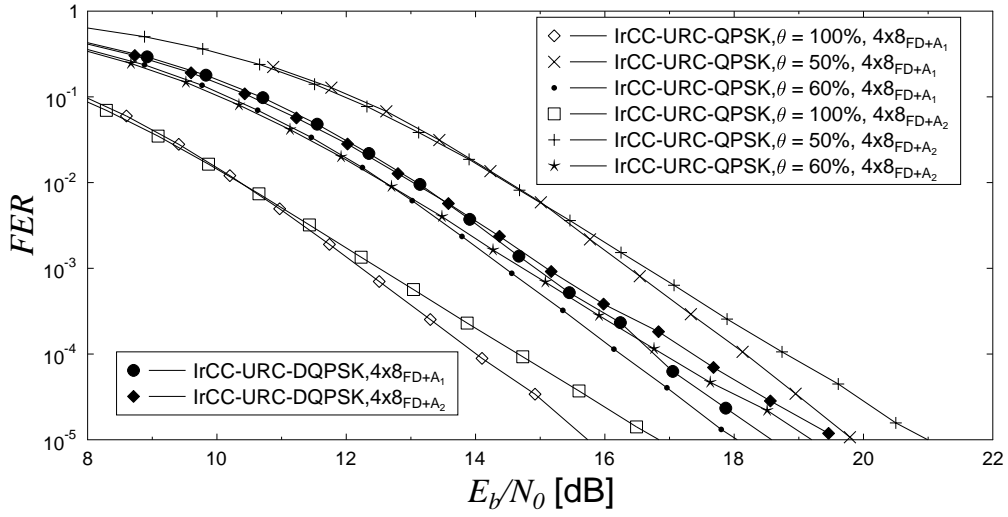
As seen in Figure 5.19, the GNCMN system supported by the coherent IrCC-URC-QPSK scheme outperforms the GNCMN system relying on the non-coherent IrCC-URC-DQPSK arrangement, when the accuracy of the channel estimation is $\theta = 100\%$. However, the performance of the system relying on the non-coherent scheme becomes superior to that of the system relying on the coherent scheme, when the channel-estimator's accuracy becomes lower than $\theta = 60\%$. Hence, we can conceive an GNCMN system capable of operating in both coherent and non-coherent modes. These modes may be switched by comparing the accuracy of the channel estimation with a pre-calculated threshold, say $\theta = 60\%$.

5.8 Chapter Summary

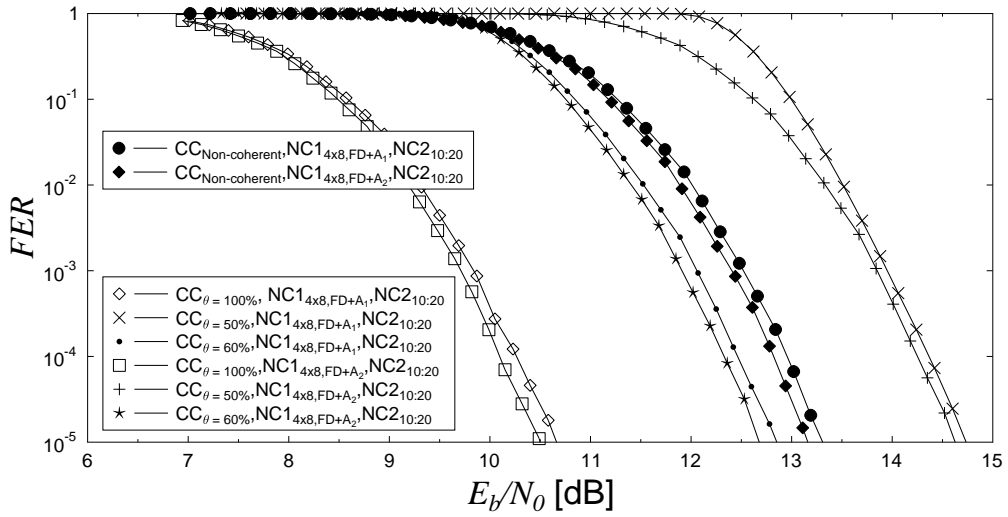
In this chapter, we have generalized the system presented in Chapter 4, in order to devise a novel system having a triple-layer coding architecture, which is named as the GNCMN system. In particular, we have developed three other single modes in addition to the existing mode of the system presented in Chapter 4 in order to form the first network coding layer, namely NC1. Furthermore, we configured the NC1 to operate in combined modes, where the single modes can be activated simultaneously, in order to attain the best possible performance. In addition to the performance bounds derived in Chapter 4 for the conventional mode of the NC1, the performance bounds for the other single modes of the NC1 have been derived for conveniently studying the system performance. We have introduced another network coding layer termed as NC2, which advocates random network codes. The outage capacity and the DCMC capacity presented in Chapter 2 is invoked for evaluating the achievable capacity of the GNCMN system. Moreover, the issue of selecting coherent or non-coherent modulation at the channel coding layer has been also discussed.

It was confirmed by our simulations results that the additional full-diversity mode devised for NC1 may assist the system in approaching its full-diversity regime, where the inter-user channels are error free. Indeed, the quantitative discrepancy is merely 0.1 dB at an $FER = 10^3$. Additionally, the two adaptive modes, namely A_1 and A_2 , are capable of improving the attainable multiplexing gain, which can reach the value of 3 dB at sufficiently high SNRs. Moreover, the FD mode and adaptive modes may be combined for exploiting the improvement of both the diversity gain and multiplexing gain.

The additional NC2 layer may be used for further improving the system's performance, albeit this is achieved at the cost of increasing both the transmission delay and complexity of the system. It was found that the optimal network coding rate of the NC2 layer is $R_{info2} = 1/2$. Given a specific network coding rate of $R_{info2} = 1/2$, a longer delay results in an improved performance supported for NC2. As a result, given a specific system performance requirement, the NC2 configuration may be optimised by determining the most appropriate network coding rate R_{info2} and the number of frames used in each coding session H .



(a) Two-layer architecture



(b) Three-layer architecture

Figure 5.19: Performance comparison of the GNCMN system comprising the NC2, NC1 and CC layers, depicted in Figure 5.1 in different configurations corresponding to different set of parameters listed in Table 5.5. The $G_{6 \times 12}$ matrix is employed at the NC1, while $H = 10$ and $\Theta = 20$ are set at the NC2 layer, as listed in Table 5.5. Both the coherent IrCC-URC-QPSK and the non-coherent IrCC-URC-DQPSK schemes are employed at the CC layer, where different levels of the channel estimation accuracy, namely $\theta = 50\%, 60\%, 100\%$, are considered for communicating over wireless channels influenced by both the fast Rayleigh and block Rayleigh fading.

The sub-frame transmission technique may also be used for improving the attainable system performance, if the system tolerates an increased delay. Then, the delays caused by the NC2 layer has to be adjusted in order for the system to meet its required performance.

Again, the channel estimation accuracy of $\theta = 60\%$ was shown to be the threshold used for deciding whether the non-coherent or the coherent modulation scheme should be used.

Conclusions and Future Works

In this chapter, we first summarise our work and findings presented throughout previous chapters in Section 6.1 before offering our future works in Section 6.2.

6.1 Conclusions

It was found in the literature of MDM presented in Section 1.1 that MDM should be concatenated with channel coding for achieving its best performance. Hence, we invoked on studying an amalgamated coded modulation scheme comprising a powerful channel code and MDM. As a result, an comparative study on the performance of the Multi-Dimensional Modulation (MDM) schemes, namely Space-Time Trellis Codes (STTCs), Space-Time Block Codes (STBCs) and Sphere-Packing-Space-Time Block Codes (SP-STBC), is presented in Section 1.1. The performance of these schemes was compared for different throughputs and frame lengths. The results of the comparison suggested in Section 1.1.4 that the STTC scheme should be favoured for its superior performance among the three schemes. As a result, the STTC scheme was chosen for our single-user cooperative system detailed in Chapter 3.

We have reviewed the literature of cooperative communications in Section 1.2.1, where a space diversity gain may be achieved by employing appropriate relays. This led to our distributed coding scheme proposed for single-user cooperative communications in Chapter 3. Based on the literature of cooperative communications in Section 1.2.1, it became explicit that network coding has been prevalently applied in cooperative communications, as shown in Figure 1.13. Hence we intensified our research on the “applications of network coding in cooperative communications”. Specifically, in Chapter 4 we proposed multi-user network coding aided cooperative systems presented and further generalised them to the multi-user multi-layer multi-mode cooperative systems detailed in Chapter 5.

In order to benchmark our near-capacity coding design, we investigated both the capacity and

the outage probability of the Continuous-input Continuous-output Memoryless Channel (CCMC), of the Discrete-input Continuous-output Memoryless Channel (DCMC) as well as that of the Differential Discrete-input Continuous-output Memoryless Channel (D-DCMC). The outage probability of the DCMC and D-DCMC may be calculated based on the associated SNR_r value corresponding to a given transmission rate R . The SNR_r value may be determined by looking up the corresponding value on the capacity curve constructed by using Equation (2.16) or by employing EXIT charts. The employment of EXIT charts used for formulating the capacity curve may be described in the following steps:

- EXIT curves pertaining to a given modulation scheme are generated for different SNR_r values.
- A single point on the capacity curves is determined by computing the area under the EXIT curve and its corresponding SNR_r .

We exemplified and formulated our near-capacity coding arrangements, namely namely our Irregular Convolutional Coded Unity Rate Coded M-ary Phase Shift Keying (IrCC-URC-MPSK), Irregular Convolutional Coded Unity Rate Coded Differential M-ary Phase Shift Keying (IrCC-URC-DMPSK) and Irregular Convolutional Coded Unity Rate Coded Space Time Trellis Coded M-ary Phase Shift Keying (IrCC-URC-STTC-MPSK) schemes, in order to approach the corresponding channel capacity. The typical three stage near-capacity coding arrangement relying on Irregular Convolutional Codes (IrCC) may be designed by carrying out the following steps:

- Optimise the inner-most two-stage coding arrangement by finding the most appropriate number of iterations associated with the affordable complexity.
- Create the EXIT curve of the amalgamated inner decoder, which has been optimised, for different SNR_r values.
- Fix the overall coding rate of the IrCC encoder and then employ the EXIT curve matching algorithm for generating the optimised weighting coefficients α_i . The number of IrCC component codes used was either 17 or 36.

For deciding whether the IrCC-URC-MPSK scheme or the IrCC-URC-DMPSK scheme should be employed, a comparison of non-coherent versus coherent systems was carried out and the effects of channel estimation were also taken into consideration. More specifically, our simulation results of Figure 2.36 suggested that a $\theta = 60\%$ channel estimation accuracy may be used for deciding whether coherent or non-coherent modulation arrangements should be activated.

The employment of sub-frame based transmissions was shown in Figure 2.33 to achieve a substantial performance improvement for our near-capacity coding scheme of Section 2.3.4 for transmission over channels subject to slow fading, where the channel coefficients varied on a frame-by-frame basis. If a system can afford a delay of $N_{sub} = 10^3$ frame duration, the performance of

the coding schemes recorded in slow-fading environment would be the same as that in fast fading environment, as evidenced by Figure 2.33.

In Section 3.3.2, we proposed a DC-IrCC-URC-STTC scheme for single-user single-antenna based cooperative relaying. In Section 3.2.4, we formulated and investigated an optimality criterion for selecting the relays by ensuring that they are capable of maintaining an open EXIT chart tunnel. The optimal relaying scheme also mitigated the problem of potential error propagation often imposed by the relays, which was achieved by selecting those specific relay nodes that were roaming near the optimal locations, where optimum in this context entailed for ensuring that the received *SNR* value required at the relay and destination nodes can be maintained simultaneously. Moreover, in Section 3.3.3.1, the dynamic relay-selection method was proposed, in order to make use of the signals transmitted from the source to the destination for the iterative decoding process employed at the destination node in order to improve the performance.

The upper and lower FER-performance bounds of Near-Capacity Multi-user Network-coding (NCMN) based systems were derived in Section 4.5. The system's FER-performance was also evaluated by Monte Carlo based simulations in Figure 4.12, in order to verify the accuracy of those bounds. These bounds guided our network coding design in Section 4.7.2 and assisted us in estimating the FER performance of the NCMN system without running extremely time-consuming Monte-Carlo simulations in Section 4.10.1. The capacity of NCMN systems was devised for the sake of benchmarking the performance of the NCMN system in different configurations. Additionally, the lower bound of the system's outage probability may be employed for estimating the size of the transfer matrix required for attaining a given diversity order.

Based on the algorithms of Section 4.3 employed for recovering the transmitted frames at the base station, we proposed a new method that we referred to as the Pragmatic Algebraic Linear Equation Method (PALEM) for accurately characterising the system's FER performance. In Section 4.9, the system's performance estimated by our PALEM was also compared to that obtained by the method used in [47], which we termed as Pure Rank Based Method (PRBM). Our proposed PALEM was shown to provide identical results in comparison to that suggested by Monte-Carlo simulations, while the PRBM always leads to optimistic results for the system performance.

We investigated our NCMN based systems combined with the IrCC-URC-MPSK and IrCC-URC-DMPSK schemes detailed in Chapter 2. These schemes approach their corresponding DCMC and D-DCMC capacities within approximately 1 dB at a *FER* of 10^{-5} . The performance of the NCMN systems relying on our realistic channel coding schemes, namely on the IrCC-URC-MPSK and IrCC-URC-DMPSK arrangement, was benchmarked against the corresponding NCMN based systems employing the idealised/perfect channel coding schemes operating at exactly the DCMC and D-DCMC capacities. The effects of errors imposed on the channel estimation were shown to be the same as those happening in the single link transmission scenario.

We generalized the NCMN system presented in Chapter 4, in order to devise a novel sys-

tem having a triple-layer coding architecture, which was termed as the Generalised Near-Capacity Multi-user Network-coding (GNCMN) system. In particular, we developed three other single modes in addition to the existing mode of the system presented in Chapter 4, in order to form the first network coding layer, namely Network Coding 1 (NC1) layer. Furthermore, we configured NC1 to operate in combined modes, where the single modes can be activated simultaneously, in order to attain the best possible performance. In addition to the performance bounds derived in Chapter 4 for the conventional mode of the NC1, the performance bounds derived for the other single modes of the NC1 have been derived for conveniently studying the system performance. We have introduced another network coding layer termed as the Network Coding 2 (NC2) layer, which advocated random network codes. The outage capacity and the DCMC capacity presented in Chapter 2 were invoked for evaluating the achievable capacity of the GNCMN system. Moreover, the issue of selecting coherent or non-coherent modulation at the physical layer has also been discussed. More specifically:

- It was confirmed by the simulations results of Figure 5.6 and Figure 5.7 that the additional full-diversity mode devised for the NC1 may assist the system in approaching its full-diversity regime, where the inter-user channels are error free. The discrepancy seen in Figure 5.6 and Figure 5.7 is merely 0.1 dB at an $FER = 10^3$. Additionally, the two adaptive modes, namely A_1 and A_2 of Section 5.1.2.3, are capable of improving the attainable multiplexing gain, which can reach the value of 3 dB at sufficiently high SNRs. Moreover, the FD mode of Section 5.1.2.2 and adaptive modes of Section 5.1.2.3 may be combined for exploiting an improved diversity gain and multiplexing gain.
- The additional NC2 layer of Section 5.1.3 may be used for further improving the system's performance at the cost of increasing both the transmission delay and complexity of the system. It was found that the optimal network coding rate of the NC2 is $R_{info2} = 1/2$. Given a specific network coding rate of $R_{info2} = 1/2$, a longer delay results in an improved performance supported by the NC2. As a result, given a specific system performance requirement, NC2 may be optimised by determining the most appropriate network coding rate R_{info2} and the number of frames H used in each coding session.
- The sub-frame transmission regime of Section 5.6.3 may also be used for improving the achievable system performance, if the system is capable of tolerating an increased delay. Once, the delay stipulated by the sub-frame transmission is fixed, the delay caused by the NC2 has to be adjusted in order for the system to meet its required performance.
- Again, in Figure 5.19 the channel estimation accuracy of $\theta = 60\%$ was shown to be the threshold used for deciding whether the non-coherent or the coherent modulation scheme should be used.

6.2 Future work

Our future work may pursue the following ideas.

In Chapter 3, the general idea of distributed coding schemes invoked for cooperative communications can be expanded to another three-stage coding arrangement, namely to IrCC-URC-STBC-SP, which was already partially investigated in Chapter 2. More specifically, it was shown in [75, 194–196] that the performance of STBC-SP systems can be further improved by concatenating SP-aided modulation with channel coding and performing symbol-to-bit demapping as well as channel decoding iteratively. A powerful IrCC-URC-STBC-SP coding scheme was designed for single-link transmission in [195]. We may apply this coding scheme for our cooperative model presented in Chapter 3. First, we may use IrCC-URC-MPSK for the source-relay link and IrCC-URC-STBC-SP for the relay-destination link. Then, we may apply SP for both the source-relay and the relay-destination links, in order to ultimately conceive a novel Distributed Concatenated IrCC-URC-STBC-SP (DC-IrCC-URC-STBC-SP) aided cooperative system.

In the Channel Coding (CC) layer of the GNCMN system presented in Figure 5.1, the coding scheme is designated for single-antenna aided transmission units. If the allocation of multiple antennas is applicable at each transmission unit in the GNCMN system, the channel coding schemes designed for our multi-antenna based system, namely for the IrCC-URC-STTC scheme detailed in Section 2.3.2, may be integrated into the CC layer of the GNCMN system, in order to conceive multi-antenna based multi-user, multi-layer, multi-mode cooperative systems.

Issues pertaining to the GNCMN optimisation need further study. As analysed in Section 5.6.5, when an adaptive mechanism is activated at both the NC1 and NC2 layers, the parameters of the two layers have to be configured so that both the information rates, namely $R_{info,A}$ of Equation (5.108) and R_{info2} of Equation (5.133), simultaneously converge to their maximum, which is equal to unity. Another suggestion was given in Section 5.5.2, where it was expected that the optimal value of the parameter Θ under the provision of other parameters in the GNCMN system may support the best possible system performance. To optimise the entire GNCMN system, a function reflecting the throughput or the diversity order of the system needs to be formed based on all the system parameters listed in Table 5.1.

The application of cognitive radio have also attracted the interest of researchers [197, 198]. Cognitive radio may be integrated into our GNCMN system at the link level, where the knowledge of channel state information may be utilised for introducing adaptive channel coding and modulation into our system. Cognitive radio may be applied at the system's scale, where the knowledge of the entire system transmission quality can be exploited for selecting the appropriate transmission regime of the system.

System's outage probability

This section is dedicated to deriving in details the performance bounds of the Near-Capacity Multi-user Network-coding (NCMN) system depicted in Figure 4.1. It should be noted that we presented an abstract version of the derivations in Section 4.5, hence the more concrete version of the derivation will be presented in the following for the sake of interested readers. Accordingly, in this section, we will first formulate the general formula of the system's outage probability in Section A.1. Major terms of the formulae derived in Section A.1 are reduced to a closed form for facilitating the derivations of the performance bounds in Section A.1.2.

A.1 Formulation of the System's Outage Probability

Let $U_{m,t} = \{u_{m,t}, u_{m,t} \in [1, \dots, M]\}$ for $\forall m \in \{1, \dots, M\}$ be a set of user indices corresponding to the specific users that are able to correctly recover an information frame $I_m(t)$ transmitted from User m during time slot t . Note that User m itself is always included in this set. Let us denote by $||U_{m,t}||$ the number of members in the set of users $U_{m,t}$, which is also the number of users that are capable of correctly detecting the information frame $I_m(t)$, and we always have

$$1 \leq ||U_{m,t}|| \leq M, \quad (\text{A.1})$$

where we use $||A||$ to represent the cardinality of the set A .

We then define the complement set of $U_{m,t}$ as $U_{m,t}^* = \{1, \dots, M\} \setminus U_{m,t}$ that comprises the indices of those users that cannot correctly recover the information frame $I_m(t)$. Hence we have

$$||U_{m,t}^*|| = M - ||U_{m,t}||. \quad (\text{A.2})$$

Let P_e be the error probability of a single link corresponding to a given SNR. Assuming that all the links/users in the network employ the same channel coding scheme, the probability that $U_{m,t}^*$ users cannot recover the information frame $I_m(t)$ is approximately $P_e^{||U_{m,t}^*||}$, which is accurate in the high SNR region.

Let us denote the set of all information frames transmitted by the users in $U_{m,t}$ during the broadcast phases as $U_{m,t}(I)$, including $I_m(t)$. Since each user broadcasts k_1 number of frames, we have:

$$||U_{m,t}(I)|| = k_1 ||U_{m,t}||. \quad (\text{A.3})$$

There are at least $||U_{m,t}(I)|| + ||U_{m,t}||k_2$ frames [47, 179], which contain the information frames transmitted by all the users of $U_{m,t}$, where the $||U_{m,t}(I)||$ information frames are transmitted during the broadcast phases, while the $||U_{m,t}||k_2$ parity frames are transmitted during the cooperative phases.

Example A.1. *In this example, we consider a system having $M = 10$ users, where each user transmits $k_1 = 2$ information frames during the broadcast phases and $k_2 = 2$ parity frames during the cooperative phases, respectively.*

Let us assume $U_{1,1} = \{1, 2, 3\}$ to be the set of user indices corresponding to the users that are able to correctly recover the information frame $I_1(1)$ transmitted by User 1 during broadcast phase 1. During the broadcast phases, the number $||U_{1,1}(I)||$ of information frames transmitted by all users of $U_{1,1}$ is $||U_{1,1}(I)|| = k_1 ||U_{1,1}|| = 6$, and all users of $U_{1,1}$ transmit $||U_{1,1}||k_2 = 6$ parity frames during the cooperative phases. We note that $||U_{1,1}(I)|| + ||U_{1,1}||k_2 = 12$ frames containing information frames are transmitted by the users in the set $U_{1,1}$.

Let us consider the information frame $I_2(2)$ transmitted by User 2 during broadcast phase 2. Assuming that we have $U_{2,2} = \{2, 4, 6\}$ and $U_{2,2} \setminus (U_{1,1} \cap U_{2,2}) = \{4, 6\}$, there are $||\{4, 6\}||k_2 = 4$ extra frames containing the information frame $I_2(2)$ transmitted by User 2 in $U_{1,1}$.

Hence, there exist at least $||U_{1,1}(I)|| + ||U_{1,1}||k_2 = 12$ frames containing information frames transmitted by all users of the set $U_{1,1}$.

It was shown in [99, 177] that there exist specific network codes that are capable of recovering X frames, if at least X frames are correctly decoded at the BS. More specifically, the network-coded codewords of such network codes are supposed to be linearly independent for all possible source-relay channel outage situations [179]. Hence, based on the assumption of having Y linearly independent frames received at the BS, a frame would be in outage only if $(Y - X + 1)$ frames or more out of Y frames were in outage, where X is the number of the information frames transmitted from the sources. Accordingly, an outage is declared for the information frame $I_m(t)$ when the direct transmission $I_m(t)$ and at least $||U_{m,t}||k_2$ out of the remaining $||U_{m,t}(I)|| - 1 + ||U_{m,t}||k_2$ received frames are in outage, which occurs with a probability given by [47, 99]

$$\begin{aligned} P_{o,m}(U_{m,t}^*) &= P_e \cdot \left[\sum_{q=0}^{||U_{m,t}(I)||-1} \binom{||U_{m,t}(I)|| - 1 + ||U_{m,t}||k_2}{||U_{m,t}||k_2 + q} P_e^{||U_{m,t}||k_2 + q} (1 - P_e)^{||U_{m,t}(I)|| - 1 - q} \right], \\ &= \sum_{q=0}^Q \binom{Q + K}{K + q} P_e^{K + q + 1} (1 - P_e)^{Q - q}, \\ &= \sum_{q=0}^Q T_q^{A_2}, \end{aligned} \quad (\text{A.4})$$

where $\binom{n}{k}$ represents the binomial coefficients, while we have Q and K defined as

$$\begin{aligned} Q &= ||U_{m,t}(I)|| - 1, \\ &= k_1 ||U_{m,t}|| - 1, \end{aligned} \quad (\text{A.5})$$

and

$$K = ||U_{m,t}|| k_2. \quad (\text{A.6})$$

However, there might be more than $||U_{m,t}(I)|| + ||U_{m,t}|| k_2$ frames [46, 47, 99, 179], which contain the information frames transmitted by all users of $U_{m,t}$. If the availability of those extra frames is taken into account, we will have

$$P_{o,m}^{True}(U_{m,t}^*) \leq P_{o,m}(U_{m,t}^*), \quad (\text{A.7})$$

where $P_{o,m}^{True}(U_{m,t}^*)$ is the true probability of the outage for the information frame $I_m(t)$. Notably, $P_{o,m}^{True}(U_{m,t}^*)$ is the outage probability for a given $U_{m,t}^*$. The system's outage probability P_o for all possible $U_{m,t}^*$ can be calculated by [99]

$$P_o = \sum_{||U_{m,t}^*||=0}^{M-1} \frac{P_e^{||U_{m,t}^*||}}{(1 - P_e)^{||U_{m,t}^*|| - M + 1}} P_{o,m}^{True}(U_{m,t}^*), \quad (\text{A.8})$$

where $\frac{P_e^{||U_{m,t}^*||}}{(1 - P_e)^{||U_{m,t}^*|| - M + 1}}$ is the probability of $||U_{m,t}^*||$ out of $M - 1$ inter-user channels in time slot t being in outage. Upon replacing Inequality (A.7) into Equation (A.8), we have:

$$P_o \leq \sum_{||U_{m,t}^*||=0}^{M-1} \frac{P_e^{||U_{m,t}^*||}}{(1 - P_e)^{||U_{m,t}^*|| - M + 1}} P_{o,m}(U_{m,t}^*), \quad (\text{A.9})$$

where $P_{o,m}(U_{m,t}^*)$ is determined by Equation (A.4).

Focusing on the region of low P_e values or small $||U_{m,t}^*||$, we always have

$$\begin{aligned} P_o &> (1 - P_e)^{M-1} P_{o,m}^{True}(U_{m,t}^*)|_{||U_{m,t}^*||=0}, \\ &> (1 - P_e)^{M-1} P_{o,m}(U_{m,t}^*)|_{||U_{m,t}^*||=0}, \end{aligned} \quad (\text{A.10})$$

since:

$$P_{o,m}^{True}(U_{m,t}^*)|_{||U_{m,t}^*||=0} = P_{o,m}(U_{m,t}^*)|_{||U_{m,t}^*||=0}. \quad (\text{A.11})$$

Bearing in mind that the condition of having linearly independent network-coded codewords at the BS is always met, when no errors are imposed by the source-relay channels, $||U_{m,t}^*|| = 0$. As a result, by replacing $||U_{m,t}^*|| = 0$ into the probability $P_{o,m}(U_{m,t}^*)$ given by Equation (A.4), the probability $P_{o,m}(U_{m,t}^*)|_{||U_{m,t}^*||=0}$ can be expressed as

$$\begin{aligned} P_{o,m}(U_{m,t}^*)|_{||U_{m,t}^*||=0} &= P_e \cdot \left[\sum_{i=0}^{Mk_1-1} \binom{Mk_1-1+Mk_2}{Mk_2+i} P_e^{Mk_2+i} (1 - P_e)^{Mk_1-1-i} \right], \\ &= \sum_{b=0}^B \binom{B+F}{F+b} P_e^{F+b+1} (1 - P_e)^{B-b}, \end{aligned} \quad (\text{A.12})$$

while for the sake of brevity we denote B and F as

$$B = Mk_1 - 1, \quad (\text{A.13})$$

and

$$F = Mk_2. \quad (\text{A.14})$$

In the next sections, we will calculate the range of the outage probabilities $P_{o,m}(U_{m,t}^*)$ and $P_{o,m}(U_{m,t}^*)|_{\|U_{m,t}^*\|=0}$, in order to determine the upper and lower bounds of the system's outage probability from Inequality (A.9) and Inequality (A.10).

A.1.1 Outage probability of a given frame

In this section, we specify the range of outage probabilities $P_{o,m}(U_{m,t}^*)$ of Equation (A.4) and $P_{o,m}(U_{m,t}^*)|_{\|U_{m,t}^*\|=0}$ of Equation (A.12), which have an identical formulation, if we consider values Q, K equivalent to B, F , respectively. Let us consider a function $f(n)$ as a ratio of two consecutive terms in either Equation (A.4) or Equation (A.12)

$$\begin{aligned} f(n) &= \frac{\text{Term}_{n+1}}{\text{Term}_n} = \frac{\binom{Q+K}{K+n+1} P_e^{K+n+1} (1-P_e)^{Q-n-1}}{\binom{Q+K}{K+n} P_e^{K+n} (1-P_e)^{Q-n}} \\ &= \frac{(Q-n)P_e}{(K+n+1)(1-P_e)}, \end{aligned} \quad (\text{A.15})$$

where we have $\text{Term}_n = \binom{Q+K}{K+n} P_e^{K+n+1} (1-P_e)^{Q-n}$. We can then find the derivative $f'(n)$ of the function $f(n)$ with respect to the variable n as follows

$$f'(n) = \frac{-(Q+K+1)P_e}{(K+n+1)^2(1-P_e)}. \quad (\text{A.16})$$

As seen in (A.16), we have $f'(n) < 0$ for $\forall n \in \{0, \dots, Q-1\}$, which suggests that the function $f(n)$ increases, as long as the variable n decreases. Thus, we have the following approximation

$$\begin{aligned} f(Q-1) &\leq f(n) \leq f(0), \\ \frac{P_e}{(K+Q)(1-P_e)} &\leq f(n) \leq \frac{QP_e}{(K+1)(1-P_e)}. \end{aligned} \quad (\text{A.17})$$

Given an arbitrary number S , we have the following series expansion [184]

$$\frac{S^{k+1} - 1}{S - 1} = 1 + S + S^2 + \dots + S^k. \quad (\text{A.18})$$

In addition, we can rewrite Equation (A.4) as

$$\begin{aligned} P_{o,m}(U_{m,t}^*) &= \sum_{q=0}^Q \text{Term}_q, \\ &= \text{Term}_0 + \text{Term}_0 f(n) + \text{Term}_0 [f(n)]^2 + \dots + \text{Term}_0 [f(n)]^Q, \\ &= \text{Term}_0 \left[1 + f(n) + [f(n)]^2 + \dots + [f(n)]^Q \right], \end{aligned} \quad (\text{A.19})$$

where we have $Term_0 = \binom{Q+K}{K} P_e^{K+1} (1 - P_e)^Q$, which comes from the general formula of Equation (A.4). Applying the series expansion of Equation (A.18) for Equation (A.19), we obtain the outage probability $P_{o,m}(U_{m,t}^*)$ as follows

$$P_{o,m}(U_{m,t}^*) = Term_0 \frac{[f(n)]^{Q+1} - 1}{f(n) - 1}. \quad (A.20)$$

It is clearly seen that the probability $P_{o,m}(U_{m,t}^*)$ in Equation (A.19) increases, as the ratio $f(n)$ increases. Taking the approximation of Inequality (A.17) into account, we arrive at the following inequalities:

$$\begin{aligned} P_{o,m}(U_{m,t}^*) &\leq P_{o,m}(U_{m,t}^*)|_{f(n)=f(0)}, \\ &\leq Term_0 \frac{[f(0)]^{Q+1} - 1}{f(0) - 1}, \\ &\leq \underbrace{\binom{Q+K}{K} P_e^{K+1} (1 - P_e)^Q}_{=Term_0} \left[\frac{[f(0)]^{Q+1} - 1}{f(0) - 1} \right], \end{aligned} \quad (A.21)$$

and

$$\begin{aligned} P_{o,m}(U_{m,t}^*) &\geq P_{o,m}(U_{m,t}^*)|_{f(n)=f(Q-1)}, \\ &\geq Term_0 \frac{[f(Q-1)]^{Q+1} - 1}{f(Q-1) - 1}, \\ &\geq \underbrace{\binom{Q+K}{K} P_e^{K+1} (1 - P_e)^Q}_{=Term_0} \left[\frac{[f(Q-1)]^{Q+1} - 1}{f(Q-1) - 1} \right]. \end{aligned} \quad (A.22)$$

Based on Inequality (A.17), we have

$$\begin{aligned} f(0) &= \frac{\overbrace{Q}^{=\beta}}{(K+1)} \frac{P_e}{(1-P_e)}, \\ &= \frac{\beta P_e}{1-P_e}, \end{aligned} \quad (A.23)$$

and

$$\begin{aligned} f(Q-1) &= \frac{\overbrace{1}^{=\alpha}}{(K+Q)} \frac{P_e}{(1-P_e)}, \\ &= \frac{\alpha P_e}{1-P_e}, \end{aligned} \quad (A.24)$$

where we have $\beta = Q/(K+1)$ and $\alpha = 1/(K+Q)$. Upon substituting Equation (A.23) into Inequality (A.21), we have

$$\begin{aligned} P_{o,m}(U_{m,t}^*) &\leq \binom{Q+K}{K} P_e^{K+1} (1 - P_e)^Q \frac{\overbrace{\left[\frac{[\frac{\beta P_e}{1-P_e}]^{Q+1} - 1}{\frac{\beta P_e}{1-P_e} - 1} \right]}^{=\frac{(\beta P_e)^{Q+1} - (1-P_e)^{Q+1}}{(1-P_e)^Q (\beta P_e + P_e - 1)}}}{\frac{\beta P_e}{1-P_e} - 1}, \\ &\leq \binom{Q+K}{K} P_e^{K+1} \left[\frac{(\beta P_e)^{Q+1} - (1-P_e)^{Q+1}}{\beta P_e + P_e - 1} \right]. \end{aligned} \quad (A.25)$$

Similarly, by substituting $f(Q - 1)$ of Equation (A.24) into Inequality (A.22), we arrive at:

$$\begin{aligned}
P_{o,m}(U_{m,t}^*) &\geq \binom{Q+K}{K} P_e^{K+1} (1-P_e)^Q \underbrace{\left[\frac{[\frac{\alpha P_e}{1-P_e}]^{Q+1} - 1}{\frac{\alpha P_e}{1-P_e} - 1} \right]}_{= \frac{(\alpha P_e)^{Q+1} - (1-P_e)^{Q+1}}{(1-P_e)^Q (\alpha P_e + P_e - 1)}}, \\
&\geq \binom{Q+K}{K} P_e^{K+1} \underbrace{\left[\frac{(\alpha P_e)^{Q+1} - (1-P_e)^{Q+1}}{\alpha P_e + P_e - 1} \right]}_{= M_u}. \tag{A.26}
\end{aligned}$$

A.1.1.1 Approximated maximum value of the probability $P_{o,m}(U_{m,t}^*)$

Let us now consider the term M_u in Inequality (A.26), where M_u can be rewritten as:

$$M_u = \frac{(1-P_e)^{Q+1} - (\beta P_e)^{Q+1}}{1-P_e - \beta P_e}. \tag{A.27}$$

Focusing our attention on the case of $P_e \ll 1$ leads to the expressions $(1-P_e)^{Q+1} < (1-P_e)$ and $(\beta P_e)^{Q+1} \approx 0$. We then take these expressions into consideration and arrive at the following approximation

$$M_u < \underbrace{\frac{1-P_e}{1-P_e - \beta P_e}}_{= M_{u1}}, \tag{A.28}$$

where M_{u1} is reformulated as

$$\begin{aligned}
M_{u1} &= \frac{1-P_e}{1-P_e - \beta P_e} \\
&= 1 + \frac{\beta P_e}{1-P_e - \beta P_e}. \tag{A.29}
\end{aligned}$$

According to Equation (A.5), Equation (A.6) and Equation (A.23), the value β may be expressed as

$$\begin{aligned}
\beta &= \frac{Q}{K+1}, \\
&= \frac{\|U_{m,t}(I)\| - 1}{\|U_{m,t}\|k_2 + 1}, \\
&= \frac{\|U_{m,t}\|k_1 - 1}{\|U_{m,t}\|k_2 + 1}. \tag{A.30}
\end{aligned}$$

It is plausible that β increases upon increasing the cardinality $\|U_{m,t}\|$, where $\|U_{m,t}\| \in [1, \dots, M]$.

Hence, we can infer that

$$\begin{aligned}
\beta &\leq \beta_{\|U_{m,t}\|=M}, \\
&\leq \underbrace{\frac{Mk_1 - 1}{Mk_2 + 1}}_{= \beta^{\max}}. \tag{A.31}
\end{aligned}$$

where we have β^{\max} given by

$$\beta^{\max} = \frac{Mk_1 - 1}{Mk_2 + 1}. \quad (\text{A.32})$$

Observing the term M_{u1} given in Equation (A.29), we find that the term M_{u1} increases as the value β increases, provided that $P_e \ll 1$. Hence, we can infer that

$$\begin{aligned} M_{u1} &\leq M_{u1} |_{\beta=\beta^{\max}}, \\ &\leq \underbrace{1 + \frac{\frac{Mk_1-1}{Mk_2+1}P_e}{1 - P_e - \frac{Mk_1-1}{Mk_2+1}P_e}}_{=M_u^{\max}}, \end{aligned} \quad (\text{A.33})$$

where M_u^{\max} is represented as

$$M_u^{\max} = 1 + \frac{\frac{Mk_1-1}{Mk_2+1}P_e}{1 - P_e - \frac{Mk_1-1}{Mk_2+1}P_e}. \quad (\text{A.34})$$

By combining the Inequality (A.28) and Inequality (A.33), we have

$$\begin{aligned} M_u &< M_{u1} \leq M_u^{\max}, \\ M_u &< M_u^{\max}. \end{aligned} \quad (\text{A.35})$$

Upon substituting M_u^{\max} of Equation (A.34) into the Inequality (A.35), we obtain

$$M_u < \underbrace{1 + \frac{\frac{Mk_1-1}{Mk_2+1}P_e}{1 - P_e - \frac{Mk_1-1}{Mk_2+1}P_e}}_{=M_u^{\max}}. \quad (\text{A.36})$$

Upon substituting the approximation of M_u given by Inequality (A.36) into Inequality (A.26), we arrive at the approximation of the probability $P_{o,m}(U_{m,t}^*)$ in the following form:

$$\begin{aligned} P_{o,m}(U_{m,t}^*) &\leq \binom{Q+K}{K} P_e^{K+1} \underbrace{\left[\frac{(\beta P_e)^{Q+1} - (1-P_e)^{Q+1}}{\beta P_e + P_e - 1} \right]}_{=M_u}, \\ &< \underbrace{\binom{Q+K}{K} P_e^{K+1} \left[1 + \frac{\frac{Mk_1-1}{Mk_2+1}P_e}{1 - P_e - \frac{Mk_1-1}{Mk_2+1}P_e} \right]}_{=M_u^{\max}} \underbrace{\phantom{\binom{Q+K}{K} P_e^{K+1} \left[1 + \frac{\frac{Mk_1-1}{Mk_2+1}P_e}{1 - P_e - \frac{Mk_1-1}{Mk_2+1}P_e} \right]}}_{=P_{o,m}^{\max}(U_{m,t}^*)}, \end{aligned} \quad (\text{A.37})$$

where the approximate maximum value $P_{o,m}^{\max}(U_{m,t}^*)$ of the probability $P_{o,m}(U_{m,t}^*)$ is given by

$$\begin{aligned} P_{o,m}^{\max}(U_{m,t}^*) &= \binom{Q+K}{K} P_e^{K+1} \underbrace{\left[1 + \frac{\frac{Mk_1-1}{Mk_2+1}P_e}{1 - P_e - \frac{Mk_1-1}{Mk_2+1}P_e} \right]}_{=M_u^{\max}}, \\ &= \binom{Q+K}{K} P_e^{K+1} M_u^{\max}. \end{aligned} \quad (\text{A.38})$$

A.1.1.2 Approximated minimum value of the probability $P_{o,m}(U_{m,t}^*)|_{\|U_{m,t}^*\|=0}$

Let us repeat the approximation given by Inequality (A.26) as follows

$$P_{o,m}(U_{m,t}^*) \geq \binom{Q+K}{K} P_e^{K+1} \left[\frac{(\alpha P_e)^{Q+1} - (1-P_e)^{Q+1}}{\alpha P_e + P_e - 1} \right], \quad (\text{A.39})$$

where $\alpha = 1/(Q+K)$. Upon replacing Q and K in Inequality (A.26) by B and F , respectively, we obtain the approximation of $P_{o,m}(U_{m,t}^*)|_{\|U_{m,t}^*\|=0}$ in Equation (A.12) with the aid of Inequality (A.39) as:

$$\begin{aligned} P_{o,m}(U_{m,t}^*)|_{\|U_{m,t}^*\|=0} &= \sum_{b=0}^B \binom{B+F}{F+b} P_e^{F+b+1} (1-P_e)^{B-b}, \\ &\geq \binom{B+F}{F} P_e^{F+1} \left[\frac{(\alpha' P_e)^{Q+1} - (1-P_e)^{Q+1}}{\alpha' P_e + P_e - 1} \right], \end{aligned} \quad (\text{A.40})$$

where $\alpha' = 1/(B+F)$. Furthermore, we substitute $B = Mk_1 - 1$ and $F = Mk_2$ into (A.40) to obtain

$$P_{o,m}(U_{m,t}^*)|_{\|U_{m,t}^*\|=0} \geq \binom{Mk_1 + Mk_2 - 1}{Mk_2} P_e^{Mk_2+1} \left[\frac{\left(\frac{P_e}{Mk_1 + Mk_2 - 1}\right)^{Mk_1} - (1-P_e)^{Mk_1}}{\frac{P_e}{Mk_1 + Mk_2 - 1} + P_e - 1} \right]. \quad (\text{A.41})$$

A.1.2 Bounding the system's outage probability

In this section, we use the probability $P_{o,m}^{\max}(U_{m,t}^*)$ of (A.38) and the approximation of $P_{o,m}(U_{m,t}^*)|_{\|U_{m,t}^*\|=0}$ given by (A.41) for deriving the upper and lower bounds of the system's outage probability P_o .

A.1.2.1 Upper bound of the system's outage probability

This section is dedicated for deriving the upper bound expression of the system's outage probability determined by Inequality (A.9), which is repeated here as:

$$P_o \leq \sum_{\|U_{m,t}^*\|=0}^{M-1} \frac{P_e^{\|U_{m,t}^*\|}}{(1-P_e)^{\|U_{m,t}^*\|-M+1}} P_{o,m}(U_{m,t}^*). \quad (\text{A.42})$$

Let us begin by replacing $P_{o,m}^{\max}(U_{m,t}^*)$ given in Equation (A.38) into Inequality (A.42), in order to arrive at

$$\begin{aligned} P_o &< \sum_{\|U_{m,t}^*\|=0}^{M-1} \frac{P_e^{\|U_{m,t}^*\|}}{(1-P_e)^{\|U_{m,t}^*\|-M+1}} \underbrace{P_{o,m}^{\max}(U_{m,t}^*)}_{> P_{o,m}(U_{m,t}^*)}, \\ &< \sum_{\|U_{m,t}^*\|=0}^{M-1} \frac{P_e^{\|U_{m,t}^*\|}}{(1-P_e)^{\|U_{m,t}^*\|-M+1}} \underbrace{\binom{Q+K}{K} P_e^{K+1} M_u^{\max}}_{= P_{o,m}^{\max}(U_{m,t}^*)}, \\ &< \sum_{\|U_{m,t}^*\|=0}^{M-1} \binom{Q+K}{K} \underbrace{\frac{P_e^{\|U_{m,t}^*\|}}{(1-P_e)^{\|U_{m,t}^*\|-M+1}} P_e^{K+1} M_u^{\max}}_{= T_o^{\text{Upper}}}. \end{aligned} \quad (\text{A.43})$$

We then define the value T_o^{Upper} as

$$\begin{aligned} T_o^{Upper} &= \frac{P_e^{||U_{m,t}^*||}}{(1 - P_e)^{||U_{m,t}^*|| - M + 1}} P_e^{K+1} M_u^{\max}, \\ &= \frac{P_e^{||U_{m,t}^*||}}{(1 - P_e)^{||U_{m,t}^*|| - M + 1}} P_e^{\overbrace{(M - ||U_{m,t}^*||)k_2}^{=K - ||U_{m,t}^*||k_2}} P_e^{||U_{m,t}^*||} M_u^{\max}. \end{aligned} \quad (\text{A.44})$$

Accordingly, Inequality (A.43) becomes

$$P_o < \sum_{||U_{m,t}^*||=0}^{M-1} \binom{Q+K}{K} T_o^{Upper}. \quad (\text{A.45})$$

Furthermore, Inequality (A.45) can be rewritten as

$$P_o < \underbrace{\sum_{||U_{m,t}^*||=0}^{M-1} \left[\binom{Q+K}{K} - \binom{B+F}{F} \right] T_o^{Upper}}_{=\Delta} + \underbrace{\sum_{||U_{m,t}^*||=0}^{M-1} \binom{B+F}{F} T_o^{Upper}}_{=\chi}. \quad (\text{A.46})$$

Bearing in mind the fact that $\binom{Q+K}{K} \leq \binom{B+F}{F}$, the term Δ defined in Inequality (A.46) always conforms to an inequality as:

$$\Delta < 0. \quad (\text{A.47})$$

Focusing our attention to the case of having $||U_{m,t}^*|| = (M - 1)$, we infer to the approximation as:

$$\Delta \leq \underbrace{\Delta_{||U_{m,t}^*||=M-1}}_{=\Omega} \quad (\text{A.48})$$

where the term Ω is defined as:

$$\begin{aligned} \Omega &= \Delta_{||U_{m,t}^*||=M-1}, \\ &= \left[\left[\binom{Q+K}{K} - \binom{B+F}{F} \right] T_o^{Upper} \right]_{||U_{m,t}^*||=M-1}, \\ &= \left[\left[\binom{k_1 - 1 + k_2}{k_2} - \binom{Mk_1 - 1 + Mk_2}{Mk_2} \right] T_o^{Upper} \right]_{||U_{m,t}^*||=M-1}. \end{aligned} \quad (\text{A.49})$$

Let us now reduce the term T_o^{Upper} given by Equation (A.44). Consider the ratio R_o of two consecutive terms T_o^{Upper} corresponding to two consecutive indices of $||U_{m,t}^*||$, we define the following ratio

$$\begin{aligned} R_o &= \frac{T_o^{Upper} ||U_{m,t}^*||}{T_o^{Upper} ||U_{m,t}^*|| + 1}, \\ &= P_e^{k_2 - 1} (1 - P_e). \end{aligned} \quad (\text{A.50})$$

Hence, we can rewrite the term χ of Inequality (A.46) as follows

$$\begin{aligned}
\chi &= \binom{B+F}{F} \sum_{\|U_{m,t}^*\|=0}^{M-1} T_o^{Upper} \|U_{m,t}^*\|, \\
&= \binom{B+F}{F} \left(T_o^{Upper}_{M-1} + T_o^{Upper}_{M-2} \dots + T_o^{Upper}_0 \right), \\
&= \binom{B+F}{F} \left(T_o^{Upper}_{M-1} + T_o^{Upper}_{M-1} (R_o)^1 + \dots + T_o^{Upper}_{M-1} (R_o)^{M-1} \right), \\
&= \binom{B+F}{F} T_o^{Upper}_{M-1} \left[1 + (R_o)^1 + \dots + (R_o)^{M-1} \right], \tag{A.51}
\end{aligned}$$

where $T_o^{Upper}_{M-1}$ is formulated as

$$\begin{aligned}
T_o^{Upper}_{M-1} &= P_e^{M-1+(M-M+1)k_2+1} (1 - P_e)^{M-1-(M-1)} M_u^{\max}, \\
&= P_e^{M+k_2} M_u^{\max}. \tag{A.52}
\end{aligned}$$

Again, let us exploit the series expansion of

$$\frac{S^{k+1} - 1}{S - 1} = 1 + S + S^2 + \dots + S^k, \tag{A.53}$$

where S is an arbitrary number.

Upon exploiting Equation (A.52) and Equation (A.53) in Equation (A.51), we finally obtain χ as follows

$$\begin{aligned}
\chi &= T_o^{Upper}_{M-1} \left[1 + (R_o)^1 + \dots + (R_o)^{M-1} \right], \\
&= T_o^{Upper}_{M-1} \left[\frac{(R_o)^M - 1}{R_o - 1} \right], \\
&= \underbrace{P_e^{M+k_2} M_u^{\max}}_{=T_o^{Upper}_{M-1}} \left[\frac{(R_o)^M - 1}{R_o - 1} \right]. \tag{A.54}
\end{aligned}$$

Upon employing the results of Equation (A.48) and Equation (A.54), we can further approximate Inequality (A.46):

$$\begin{aligned}
P_o &< \underbrace{\sum_{\|U_{m,t}^*\|=0}^{M-1} \left[\binom{Q+K}{K} - \binom{B+F}{F} \right] T_o^{Upper}}_{=\Delta} + \underbrace{\sum_{\|U_{m,t}^*\|=0}^{M-1} \binom{B+F}{F} T_o^{Upper}}_{=\chi}, \\
&< \underbrace{\underbrace{\Omega}_{\geq \Delta} + \underbrace{\binom{B+F}{F} P_e^{M+k_2} M_u^{\max} \left[\frac{(R_o)^M - 1}{R_o - 1} \right]}_{=\chi}}_{=P_o^{Upper}}. \tag{A.55}
\end{aligned}$$

Hence, we define the strict upper bound of the system's outage probability as:

$$P_o^{Upper} = \Omega + \binom{B+F}{F} P_e^{M+k_2} M_u^{\max} \left[\frac{(R_o)^M - 1}{R_o - 1} \right], \tag{A.56}$$

where the terms of Ω , M_u^{\max} and R_o are defined by Equation (A.49), Equation (A.34) and Equation (A.50), respectively.

A.1.2.2 Lower bound of system's outage probability

Below we repeat Inequality (A.10), which provides the formula for determining the lower bound of system's outage probability as

$$P_o > (1 - P_e)^{M-1} P_{o,m}(U_{m,t}^*)|_{\|U_{m,t}^*\|=0}. \quad (\text{A.57})$$

By combining Inequality (A.57) and the approximation of Inequality (A.41) for expressing the probability $P_{o,m}(U_{m,t}^*)|_{\|U_{m,t}^*\|=0}$, which is repeated as follows:

$$P_{o,m}(U_{m,t}^*)|_{\|U_{m,t}^*\|=0} \geq \binom{Mk_1 + Mk_2 - 1}{Mk_2} P_e^{Mk_2+1} \left[\frac{\left(\frac{P_e}{Mk_1 + Mk_2 - 1}\right)^{Mk_1} - (1 - P_e)^{Mk_1}}{\frac{P_e}{Mk_1 + Mk_2 - 1} + P_e - 1} \right], \quad (\text{A.58})$$

we arrive at

$$\begin{aligned} P_o &> (1 - P_e)^{M-1} P_{o,m}(U_{m,t}^*)|_{\|U_{m,t}^*\|=0}, \\ &> \underbrace{(1 - P_e)^{M-1} \binom{Mk_1 + Mk_2 - 1}{Mk_2} P_e^{Mk_2+1} \left[\frac{\left(\frac{P_e}{Mk_1 + Mk_2 - 1}\right)^{Mk_1} - (1 - P_e)^{Mk_1}}{\frac{P_e}{Mk_1 + Mk_2 - 1} + P_e - 1} \right]}_{=P_o^{Lower}}, \end{aligned} \quad (\text{A.59})$$

where we define P_o^{Lower} as the strict lower bound of the system's outage probability, which is given by

$$P_o^{Lower} = \binom{Mk_1 + Mk_2 - 1}{Mk_2} \frac{P_e^{Mk_2+1}}{(1 - P_e)^{1-M}} \left[\frac{\left(\frac{P_e}{Mk_1 + Mk_2 - 1}\right)^{Mk_1} - (1 - P_e)^{Mk_1}}{\frac{P_e}{Mk_1 + Mk_2 - 1} + P_e - 1} \right]. \quad (\text{A.60})$$

Modem Channel Emulator

The Modem Channel Emulator Method (MCEM) is used for avoiding repeating the same simulation by employing simulation results previously produced. It is especially beneficial for running simulation, in order to obtain performances of systems comprising a large number of transmission links, namely the NCMN system presented in Figure 4.1 and the GNCMN system portrayed in Figure 5.1. Hence, the MCEM was employed for obtaining the simulation results presented in Chapter 4 and Chapter 5.

Assume that in a simulation we have transmitted N_f number of frames, which were built from N_b number of bits. The length L of the frame is given by

$$N = \frac{N_b}{N_f}. \quad (\text{B.1})$$

The average FER given by simulation has to obey:

$$FER = \frac{E_f}{N_f}, \quad (\text{B.2})$$

where E_f is the number of erroneous frames within the N_f transmitted frames. Similarly, the corresponding average BER has to satisfy:

$$BER = \frac{E_b}{N_b}, \quad (\text{B.3})$$

where E_b is the number of erroneous bits within the N_b number of transmitted bits.

It is desirable to calculate BER for a given transmitted frame, which is erroneous. We assume that these erroneous bits are distributed equally to all erroneous frames, then the number of erroneous bits within an erroneous frame is represented by:

$$E_b^f = \frac{E_b}{E_f}. \quad (\text{B.4})$$

Since we have the frame length N specified in (B.1), the BER_f calculated for an erroneous frame

is given by:

$$\begin{aligned}
 BER_f &= \frac{E_b^f}{L}, \\
 &= \frac{E_b/E_f}{N_b/N_f'}, \\
 &= \frac{BER}{FER'} \tag{B.5}
 \end{aligned}$$

If BER and FER are known by simulations, which have been conducted, then it is possible to emulate the system without having to rerun the simulations. As a result, the operation of the MCEM can be carried out by following two main steps.

1. Firstly, from the known FER , a new transmission frame is judged to be erroneous or not by using a process briefly illustrated in Figure B.1. The FER is equal to the occurrence's probability P_e of an erroneous frame, which is proportional to the shaded region. An error-free frame occurs with a probability of $P_c = (1 - FER)$, which is also proportional to the unshaded region. Then, this process is akin to throwing a stone/dart onto the circular chart of Figure B.1. Accordingly, the frame will be considered erroneous if the stone lands on the shaded region. By contrast, if the stone lands on the unshaded region, the frame is then considered error free.
2. The second step in the emulation is as follows. If the frame is error free, then we do not corrupt the frame. Otherwise, we need to decide if each of the bits within the frame is erroneous. Similar to the manner conducted in the previous step for frames, we again can corrupt the bits within the erroneous frame according the BER for the erroneous frame. More specifically, we need to throw E_b^f number of stones onto another circular chart, where the shaded region is proportional to $P_e = BER_f$. Each time a stone lands on the shaded region, we corrupt one corresponding bit.

In order to obtain BER and FER associated with a given SNR value, which is between two SNR points of the previous simulation, interpolation method can be applied to get the associated BER and FER .

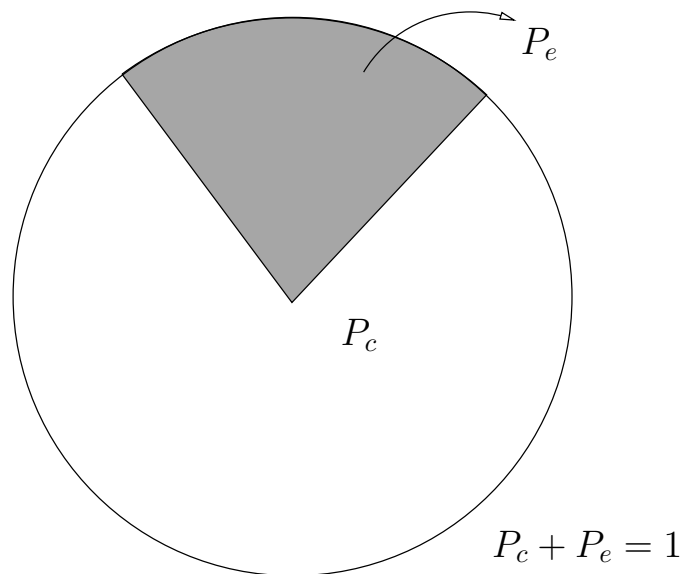


Figure B.1: Illustration of probabilities, where P_e is the probability of erroneous detection and P_c is the probability of correct detection.

Adaptive mode 2: Performance Bound of the System Performance

This section is dedicated to deriving in details the performance bounds of the GNCCMN system depicted in Figure 5.1. The GNCCMN system comprises the Channel Code (CC) and Network Coding 1 (NC1), where NC1 operates in the A_2 mode detailed in Section 5.1.2.3. Note that we presented an abstract version of the derivation in Section 5.2.2.2, hence the more concrete version of the derivation will be presented in the following for the sake of interested readers.

In contrast to the A_1 mode of Figure 5.1, it is suggested by Equation (5.59) and Equation (5.60) that changing the number of parity frames k_2 transmitted in the cooperative phases results in an increased multiplexing gain at the cost of a reduced diversity gain. As a result of the decreased diversity gain, the condition given in Equation (5.86) is no longer satisfied, thus the procedure used for estimating the performance bounds associated with the A_1 mode presented in Section 5.2.2.1 cannot be employed for formulating the performance bounds of the system employing the A_2 mode.

Alternative, we need to derive the two components affecting the performance of the system, namely the outage probability of the system associated with the reduced diversity gain and the increased multiplexing gain achieved by activating the A_2 mode. Accordingly,

- In Section C.1, the system's outage probability corresponding to the scenario of applying the A_2 mode is formulated in Section C.1.
- In Section C.2, the important terms in the formula of the system's outage probability derived in Section C.1 are reduced for facilitating the derivations of the performance bounds.
- In Section C.3, the system's performance bounds are derived by combining the two components affecting the system performance.

C.1 Outage Probability of the System Employing the A_2 Mode

Let us now invoke the approach exploited in Section 4.5 for determining the performance bounds of the system having the NC1 layer operating in the C mode of Figure 5.1. Let $U_{m,t} = \{u_{m,t}, u_{m,t} \in [1, \dots, M]\}$ for $\forall m \in \{1, \dots, M\}$ be a set of user indices corresponding to the specific users that are able to correctly recover an Information Frame (IF) $I_m(t)$ transmitted from User m during time slot t . Note that User m is always included in this set. Let us denote the number of members in the set of users $U_{m,t}$, which also represents the number of users capable of correctly detecting the information frame $I_m(t)$ by $||U_{m,t}||$, and we always have

$$1 \leq ||U_{m,t}|| \leq M, \quad (\text{C.1})$$

where we use $||A||$ to represent the cardinality of the set A .

We then define the complement set of $U_{m,t}$ as $U_{m,t}^* = \{1, \dots, M\} \setminus U_{m,t}$ that comprises the indices of those users that cannot correctly recover the information frame $I_m(t)$. Hence we have

$$||U_{m,t}^*|| = M - ||U_{m,t}||. \quad (\text{C.2})$$

Let P_e be the error probability of a single link corresponding to a given SNR. Assuming that all the links/users in the network employ the same channel coding scheme, the probability that $U_{m,t}^*$ users cannot recover the information frame $I_m(t)$ is approximately $P_e^{||U_{m,t}^*||}$, which is accurate in the high SNR region.

Let us denote the set of all IFs transmitted by the users in $U_{m,t}$ during the broadcast phases by $U_{m,t}(I)$, including $I_m(t)$. Since each user broadcasts k_1 number of frames, we have:

$$||U_{m,t}(I)|| = k_1 ||U_{m,t}||. \quad (\text{C.3})$$

Let us additionally define $D_{m,t} = \{d_{m,t}, d_{m,t} \in [1, \dots, ||U_{m,t}|| - 1]\}$ as the set of user indices belonging to $U_{m,t}$ but excluding User m , provided that all the IFs transmitted by all users of $D_{m,t}$ have been successfully recovered by the BS by the end of BPs. Accordingly, we have [12]

$$||U_{m,t}|| - ||D_{m,t}|| \geq 1. \quad (\text{C.4})$$

Bearing in mind Equation (5.59) and Equation (5.60), there are at least Γ frames containing the IF transmitted by all the users of $U_{m,t}$, where the value of Γ is specified by:

$$\Gamma = ||U_{m,t}(I)|| + (||U_{m,t}|| - ||D_{m,t}||)k_2 + ||D_{m,t}||, \quad (\text{C.5})$$

where the $||U_{m,t}(I)||$ IFs are transmitted during the broadcast phases, while the $||U_{m,t}||$ PFs are transmitted during the cooperative phases. Taking Inequality (C.4) into consideration, we may arrive at an approximation of Γ as:

$$||U_{m,t}(I)|| + k_2 + ||U_{m,t}|| - 1 \leq \Gamma \leq ||U_{m,t}(I)|| + ||U_{m,t}||k_2, \quad (\text{C.6})$$

It was proved in [99, 177] that there exist network codes that facilitate recovery of X information frames, provided that at least X frames are correctly decoded at the BS. More specifically, the network codewords of such network codes are supposed to be linearly independent for all possible source-relay channel outage situations [179]. Hence, under the assumption of having Y linearly independent frames received at the BS, a frame would be in outage only if at least $(Y - X + 1)$ frames out of Y frames were in outage, where X is the number of the IFs transmitted from the sources. Then, it may be shown that the outage probability is given by:

$$P_m^{A_2}(U_{m,t}^*) = P_e \cdot \left[\sum_{i=0}^{||U_{m,t}(I)||-1} \frac{\binom{||U_{m,t}(I)||+(||U_{m,t}||-||D_{m,t}||)k_2+||D_{m,t}||-1}{(||U_{m,t}||-||D_{m,t}||)k_2+||D_{m,t}||+i} P_e^{||U_{m,t}||k_2+i}}{(1-P_e)^{i+1-||U_{m,t}(I)||}} \right], \quad (\text{C.7})$$

where $\binom{||U_{m,t}(I)||+(||U_{m,t}||-||D_{m,t}||)k_2+||D_{m,t}||-1}{(||U_{m,t}||-||D_{m,t}||)k_2+||D_{m,t}||+i}$ is the binomial coefficients. By substituting Inequality (C.6) into Equation (C.7), we arrive at :

$$P_m^{A_2}(U_{m,t}^*) \geq \underbrace{P_e \cdot \left[\sum_{i=0}^{||U_{m,t}(I)||-1} \frac{\binom{||U_{m,t}(I)||+||U_{m,t}||k_2-1}{||U_{m,t}||k_2+i} P_e^{||U_{m,t}||k_2+i}}{(1-P_e)^{i+1-||U_{m,t}(I)||}} \right]}_{=P_m(U_{m,t}^*)}}, \quad (\text{C.8})$$

$$P_m^{A_2}(U_{m,t}^*) \leq P_e \cdot \left[\sum_{i=0}^{||U_{m,t}(I)||-1} \frac{\binom{||U_{m,t}(I)||+k_2+||U_{m,t}||-2}{k_2+||U_{m,t}||-1+i} P_e^{||U_{m,t}||k_2+i}}{(1-P_e)^{i+1-||U_{m,t}(I)||}} \right]. \quad (\text{C.9})$$

For the sake of brevity, we define Q , V and K as:

$$Q = ||U_{m,t}(I)|| - 1 = k_1 ||U_{m,t}|| - 1, \quad (\text{C.10})$$

$$V = k_2 + ||U_{m,t}|| - 1, \quad (\text{C.11})$$

$$K = k_2 ||U_{m,t}||. \quad (\text{C.12})$$

As a result, Inequality (C.8) may be rewritten as:

$$\begin{aligned} P_m^{A_2}(U_{m,t}^*) &\geq P_e \cdot \left[\sum_{i=0}^{||U_{m,t}(I)||-1} \frac{\binom{||U_{m,t}(I)||+||U_{m,t}||k_2-1}{||U_{m,t}||k_2+i} P_e^{||U_{m,t}||k_2+i}}{(1-P_e)^{i+1-||U_{m,t}(I)||}} \right], \\ &\geq \sum_{i=0}^Q \binom{Q+K}{K+i} P_e^{K+i+1} (1-P_e)^{Q-i}, \\ &\geq \sum_{i=0}^Q Y_i^{A_2}, \end{aligned} \quad (\text{C.13})$$

where the term $Y_i^{A_2}$ is defined as

$$Y_i^{A_2} = \binom{Q+K}{K+i} P_e^{K+i+1} (1-P_e)^{Q-i}. \quad (\text{C.14})$$

Accordingly, Inequality (C.9) can be rewritten as:

$$\begin{aligned}
P_m^{A_2}(U_{m,t}^*) &\leq P_e \cdot \left[\sum_{i=0}^{||U_{m,t}(I)||-1} \frac{(\|U_{m,t}(I)\|+k_2+\|U_{m,t}\|-2)P_e^{k_2+\|U_{m,t}\|-1+i}}{(1-P_e)^{i+1-\|U_{m,t}(I)\|}} \right], \\
&\leq \sum_{i=0}^Q \binom{Q+V}{V+i} P_e^{V+i+1} (1-P_e)^{Q-i}, \\
&\leq \sum_{i=0}^Q T_i^{A_2},
\end{aligned} \tag{C.15}$$

where the term $T_i^{A_2}$ is defined as

$$T_i^{A_2} = \binom{Q+V}{V+i} P_e^{V+i+1} (1-P_e)^{Q-i}. \tag{C.16}$$

However, there might be more than Γ frames [46,47,99,179], which contain the IFs transmitted by all users of $U_{m,t}$. If the availability of those extra frames is taken into account, we will have

$$P_m^{A_2,true}(U_{m,t}^*) \leq P_m^{A_2}(U_{m,t}^*), \tag{C.17}$$

where $P_m^{A_2,true}(U_{m,t}^*)$ is the true probability of outage for the information frame $I_m(t)$.

Notably, $P_m^{A_2,true}(U_{m,t}^*)$ is the true outage probability for a given $U_{m,t}^*$. The system's outage probability P^{A_2} for all possible $U_{m,t}^*$ can be calculated by

$$P^{A_2} = \sum_{||U_{m,t}^*||=0}^{M-1} \frac{P_e^{||U_{m,t}^*||}}{(1-P_e)^{||U_{m,t}^*||-M+1}} P_m^{A_2,true}(U_{m,t}^*). \tag{C.18}$$

Regarding the *upper bound* of P^{A_2} specified in Equation (C.18), Inequality (C.9) and Inequality (C.17) may be substituted into Equation (C.18) in order to infer that

$$\begin{aligned}
P^{A_2} &= \sum_{||U_{m,t}^*||=0}^{M-1} \frac{P_e^{||U_{m,t}^*||}}{(1-P_e)^{||U_{m,t}^*||-M+1}} P_m^{A_2,true}(U_{m,t}^*), \\
&\leq \sum_{||U_{m,t}^*||=0}^{M-1} \frac{P_e^{||U_{m,t}^*||}}{(1-P_e)^{||U_{m,t}^*||-M+1}} P_m^{A_2}(U_{m,t}^*), \\
&\leq \sum_{||U_{m,t}^*||=0}^{M-1} \frac{P_e^{||U_{m,t}^*||}}{(1-P_e)^{||U_{m,t}^*||-M+1}} \sum_{i=0}^Q T_i^{A_2}.
\end{aligned} \tag{C.19}$$

As regards to the *lower bound*, we can further employ the approximation of $P_m^{A_2}(U_{m,t}^*)$ mentioned in Inequality (C.8) as

$$P_m(U_{m,t}^*) = P_e \cdot \left[\sum_{i=0}^{||U_{m,t}(I)||-1} \frac{(\|U_{m,t}(I)\|+\|U_{m,t}\|k_2-1)P_e^{||U_{m,t}\|k_2+i}}{(1-P_e)^{i+1-\|U_{m,t}(I)\|}} \right], \tag{C.20}$$

By focusing our attention on the region corresponding to a low P_e or small $||U_{m,t}^*||$, we have

$$\begin{aligned}
P^{A_2} &> (1-P_e)^{M-1} P_m^{A_2,true}(U_{m,t}^*)|_{||U_{m,t}^*||=0}, \\
&> (1-P_e)^{M-1} P_m(U_{m,t}^*)|_{||U_{m,t}^*||=0},
\end{aligned} \tag{C.21}$$

where we exploited:

$$\begin{aligned} P_m(U_{m,t}^*)|_{\|U_{m,t}^*\|=0} &= P_m^{A_2,true}(U_{m,t}^*)|_{\|U_{m,t}^*\|=0}, \\ &= P_e \cdot \left[\sum_{i=0}^{Mk_1-1} \binom{Mk_1-1+Mk_2}{Mk_2+i} P_e^{Mk_2+i} (1-P_e)^{Mk_1-1-i} \right], \end{aligned} \quad (C.22)$$

Upon substituting Inequality (C.20) into Inequality (C.21), we arrive at

$$\begin{aligned} P^{A_2} &> (1-P_e)^{M-1} P_m(U_{m,t}^*)|_{\|U_{m,t}^*\|=0}, \\ &> (1-P_e)^{M-1} \sum_{i=0}^Q Y_i^{A_2}|_{\|U_{m,t}^*\|=0}, \end{aligned} \quad (C.23)$$

where we have

$$\sum_{i=0}^Q Y_i^{A_2}|_{\|U_{m,t}^*\|=0} = \sum_{i=0}^Q \binom{E+F}{F+i} P_e^{F+i+1} (1-P_e)^{E-i}. \quad (C.24)$$

For the sake of brevity, we define E and F as

$$E = Mk_1 - 1, \quad (C.25)$$

$$F = Mk_2. \quad (C.26)$$

C.2 Outage Probability of an Information Frame in Adaptive 2

In order to derive the upper bound for the system's probability P^{A_2} of Equation (C.18), which contains the $P_m^{A_2,true}(U_{m,t}^*)$ referred to as the true probability of outage for the information frame $I_m(t)$, we employ the connection between the two probabilities, namely $P_m^{A_2,true}(U_{m,t}^*)$ and $P_m^{A_2}(U_{m,t}^*)$, represented in Inequality (C.17). Likewise, we may derive the lower bound of the system's probability represented by Inequality (C.21) by considering the term $P_m^{A_2}(U_{m,t}^*)|_{\|U_{m,t}^*\|=0}$.

Let us now specify the range of the outage probabilities $P_m^{A_2}(U_{m,t}^*)$ of Equation (C.15) and $P_m^{A_2}(U_{m,t}^*)|_{\|U_{m,t}^*\|=0}$ of Equation (C.23). It is noted that the term $T_i^{A_2}$ of Equation (C.16) and the term $Y_i^{A_2}|_{\|U_{m,t}^*\|=0}$ of Equation (C.24) have an identical formulation, if we conceive values Q of Equation (C.10), V of Equation (C.11) equivalent to E of Equation (C.25), F of Equation (C.26), respectively. As a result, the close form for the term $P_m^{A_2}(U_{m,t}^*)$ may be also applied for formulating the term $P_m^{A_2}(U_{m,t}^*)|_{\|U_{m,t}^*\|=0}$. Accordingly, let us consider a function $f(n)$ as a ratio of two consecutive terms in Equation (C.15), which is formulated as:

$$\begin{aligned} f(n) = \frac{T_{n+1}^{A_2}}{T_n^{A_2}} &= \frac{\binom{Q+V}{V+n+1} P_e^{V+n+1} (1-P_e)^{Q-n-1}}{\binom{Q+V}{V+n} P_e^{V+n} (1-P_e)^{Q-n}} \\ &= \frac{(Q-n)P_e}{(V+n+1)(1-P_e)}, \end{aligned} \quad (C.27)$$

where we have $T_n^{A_2} = \binom{Q+V}{V+n} P_e^{V+n+1} (1-P_e)^{Q-n}$. Following a few steps, we can express the derivative $f'(n)$ of the function $f(n)$ with respect to the variable n as follows

$$f'(n) = \frac{-(Q+V+1)P_e}{(V+n+1)^2(1-P_e)}. \quad (C.28)$$

As seen in Equation (C.28), we have $f'(n) < 0$ for $\forall n \in \{0, \dots, Q-1\}$, which suggests that the function $f(n)$ increases, as long as the variable n decreases. Thus, we use the following series expansion:

$$\begin{aligned} f(Q-1) &\leq f(n) \leq f(0), \\ \frac{P_e}{(V+Q)(1-P_e)} &\leq f(n) \leq \frac{QP_e}{(V+1)(1-P_e)}. \end{aligned} \quad (\text{C.29})$$

Given an arbitrary number S , we have the equation

$$\frac{S^{k+1} - 1}{S - 1} = 1 + S + S^2 + \dots + S^k. \quad (\text{C.30})$$

Furthermore, we can rewrite Equation (C.15) as

$$\begin{aligned} P_m^{A_2}(U_{m,t}^*) &= \sum_{i=0}^Q T_i^{A_2}, \\ &= T_0^{A_2} + T_0^{A_2} f(n) + T_0^{A_2} [f(n)]^2 + \dots + T_0^{A_2} [f(n)]^Q, \\ &= T_0^{A_2} \left[1 + f(n) + [f(n)]^2 + \dots + [f(n)]^Q \right], \end{aligned} \quad (\text{C.31})$$

where we have $T_0^{A_2} = \binom{Q+V}{V} P_e^{V+1} (1-P_e)^Q$, which transpires from the general formula of Equation (C.15). Upon substituting Equation (C.30) into Equation (C.31), we arrive at the outage probability expression $P_m^{A_2}(U_{m,t}^*)$ as follows

$$P_m^{A_2}(U_{m,t}^*) = T_0^{A_2} \frac{[f(n)]^{Q+1} - 1}{f(n) - 1}, \quad (\text{C.32})$$

Observe the probability $P_m^{A_2}(U_{m,t}^*)$ in Equation (C.31) increases, as the function $f(n)$ increases. Taking Inequality (C.29) into account, we arrive at the following inequalities:

$$\begin{aligned} P_m^{A_2}(U_{m,t}^*) &\leq P_m^{A_2}(U_{m,t}^*)|_{f(n)=f(0)}, \\ &\leq T_0^{A_2} \frac{[f(0)]^{Q+1} - 1}{f(0) - 1}, \\ &\leq \underbrace{\left(\binom{Q+V}{V} P_e^{V+1} (1-P_e)^Q \right)}_{=T_0^{A_2}} \left[\frac{[f(0)]^{Q+1} - 1}{f(0) - 1} \right], \end{aligned} \quad (\text{C.33})$$

and

$$\begin{aligned} P_m^{A_2}(U_{m,t}^*) &\geq P_m^{A_2}(U_{m,t}^*)|_{f(n)=f(Q-1)}, \\ &\geq T_0^{A_2} \frac{[f(Q-1)]^{Q+1} - 1}{f(Q-1) - 1}, \\ &\geq \underbrace{\left(\binom{Q+V}{V} P_e^{V+1} (1-P_e)^Q \right)}_{=T_0^{A_2}} \left[\frac{[f(Q-1)]^{Q+1} - 1}{f(Q-1) - 1} \right]. \end{aligned} \quad (\text{C.34})$$

Upon recalling Inequality (C.29), we may arrive at:

$$\begin{aligned} f(0) &= \frac{\overbrace{Q}^{=\beta_{A_2}}}{(V+1)} \frac{P_e}{(1-P_e)}, \\ &= \frac{\beta_{A_2} P_e}{1-P_e}, \end{aligned} \quad (\text{C.35})$$

and

$$\begin{aligned} f(Q-1) &= \frac{\overbrace{1}^{=\alpha}}{(V+Q)} \frac{P_e}{(1-P_e)}, \\ &= \frac{\alpha P_e}{1-P_e}, \end{aligned} \tag{C.36}$$

where we have $\beta_{A_2} = Q/(V+1)$ and $\alpha_{A_2} = 1/(V+Q)$. Upon substituting Equation (C.35) into Inequality (C.33), we have

$$\begin{aligned} P_m^{A_2}(U_{m,t}^*) &\leq \binom{Q+V}{V} P_e^{V+1} (1-P_e)^Q \frac{\overbrace{\left[\frac{\beta_{A_2} P_e}{1-P_e} \right]^{Q+1} - 1}}{\frac{\beta_{A_2} P_e}{1-P_e} - 1}, \\ &\leq \binom{Q+V}{V} P_e^{V+1} \underbrace{\left[\frac{(\beta_{A_2} P_e)^{Q+1} - (1-P_e)^{Q+1}}{\beta_{A_2} P_e + P_e - 1} \right]}_{=M_{u,A_2}}. \end{aligned} \tag{C.37}$$

Similarly, by substituting $f(Q-1)$ of Equation (C.36) into Equation (C.34), we obtain

$$\begin{aligned} P_m^{A_2}(U_{m,t}^*) &\geq \binom{Q+V}{V} P_e^{V+1} (1-P_e)^Q \frac{\overbrace{\left[\frac{\alpha_{A_2} P_e}{1-P_e} \right]^{Q+1} - 1}}{\frac{\alpha_{A_2} P_e}{1-P_e} - 1}, \\ &\geq \binom{Q+V}{V} P_e^{V+1} \left[\frac{(\alpha_{A_2} P_e)^{Q+1} - (1-P_e)^{Q+1}}{\alpha_{A_2} P_e + P_e - 1} \right]. \end{aligned} \tag{C.38}$$

Having formulated the range of the term $P_m^{A_2}(U_{m,t}^*)$ in Inequality (C.37) and Inequality (C.38), let us now dedicate Section C.2.1 to further simplifying the term M_{u,A_2} of Inequality (C.37) before forming the upper bound of the $P_m^{A_2}(U_{m,t}^*)$. Then, in Section C.2.2, the probability $P_m(U_{m,t}^*)|_{\|U_{m,t}^*\|=0}$ of Equation (C.22) is also approximated for facilitating the lower bound derivations.

C.2.1 Approximation of the Probability $P_m^{A_2}(U_{m,t}^*)$

In order to further approximate the probability $P_m^{A_2}(U_{m,t}^*)$ of Inequality (C.37), let us now consider the term M_u in Inequality (C.37), where M_{u,A_2} may be rewritten as:

$$M_{u,A_2} = \frac{(1-P_e)^{Q+1} - (\beta_{A_2} P_e)^{Q+1}}{1-P_e - \beta_{A_2} P_e}. \tag{C.39}$$

Paying more attention to the case of $P_e \ll 1$ in Equation (C.39) leads to the expressions $(1-P_e)^{Q+1} < (1-P_e)$ and $(\beta_{A_2} P_e)^{Q+1} \approx 0$. We can then take these expressions into consideration to arrive at the following approximation

$$M_{u,A_2} < \frac{1-P_e}{\underbrace{1-P_e - \beta_{A_2} P_e}_{=M_{u1,A_2}}}. \tag{C.40}$$

where M_{u1,A_2} is reformulated as

$$\begin{aligned} M_{u1,A_2} &= \frac{1 - P_e}{1 - P_e - \beta_{A_2} P_e}, \\ &= 1 + \frac{\beta_{A_2} P_e}{1 - P_e - \beta_{A_2} P_e}. \end{aligned} \quad (C.41)$$

According to Equation (C.10) and Equation (C.11), the value β_{A_2} of Equation (C.35) may be expressed as

$$\begin{aligned} \beta_{A_2} &= \frac{Q}{V + 1}, \\ &= \frac{||U_{m,t}(I)|| - 1}{k_2 + ||U_{m,t}|| - 1 + 1}, \\ &= \frac{||U_{m,t}|| k_1 - 1}{k_2 + ||U_{m,t}||}. \end{aligned} \quad (C.42)$$

It is plausible that β_{A_2} of Equation (C.42) increases upon increasing the cardinality $||U_{m,t}||$, where $||U_{m,t}|| \in [1, \dots, M]$. Hence, we can infer that

$$\begin{aligned} \beta_{A_2} &\leq \beta_{A_2} |_{||U_{m,t}||=M}, \\ &\leq \underbrace{\frac{Mk_1 - 1}{k_2 + M}}_{=\beta_{A_2}^{\max}}, \end{aligned} \quad (C.43)$$

where we have

$$\beta_{A_2}^{\max} = \frac{Mk_1 - 1}{k_2 + M}. \quad (C.44)$$

Observing the term M_{u1,A_2} in Equation (C.41), we find that the term M_{u1,A_2} increases, as the value of β increases, provided that $P_e \ll 1$. Hence, we can infer from Equation (C.41) that

$$\begin{aligned} M_{u1,A_2} &\leq M_{u1,A_2} |_{\beta=\beta^{\max}}, \\ &\leq \underbrace{1 + \frac{\frac{Mk_1-1}{k_2+M} P_e}{1 - P_e - \frac{Mk_1-1}{k_2+M} P_e}}_{=M_{u,A_2}^{\max}}, \end{aligned} \quad (C.45)$$

where M_{u,A_2}^{\max} is represented as

$$M_{u,A_2}^{\max} = 1 + \frac{\frac{Mk_1-1}{k_2+M} P_e}{1 - P_e - \frac{Mk_1-1}{k_2+M} P_e}. \quad (C.46)$$

By combining Inequality (C.40) and Inequality (C.45), we come up with

$$\begin{aligned} M_{u,A_2} &< M_{u1,A_2} \leq M_{u,A_2}^{\max}, \\ M_{u,A_2} &< M_{u,A_2}^{\max}. \end{aligned} \quad (C.47)$$

Substituting M_{u,A_2}^{\max} of Equation (C.46) into Inequality (C.47), we arrive at

$$M_{u,A_2} < \underbrace{1 + \frac{\frac{Mk_1-1}{k_2+M} P_e}{1 - P_e - \frac{Mk_1-1}{k_2+M} P_e}}_{=M_{u,A_2}^{\max}}. \quad (C.48)$$

Then substituting M_{u,A_2} given by Inequality (C.48) into Inequality (C.37) yields:

$$\begin{aligned}
 P_m^{A_2}(U_{m,t}^*) &\leq \left(\frac{Q+V}{V}\right) P_e^{V+1} \underbrace{\left[\frac{(\beta P_e)^{Q+1} - (1-P_e)^{Q+1}}{\beta P_e + P_e - 1}\right]}_{=M_{u,A_2}}, \\
 &< \underbrace{\left(\frac{Q+V}{V}\right) P_e^{V+1} \left[1 + \frac{\frac{Mk_1-1}{k_2+M} P_e}{1 - P_e - \frac{Mk_1-1}{k_2+M} P_e}\right]}_{=M_{u,A_2}^{\max}}}, \tag{C.49} \\
 &= P_m^{\max,A_2}(U_{m,t}^*)
 \end{aligned}$$

where the maximum value $P_m^{\max,A_2}(U_{m,t}^*)$ of the probability $P_m^{A_2}(U_{m,t}^*)$ is given by

$$\begin{aligned}
 P_m^{\max,A_2}(U_{m,t}^*) &= \left(\frac{Q+V}{V}\right) P_e^{V+1} \underbrace{\left[1 + \frac{\frac{Mk_1-1}{k_2+M} P_e}{1 - P_e - \frac{Mk_1-1}{k_2+M} P_e}\right]}_{=M_{u,A_2}^{\max}}, \\
 &= \left(\frac{Q+V}{V}\right) P_e^{V+1} M_{u,A_2}^{\max}. \tag{C.50}
 \end{aligned}$$

C.2.2 Approximation of the probability $P_m(U_{m,t}^*)|_{||U_{m,t}^*||=0}$

As afore-mentioned, we may exploit the similarity in the formulae of $P_m^{A_2}(U_{m,t}^*)$ given in Equation (C.15) and of $P_m^{A_2}(U_{m,t}^*)|_{||U_{m,t}^*||=0}$ provided by Equation (C.23), in order to approximate the probability $P_m(U_{m,t}^*)|_{||U_{m,t}^*||=0}$. The approximation is then employed for deriving the system's lower bound in Section C.3.2.

For convenience, let us repeat Inequality (C.38) here as follows

$$P_m^{A_2}(U_{m,t}^*) \geq \left(\frac{Q+V}{V}\right) P_e^{V+1} \left[\frac{(\alpha_{A_2} P_e)^{Q+1} - (1-P_e)^{Q+1}}{\alpha_{A_2} P_e + P_e - 1}\right], \tag{C.51}$$

where we have $\alpha_{A_2} = 1/(Q+V)$. Upon replacing Q and V in Inequality (C.51) by E and F , respectively, into Inequality (C.51), Equation (C.22) may be rewritten as:

$$\begin{aligned}
 P_m^{A_2}(U_{m,t}^*)|_{||U_{m,t}^*||=0} &= P_e \cdot \left[\sum_{i=0}^{Mk_1-1} \binom{Mk_1-1+Mk_2}{Mk_2+i} P_e^{Mk_2+i} (1-P_e)^{Mk_1-1-i}\right], \\
 &= \sum_{i=0}^E \binom{E+F}{F+i} P_e^{F+i+1} (1-P_e)^{E-i}, \\
 &\geq \left(\frac{E+F}{F}\right) P_e^{F+1} \left[\frac{(\alpha'_{A_2} P_e)^{Q+1} - (1-P_e)^{Q+1}}{\alpha'_{A_2} P_e + P_e - 1}\right], \tag{C.52}
 \end{aligned}$$

where we have $\alpha'_{A_2} = 1/(E+F)$. We further substitute $E = Mk_1 - 1$ into Equation (C.52) to arrive at

$$P_m^{A_2}(U_{m,t}^*)|_{||U_{m,t}^*||=0} \geq \binom{Mk_1+F-1}{F} \frac{P_e^{F+1} \left[\left(\frac{P_e}{Mk_1+F-1}\right)^{Mk_1} - (1-P_e)^{Mk_1}\right]}{\frac{P_e}{Mk_1+F-1} + P_e - 1}. \tag{C.53}$$

C.3 Adaptive mode 2: Upper and Lower Bounds

In this section, we use the probability $P_m^{\max, A_2}(U_{m,t}^*)$ of Equation (C.50) and the bound of $P_m^{A_2}(U_{m,t}^*)|_{\|U_{m,t}^*\|=0}$ given by Inequality (C.53) for deriving the upper bound and lower bound of the system's outage probability P_o .

C.3.1 Upper bound in Adaptive mode 2

This section is dedicated to the derivation of formula for the upper bound of the system's outage probability determined by Inequality (C.19), which is repeated here for convenience:

$$P^{A_2} \leq \sum_{\|U_{m,t}^*\|=0}^{M-1} \frac{P_e^{\|U_{m,t}^*\|}}{(1-P_e)^{\|U_{m,t}^*\|-M+1}} P_m^{A_2}(U_{m,t}^*), \quad (C.54)$$

By substituting $P_m^{\max, A_2}(U_{m,t}^*)$ given in Equation (C.50) into Inequality (C.54), we arrive at:

$$\begin{aligned} P^{A_2} &< \sum_{\|U_{m,t}^*\|=0}^{M-1} \frac{P_e^{\|U_{m,t}^*\|}}{(1-P_e)^{\|U_{m,t}^*\|-M+1}} \underbrace{P_m^{\max, A_2}(U_{m,t}^*)}_{> P_m^{A_2}(U_{m,t}^*)}, \\ &< \sum_{\|U_{m,t}^*\|=0}^{M-1} \frac{P_e^{\|U_{m,t}^*\|}}{(1-P_e)^{\|U_{m,t}^*\|-M+1}} \underbrace{\binom{Q+V}{V} P_e^{V+1} M_{u, A_2}^{\max}}_{= P_m^{\max, A_2}(U_{m,t}^*)}, \\ &< \sum_{\|U_{m,t}^*\|=0}^{M-1} \binom{Q+V}{V} \underbrace{\frac{P_e^{\|U_{m,t}^*\|}}{(1-P_e)^{\|U_{m,t}^*\|-M+1}} P_e^{V+1} M_{u, A_2}^{\max}}_{= T_{o, A_2}^{Upper}}. \end{aligned} \quad (C.55)$$

We then define the value T_{o, A_2}^{Upper} as

$$\begin{aligned} T_{o, A_2}^{Upper} &= \frac{P_e^{\|U_{m,t}^*\|}}{(1-P_e)^{\|U_{m,t}^*\|-M+1}} P_e^{\overbrace{V}^{=k_2+\|U_{m,t}^*\|-1}} + 1 M_{u, A_2}^{\max}, \\ &= \frac{P_e^{k_2+M}}{(1-P_e)^{\|U_{m,t}^*\|-M+1}} M_{u, A_2}^{\max}. \end{aligned} \quad (C.56)$$

Accordingly, Inequality (C.55) becomes

$$P^{A_2} < \sum_{\|U_{m,t}^*\|=0}^{M-1} \binom{Q+V}{V} T_{o, A_2}^{Upper}. \quad (C.57)$$

Furthermore, Inequality (A.43) can be rewritten as

$$P_o < \underbrace{\sum_{\|U_{m,t}^*\|=0}^{M-1} \left[\binom{Q+V}{V} - \binom{E+G}{G} \right] T_{o, A_2}^{Upper}}_{=\Delta_{A_2}} + \underbrace{\sum_{\|U_{m,t}^*\|=0}^{M-1} \binom{E+G}{G} T_{o, A_2}^{Upper}}_{=\chi_{A_2}}, \quad (C.58)$$

where G is defined as

$$G = k_2 + M - 1. \quad (C.59)$$

Bearing in mind the fact that $\binom{Q+V}{V} \leq \binom{E+G}{G}$, the term Δ_{A_2} defined by Inequality (C.58) always satisfies

$$\Delta_{A_2} < 0. \quad (C.60)$$

Paying more attention to the case of having $\|U_{m,t}^*\| = (M-1)$, we infer the following bound:

$$\Delta_{A_2} \leq \underbrace{\Delta_{A_2|_{\|U_{m,t}^*\|=M-1}}}_{=\Omega_{A_2}} \quad (C.61)$$

where the term Ω_{A_2} is defined as:

$$\begin{aligned} \Omega_{A_2} &= \Delta_{A_2|_{\|U_{m,t}^*\|=M-1}} \\ &= \left[\left[\binom{Q+V}{V} - \binom{E+G}{G} \right] T_{o,A_2}^{Upper} \right]_{\|U_{m,t}^*\|=M-1}, \\ &= \left[\left[\binom{k_1-1+k_2+1-1}{k_2} - \binom{Mk_1-1+k_2+M-1}{k_2+M-1} \right] T_{o,A_2}^{Upper} \right]_{\|U_{m,t}^*\|=M-1}, \\ &= \left[\left[\binom{k_1+k_1-1}{k_2} - \binom{Mk_1-2+k_2+M}{k_2+M-1} \right] T_{o,A_2}^{Upper} \right]_{\|U_{m,t}^*\|=M-1}, \\ &= \left[\binom{k_1+k_2-1}{k_2} - \binom{Mk_1-2+k_2+M}{k_2+M-1} \right] P_e^{k_2+M} M_{u,A_2}^{\max}. \end{aligned} \quad (C.62)$$

Let us now reduce the χ_{A_2} of Inequality (C.58) containing the term T_{o,A_2}^{Upper} given by Equation (C.56), which may be reduced by considering the ratio R_{o,A_2} of two consecutive terms $T_{o,A_2}^{Upper|_{\|U_{m,t}^*\|}}$ corresponding to two consecutive indices of $\|U_{m,t}^*\|$, yielding

$$\begin{aligned} R_{o,A_2} &= \frac{T_{o,A_2}^{Upper|_{\|U_{m,t}^*\|}}}{T_{o,A_2}^{Upper|_{\|U_{m,t}^*\|+1}}}, \\ &= 1 - P_e. \end{aligned} \quad (C.63)$$

Accordingly, we can rewrite the term χ_{A_2} of Inequality (C.58) as follows

$$\begin{aligned} \chi_{A_2} &= \binom{E+G}{G} \sum_{\|U_{m,t}^*\|=0}^{M-1} T_{o,A_2}^{Upper|_{\|U_{m,t}^*\|}} \\ &= \binom{E+G}{G} \left(T_{o,A_2}^{Upper|_{M-1}} + T_{o,A_2}^{Upper|_{M-2}} \cdots + T_{o,A_2}^{Upper|_0} \right), \\ &= \binom{E+G}{G} \left(T_{o,A_2}^{Upper|_{M-1}} + T_{o,A_2}^{Upper|_{M-1}} (R_{o,A_2})^1 + \cdots + T_{o,A_2}^{Upper|_{M-1}} (R_{o,A_2})^{M-1} \right), \\ &= \binom{E+G}{G} T_{o,A_2}^{Upper|_{M-1}} \left[1 + (R_{o,A_2})^1 + \cdots + (R_{o,A_2})^{M-1} \right], \end{aligned} \quad (C.64)$$

where $T_{o,A_2}^{Upper} M_{-1}$ is formulated as

$$T_{o,A_2}^{Upper} M_{-1} = P_e^{k_2+M} M_{u,A_2}^{\max}, \quad (C.65)$$

and M_{u,A_2}^{\max} is given by Equation (C.46).

Again, we exploit the series expansion of

$$\frac{S^{k+1} - 1}{S - 1} = 1 + S + S^2 + \dots + S^k, \quad (C.66)$$

where S is an arbitrary number. By substituting Equation (C.65) and Equation (C.66) into Equation (C.64), we arrive at

$$\begin{aligned} \chi_{A_2} &= \binom{E+G}{G} T_{o,A_2}^{Upper} M_{-1} \left[1 + (R_{o,A_2})^1 + \dots + (R_{o,A_2})^{M-1} \right], \\ &= \binom{E+G}{G} T_{o,A_2}^{Upper} M_{-1} \left[\frac{(R_{o,A_2})^M - 1}{R_{o,A_2} - 1} \right], \\ &= \binom{E+G}{G} P_e^{k_2+M} M_{u,A_2}^{\max} \left[\frac{(R_{o,A_2})^M - 1}{R_{o,A_2} - 1} \right], \\ &= \binom{k_1M + k_2 + M - 2}{k_2 + M - 1} P_e^{k_2+M} M_{u,A_2}^{\max} \left[\frac{(R_{o,A_2})^M - 1}{R_{o,A_2} - 1} \right]. \end{aligned} \quad (C.67)$$

Upon employing the results of Equation (C.61) and Equation (C.67), we can further approximate Inequality (C.58) as

$$\begin{aligned} P^{A_2} &< \underbrace{\sum_{\|U_{m,t}^*\|=0}^{M-1} \left[\binom{Q+V}{V} - \binom{E+G}{G} \right] T_{o,A_2}^{Upper}}_{=\Delta_{A_2}} + \underbrace{\sum_{\|U_{m,t}^*\|=0}^{M-1} \binom{E+M}{M} T_{o,A_2}^{Upper}}_{=\chi_{A_2}}, \\ &< \underbrace{\underbrace{\Omega_{A_2}}_{\geq \Delta_{A_2}} + \underbrace{\binom{E+G}{G} P_e^{k_2+M} M_{u,A_2}^{\max} \left[\frac{(R_{o,A_2})^M - 1}{R_{o,A_2} - 1} \right]}_{=\chi_{A_2}}}_{=P^{U,A_2}}, \\ &< \underbrace{\left[\binom{k_1 + k_2 - 1}{k_2} - \binom{Mk_1 - 2 + k_2 + M}{k_2 + M - 1} \right] P_e^{k_2+M} M_{u,A_2}^{\max}}_{=\Omega_{A_2}} \\ &\quad + \underbrace{\binom{k_1M + k_2 + M - 2}{k_2 + M - 1} P_e^{k_2+M} M_{u,A_2}^{\max} \left[\frac{(R_{o,A_2})^M - 1}{R_{o,A_2} - 1} \right]}_{=\chi_{A_2}}, \\ &< \underbrace{\Omega_{A_2} + \chi_{A_2}}_{=P^{U,A_2}}, \end{aligned} \quad (C.68)$$

where M_{u,A_2}^{\max} and R_{o,A_2} are defined in Equation (C.46) and Equation (C.63), respectively, while the probability P^{U,A_2} is given by:

$$P^{U,A_2} = \Omega_{A_2} + \chi_{A_2}. \quad (C.69)$$

Notably, the outage probability of the network coding system supported by the A_2 mode is also affected by the multiplexing gain Ω_2 , which is given by Equation (5.66) as:

$$\Omega_2 = \frac{k_1 + k_2}{k_1 + k_2 \left(1 - (1 - P_e)^{Mk_1}\right) - (1 - P_e)^{k_1} (k_2 - 1) \left(1 - (1 - P_e)^{(M-1)k_1}\right)} \quad (\text{C.70})$$

Bearing in mind the influence of both the diversity and multiplexing aspects, the upper bound of the system's outage probability in the A_2 mode may be expressed as:

$$\underbrace{\Omega_2 P^{A_2}}_{=P_o^{A_2}} < \underbrace{\Omega_2 P^{A_2, U}}_{=P_o^{A_2, Upper}} \quad (\text{C.71})$$

where $P_o^{A_2}$ is the system's outage probability when A_2 is activated, while $P_o^{A_2, Upper}$ is the corresponding upper bound of $P_o^{A_2}$.

C.3.2 Lower bound in Adaptive mode 2

For convenience, let us repeat Inequality (C.21) here, which formulates the lower bound of the system's outage probability as

$$P^{A_2} > (1 - P_e)^{M-1} P_m^{A_2}(U_{m,t}^*)|_{\|U_{m,t}^*\|=0}. \quad (\text{C.72})$$

Again, for convenience, let us repeat the Inequality (C.53) formulating the bound of the probability $P_m(U_{m,t}^*)|_{\|U_{m,t}^*\|=0}$:

$$P_m^{A_2}(U_{m,t}^*)|_{\|U_{m,t}^*\|=0} \geq \binom{Mk_1 + M - 1}{M} P_e^{M+1} \left[\frac{\left(\frac{P_e}{Mk_1 + M - 1}\right)^{Mk_1} - (1 - P_e)^{Mk_1}}{\frac{P_e}{Mk_1 + M - 1} + P_e - 1} \right], \quad (\text{C.73})$$

By combining Inequality (C.72) and Inequality (C.73), we obtain the following

$$\begin{aligned} P^{A_2} &> (1 - P_e)^{M-1} P_m^{A_2}(U_{m,t}^*)|_{\|U_{m,t}^*\|=0}, \\ &> \underbrace{(1 - P_e)^{M-1} \binom{Mk_1 + M - 1}{M} P_e^{M+1} \left[\frac{\left(\frac{P_e}{Mk_1 + M - 1}\right)^{Mk_1} - (1 - P_e)^{Mk_1}}{\frac{P_e}{Mk_1 + M - 1} + P_e - 1} \right]}_{=P^{L, A_2}}, \end{aligned} \quad (\text{C.74})$$

where we define P^{L, A_2} as the strict lower bound of the system's outage probability, which is given by

$$P^{L, A_2} = \binom{Mk_1 + M - 1}{M} \frac{P_e^{M+1}}{(1 - P_e)^{1-M}} \left[\frac{\left(\frac{P_e}{Mk_1 + M - 1}\right)^{Mk_1} - (1 - P_e)^{Mk_1}}{\frac{P_e}{Mk_1 + M - 1} + P_e - 1} \right]. \quad (\text{C.75})$$

Similarly to the above derivation of the upper bound expressed in Inequality (C.71), the system's outage probability is also affected by the associated multiplexing aspects. Hence, the lower

bound of the system's outage probability in the A_2 mode may be represented by:

$$\underbrace{\Omega_2 P^{A_2,L}}_{=P_0^{A_2,Lower}} < \underbrace{\Omega_2 P^{A_2}}_{=P_0^{A_2}} \quad (C.76)$$

where $P_0^{A_2}$ is the system's outage probability when A_2 is activated, while $P_0^{A_2,Lower}$ is the corresponding lower bound of $P_0^{A_2}$. Combining Inequality (C.71) and Inequality (C.76), we have

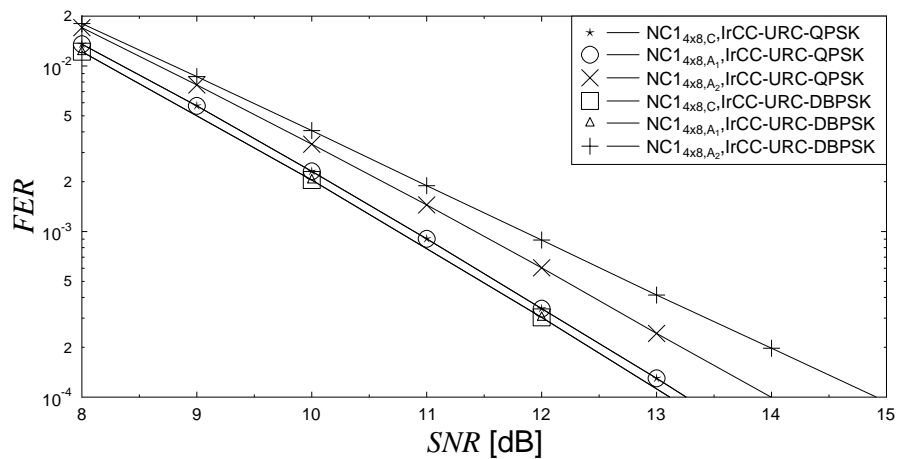
$$\underbrace{\Omega_2 P^{A_2,L}}_{=P_0^{A_2,Lower}} < \underbrace{\Omega_2 P^{A_2}}_{=P_0^{A_2}} < \underbrace{\Omega_2 P^{A_2,U}}_{=P_0^{A_2,Upper}} \quad (C.77)$$

where $P_0^{A_2,Lower}$ and $P_0^{A_2,Upper}$ are the corresponding lower and upper bounds of $P_0^{A_2}$, respectively. Finally, the probabilities $P^{A_2,U}$, $P^{A_2,L}$ and Ω_2 are given by Equation (C.69), Equation (C.75) and Equation (C.70), respectively.

Additional Results

D.1 The FER-versus-SNR performance of the A_1 and A_2 modes

This section presents the SNR-versus-FER performance of the system of Figure 5.1 discussed in Section 5.3.2.2 regarding the multiplexing gain versus diversity gain in the adaptive network coding. More specifically, Figure D.1 characterises the $G_{4 \times 8}$ based systems in both the non-coherent and coherent scenarios, which were presented in Figure 5.5. As seen in Figure D.1, the FER vs SNR performance curves of the C mode and the A_1 mode are identical, hence there is no change in diversity gain, when the system switches to the A_1 mode from the C mode of Figure 5.1. As a result, a diversity gain of zero is seen in Figure 5.5. By contrast, when switching to the A_2 mode from the C mode, a degradation is experienced in the FER vs SNR performance, as seen in Figure D.1. As a result, a negative diversity gain is observed in Figure 5.5.



(a) Coherent IrCC-URC-QPSK scheme

Figure D.1: The FER-versus-SNR performance reflecting the diversity gain of the system portrayed in Figure 5.1. The system comprise the Channel Coding (CC) and Network Coding 1 (NC1) layers, where the NC1 layer employed the $\mathbf{G}_{4 \times 8}$ matrix operating in both the A_1 and A_2 modes. The CC layer was supported by both the non-coherent IrCC-URC-DPSK scheme and coherent IrCC-URC-QPSK scheme, for supporting the $N_{sub} = 1$ sub-frame transmission regime over wireless channels influenced by both the uncorrelated Rayleigh and block Rayleigh fadings, as presented in Figure 5.5.

Bibliography

- [1] W. T. Webb and L. Hanzo, *Modern Quadrature Amplitude Modulation : Principles and Applications for Fixed and Wireless Channels*. London: IEEE Press, and John Wiley & Sons, 1994.
- [2] L. Hanzo, T.H. Liew and B.L. Yeap, *Turbo Coding, Turbo Equalisation and Space Time Coding for Transmission over Wireless channels*. New York, USA: John Willy IEEE Press, 2002.
- [3] H. V. Nguyen, C. Xu, S. X. Ng, and L. Hanzo, "Non-coherent near-capacity network coding for cooperative multi-user communications," *IEEE Transactions on Communications*, vol. 60, no. 10, pp. 3059–3070, 2012.
- [4] H. V. Nguyen, S. X. Ng, and L. Hanzo, "Irregular convolution and unity-rate coded network-coding for cooperative multi-user communications," *IEEE Transactions on Wireless Communications*, vol. 12, no. 3, pp. 1231–1243, 2013.
- [5] H. V. Nguyen, C. Xu, S. X. Ng, J. L. Rebelatto, Y. Li, and L. Hanzo, "Near-capacity non-coherent network-coding aided scheme for cooperative multi-user communications," in *2011 IEEE Vehicular Technology Conference (VTC Fall)*, pp. 1 –5, Sept. 2011.
- [6] H. V. Nguyen, S. X. Ng, J. L. Rebelatto, Y. Li, and L. Hanzo, "Near-capacity network coding for cooperative multi-user communications," in *IEEE Vehicular Technology Conference (VTC Fall 2011)*, pp. 1 –5, Sept. 2011.
- [7] J. N. Laneman, D. N. C. Tse, and G. W. Wornell, "Cooperative diversity in wireless networks: Efficient protocols and outage behavior," *IEEE Transactions on Information Theory*, vol. 50, pp. 3062–3080, Dec. 2004.
- [8] S. Yiu, R. Schober, and L. Lampe, "Distributed space-time block coding," *IEEE Transactions on Communications*, vol. 54, pp. 1195–1206, July 2006.
- [9] H. V. Nguyen, S. X. Ng, and L. Hanzo, "Distributed three-stage concatenated irregular convolutional, unity-rate and space-time trellis coding for single-antenna aided cooperative

- communications,” in *Vehicular Technology Conference Fall (VTC 2010-Fall), 2010 IEEE 72nd*, pp. 1–5, 2010.
- [10] H. V. Nguyen, S. X. Ng, and L. Hanzo, “Performance bounds of network coding aided cooperative multiuser systems,” *Signal Processing Letters, IEEE*, vol. 18, no. 7, pp. 435–438, 2011.
- [11] J. L. Rebelatto, B. F. Uchoa-Filho, and D. Silva, “Full-diversity network coding for two-user cooperative communications,” in *2011 IEEE Information Theory Workshop (ITW)*, pp. 543–547, Oct. 2011.
- [12] J. Rebelatto, B. Uchoa-Filho, Y. Li, and B. Vucetic, “Adaptive distributed network-channel coding,” *IEEE Transactions on Wireless Communications*, vol. 10, pp. 2818–2822, Sep. 2011.
- [13] C. E. Shannon, “A mathematical theory of communication,” *Bell Syst. Tech. J.*, vol. 27, pp. 379/623–423/656, 1948.
- [14] R. Hamming, “Error detecting and error correcting codes,” *Bell System Technical Journal*, vol. 29, pp. 147–160, 1950.
- [15] P. Elias, “Coding for noisy channels,” *IRE Conv. Rec. pt.4*, pp. 37–47, 1955.
- [16] E. Prange, “Cyclic error-correcting codes in two symbols,” *AFCRC-TN-57, 103, Air Force Cambridge Research Center, Cambridge, Mass.*, 1972.
- [17] D. Brennan, “Linear diversity combining techniques,” *Proceedings of the IRE*, vol. 47, pp. 1075–1102, June 1959.
- [18] I. Reed and G. Solomon, “Polynomial codes over certain finite fields,” *J. Soc. Ind. Appl. Math.*, vol. 8, pp. 300–304, June 1960.
- [19] C. Forney, “Concatenated codes,” *Cambridge: MIT Press*, 1966.
- [20] E. C. van der Meulen, “Three-terminal communication channels,” *Advanced Applied Probability*, vol. 3, no. 1, pp. 120–154, 1971.
- [21] L. Bahl, C. Cullum, W. Frazer, and F. Jelinek, “An efficient algorithm for computing free distance,” *IEEE Transactions on Information Theory*, vol. 18, pp. 437–439, May 1972.
- [22] L. Bahl, J. Cocke, F. Jelinek, and J. Raviv, “Optimal decoding of linear codes for minimizing symbol error rate,” *IEEE Transactions on Information Theory*, vol. 20, pp. 284–287, Mar. 1974.
- [23] E. van der Meulen, “A survey of multi-way channels in information theory: 1961-1976,” *IEEE Transactions on Information Theory*, vol. 23, pp. 1–37, Jan. 1977.

- [24] T. Cover and A. Gamal, "Capacity theorems for the relay channel," *IEEE Transactions on Information Theory*, vol. 25, pp. 572 – 584, Sep. 1979.
- [25] C. Berrou, A. Glavieux, and P. Thitimajshima, "Near shannon limit error-correcting coding and decoding: Turbo-codes. 1," in *IEEE International Conference on Communications, 1993. ICC '93 Geneva. Technical Program, Conference Record*, vol. 2, pp. 1064 –1070 vol.2, May 1993.
- [26] V. Tarokh and N. Seshadri and A. Calderbank, "Space-time codes for high data rate wireless communications: Performance criterion and code construction," in *Proc IEEE International Conference on Communications '97*, (Montreal, Canada), pp. 299–303, 1997.
- [27] G. J. Foschini, "Layered space-time architecture for wireless communication in a fading environment when using multiple antennas," *Bell Labs. Tech. J.*, vol. 1, pp. 198–212, Autumn 1996.
- [28] S. M. Alamouti, "A simple transmit diversity technique for wireless communications," *IEEE Journal on Selected Areas in Commu.*, vol. 16, Oct. 1998.
- [29] A. Sendonaris, E. Erkip, and B. Aazhang, "Increasing uplink capacity via user cooperation diversity," in *IEEE International Symposium on Information Theory, 1998*, p. 156, Aug. 1998.
- [30] V. Tarokh, H. Jafarkhani, and A. R. Calderbank, "Space-time block codes from orthogonal designs," *IEEE Trans. Inform. Theory*, vol. 45, July 1999.
- [31] V. Tarokh, A. Naguib, N. Seshadri, and A. R. Calderbank, "Space-time codes for high data rate wireless communication: Performance criteria in the presence of channel estimation errors, mobility, and multiple paths," *IEEE Transactions on Communications*, vol. 47, no. 2, pp. 199–207, 1999.
- [32] H. J. V. Tarokh and A. Calderbank, "Space-time block codes from orthogonal designs," *IEEE Transactions on Information Theory*, vol. 45, pp. 1456–1467, May 1999.
- [33] R. Ahlswede, N. Cai, S.-Y. Li, and R. Yeung, "Network information flow," *IEEE Transactions on Information Theory*, vol. 46, pp. 1204 –1216, July 2000.
- [34] J. N. Laneman and G. W. Wornell, "Distributed space-time-coded protocols for exploiting cooperative diversity in wireless networks," *IEEE Transactions on Information Theory*, vol. 49, pp. 2415–2425, Oct. 2003.
- [35] M. Janani, A. Hedayat, T. Hunter, and A. Nosratinia, "Coded cooperation in wireless communications: space-time transmission and iterative decoding," *IEEE Transactions on Signal Processing*, vol. 52, pp. 362 – 371, Feb. 2004.

- [36] H. H. Sneessens and L. Vandendorpe, "Soft decode and forward improves cooperative communications," in *6th IEE International Conference on 3G and Beyond*, pp. 1–4, Nov. 2005.
- [37] R. Hu and J. Li, "Exploiting slepian-wolf codes in wireless user cooperation," in *IEEE 6th Workshop on Signal Processing Advances in Wireless Communications, 2005*, pp. 275–279, June 2005.
- [38] Y. Li, B. Vucetic, T. Wong, and M. Dohler, "Distributed turbo coding with soft information relaying in multihop relay networks," *IEEE Journal on Selected Areas in Communications*, vol. 24, pp. 2040–2050, Nov. 2006.
- [39] R. Hu and J. Ti, "Practical compress-forward in user cooperation: Wyner-ziv cooperation," in *IEEE International Symposium on Information Theory*, pp. 489–493, July 2006.
- [40] R. W. Yeung and N. Cai, "Network error correction, part I: Basic concepts and upper bounds," *Communications in Information and Systems*, vol. 6, no. 1, pp. 19–36, 2006.
- [41] R. W. Yeung and N. Cai, "Network error correction, part II: Lower bounds," *Communications in Information and Systems*, vol. 6, no. 1, pp. 37–54, 2006.
- [42] T. Ho, M. Medard, R. Koetter, D. Karger, M. Effros, J. Shi, and B. Leong, "A random linear network coding approach to multicast," *IEEE Transactions on Information Theory*, vol. 52, pp. 4413–4430, Oct. 2006.
- [43] L. Xiao, T. Fuja, J. Kliewer, and D. Costello, "A network coding approach to cooperative diversity," *IEEE Transactions on Information Theory*, vol. 53, pp. 3714–3722, Oct. 2007.
- [44] T. Wang and G. Giannakis, "Complex field network coding for multiuser cooperative communications," *IEEE Journal on Selected Areas in Communications*, vol. 26, pp. 561–571, April 2008.
- [45] L. Hanzo, O. Alamri, M. E. Hajjar and N. Wu, *Near-Capacity Multi-Functional MIMO Systems*. New York, USA : John Wiley and Sons, 2009.
- [46] M. Xiao and M. Skoglund, "M-user cooperative wireless communications based on nonbinary network codes," in *IEEE Information Theory Workshop on Networking and Information Theory 2009 (ITW 2009)*, pp. 316–320, June 12-10, 2009.
- [47] J. L. Rebelatto, B. F. Uchôa-Filho, Y. Li, and B. Vucetic, "Generalized distributed network coding based on nonbinary linear block codes for multi-user cooperative communications," in *2010 IEEE International Symposium on Information Theory (ISIT 2010)*, pp. 943–947, June 2010.
- [48] J. Rebelatto, B. Uchoa-Filho, Y. Li, and B. Vucetic, "Adaptive distributed network-channel coding for cooperative multiple access channel," in *Communications (ICC), 2011 IEEE International Conference on*, pp. 1–5, June 2011.

- [49] I. Maric, A. Goldsmith, and M. Medard, "Multihop analog network coding via amplify-and-forward: The high snr regime," *IEEE Transactions on Information Theory*, vol. 58, pp. 793–803, Feb. 2012.
- [50] M. Xiao, J. Kliewer, and M. Skoglund, "Design of network codes for multiple-user multiple-relay wireless networks," *IEEE Transactions on Communications*, vol. 60, pp. 3755–3766, Dec. 2012.
- [51] E. Biglieri and M. Elia, "Multidimensional modulation and coding for band-limited digital channels," *IEEE Transactions on Information Theory*, vol. 34, pp. 803–809, July 1988.
- [52] D. Slepian, "Permutation modulation," *IEEE Proceedings of the IEEE*, vol. 53, pp. 228–236, Mar. 1965.
- [53] R. Ottoson, "Group codes for phase- and amplitude-modulated signals on a Gaussian channel," *IEEE Transactions on Information Theory*, vol. 17, pp. 315–321, May 1971.
- [54] H. Sari, "A generalization of multidimensional modulation," in *Proc. IEEE International Conference on Communications ICC 95 Seattle, Gateway to Globalization*, vol. 2, pp. 683–687, June 18–22, 1995.
- [55] G. Welti, J. Lee, G. J. Foschini, and M. J. Gans, "Digital transmission with coherent four-dimensional modulation," *IEEE Transactions on Information Theory*, vol. 6, March 1998.
- [56] L. Zetterberg and H. Brandstrom, "Codes for combined phase and amplitude modulated signals in a four-dimensional space," *IEEE Transactions on Communications*, vol. 25, no. 9, pp. 943–950, 1977.
- [57] M. Visintin, E. Biglieri, and V. Castellani, "Four-dimensional signaling for bandlimited channels," *IEEE Transactions on Communications*, vol. 42, no. 234, pp. 403–409, 1994.
- [58] D. Saha and T. G. Birdsall, "Quadrature-quadrature phase-shift keying," *IEEE Transactions on Communications*, vol. 37, pp. 437–448, May 1989.
- [59] L.-F. Wei, "Trellis-coded modulation with multidimensional constellations," *IEEE Transactions on Information Theory*, vol. 33, pp. 483–501, July 1987.
- [60] D. Saha, "Channel coding with quadrature-quadrature phase shift-keying (Q^2 PSK) signals," *IEEE Transactions on Communications*, vol. 38, pp. 409–417, Apr. 1990.
- [61] F. Simoens, H. Wymeersch, and M. Moeneclaey, "Spatial mapping for mimo systems," in *Proc. IEEE Information Theory Workshop*, pp. 187–192, Oct. 24–29, 2004.
- [62] F. Simoens, H. Wymeersch, H. Bruneel, and M. Moeneclaey, "Multidimensional mapping for bit-interleaved coded modulation with BPSK/QPSK signaling," *IEEE Communications Letters*, vol. 9, pp. 453–455, May 2005.

- [63] W. Lee, J. Cho, C.-K. Sung, H. Song, and I. Lee, "Mapping optimization for spacetime bit-interleaved coded modulation with iterative decoding," *IEEE Transactions on Communications*, vol. 55, pp. 650–655, Apr. 2007.
- [64] N. Gresset, L. Brunel, and J. J. Boutros, "Spacetime coding techniques with bit-interleaved coded modulations for mimo block-fading channels," *IEEE Transactions on Information Theory*, vol. 54, pp. 2156–2178, May 2008.
- [65] C. Stierstorfer and R. F. H. Fischer, "Asymptotically optimal mappings for BICM with M-QAM and M^2 -QAM," *Electronics Letters*, vol. 45, pp. 173–174, Jan. 2009.
- [66] M. Teimouri, A. Hedayat, and M. Shiva, "Concatenated bit-interleaved coded modulation and orthogonal space-time block codes over fading channels," *IET Communications*, vol. 3, pp. 1354–1362, Aug. 2009.
- [67] J. H. Winters, J. Salz, and R. D. Gitlin, "The impact of antenna diversity on the capacity of wireless communication systems," *IEEE Transactions on Communications*, vol. 42, no. 234, pp. 1740–1751, 1994.
- [68] V. Tarokh, N. Seshadri, and A. R. Calderbank, "Space-time codes for high data rate wireless communication: Performance criterion and code construction," *IEEE Transactions on Information Theory*, vol. 44, pp. 744–765, Mar. 1998.
- [69] N. S. V. Tarokh, A. Naguib and A. Calderbank, "Space-time codes for high data rate wireless communications: Mismatch analysis," in *Proc IEEE International Conference on Communications '97*, (Montreal, Canada), pp. 309–313, 1997.
- [70] A. F. Naguib, V. Tarokh, N. Seshadri, and A. R. Calderbank, "A space-time coding modem for high-data-rate wireless communications," *IEEE Journal on Selected Areas in Communications*, vol. 16, pp. 1459–1478, Oct. 1998.
- [71] L. Hanzo, S. X. Ng, W. Webb and T.Keller, *Quadrature Amplitude Modulation: From Basics to Adaptive Trellis-Coded, Turbo-Equalised and Space-Time Coded OFDM, CDMA and MC-CDMA Systems, Second Edition*. New York, USA : John Wiley and Sons, 2004.
- [72] S. M. Alamouti, "A simple transmit diversity technique for wireless communications," *IEEE Journal on Selected Areas in Communications*, vol. 16, pp. 1451–1458, Oct. 1998.
- [73] L. Hanzo, O. Alamri, M. El-Hajjar, and N. Wu, *Near-Capacity Multi-Functional MIMO Systems*. New York, USA: John Wiley IEEE Press, 2009.
- [74] O. Alamri, B. L. Yeap, and L. Hanzo, "Turbo detection of channel-coded space-time signals using sphere packing modulation," in *Proc. VTC2004-Fall Vehicular Technology Conference 2004 IEEE 60th*, vol. 4, pp. 2498–2502, Sept. 26–29, 2004.

- [75] O. Alamri, S. X. Ng, F. Guo, and L. Hanzo, "A purely symbol-based precoded and ldpc-coded iterative-detection assisted sphere-packing modulated space-time coding scheme," in *Proc. IEEE Wireless Communications and Networking Conference WCNC 2006*, vol. 3, pp. 1201–1206, Apr. 3–6, 2006.
- [76] R. Tee, R. G. Maunder, and L. Hanzo, "Exit-chart aided near-capacity irregular bit-interleaved coded modulation design," *IEEE Transactions on Wireless Communications*, vol. 8, pp. 32–37, Jan. 2009.
- [77] J. Yater, "Signal relay systems using large space arrays," *IEEE Transactions on Communications*, vol. 20, pp. 1108 – 1121, Dec. 1972.
- [78] M. Hasna and M.-S. Alouini, "End-to-end performance of transmission systems with relays over rayleigh-fading channels," *IEEE Transactions on Wireless Communications*, vol. 2, pp. 1126 – 1131, Nov. 2003.
- [79] L. Yang, M. Hasna, and M.-S. Alouini, "Average outage duration of multihop communication systems with regenerative relays," *IEEE Transactions on Wireless Communications*, vol. 4, pp. 1366 – 1371, July 2005.
- [80] M. Gastpar and M. Vetterli, "On the capacity of large gaussian relay networks," *IEEE Transactions on Information Theory*, vol. 51, pp. 765 – 779, Mar. 2005.
- [81] Z. Zhang and T. Duman, "Capacity-approaching turbo coding and iterative decoding for relay channels," *IEEE Transactions on Communications*, vol. 53, pp. 1895 – 1905, Nov. 2005.
- [82] A. Host-Madsen and J. Zhang, "Capacity bounds and power allocation for wireless relay channels," *IEEE Transactions on Information Theory*, vol. 51, pp. 2020 – 2040, June 2005.
- [83] W. Chin, Y. Qian, and G. Giambene, "Advances in cooperative and relay communications [guest editorial]," *IEEE Communications Magazine*, vol. 47, pp. 100 – 101, Feb. 2009.
- [84] K. Loa, C.-C. Wu, S.-T. Sheu, Y. Yuan, M. Chion, D. Huo, and L. Xu, "Imt-advanced relay standards [wimax/lte update]," *IEEE Communications Magazine*, vol. 48, pp. 40 – 48, Aug. 2010.
- [85] Y. Yu, R. Hu, C. Bontu, and Z. Cai, "Mobile association and load balancing in a cooperative relay cellular network," *IEEE Communications Magazine*, vol. 49, pp. 83 – 89, May 2011.
- [86] D. Hwang, J. Choi, B. Clerckx, and G. Kim, "Mimo precoder selections in decode-forward relay networks with finite feedback," *IEEE Transactions on Communications*, vol. 59, pp. 1785 – 1790, July 2011.

- [87] X. Xie, B. Rong, T. Zhang, and W. Lei, "Improving physical layer multicast by cooperative communications in heterogeneous networks," *IEEE Wireless Communications*, vol. 18, pp. 58–63, June 2011.
- [88] Z. Ding, K. Leung, D. Goeckel, and D. Towsley, "Opportunistic relaying for secrecy communications: Cooperative jamming vs. relay chatting," *IEEE Transactions on Wireless Communications*, vol. 10, pp. 1725–1729, June 2011.
- [89] T. Korakis, M. Knox, E. Erkip, and S. Panwar, "Cooperative network implementation using open-source platforms," *IEEE Communications Magazine*, vol. 47, pp. 134–141, Feb. 2009.
- [90] L. Chen, R. Carrasco, and I. Wassell, "Opportunistic nonorthogonal amplify-and-forward cooperative communications," *Electronics Letters*, vol. 47, pp. 626–628, Dec. 2011.
- [91] M. Yassaee and M. Aref, "Slepian wolf coding over cooperative relay networks," *IEEE Transactions on Information Theory*, vol. 57, pp. 3462–3482, June 2011.
- [92] F. Tian, W. Zhang, W.-K. Ma, P. Ching, and H. Poor, "An effective distributed space-time code for two-path successive relay network," *IEEE Transactions on Communications*, vol. 59, pp. 2254–2263, Aug. 2011.
- [93] Y. Chen, J. Zhang, and I. Marsic, "Link-layer-and-above diversity in multihop wireless networks," *IEEE Communications Magazine*, vol. 47, pp. 118–124, Feb. 2009.
- [94] Y. Rong and Y. Xiang, "Multiuser multi-hop mimo relay systems with correlated fading channels," *IEEE Transactions on Wireless Communications*, vol. 10, pp. 2835–2840, Sep. 2011.
- [95] X. S. Shen, A. Hjrungnes, Q. Zhang, P. Kumar, and Z. Han, "Guest editorial cooperative networking – challenges and applications (part i)," *IEEE Journal on Selected Areas in Communications*, vol. 30, pp. 241–244, Feb. 2012.
- [96] X. S. Shen, A. Hjrungnes, Q. Zhang, P. Kumar, and Z. Han, "Guest editorial cooperative networking – challenges and applications (part ii)," *IEEE Journal on Selected Areas in Communications*, vol. 30, pp. 1593–1596, Oct. 2012.
- [97] J. Cloud, L. Zeger, and M. Medard, "Mac centered cooperation – synergistic design of network coding, multi-packet reception, and improved fairness to increase network throughput," *IEEE Journal on Selected Areas in Communications*, vol. 30, pp. 341–349, Feb. 2012.
- [98] R. Cao and L. Yang, "Decomposed It codes for cooperative relay communications," *IEEE Journal on Selected Areas in Communications*, vol. 30, pp. 407–414, Feb. 2012.
- [99] J. Rebelatto, B. Uchoa Filho, Y. Li, and B. Vucetic, "Multi-user cooperative diversity through network coding based on classical coding theory," *IEEE Transactions on Signal Processing*, vol. 60, pp. 916–926, Feb. 2012.

- [100] S. Chiochan and E. Hossain, "Cooperative relaying in wi-fi networks with network coding," *IEEE Wireless Communications*, vol. 19, pp. 57–65, April 2012.
- [101] S. Sharma, Y. Shi, J. Liu, Y. Hou, S. Kompella, and S. Midkiff, "Network coding in cooperative communications: Friend or foe?," *IEEE Transactions on Mobile Computing*, vol. 11, pp. 1073–1085, July 2012.
- [102] L. Wei and W. Chen, "Compute-and-forward network coding design over multi-source multi-relay channels," *IEEE Transactions on Wireless Communications*, vol. 11, pp. 3348–3357, Sept. 2012.
- [103] M. Peng, C. Yang, Z. Zhao, W. Wang, and H.-H. Chen, "Cooperative network coding in relay-based imt-advanced systems," *IEEE Communications Magazine*, vol. 50, pp. 76–84, April 2012.
- [104] R. Niati, A. Banihashemi, and T. Kunz, "Throughput and energy optimization in wireless networks: Joint mac scheduling and network coding," *IEEE Transactions on Vehicular Technology*, vol. 61, pp. 1372–1382, Mar. 2012.
- [105] J. Liu, N. Shroff, and H. Sherali, "Optimal power allocation in multi-relay mimo cooperative networks: Theory and algorithms," *IEEE Journal on Selected Areas in Communications*, vol. 30, pp. 331–340, Feb. 2012.
- [106] S. Huang, H. Chen, and Y. Zhang, "Optimal power allocation for spectrum sensing and data transmission in cognitive relay networks," *IEEE Wireless Communications Letters*, vol. 1, pp. 26–29, Feb. 2012.
- [107] P. Ubaidulla and S. Aissa, "Optimal relay selection and power allocation for cognitive two-way relaying networks," *IEEE Wireless Communications Letters*, vol. 1, pp. 225–228, June 2012.
- [108] H. Kim, S. Lim, H. Wang, and D. Hong, "Optimal power allocation and outage analysis for cognitive full duplex relay systems," *IEEE Transactions on Wireless Communications*, vol. 11, pp. 3754–3765, Oct. 2012.
- [109] H. Yu, W. Tang, and S. Li, "Joint optimal sensing time and power allocation for amplify-and-forward cognitive relay networks," *IEEE Communications Letters*, vol. 16, pp. 1948–1951, Dec. 2012.
- [110] J. C. Park, I. Song, and Y. H. Kim, "Outage-optimal allocation of relay power for analog network coding with three transmission phases," *IEEE Communications Letters*, vol. 16, pp. 838–841, June 2012.

- [111] J. M. Park, S.-L. Kim, and J. Choi, "Hierarchically modulated network coding for asymmetric two-way relay systems," *IEEE Transactions on Vehicular Technology*, vol. 59, pp. 2179–2184, June 2010.
- [112] W. Guo and I. Wassell, "Capacity-outage-tradeoff (cot) for cooperative networks," *IEEE Journal on Selected Areas in Communications*, vol. 30, pp. 1641–1648, Oct. 2012.
- [113] X. Gong, T. Chandrashekar, J. Zhang, and H. Poor, "Opportunistic cooperative networking: To relay or not to relay?," *IEEE Journal on Selected Areas in Communications*, vol. 30, pp. 307–314, Feb. 2012.
- [114] S. Sharma, Y. Shi, Y. Hou, H. Sherali, S. Kompella, and S. Midkiff, "Joint flow routing and relay node assignment in cooperative multi-hop networks," *IEEE Journal on Selected Areas in Communications*, vol. 30, pp. 254–262, Feb. 2012.
- [115] S.-J. Syue, C.-L. Wang, T. Aguilar, V. Gauthier, and H. Afifi, "Cooperative geographic routing with radio coverage extension for ser-constrained wireless relay networks," *IEEE Journal on Selected Areas in Communications*, vol. 30, pp. 271–279, Feb. 2012.
- [116] R. Zhang, J. Shi, Y. Zhang, and J. Sun, "Secure cooperative data storage and query processing in unattended tiered sensor networks," *IEEE Journal on Selected Areas in Communications*, vol. 30, pp. 433–441, Feb. 2012.
- [117] A. Le and A. Markopoulou, "Cooperative defense against pollution attacks in network coding using spacemac," *IEEE Journal on Selected Areas in Communications*, vol. 30, pp. 442–449, Feb. 2012.
- [118] Q. Yan, M. Li, Z. Yang, W. Lou, and H. Zhai, "Throughput analysis of cooperative mobile content distribution in vehicular network using symbol level network coding," *IEEE Journal on Selected Areas in Communications*, vol. 30, pp. 484–492, Feb. 2012.
- [119] Z. Zhang and H. Jiang, "Distributed opportunistic channel access in wireless relay networks," *IEEE Journal on Selected Areas in Communications*, vol. 30, pp. 1675–1683, Oct. 2012.
- [120] S. Singh and M. Motani, "Cooperative multi-channel access for 802.11 mesh networks," *IEEE Journal on Selected Areas in Communications*, vol. 30, pp. 1684–1693, Oct. 2012.
- [121] K.-H. Liu and H.-H. Chen, "Performance analysis of threshold relaying with random channel access over non-identically distributed rayleigh-fading channels," *IEEE Journal on Selected Areas in Communications*, vol. 30, pp. 1703–1710, Oct. 2012.
- [122] X. Li, J. Yang, A. Nayak, and I. Stojmenovic, "Localized geographic routing to a mobile sink with guaranteed delivery in sensor networks," *IEEE Journal on Selected Areas in Communications*, vol. 30, pp. 1719–1729, Oct. 2012.

- [123] R. Urgaonkar and M. Neely, "Optimal routing with mutual information accumulation in wireless networks," *IEEE Journal on Selected Areas in Communications*, vol. 30, pp. 1730–1737, Oct. 2012.
- [124] P. Zhang, C. Lin, Y. Jiang, P. Lee, and J. Lui, "Anoc: Anonymous network-coding-based communication with efficient cooperation," *IEEE Journal on Selected Areas in Communications*, vol. 30, pp. 1738–1745, Oct. 2012.
- [125] H. Al-Zubaidy, C. Huang, and J. Yan, "Dynamic packet scheduler optimization in wireless relay networks," *IEEE Journal on Selected Areas in Communications*, vol. 30, pp. 1746–1753, Oct. 2012.
- [126] J. Jose, S. Vishwanath, and L. Ying, "Queue-architecture and stability analysis in cooperative relay networks," *IEEE Journal on Selected Areas in Communications*, vol. 30, pp. 1754–1761, Oct. 2012.
- [127] J. Yu, H. Roh, W. Lee, S. Pack, and D.-Z. Du, "Topology control in cooperative wireless ad-hoc networks," *IEEE Journal on Selected Areas in Communications*, vol. 30, pp. 1771–1779, Oct. 2012.
- [128] Y. Liu, L. Ni, and C. Hu, "A generalized probabilistic topology control for wireless sensor networks," *IEEE Journal on Selected Areas in Communications*, vol. 30, pp. 1780–1788, Oct. 2012.
- [129] K. Zhu, D. Niyato, and P. Wang, "Dynamic service selection and bandwidth allocation in IEEE 802.16m mobile relay networks," *IEEE Journal on Selected Areas in Communications*, vol. 30, pp. 1798–1805, Oct. 2012.
- [130] M. Hajiaghayi, M. Dong, and B. Liang, "Jointly optimal channel and power assignment for dual-hop multi-channel multi-user relaying," *IEEE Journal on Selected Areas in Communications*, vol. 30, pp. 1806–1814, Oct. 2012.
- [131] P. Chou and Y. Wu, "Network coding for the internet and wireless networks," *IEEE Signal Processing Magazine*, vol. 24, no. 5, pp. 77–85, 2007.
- [132] E. Soljanin, "Network multicast with network coding [lecture notes]," *IEEE Signal Processing Magazine*, vol. 25, no. 5, pp. 109–112, 2008.
- [133] Y. Chen and S. Kishore, "On the tradeoffs of implementing randomized network coding in multicast networks," *IEEE Transactions on Communications*, vol. 58, pp. 2107–2115, July 2010.
- [134] C. Fragouli and E. Soljanin, "Network coding fundamentals," *Foundation and Trends in Networking*, vol. 2, no. 1, pp. 1–133, 2007.

- [135] R. Dougherty, C. Freiling, and K. Zeger, "Network coding and matroid theory," *Proceedings of the IEEE*, vol. 99, pp. 388–405, Mar. 2011.
- [136] Z. Zhang, "Theory and applications of network error correction coding," *Proceedings of the IEEE*, vol. 99, pp. 406–420, Mar. 2011.
- [137] N. Cai and T. Chan, "Theory of secure network coding," *Proceedings of the IEEE*, vol. 99, pp. 421–437, Mar. 2011.
- [138] Y. R.W., C. N. Li S.-Y.R., and Z. Z., "Network coding theory," *Network Coding Theory, Foundations and Trends in Communication and Information Theory*, vol. 2, no. 4 and 5, pp. 241–381, 2006.
- [139] D. Traskov, M. Heindlmaier, M. Medard, and R. Koetter, "Scheduling for network-coded multicast," *Networking, IEEE/ACM Transactions on*, vol. 20, pp. 1479–1488, Oct. 2012.
- [140] B. Li and Y. Wu, "Network coding [scanning the issue]," *Proceedings of the IEEE*, vol. 99, pp. 363–365, Mar. 2011.
- [141] S.-Y. Li, Q. Sun, and Z. Shao, "Linear network coding: Theory and algorithms," *Proceedings of the IEEE*, vol. 99, pp. 372–387, Mar. 2011.
- [142] R. W. Yeung, *Information Theory and Network Coding*. New York, USA: Springer, 2010.
- [143] N. Cai and R. Yeung, "Secure network coding," in *IEEE International Symposium on Information Theory, 2002*, p. 323, June-July 2002.
- [144] N. Cai and R. Yeung, "Secure network coding on a wiretap network," *IEEE Transactions on Information Theory*, vol. 57, pp. 424–435, Jan. 2011.
- [145] S. El Rouayheb, E. Soljanin, and A. Sprintson, "Secure network coding for wiretap networks of type ii," *IEEE Transactions on Information Theory*, vol. 58, pp. 1361–1371, Mar. 2012.
- [146] R. Ahlswede, N. Cai, and R. Yeung, "Network information flow theory," in *IEEE International Symposium on Information Theory, 1998*, p. 186, Aug. 1998.
- [147] R. Koetter and F. R. Kschischang, "Coding for errors and erasures in random network coding," in *IEEE International Symposium on Information Theory, 2007 (ISIT 2007)*, pp. 791–795, June 2007.
- [148] R. Koetter and F. Kschischang, "Coding for errors and erasures in random network coding," *IEEE Transactions on Information Theory*, vol. 54, pp. 3579–3591, Aug. 2008.
- [149] Z. Zhang, "Linear network error correction codes in packet networks," *IEEE Transactions on Information Theory*, vol. 54, pp. 209–218, Jan. 2008.

- [150] C. Wang, M. Xiao, and M. Skoglund, "Diversity-multiplexing tradeoff analysis of coded multi-user relay networks," *IEEE Transactions on Communications*, vol. 59, pp. 1995–2005, July 2011.
- [151] D. Tse and P. Viswanath, *Fundamentals of Wireless Communications*. Englewood Cliffs, NJ, USA: Cambridge: Cambridge University Press, 2005.
- [152] J. Laneman, D. Tse, and G. Wornell, "Cooperative diversity in wireless networks: Efficient protocols and outage behavior," *IEEE Transactions on Information Theory*, vol. 50, pp. 3062–3080, Dec. 2004.
- [153] I. S. Gradshteyn and I. M. Ryzhik, *Table of Integrals, Series, and Products, Sixth Edition*. CA: Academic Press, 2000.
- [154] P. Ho and D. Fung, "Error performance of multiple-symbol differential detection of PSK signals transmitted over correlated Rayleigh fading channels," *IEEE Transactions on Communications*, vol. 40, pp. 1566–1569, Oct. 1992.
- [155] V. Pauli, L. Lampe, and R. Schober, "'Turbo DPSK' using soft multiple-symbol differential sphere decoding," *IEEE Transactions on Information Theory*, vol. 52, pp. 1385–1398, April 2006.
- [156] S. X. Ng and L. Hanzo, "On the mimo channel capacity of multidimensional signal sets," *IEEE Transactions on Vehicular Technology*, vol. 55, pp. 528–536, Mar. 2006.
- [157] A. Ashikhmin, G. Kramer, and S. ten Brink, "Extrinsic information transfer functions: model and erasure channel properties," *IEEE Transactions on Information Theory*, vol. 50, pp. 2657–2673, Nov. 2004.
- [158] M. Tücher and J. Hagenauer, "Exit charts of irregular codes," in *Proceeding of the 36th Annual Conference on Information Sciences and Systems [CDROM], (Princeton, NJ, USA)*, Mar. 2002.
- [159] M. Tüchler, "Design of serially concatenated systems depending on the block length," *IEEE Transactions on Communications*, vol. 52, pp. 209–218, Feb. 2004.
- [160] S. ten Brink, "Convergence behavior of iteratively decoded parallel concatenated codes," *IEEE Transactions on Communications*, vol. 49, pp. 1727–1737, Oct. 2001.
- [161] S. X. Ng, S. Das, J. Wang, and L. Hanzo, "Near-Capacity Iteratively Decoded Space-Time Block Coding," in *Proc. IEEE Vehicular Technology Conference VTC Spring 2008*, pp. 590–594, May 11–14, 2008.
- [162] S. ten Brink, "Rate one-half code for approaching the Shannon limit by 0.1 dB," *Electronics Letters*, vol. 36, pp. 1293–1294, July 20, 2000.

- [163] M. Tuchler, "Convergence prediction for iterative decoding of threefold concatenated systems," in *Proc. IEEE Global Telecommunications Conference GLOBECOM '02*, vol. 2, pp. 1358–1362, Nov. 17–21, 2002.
- [164] S. X. Ng, J. Wang, M. Tao, L.-L. Yang, and L. Hanzo, "Iteratively decoded variable length space-time coded modulation: Code construction and convergence analysis," *IEEE Transactions on Wireless Communications*, vol. 6, pp. 1953–1963, May 2007.
- [165] A. Ghosh, R. Ratasuk, B. Mondal, N. Mangalvedhe, and T. Thomas, "LTE-advanced: next-generation wireless broadband technology [Invited Paper]," *IEEE Wireless Communications*, vol. 17, pp. 10–22, June 2010.
- [166] G. Piro, L. Grieco, G. Boggia, F. Capozzi, and P. Camarda, "Simulating LTE cellular systems: An open-source framework," *IEEE Transactions on Vehicular Technology*, vol. 60, pp. 498–513, Feb. 2011.
- [167] S. X. Ng, J. Wang, and L. Hanzo, "Unveiling Near-Capacity Code Design: The Realization of Shannon's Communication Theory for MIMO Channels," in *Proc. IEEE International Conference on Communications ICC '08*, pp. 1415–1419, May 19–23, 2008.
- [168] J. Zuo, H. V. Nguyen, S. X. Ng, and L. Hanzo, "Energy-efficient relay aided ad hoc networks using iteratively detected irregular convolutional coded, unity-rate coded and space-time trellis coded transceivers," in *Wireless Communications and Networking Conference (WCNC), 2011 IEEE*, pp. 1179–1184, March 2011.
- [169] H. Ochiai, P. Mitran, and V. Tarokh, "Design and analysis of collaborative diversity protocols for wireless sensor networks," in *Proc. VTC2004-Fall Vehicular Technology Conference 2004 IEEE 60th*, vol. 7, pp. 4645–4649, Sept. 26–29, 2004.
- [170] L. Kong, S. Ng, R. Tee, R. Maunder, and L. Hanzo, "Reduced-complexity near-capacity downlink iteratively decoded generalized multi-layer space-time coding using irregular convolutional codes," *IEEE Transactions on Wireless Communications*, vol. 9, pp. 684–695, February 2010.
- [171] M. C. Valenti and B. Zhao, "Distributed turbo codes: towards the capacity of the relay channel," in *IEEE 58th Proc. VTC 2003-Fall Vehicular Technology Conference 2003*, vol. 1, pp. 322–326, Oct. 6–9, 2003.
- [172] A. Sendonaris, E. Erkip, and B. Aazhang, "User cooperation diversity. Part I. System description," *IEEE Transactions on Communications*, vol. 51, pp. 1927–1938, Nov. 2003.
- [173] A. Host-Madsen and J. Zhang, "Capacity bounds and power allocation for wireless relay channels," *IEEE Transactions on Information Theory*, vol. 51, pp. 2020–2040, June 2005.

- [174] L. Kong, S. X. Ng, R. G. Maunder, and L. Hanzo, "Successive Relaying Aided Near-Capacity Irregular Distributed Space-Time Coding," in *IEEE Global Telecommunications Conference, 2009. GLOBECOM 2009*, pp. 1–5, Nov. 30–Dec. 4, 2009.
- [175] L. Wang and L. Hanzo, "Dispensing with channel estimation: Differentially modulated cooperative wireless communications," *Communications Surveys Tutorials, IEEE*, vol. 14, no. 3, pp. 836–857, 2012.
- [176] A. Asterjadhi, E. Fasolo, M. Rossi, J. Widmer, and M. Zorzi, "Toward network coding-based protocols for data broadcasting in wireless ad hoc networks," *IEEE Transactions on Wireless Communications*, vol. 9, pp. 662–673, Feb. 2010.
- [177] R. Koetter and M. Medard, "An algebraic approach to network coding," *Networking, IEEE/ACM Transactions on*, vol. 11, pp. 782–795, Oct. 2003.
- [178] M. Jafari, L. Keller, C. Fragouli, and K. Argyraki, "Compressed network coding vectors," pp. 109–113, June 2009.
- [179] M. Xiao and M. Skoglund, "Design of network codes for multiple-user multiple-relay wireless networks," in *IEEE International Symposium on Information Theory, 2009. (ISIT 2009)*, pp. 2562–2566, June 2009.
- [180] C. Hausl and P. Dupraz, "Joint Network-Channel Coding for the Multiple-Access Relay Channel," in *3rd Annual IEEE Communications Society on Sensor and Ad Hoc Communications and Networks, 2006. SECON '06*, vol. 3, pp. 817–822, Sept. 2006.
- [181] SAGE, "Open source mathematics software," in *online source available at <http://www.sagemath.org/>*.
- [182] C. F. Golub, Gene H.; Van Loan, *Matrix Computations*. Johns Hopkins Studies in Mathematical Sciences: Johns Hopkins University Press, 1996.
- [183] M. Xiao and M. Skoglund, "Multiple-user cooperative communications based on linear network coding," *IEEE Transactions on Communications*, vol. 58, pp. 3345–3351, Dec. 2010.
- [184] Bromwich, T.J., *An Introduction to the Theory of Infinite Series*. MacMillan, 1965.
- [185] L. Kong, S. X. Ng, R. Maunder, and L. Hanzo, "Maximum-throughput irregular distributed space-time code for near-capacity cooperative communications," *IEEE Transactions on Vehicular Technology*, vol. 59, pp. 1511–1517, Mar. 2010.
- [186] S. X. Ng, C. Qian, D. Liang, and L. Hanzo, "Adaptive turbo trellis coded modulation aided distributed space-time trellis coding for cooperative communications," in *2010 IEEE 71st Vehicular Technology Conference (VTC 2010-Spring)*, pp. 1–5, May 2010.

- [187] R. Tee, T. Nguyen, S. Ng, L.-L. Yang, and L. Hanzo, "Luby transform coding aided bit-interleaved coded modulation for the wireless internet," in *2007 IEEE 66th Vehicular Technology Conference, 2007. VTC-2007 Fall*, pp. 2025–2029, Oct. 2007.
- [188] T. Nguyen, M. El-Hajjar, L. Yang, and L. Hanzo, "A systematic luby transform coded v-blast system," in *IEEE International Conference on Communications, 2008. ICC '08.*, pp. 775–779, May 2008.
- [189] O. Iscan and C. Hausl, "Iterative network and channel decoding for the relay channel with multiple sources," in *2011 IEEE Vehicular Technology Conference (VTC-2011 Fall)*, pp. 1–5, Sept. 2011.
- [190] F. Sun, "Two-layer coding rate optimization in relay-aided systems," in *Vehicular Technology Conference (VTC Fall), 2011 IEEE*, pp. 1–5, Sept. 2011.
- [191] B. Li and D. Niu, "Random network coding in peer-to-peer networks: From theory to practice," *Proceedings of the IEEE*, vol. 99, pp. 513–523, march 2011.
- [192] R. Kim, J. Jin, and B. Li, "Scattered random network coding for efficient transmission in multihop wireless networks," *IEEE Transactions on Vehicular Technology*, vol. 60, pp. 2383–2389, jun 2011.
- [193] Hoffman, K. M. and Kunze, R., *Linear Algebra, Second Edition*. Englewood Cliffs, NJ: Prentice Hall, 1971.
- [194] O. Alamri, B. Yeap, and L. Hanzo, "A Turbo Detection and Sphere-Packing-Modulation-Aided Space-Time Coding Scheme," *IEEE Transactions on Vehicular Technology*, vol. 56, pp. 575–582, March 2007.
- [195] O. Alamri, J. Wang, S. X. Ng, L.-L. Yang, and L. Hanzo, "Near-Capacity Transceiver Design Using Exit-Curve Fitting: Three-Stage Turbo Detection of Irregular Convolutional Coded Joint Sphere-Packing Modulation and Space-Time Coding," in *IEEE International Conference on Communications, 2007, ICC '07*, pp. 4028–4033, June 2007.
- [196] O. Alamri, J. Wang, S. X. Ng, L.-L. Yang, and L. Hanzo, "Near-Capacity Three-Stage Turbo Detection of Irregular Convolutional Coded Joint Sphere-Packing Modulation and Space-Time Coding," *IEEE Transactions on Communications*, vol. 57, pp. 1486–1495, May 2009.
- [197] D. Nguyen and M. Krunz, "Price-based joint beamforming and spectrum management in multi-antenna cognitive radio networks," *IEEE Journal on Selected Areas in Communications*, vol. 30, pp. 2295–2305, Dec. 2012.

-
- [198] Q. Liang, S. Han, F. Yang, G. Sun, and X. Wang, "A distributed-centralized scheme for short- and long-term spectrum sharing with a random leader in cognitive radio networks," *IEEE Journal on Selected Areas in Communications*, vol. 30, pp. 2274 –2284, Dec. 2012.

Subject Index

Symbols

<i>C</i> mode	152
<i>FD</i> mode	152, 154
16PSK	34
17co-IrCC	59, 63
36co-IrCC	59, 63
4PSK	8
8PSK	34

A

AF	6, 76
AWGN	7

B

BER	ii, 1, 39
BICM	7
BM	9
BP	103
BPS	9, 35, 123, 164
BPs	103, 152
BPSK	34
BS	3, 103

C

CAF	6
CC	iii, 150, 209, 224, 239
CCDF	39
CCMC	ii, 27, 29, 102, 206
CDD	31
CNC	25
CP	103

CPs	103, 149
CSI	31

D

D-DCMC	ii, 27, 29, 35, 206
DBPSK	36
DC-IrCC-URC-STBC-SP	209
DC-IRCC-URC-STTC	76
DC-IrCC-URC-STTC	ii
DCMC	ii, 27, 29, 206
DF	6, 76
DMPSK	31, 65
DMT	26
DNC	103
DNCs	103
DQPSK	36

E

EGC	5
EXIT	ii, 29, 35, 46, 48, 65

F

FEC	46
FER	iii, 3, 9, 30

G

GDNC	6, 25, 26, 103
GDNCs	103
GF	103
GNC	25
GNCMN	149, 208

H

HNC.....23

I

i.i.d.....30

IF.....103, 152, 225

IFs.....103, 150

IIR.....46

IrCC.....46

IrCC-URC.....80

IrCC-URC-DBPSK.....65

IrCC-URC-DMPSK.....ii, 3, 47, 149, 206

IrCC-URC-DQPSK.....36

IrCC-URC-MPSK.....ii, 3, 47, 81, 149, 206

IrCC-URC-QPSK.....56

IrCC-URC-STTC.....48, 77

IrCC-URC-STTC-MPSK.....ii, 47, 206

IrCC-URC-STTC2x1.....99

IrCCs.....44

L

LDPC.....15

LNC.....23

LTE.....143

LTE-Advanced.....193

M

MAC.....20

MAP.....5

MCEM.....221

MDM.....1, 205

MDS.....6, 25, 26, 106

MIMO.....ii, 1, 4, 48, 125

ML.....31

MRC.....5

MRRC.....11

MSDD.....31

MSDD-aided-DEM.....65

MSDD-aided-DMPSK.....33

MSDSD.....31

N

NC1.....iii, 150, 208, 224, 239

NC2.....iii, 150, 208

NCMN.....iii, 102, 149, 199, 207, 210

NLNC.....23

NNCNM.....iii

P

PALEM.....iii, 3, 115, 207

PAM.....4

PC.....25

PFs.....103, 149

PHY.....20

PRBM.....103, 207

PSK.....7

QQ²PSK.....7

QAM.....4

QPSK.....7, 34

R

R-D.....125

RNC.....6, 25, 26

RS.....5, 25, 106

RSC.....32

S

S-D.....125

S-R.....125

SC.....5, 26

SISO.....125

SNC.....25

SNR.....ii, 4

SP.....14

SP-STBC.....ii, 205

STBC.....4, 5, 8, 11

STBC-PSK/QAM.....ii

STBC-SP.....4, 8

STBCs.....ii, 205

STC.....7

STTC.....	4, 5, 8, 47, 48
STTC-PSK/QAM.....	ii
STTC-QPSK.....	48
STTCs.....	ii, 8, 205

T

TS.....	103
---------	-----

U

URC.....	46
URC-DMPSK.....	65
URC-DQPSK.....	36
URC-QPSK.....	56
URC-STTC _{2×1} -QPSK.....	50
URC-STTC-MPSK.....	48
URC-STTC-QPSK.....	48

V

VMIMO.....	76
------------	----

Author Index

Cover, [24] 5, 20
Yater, [77] 20

A

A., [35] 6
A., [82] 20
A., [25] 5
A., [176] 103
A., [165] 46, 69, 143, 194
A., [117] 22
A., [49] 6, 26
A., [145] 25
A., [122] 22
A., [29] 5
A., [157] 35, 46–48, 50, 57, 59, 65
A., [173] 76, 84, 97, 123, 125
A.E., [24] 5, 20
A.H., [104] 22
Aazhang, [29] 5
Afifi, [115] 22
Aguilar, [115] 22
Ahlsvede, [146] 25, 26
Ahlsvede, [33] 5, 26
Aissa, [107] 22
Al-Zubaidy, [125] 22
Alamouti, S.M. [28] 5
Alamouti, [72] 11, 13, 76
Alamri, [74] 14
Alamri, [75] 15
Alouini, [78] 20
Alouini, [79] 20

Anh Le, [117] 22
Are, [95] 22
Are, [96] 22
Aref, [91] 22
Argyraki, [178] 103
Ashikhmin, [157] . 35, 46–48, 50, 57, 59, 65
Asterjadhi, [176] 103

B

B., [42] 6, 25, 26, 103, 162
B., [38] 6
B., [165] 46, 69, 143, 194
B., [140] 24, 27
B., [86] 20
B., [48] 6, 26
B., [12] .. 6, 25, 26, 147, 149, 159–161, 168,
181
B., [99] . 22, 25, 26, 103, 106, 107, 113, 115,
118, 119, 122, 123, 127, 134, 136,
147, 154, 169, 172, 211, 212
B., [29] 5
B.F., [48] 6, 26
B.F., [12] 6, 25, 26, 147, 149, 159–161, 168,
181
B.F., [99] 22, 25, 26, 103, 106, 107, 113,
115, 118, 119, 122, 123, 127, 134,
136, 147, 154, 169, 172, 211, 212
Bahl, [21] 5
Bahl, [22] 5
Banihashemi, [104] 22
Baochun Li, [191] 162, 181

- Baochun Li, [192]..... 181
 Bartolomeu F., [11]..... 145, 149, 173
 Ben Liang, [130]..... 22
 Berrou, [25]..... 5
 Biglieri, [51]..... 4, 7
 Bo Rong, [87]..... 20
 Boggia, [166]..... 46, 69, 143
 Bontu, [85]..... 20
 Boutros, [64]..... 7
 Brennan, [17]..... 5
 Brunel, [64]..... 7
- C**
- C van der Meulen, E. [20]..... 5
 C., D.N. [7]..... 6, 76, 77
 C., [21]..... 5
 C., [25]..... 5
 C., [180]..... 106
 C., [178]..... 103
 C., [135]..... 23
 C., [134]..... 23, 24
 C.S., [85]..... 20
 Cai, [146]..... 25, 26
 Cai N., [138]..... 23
 Calderbank, [70]..... 8
 Camarda, [166]..... 46, 69, 143
 Capozzi, [166]..... 46, 69, 143
 Carrasco, [90]..... 22
 Chan, [137]..... 23
 Chandrashekar, [113]..... 22
 Chang-Kyung Sung, [63]..... 7
 Changcheng Huang, [125]..... 22
 Changqing Yang, [103]..... 22
 Chao, [5]..... 3
 Chao Wang, [150]..... 25, 26
 Chao Xu, [3]..... 3
 Charles F., [182]..... 114
 Chen, [133]..... 22
 Chen, [90]..... 22
- Chieochan, [100]..... 22
 Chih-Chiang Wu, [84]..... 20, 194
 Chin, [83]..... 20, 22
 Chin-Liang Wang, [115]..... 22
 Ching, [92]..... 22
 Chion, [84]..... 20, 194
 Chou, [131]..... 22
 Christoph, [189]..... 147, 159
 Chuang Lin, [124]..... 22
 Chuanping Hu, [128]..... 22
 Chuyi Qian, [186]..... 146
 Clerckx, [86]..... 20
 Cloud, [97]..... 22
 Cocke, [22]..... 5
 Costello, [43]..... 6, 26
 Cullum, [21]..... 5
- D**
- D., [154]..... 31, 32
 D., [43]..... 6, 26
 D., [84]..... 20, 194
 D., [88]..... 20, 22
 D., [139]..... 23
 D., [129]..... 22
 D.G., [17]..... 5
 D.L., [88]..... 20, 22
 D.N., [197]..... 209
 D.N.C., [152]..... 30, 118
 D.R., [42]..... 6, 25, 26, 103, 162
 D.Tse, [151]..... 30, 39, 69
 Daesik Hong, [108]..... 22
 Dandan Liang, [186]..... 146
 Danilo, [11]..... 145, 149, 173
 Das, [161]..... 46, 76, 77
 Di Niu, [191]..... 162, 181
 Ding-Zhu Du, [127]..... 22
 Dohler, [38]..... 6
 Dougherty, [135]..... 23
 Duckdong Hwang, [86]..... 20

- Duman, [81] 20
 Dupraz, [180] 106
- E**
- E., [23] 5
 E., [132] 22
 E., [89] 22
 E., [176] 103
 E., [145] 25
 E., [100] 22
 E., [29] 5
 E., [51] 4, 7
 E., [134] 23, 24
 E.Hajjar, M. [45] . 6, 8, 16, 44, 56, 57, 66, 77
 Effros, [42] 6, 25, 26, 103, 162
 El Rouayheb, [145] 25
 El-Hajjar, M. [73] 12
 El-Hajjar, [188] 146, 159
 Elia, [51] 4, 7
 Elias, P. [15] 5
 Erkip, [89] 22
 Erkip, [29] 5
- F**
- F., A. [70] 8
 F., [21] 5
 F., [22] 5
 F., [166] 46, 69, 143
 F., [75] 15
 F.R., [148] 25, 26
 Fan Sun, [190] 149
 Fasolo, [176] 103
 Feng Tian, [92] 22
 Feng Yang, [198] 209
 Forney, C. [19] 5
 Foschini, G.J. [27] 5
 Fragouli, [178] 103
 Fragouli, [134] 23, 24
 Frank R., [147] 25, 26
 Frazer, [21] 5
- Freiling, [135] 23
 Fuja, [43] 6, 26
 Fung, [154] 31, 32
- G**
- G., [83] 20, 22
 G., [166] 46, 69, 143
 G., [157] 35, 46–48, 50, 57, 59, 65
 G.B., [44] 6
 G.W., [152] 30, 118
 Gamal, [24] 5, 20
 Gaofei Sun, [198] 209
 Gastpar, [80] 20
 Gauthier, [115] 22
 Gene H.; Van Loan, [182] 114
 Ghosh, [165] 46, 69, 143, 194
 Giambene, [83] 20, 22
 Giannakis, [44] 6
 Gil Kim, [86] 20
 Glavieux, [25] 5
 Goeckel, [88] 20, 22
 Goldsmith, [49] 6, 26
 Golub, [182] 114
 Gradshteyn, I.S. [153] 30
 Gresset, [64] 7
 Grieco, [166] 46, 69, 143
 Guo, [75] 15
- H**
- H., [115] 22
 H., [125] 22
 H., [169] 63, 78, 79
 H.D., [114] 22
 H.D., [105] 22
 H.V., [92] 22
 H.V., [113] 22
 Hagenauer, J. [158] 44, 46, 47, 49, 56
 Hai Jiang, [119] 22
 Hajiaghayi, [130] 22
 Hamming, R.W. [14] 5

- Han, [95] 22
- Han, [96] 22
- Hano Wang, [108] 22
- Hanzo, L. [73] 12
- Hanzo, L. [45] ... 6, 8, 16, 44, 56, 57, 66, 77
- Hanzo, L. [71] 8
- Hanzo, L. [1] 1, 2
- Hanzo, [156] 33
- Hanzo, [187] 146, 159
- Hanzo, [188] 146, 159
- Hanzo, [185] 125
- Hanzo, [170] 66
- Hanzo, [174] 77
- Hanzo, [186] 146
- Hanzo, [9] 3
- Hanzo, [10] 3
- Hanzo, [168] 52
- Hanzo, [175] 87
- Hanzo, [5] 3
- Hanzo, [6] 3
- Hanzo, [3] 3
- Hanzo, [4] 3, 4
- Hanzo, [74] 14
- Hanzo, [75] 15
- Hanzo, [164] 46, 150
- Hanzo, [167] 48
- Hanzo, [161] 46, 76, 77
- Harold H., [36] 6
- Hasna, [78] 20
- Hasna, [79] 20
- Hausl, [180] 106
- Hausl, [189] 147, 159
- Hedayat, [35] 6
- Heejun Roh, [127] 22
- Heindlmaier, [139] 23
- Hjorungnes, [96] 22
- Hjrunngnes, [95] 22
- Ho, [154] 31, 32
- Ho, [42] 6, 25, 26, 103, 162
- Hoffman, [193] 181
- Hongbin Chen, [106] 22
- Hongqiang Zhai, [118] 22
- Hossain, [100] 22
- Host-Madsen, [82] 20
- Host-Madsen, [173] 76, 84, 97, 123, 125
- Hou, [114] 22
- Hou, [101] 22
- Hsiao-Hwa Chen, [103] 22
- Hsiao-Hwa Chen, [121] 22
- Hu, [37] 6
- Hu, [85] 20
- Hung Viet, [5] 3
- Hung Viet, [6] 3
- Hung Viet, [4] 3, 4
- Hung Viet Nguyen, [9] 3
- Hung Viet Nguyen, [10] 3
- Hung Viet Nguyen, [168] 52
- Hung Viet Nguyen, [3] 3
- Hunter, [35] 6
- Huo, [84] 20, 194
- Huogen, [109] 22
- Hwangjun Song, [63] 7
- Hyungjong Kim, [108] 22
- I**
- I., [93] 22
- I., [49] 6, 26
- I., [122] 22
- I.J., [90] 22
- I.J., [112] 22
- Ickho Song, [110] 22
- Inkyu Lee, [63] 7
- Iscan, [189] 147, 159
- J**
- J., J. [64] 7
- J., [22] 5
- J., [77] 20
- J., [82] 20

- J., [37] 6
- J., [43] 6, 26
- J., [176] 103
- J., [99] . 22, 25, 26, 103, 106, 107, 113, 115,
118, 119, 122, 123, 127, 134, 136,
147, 154, 169, 172, 211, 212
- J., [97] 22
- J., [50] 6, 26
- J., [125] 22
- J., [126] 22
- J., [173] 76, 84, 97, 123, 125
- J.C.S., [124] 22
- J.L., [48] 6, 26
- J.L., [12] 6, 25, 26, 147, 149, 159–161, 168,
181
- J.N., [152] 30, 118
- Jae Cheol Park, [110] 22
- Jafari, [178] 103
- Janani, [35] 6
- Jelinek, [21] 5
- Jelinek, [22] 5
- Jia Liu, [105] 22
- Jia Liu, [101] 22
- Jian Zhang, [93] 22
- Jieun Yu, [127] 22
- Jin Jin, [192] 181
- Jin Wang, [164] 46, 150
- Jin Wang, [167] 48
- Jin Wang, [161] 46, 76, 77
- Jing Shi, [116] 22
- Jing Ti, [39] 6
- Jing Zuo, [168] 52
- Jinho Choi, [111] 22
- Jinyuan Sun, [116] 22
- Jiulin Yang, [122] 22
- Joao Luiz, [47] 6, 25, 26, 103, 106, 107, 113,
115, 118, 119, 122, 123, 127, 134,
136, 147, 165, 166, 169, 172, 207,
211, 212
- Joao Luiz, [11] 145, 149, 173
- Joao Luiz, [5] 3
- Joao Luiz, [6] 3
- Jose, [126] 22
- Jun Shi, [42] 6, 25, 26, 103, 162
- Jung Min Park, [111] 22
- Jungho Cho, [63] 7
- Junil Choi, [86] 20
- Junshan Zhang, [113] 22
- K**
- K., [178] 103
- K., [84] 20, 194
- K., [135] 23
- K.K., [88] 20, 22
- Karger, [42] 6, 25, 26, 103, 162
- Keller, [178] 103
- Kim, [192] 181
- Kishore, [133] 22
- Kliwer, [43] 6, 26
- Kliwer, [50] 6, 26
- Knox, [89] 22
- Koetter, [177] 103, 211
- Koetter, [42] 6, 25, 26, 103, 162
- Koetter, [147] 25, 26
- Koetter, [148] 25, 26
- Koetter, [139] 23
- Kompella, [114] 22
- Kompella, [101] 22
- Kong, [174] 77
- Korakis, [89] 22
- Kramer, [157] 35, 46–48, 50, 57, 59, 65
- Krunz, [197] 209
- Kschischang, [147] 25, 26
- Kschischang, [148] 25, 26
- Kuang-Hao Liu, [121] 22
- Kumar, [95] 22
- Kumar, [96] 22
- Kun Zhu, [129] 22

- Kunz, [104] 22
 Kunze, [193] 181
- L**
- L., B. [74] 14
 L., [21] 5
 L., [22] 5
 L., [156] 33
 L., [155] 32
 L., [187] 146, 159
 L., [188] 146, 159
 L., [178] 103
 L., [185] 125
 L., [170] 66
 L., [186] 146
 L., [9] 3
 L., [10] 3
 L., [90] 22
 L., [168] 52
 L., [175] 87
 L., [3] 3
 L., [128] 22
 L., [74] 14
 L., [64] 7
 L., [164] 46, 150
 L., [167] 48
 L.-L., [187] 146, 159
 L.A., [166] 46, 69, 143
 L.L., [188] 146, 159
 L.M., [97] 22
 Lajos, [174] 77
 Lajos, [5] 3
 Lajos, [6] 3
 Lajos, [4] 3, 4
 Lampe, [155] 32
 Laneman, [152] 30, 118
 Laneman, [34] 5, 76
 Laneman, [7] 6, 76, 77
 Lee, [124] 22
 Lei Xiao, [43] 6, 26
 Lei Ying, [126] 22
 Leong, [42] 6, 25, 26, 103, 162
 Leung, [88] 20, 22
 Li, [37] 6
 Li, [141] 24
 Li, [140] 24, 27
 Li, [99] 22, 25, 26, 103, 106, 107, 113, 115,
 118, 119, 122, 123, 127, 134, 136,
 147, 154, 169, 172, 211, 212
 Li, [5] 3
 Li, [6] 3
 Li, [109] 22
 Li, [33] 5, 26
 Li S.-Y.R., [138] 23
 Li Wang, [175] 87
 Lie-Liang Yang, [164] 46, 150
 Lili Wei, [102] 22
 Lin Yang, [79] 20
 Ling Xu, [84] 20, 194
 Lingkun, [174] 77
 Lingkun Kong, [185] 125
 Lingkun Kong, [170] 66
 Liuqing Yang, [98] 22
 Loa, [84] 20, 194
 Luc, [36] 6
 Lui, [124] 22
- M**
- M., K. [193] 181
 M., S. [72] 11, 13, 76
 M., [177] 103, 211
 M., [35] 6
 M., [80] 20
 M., [42] 6, 25, 26, 103, 162
 M., [38] 6
 M., [188] 146, 159
 M., [89] 22

- M., [46] . 6, 25, 26, 103, 104, 107, 118, 119,
122, 166, 169, 212
- M., [179] 103, 104, 118, 119, 122, 165, 166,
169, 211, 212
- M., [178] 103
- M., [176] 103
- M., [84] 20, 194
- M., [183] 118, 119, 166
- M., [150] 25, 26
- M., [139] 23
- M., [97] 22
- M., [49] 6, 26
- M., [50] 6, 26
- M., [120] 22
- M., [130] 22
- M., [197] 209
- M., [51] 4, 7
- M.-S., [78] 20
- M.-S., [79] 20
- M.H., [91] 22
- M.J., [123] 22
- M.O., [78] 20
- M.O., [79] 20
- M.R., [91] 22
- M.Tücher, [158] 44, 46, 47, 49, 56
- Mangalvedhe, [165] 46, 69, 143, 194
- Maric, [49] 6, 26
- Markopoulou, [117] 22
- Marsic, [93] 22
- Maunder, [185] 125
- Maunder, [170] 66
- Maunder, [174] 77
- Medard, [177] 103, 211
- Medard, [42] 6, 25, 26, 103, 162
- Medard, [139] 23
- Medard, [97] 22
- Medard, [49] 6, 26
- Meixia Tao, [164] 46, 150
- Midkiff, [114] 22
- Midkiff, [101] 22
- Min Dong, [130] 22
- Ming Li, [118] 22
- Ming Xiao, [46] ... 6, 25, 26, 103, 104, 107,
118, 119, 122, 166, 169, 212
- Ming Xiao, [179] .. 103, 104, 118, 119, 122,
165, 166, 169, 211, 212
- Ming Xiao, [183] 118, 119, 166
- Ming Xiao, [150] 25, 26
- Ming Xiao, [50] 6, 26
- Mitran, [169] 63, 78, 79
- Mondal, [165] 46, 69, 143, 194
- Motani, [120] 22
- Mugen Peng, [103] 22
- N**
- N., J. [34] 5, 76
- N., J. [7] 6, 76, 77
- N., [165] 46, 69, 143, 194
- N., [146] 25, 26
- N., [64] 7
- N., [70] 8
- N.B., [105] 22
- N.Wu, [45] 6, 8, 16, 44, 56, 57, 66, 77
- Naguib, [70] 8
- Nayak, [122] 22
- Neely, [123] 22
- Ng, S.X. [71] 8
- Ng, [187] 146, 159
- Ng, [174] 77
- Ng, [5] 3
- Ng, [6] 3
- Ng, [4] 3, 4
- Ng, [75] 15
- Nguyen, [187] 146, 159
- Nguyen, [188] 146, 159
- Nguyen, [5] 3
- Nguyen, [6] 3
- Nguyen, [197] 209

Nguyen, [4].....3, 4
 Ni, [128] 22
 Niati, [104] 22
 Ning Cai, [143] 25
 Ning Cai, [144] 25
 Ning Cai, [137] 23
 Ning Cai, [33] 5, 26
 Niyato, [129].....22
 Nosratinia, [35].....6

O

O., [74].....14
 O., [75].....15
 O.Alamri, [73] 12
 O.Alamri, [45]...6, 8, 16, 44, 56, 57, 66, 77
 Ochiai, [169].....63, 78, 79
 Onurcan, [189] 147, 159
 Ottoson, [53].....4, 7

P

P., [154].....31, 32
 P., [25] 5
 P., [180] 106
 P., [166] 46, 69, 143
 P., [107] 22
 P., [169] 63, 78, 79
 P.A., [131] 22
 P.C., [92] 22
 P.P.C., [124] 22
 P.R., [95] 22
 P.R., [96] 22
 Panwar, [89] 22
 Pauli, [155] 32
 Peng Zhang, [124] 22
 Ping Wang, [129] 22
 Piro, [166] 46, 69, 143
 Poor, [92] 22
 Poor, [113] 22
 Prange, E. [16].....5

Q

Q.T., [141] 24
 Qian, [83] 20, 22
 Qian, [95] 22
 Qian, [96] 22
 Qiben Yan, [118] 22
 Qingkai Liang, [198] 209

R

R., A. [70].....8
 R., [177] 103, 211
 R., [37] 6
 R., [155] 32
 R., [42] 6, 25, 26, 103, 162
 R., [148] 25, 26
 R., [170] 66
 R., [165] 46, 69, 143, 194
 R., [135] 23
 R., [139] 23
 R., [104] 22
 R., [123] 22
 R., [146] 25, 26
 R., [33] 5, 26
 R., [193] 181
 R.A., [90] 22
 R.G., [185] 125
 R.Q., [85] 20
 R.W., [143] 25
 R.W., [144] 25
 R.W., [146] 25, 26
 R.W., [33] 5, 26
 R.Y., [192] 181
 R.Y.S., [187] 146, 159
 Ralf, [147] 25, 26
 Ratasuk, [165] 46, 69, 143, 194
 Raviv, [22] 5
 Rebelatto, [47]6, 25, 26, 103, 106, 107, 113,
 115, 118, 119, 122, 123, 127, 134,
 136, 147, 165, 166, 169, 172, 207,

- 211, 212
 Rebelatto, [48] 6, 26
 Rebelatto, [12] 6, 25, 26, 147, 149, 159–161,
 168, 181
 Rebelatto, [99] ... 22, 25, 26, 103, 106, 107,
 113, 115, 118, 119, 122, 123, 127,
 134, 136, 147, 154, 169, 172, 211,
 212
 Rebelatto, [11] 145, 149, 173
 Rebelatto, [5] 3
 Rebelatto, [6] 3
 Reed, I.S. [18] 5
 Robert G., [174] 77
 Rong, [94] 22
 Rossi, [176] 103
 Rui Cao, [98] 22
 Rui Zhang, [116] 22
 Ruiyuan Hu, [39] 6
 Ryzhik, I.M. [153] 30
- S**
- S., [89] 22
 S., [114] 22
 S., [145] 25
 S., [107] 22
 S., [100] 22
 S., [101] 22
 S., [126] 22
 S., [157] 35, 46–48, 50, 57, 59, 65
 S., [162] 46, 50, 57, 59
 S., [160] 46
 S., [161] 46, 76, 77
 S.-Y.R., [141] 24
 S.-Y.R., [33] 5, 26
 S.F., [114] 22
 S.F., [101] 22
 S.R., [120] 22
 S.X., [187] 146, 159
 SAGE, [181] 106
- Sangheon Park, [127] 22
 Schober, [155] 32
 Sendonaris, [29] 5
 Seong-Lyun Kim, [111] 22
 Seshadri, [70] 8
 Shalinee, [133] 22
 Shaoqian, [109] 22
 Sharma, [114] 22
 Sharma, [101] 22
 Shen, [95] 22
 Shen, [96] 22
 Sherali, [114] 22
 Sherali, [105] 22
 Shi, [114] 22
 Shiann-Tsong Sheu, [84] 20, 194
 Shiwei Huang, [106] 22
 Shroff, [105] 22
 Sihui Han, [198] 209
 Silva, [11] 145, 149, 173
 Singh, [120] 22
 Skoglund, [46] 6, 25, 26, 103, 104, 107, 118,
 119, 122, 166, 169, 212
 Skoglund, [179] ... 103, 104, 118, 119, 122,
 165, 166, 169, 211, 212
 Skoglund, [183] 118, 119, 166
 Skoglund, [150] 25, 26
 Skoglund, [50] 6, 26
 Sneessens, [36] 6
 Soljanin, [132] 22
 Soljanin, [145] 25
 Soljanin, [134] 23, 24
 Solomon, G. [18] 5
 Soon Ng, [170] 66
 Soon Xin, [174] 77
 Soon Xin, [5] 3
 Soon Xin, [6] 3
 Soon Xin, [4] 3, 4
 Soon Xin, [75] 15
 Soon Xin Ng, [156] 33

- Soon Xin Ng, [185].....125
 Soon Xin Ng, [186].....146
 Soon Xin Ng, [9]3
 Soon Xin Ng, [10].....3
 Soon Xin Ng, [168].....52
 Soon Xin Ng, [3]3
 Soon Xin Ng, [164] 46, 150
 Soon Xin Ng, [167].....48
 Soon Xin Ng, [161].....46, 76, 77
 Sprintson, [145]25
 Stojmenovic, [122] 22
 Sun, [141] 24
 Sungmook Lim, [108] 22
 Syue-Ju Syue, [115] 22
- T**
- T., [24].....5, 20
 T., [42] 6, 25, 26, 103, 162
 T., [43].....6, 26
 T., [89].....22
 T., [165] 46, 69, 143, 194
 T., [137].....23
 T., [104].....22
 T., [115].....22
 T.D., [187] 146, 159
 T.D., [188] 146, 159
 T.E., [35] 6
 T.F., [38].....6
 T.Keller, [71].....8
 T.M., [81] 20
 T.P.S., [113].....22
 Tairan Wang, [44] 6
 Tang, [109] 22
 Tao Zhang, [87] 20
 Tarokh, [70].....8
 Tarokh, [169].....63, 78, 79
 Tee, [187].....146, 159
 Tee, [170] 66
 ten Brink, [157]...35, 46–48, 50, 57, 59, 65
 ten Brink, [162]46, 50, 57, 59
 ten Brink, [160] 46
 Thitimajshima, [25].....5
 Thomas, [165]46, 69, 143, 194
 Towsley, [88] 20, 22
 Traskov, [139].....23
 Tse, [152].....30, 118
 Tse, [7] 6, 76, 77
- U**
- Ubaidulla, [107]22
 Uchô, [47] ... 6, 25, 26, 103, 106, 107, 113,
 115, 118, 119, 122, 123, 127, 134,
 136, 147, 165, 166, 169, 172, 207,
 211, 212
 Uchoa Filho, [99].22, 25, 26, 103, 106, 107,
 113, 115, 118, 119, 122, 123, 127,
 134, 136, 147, 154, 169, 172, 211,
 212
 Uchoa-Filho, [48] 6, 26
 Uchoa-Filho, [12] 6, 25, 26, 147, 149,
 159–161, 168, 181
 Uchoa-Filho, [11] 145, 149, 173
 Urgaonkar, [123] 22
- V**
- V., [155].....32
 V., [115].....22
 V., [70].....8
 V., [169].....63, 78, 79
 van der Meulen, [23].....5
 Vandendorpe, [36] 6
 Vetterli, [80] 20
 Vishwanath, [126].....22
 Viswanath, P. [151]30, 39, 69
 Vucetic, [38] 6
 Vucetic, [48].....6, 26
 Vucetic, [12]..6, 25, 26, 147, 149, 159–161,
 168, 181

Vucetic, [99] 22, 25, 26, 103, 106, 107, 113,
115, 118, 119, 122, 123, 127, 134,
136, 147, 154, 169, 172, 211, 212

W

W., G. [34] 5, 76
W., G. [7] 6, 76, 77
W., [21] 5
W.H., [83] 20, 22
Wanbin, [109] 22
Wassell, [90] 22
Wassell, [112] 22
Webb, W.T. [1] 1, 2
Webb, W. [71] 8
Wei Zhang, [92] 22
Weijia Lei, [87] 20
Weisi Guo, [112] 22
Wen Chen, [102] 22
Wenbo Wang, [103] 22
Wenjing Lou, [118] 22
Widmer, [176] 103
Wing-Kin Ma, [92] 22
Wong, [38] 6
Wonjun Lee, [127] 22
Wookbong Lee, [63] 7
Wornell, [152] 30, 118
Wornell, [34] 5, 76
Wornell, [7] 6, 76, 77
Wu, N. [73] 12
Wu, [140] 24, 27

X

Xiang, [94] 22
Xianzhong Xie, [87] 20
Xiaowen Gong, [113] 22
Xinbing Wang, [198] 209
Xu, [5] 3
Xu Li, [122] 22
Xuemin Sherman, [95] 22
Xuemin Sherman, [96] 22

Y

Y., [83] 20, 22
Y., [140] 24, 27
Y., [114] 22
Y.H., [99] ... 22, 25, 26, 103, 106, 107, 113,
115, 118, 119, 122, 123, 127, 134,
136, 147, 154, 169, 172, 211, 212
Y.T., [114] 22
Y.T., [101] 22
Yan, [125] 22
Yan Zhang, [106] 22
Yanchao Zhang, [116] 22
Yang, [187] 146, 159
Yang, [188] 146, 159
Yassae, [91] 22
Yeap, [74] 14
Yeung, Raymond W. [142] 25
Yeung, [143] 25
Yeung, [144] 25
Yeung, [146] 25, 26
Yeung, [33] 5, 26
Yeung R.W., [138] 23
Yi Shi, [101] 22
Yi Yu, [85] 20
Yifei Yuan, [84] 20, 194
Yingda, [133] 22
Yixin Jiang, [124] 22
Yong, [94] 22
Yonghui, [5] 3
Yonghui, [6] 3
Yonghui Li, [38] 6
Yonghui Li, [48] 6, 26
Yonghui Li, [12] 6, 25, 26, 147, 149,
159–161, 168, 181
Yu, [109] 22
Yuanzhu Chen, [93] 22
Yue, [94] 22
Yun Hee Kim, [110] 22
Yunhuai Liu, [128] 22

Yunnan Wu, [131] 22

Z

Zeger, [135] 23

Zeger, [97] 22

Zhang, [82] 20

Zhang, [95] 22

Zhang, [96] 22

Zhang, [173] 76, 84, 97, 123, 125

Zhang Z., [138] 23

Zhen Zhang, [149] 25, 26

Zhen Zhang, [136] 23, 25

Zheng Zhang, [81] 20

Zhenyu Yang, [118] 22

Zhiguo Ding, [88] 20, 22

Zhijun Cai, [85] 20

Zhongyuan Zhao, [103] 22

Zhou Zhang, [119] 22

Zhu, [95] 22

Zhu, [96] 22

Ziyu Shao, [141] 24

Zorzi, [176] 103